SAFIR

Safe and High Quality Food Production using Low Quality Waters and Improved Irrigation Systems and Management (SAFIR)

Contract-No. FOOD-CT-2005-023168

A Specific Targeted Research Project

under the Thematic Priority ' Food Quality and Safety '

WP 3• Single Crop Modelling

D3_2 Final version and documented models available

Due date:	30-04-09
Actual submission date:	30-04-09
Start date of project:	01-10-05 Duration: 48 months
Deliverable Lead contractor:	Natural Environment Research Council
Participant(s) (Partner short names)	DIAS, CER, LIFE-KU, NERC, UB, CAU, CAAS
Author(s) in alphabetic order:	Ragab Ragab
Contact for queries:	Natural Environment Research Council Centre for Ecology and Hydrology Maclean Building Crowmarsh Gifford Wallingford, OXON OX10 8BB, UK United Kingdom Rag@ceh.ac.uk
Dissemination Level: (PUblic, Restricted to other Programmes Participants, REstricted to a group specified by the consortium, COnfidential only for members of the consortium)	PU
Deliverable Status:	Revision 1.0

Project co-funded by the European Commission within the Sixth Framework Programme (2002-2006)

Contents

The Daisy model description (Summary)

Daisy is a field scale model for simulating nitrogen, carbon and water dynamics. It has been used for assessing both production and environmental impact of farm management. In the SAFIR project the model has been extended in order to be able to simulate the effect of PRD irrigation in row crops. The complete model (including documentation) can be downloaded from the Daisy homepage:

http://code.google.com/p/daisy-model/

The changes can roughly be divided into three areas: soil physics, the crop model, and the soil vegetation atmosphere transfer system.

2D Soil Physics

The original Daisy model is based on a vertical 1D description of the field, with finite difference solutions to Richard's equation for water flow, convection-dispersion for solute (nutrients and pesticides) transport, and the heat transfer equation. To support row crops and PRD irrigation, a 2D description of the field has been introduced based on finite volume solutions to the same equations. These numerical schemes have been documented in Annex 3.1. The principles for integrating them with the existing Daisy code can be found in Annex 3.2

Changes to the crop model

The original Daisy photosynthesis model is based on radiation intensity (Goudriaan and Laar, 1978), with separately calculated water and nitrogen stress factors. The canopy is divided into 30 layers, with a single light extinction coefficient. To better support the effect of ABA on production, a new photosynthesis model based on Farquhar et al (1980) and Ball et al (1987), with Stomata conductance model coupled as described by Collatz et al., 1991, has been added. This is supplemented by a new light distribution model that includes sunlit and shaded leaves, as well as the effect of the sun angle on diffuse radiation, as per de Pury and Farquhar (1997). This work is described in Annex 3.3.

A new 2D root distribution model has been included for row crops. It is based on a simple 2D extension of the empirical relationship found in Gerwitz and Page, 1974, as detailed in Annex 3.4.

Binding the two together is the plant hormone ABA. The ABA generation is based on work by Liu et al. (2008). Its implementation in Daisy, as well as the effect on stomata conductivity, is described in Annex 3.5.

New SVAT model

To support the more complex photosynthesis model, a new SVAT (Soil Vegetation Atmosphere Transfer) model has been introduced. The model divides the canopy into sunlit and shaded leaves, and a set of equations describing the energy flow between laves, canopy air, soil surface, and the above canopy atmosphere is introduced. By solving this equation system, we can find the temperature of sunlit and shaded laves, canopy air humidity, as well as transpiration. Since the temperature and humidity affects photosynthesis and stomata conductance, and stomata conductance is an important element of the equation system, an iterative process is used.

The equation system is described in Annex 3.6. The components of the equation system are too numerous to mention here, but most can be found in Houborg (2006), on which this work is based.

References:

Ball, J.T., Woodrow, I.E. and Berry, J.A. (1987) A model predicting stomatal conductance and its contribution to the control of photosynthesis under different environmental conditions. In: I.Biggins (Editor), *Progress in Photosynthesis Research*. Martinus Nijhoff Publishers, Netherlands, pp. 221-224.

Collatz, G.J., Ball, J.T., Grivet, C. and Berry, J.A. (1991) Physiological and Environmental-Regulation of Stomatal Conductance, Photosynthesis and Transpiration - A Model That Includes A Laminar Boundary-Layer. *Agricultural and Forest Meteorology*, 54(2-4): 107-136.

de Pury, D.G.G. and Farquhar, G.D. (1997) Simple scaling of photosynthesis from leaves to canopies without the errors of big-leaf models. *Plant Cell and Environment*, 20(5): 537-557.

Farquhar, G.D., Caemmerer, S.V. and Berry, J.A. (1980) A Biochemical-Model of Photosynthetic Co2 Assimilation in Leaves of C-3 Species. *Planta*, 149(1): 78-90

Gerwitz, A., and Page, E. R (1974) An empirical mathematical model to describe plant root systems.*The Journal of Applied Ecology* 11, 773-781

Goudriaan, J., Laar, H.H. van **(**1978) Calculation of daily totals of the gross CO2 assimilation of leaf canopies. *Journal of Agricultural Science (Netherlands)* 26(4) p. 373-382

Houborg, R (2006) Inferences of key environmental an vegetation biophysical controls for use in regional-scale SVAT modeling using Terra and Agua MODIS and weather prediction data. PhD dissertation, Institute of Geography, University of Copenhagen,

Liu, F., Song, R., Zhang., X., Shahnazari, A., Andersen, M. N., Plauborg, F., Jacobsen, S-E. and Jensen, C. R. (2008) Measurement and modelling of ABA signalling in potato (Solanum tuberosum L.) during partial root-zone drying. *Environmental and Experimental Botany* 63, 385-391

The SALTMED model description (Summary)

In this part a summary of SALTMED model processes will be given, however more detailed description of the processes and the main equations are given in Annex 3.7. SALTMED model user interface and examples of input and output are given in Annex 3.8.

The SALTMED model was designed to include a number of physical processes acting simultaneously under field conditions. It was also designed to be, generic, physically based, and friendly to use. The model contained the following key processes:

1. **Evapotranspiration: several options to calculate the evapotranspiraion that include:**

- Penman-Monteith equation according to the modified version of FAO - 56 (1998) with average seasonal value of surface conductance.
- Penman Monteith equation with options to specify the surface conductance. The latter is calculated by different methods:

A. ***Applying Penman – Monteith equation using stomata Conductance calculated from environmental parameters*****: A**ccording to Jarvis 1976 and modified by Korner et al. (1995). It is based on multiplication of maximum stomata conductance by the relative effects of environmental stress factors such as Vapour Pressure Deficit, VPD, temperature, soil water availability and radiation.

B. ***Applying Penman – Monteith equation using stomata Conductance calculated from the Absecic Acid, ABA and leaf water potential***
The equation suggested by Tardieu et al. 1993 was implemented. The equation is based on minimum stomata conductance, leaf water potential, Absecic Acid concentration, and other fitting coefficients.

C. Applying Penman – Monteith equation using average value of stomata Conductance

D. ***Applying Penman – Monteith equation using measured daily value of stomata Conductance***

2. **Modelling Crop Growth, Biomass / Dry Matter production and Yield**
The crop growth, biomass / dry matter production and yield have been calculated based on: radiation, photosynthetic efficiency, water uptake, air temperature, leaf nitrogen content, leaf area index, respiration losses and the harvest index.

3. **Modelling Soil Nitrogen Dynamics**
Soil nitrogen dynamics based largely on the approach of Johnsson et al. 1987 in SOIL – N model have been adapted and coded. The model takes into account the different external N-sources as:
1-Dry deposition from the atmosphere
2-Wet deposition with rainfall
3- Commercial Fertilizers add as dry chemicals (Urea, Ammonium based fertilizer, Nitrate based Fertilizer and mixed Ammonium Nitrate Fertilizer etc.)
4- Commercial fertilizers added with the irrigation water
(Fertigation) these are as above (Urea, Ammonium based fertilizer, Nitrate based Fertilizer and mixed Ammonium Nitrate Fertilizer etc.)
5- Manure
6- Incorporated crop residues of previous crop on ploughing day before sowing

The model implemented the following processes:

- Mineralization, Immobilization, Nitrification, Denitrification
- N-Leaching
- Plant N Uptake

.

4. **Modelling Soil Temperature**
   Soil temperature has been calculated from air temperature according to the approach of Kang et al. 2000 and Zheng et al. 1993. It is based on average air temperature, damping ratio, thermal diffusivity as a function of soil water, air and mineral content, Leaf Area Index, LAI and litter fraction.

5. **Modelling water uptake**: Plant water uptake was calculated according to Cardon and Letey (1992) taking into account the water stress and the salinity stress in case of using saline water.
6. **Modelling soil water and solute movement**: The water flow in soil was described mathematically using Richard's equation. The movement of solute in the soil system was described by the convection–dispersion equation. Under irrigation from a trickle line source, the water and solute transport can be viewed as two-dimensional flow. In the model, sprinkler, flood and basin irrigation are described by one-dimensional flow equations. Furrow and trickle line source are described by 2-dimensional equations. Trickle point source is described by cylindrical flow equations.

Default Data in the Databases
The model has 3 built-in databases:
Crop database (based largely on the FAO 1992 & 1998), contains different crops, trees and shrubs (>200) from different regions, duration of each growth stage, sowing and harvest dates, K_c & K_{cb} values for each growth stage, maximum height and maximum rooting depth. The model uses K_{cb} as it runs on a daily time step.
Soils database: Contains the hydraulic characteristics and solute transport parameters of more than 40 different soil types.
Irrigation system database: Contains information on the wetting fraction and the frequency of application of the irrigation systems

Data Requirements
Plant characteristics: these include for each growth stage; the crop coefficient, K_c , K_{cb}, root depth and lateral expansion, crop height and maximum / potential final yield observed in the region under optimum conditions.
Soil characteristics: include depth of each soil horizon, saturated hydraulic conductivity, saturated soil water content, salt diffusion coefficient, longitudinal and transversal dispersion coefficient, initial condition of : soil moisture, NO^3-N, NH^4-N and salinity in each soil layer, tabulated data of soil moisture versus soil water potential and soil moisture versus hydraulic conductivity.
Meteorological data: include daily values of temperature (maximum), temperature (minimum), relative humidity, total or net radiation, wind speed, and daily rainfall.
Water management data: include the date and amount of irrigation water and fertilizers applied (fertigation) and the salinity of applied irrigation.
Nitrogent fertilization data: This includes amount and date of dry fertilizers added, dry and wet N deposition, initial soil humus and litter contents.

Model parameters: include the number of compartments in both vertical and horizontal direction, tortuosity parameters, diffusion parameters, uptake parameters, position of plant relative to irrigation source and the maximum time step for calculation.
Model run: The model runs at maximum time step of 200 seconds and output values on daily basis. The model calculates the water and solute movement on grid square basis. The default grid size is 4 by 4 cm. The model considers different plant positions from the irrigation source and accommodates rainfed as well as subsurface irrigation including deficit irrigation and Partial Root Drying, PRD.

Model structure and equations used to describe each processes are given in Ragab, 2002.
The model is friendly and easy to use benefiting from the Windows™ environment. The model is freely available at: http://www.safir4eu.org

Published SALTMED References:

Ragab, R. 2002. A holistic generic integrated approach for irrigation, crop and field management: the SALTMED model. Environmental Modelling and Software 17: 345-361.

R. Ragab, (Editor), 2005. Advances in integrated management of fresh and saline water for sustainable crop production: Modelling and practical solutions. International Journal of Agricultural Water Management (Special Issue), volume 78- Issues 1-2, pages 1-164. Elsevier, Amsterdam. The Netherlands.

Supporting development References

Cardon, E.G., Letey, J., 1992. Plant water uptake terms evaluated for soil water and solute movement models. Soil Sci. Soc. Am. J. 56, 1876-1880.

FAO, 1998. Crop evapotranspiration, Irrigation and Drainage Paper No 56. Rome, Italy.
Jarvis, P. G. 1976. The iterepretation of the variations in leaf water potential and stomatal conductance found in canopies in the field. Philosophical. Transactions of the Royal Society. B273:593-610.

Pleijel, H., Danielsson, H., Vandermeiren, K., Blum, C., Colls, J, and Ojanpera, K. 2002. Stomatal conductance and ozone exposure in relation to potato tuber yield-results from the European CHIP programme. European J.of Agronomy, 17:303-317.

Tardieu, F, Zhang, J. and Gowing, D. J. G. 1993. Stomatal control by both [ABA] in the xylem sap and leaf water status: a test of a model for droughted or ABA-fed field-grown maize. Plant, Cell and environment .16:413-420.

Eckersten, H and Jansson, P,.- E. 1991. Modelling water flow, nitrogen uptake and production for wheat. Fertilizer Research 27: 313-329.

Johnsson, H., Bergstrom, L and Jansson, P.-E.. 1987. Simulated nitrogen dynamics and losses in a layered agricultural soil. Agriculture, Ecosystems and Environment, 18:333-356.

Wu, L., McGechan, M., B., Lewis, D. R., Hooda, P. S., and Vinten, A., J., A. 1998. Parameter selection and testing the soil nitrogen dynamics model SOILN. Soil Use and Management, 14: 170-181

Kang, S., Kim, S., Oh, S. and Lee, D. 2000. Predicting spatial and temporal patterns of soil temperature based on topography, surface cover and air temperature. Forest Ecology and Management 136:173-184.

Marshall, T.J., Holmes, J. W., and Rose, C.W. (editors). 1996. Soil Physics (3rd edition) , 358-376. Cambridge University Press. Cambridge, UK.

Zheng, D., Hunt, Jr., Running, S.W. 1993. A daily soil temperature model based on air temperature and precipitation for continental applications. Climate Research 2: 183-191.

Annex 3.1 Water movement in Daisy model

Chapter 1

Water movement

The soil water, θ is in the model divided into 3 parts:

$$\theta = \theta_1 + \theta_2 + \theta_3 \tag{1.1}$$

The third domain is made for describing the macroporous flow whereas the primary and secondary domain are representing the water in the soil matrix

$$\theta_{\mathrm{m}} = \theta_1 + \theta_2 \tag{1.2}$$

where θ_{m} is volumetric water content in the matrix domain. The division of the matrix domain into 2 subdomains is solely made for a better description of solute movement - see more in chapter 2.

1.1 Richards' Equation

The water flow in porous media can be described with the formula of Richard. The equation is derived here. The water flux density vector, $\mathbf{q}_{\mathrm{m}}$ can be calculated by the Darcy´s law. For a two-dimensional vertical transect it yields:

$$\mathbf{q}_{\mathrm{m}} = -\mathbf{K}(\psi)\nabla(\psi + z) \tag{1.3}$$

where $\mathbf{K}(\psi)$ is the hydraulic conductivity tensor, ψ is the potential head. The x-axis is chosen in horizontal direction and the z-axis is positive upwards. The conductivity tensor can be expressed as:

$$\mathbf{K} = \begin{bmatrix} K_{xx} & K_{xz} \\ K_{zx} & K_{zz} \end{bmatrix} \tag{1.4}$$

For a model with rectangular cells we have chosen that the principal directions of the anisotropic medium are parallel to the x- and z-axis, i.e.

$$\mathbf{K} = \begin{bmatrix} K_{xx} & 0 \\ 0 & K_{zz} \end{bmatrix} \tag{1.5}$$

The mass balance for the system gives

$$\frac{\partial \theta_{\mathrm{m}}}{\partial t} = -\nabla \cdot \mathbf{q}_{\mathrm{m}} - \Gamma_{\mathrm{wm}} \tag{1.6}$$

where θ_{m} is the volumetric water content and Γ_{wm} is the sink term for water. The partial differential equation can be developed by combining Darcy´s law, equation (1.3) and the mass balance, equation (1.6), thus

$$\frac{\partial \theta_{\mathrm{m}}}{\partial t} = \nabla \cdot (\mathbf{K}(\psi)\nabla(\psi + z)) - \Gamma_{\mathrm{wm}} \tag{1.7}$$

This is known as Richard's equation. For the modeling is assumed that the soil-water retention is without hysteresis, i.e. there is a unique relation between the matrix pressure potential and the water content.

To solve Richard's equation it is necessary to specify initial and boundary conditions. The boundary conditions specify a combination of ψ and its derivative on the boundary. Furthermore it is possible to use different forms of flux (Neumann) and predescribed pressure (Dirichlet) boundary conditions. The problem to be solved for determining the water movement can be summarized to

$$\begin{cases} \frac{\partial \theta_{\mathrm{m}}}{\partial t} = \nabla \cdot (\mathbf{K}(\psi)\nabla(\psi + z)) - \Gamma_{\mathrm{wm}} & \text{in } \Omega \\ \bar{\mathbf{n}} \cdot (\mathbf{K}(\psi)\nabla(\psi + z)) = -q_{\mathrm{m}} & \text{on } \partial\Omega^N \\ \psi = \psi_0 & \text{on } \partial\Omega^D \end{cases} \tag{1.8}$$

where $\bar{\mathbf{n}}$ is the outward unit normal, and q_{m} is the magnitude of the outward flow from the domain. ψ_0 is the predescribed pressure at the boundary. Ω is the soil domain. $\partial\Omega^N$ and $\partial\Omega^D$ are part of the boundary of Ω with Neumann and Dirichlet boundaries, respectively such that $\partial\Omega = \partial\Omega^N \cup \partial\Omega^D$. Each of $\partial\Omega^N$ and $\partial\Omega^D$ are not necessarily one continuous curve piece. A special case of the Neumann boundary conditions is often applied for the lower boundary condition, viz. it is assumed that the flow it is only driven by gravity (gravity boundary condition), i.e. $\partial\psi/\partial x = \partial\psi/\partial z = 0$ which gives

$$q_{\mathrm{m}} = \bar{\mathbf{n}} \cdot \begin{bmatrix} 0 \\ K_{zz} \end{bmatrix} \tag{1.9}$$

Another often used boundary condition is the seepage boundary condition for atmospheric boundaries. If a seepage face does not develop, the boundary acts as no flow. If a seepage face occurs we have a Dirichlet boundary condition with $\psi = 0$ and allow water to flow out of the domain. The condition can for instance be applied in connection with estuaries or streams.

1.2 Macropore flow

In the concept all macropores are vertical oriented. The macropore (tertiary) domain in the model contains a number of user specified macropore clases. In

a macropores class all the macropores have the same physical properties such as length. Each of the classes are characterized by distribution in the horizontal plane, radius of the pores and depth where the macropores start and ends. Also the pressures where the water starts and stops moving from the matrix to the macropore domain must be known. The macropores are also characterized by resistance for transferring water from a filled macropore to the matrix domain. The macropores can either end in the soil matrix or in a drain. When the macropores ends in a drain, matrix water which flows intro the macropore is instantaneously moved to the drain, and as consequence can macropores connected with drains newer be filled, and water can not be moved from the macropore to the matrix. The pressures where the water starts and stops moving from the matrix to the macropore domain must be known and the values are common for all the classes.

1.2.1 Macropore interaction with matrix water

The condition for macroporous flow to initiate and water move from the matrix to macropores in a macropores class is that the matrix pressure exceeds a certain value ψ_{initiate}.

$$\psi \geq \psi_{\text{initiate}} \tag{1.10}$$

When water is transferred from the matrix to the macroporous domain, the water is instantaneously moved to the top of the current water level in the macropores. If the whole macropore is empty, the incoming water is moved instantaneous to the bottom of the macropore or alternatively to the drain (if the macropore ends in a drain).

The water transfer from the matrix domain to the macroporous domain terminates if the matrix pressure is below a certain level, i.e.

$$\psi < \psi_{\text{terminate}} \tag{1.11}$$

In a location where the macropore class is filled with water, water is transferred from the macropore to the matrix domain if

$$\psi_{3,\,\text{c}} > \psi \tag{1.12}$$

where $\psi_{3,\,\text{c}}$ is the pressure potential in the macropore.

The quantification of the water movement toward a macropore is based on a relatively simple approach, very similar to theory of water the movement in a confined aquifer towards a well. For a confined aquifer of thickness D the stationary solution for water movement towards a well is

$$Q = \frac{2\pi K D(s_{\text{well}} - s)}{\ln(\frac{r}{r_{\text{well}}})} \tag{1.13}$$

where K is the (saturated) hydraulic conductivity, r_{well} is the radius of the well, s_{well} is the drawdown at the wall of well and s is the drawdown at the distance r from the center of the well.

If the macropores are equidistant placed, the density in the horizontal plane M_{c} can be approximated as:

$$M_{\text{c}} \approx \frac{1}{\pi r_{\text{c, mean}}^2} \tag{1.14}$$

where $2r_{\text{c, mean}}$ is the mean distance between the macropores.

In a small time step, the flow towards a macropore is considered as stationary and at the distance $r_{\text{c, mean}}$, the pressure in the current time step is considered as unaffected of the macropore, i.e. no pressure drawdown. Thus the flow to a piece of a single macropore with the height, Δz can be approximated as

$$Q_{\text{c, macro}} = \frac{2\pi K(\psi)\Delta z(\psi - \psi_{3,\text{ c}})}{\ln(\frac{r_{\text{c, mean}}}{r_{\text{c, macro}}})} \tag{1.15}$$

where $\psi_{3,\text{ c}}$ is the pressure potential in the macropores and $r_{\text{c, macro}}$ is the radius of the macropore and $K(\psi)$ is the hydraulic conductivity. Preventing that the hydraulic conductivity is very high in fractured media the $K(\psi)$ is computed as

$$K(\psi) = \min(K_{xx}(\psi), K_{xx}(\psi_{\text{initiate}})) = K_{xx}(\min(\psi, \psi_{\text{initiate}})) \tag{1.16}$$

where K_{xx} is the conductivity in the x-direction (see equation (1.5)). It is assumed that the flow towards the macropores is horizontal. Using equation (1.14) the sink term can be calculated

$$\Gamma_{\text{wm, c}} = \frac{M_{\text{c}} Q_{\text{c, macro}}}{\Delta z} = \frac{-4\pi M_{\text{c}} K_{xx}(\psi)(\psi - \psi_{3,\text{ c}})}{\ln(\pi M_{\text{c}} r_{\text{c, macro}}^2)} \tag{1.17}$$

For flow from the macropore domain into the matrix domain are the calculations made in a similar manner, but instead of using the conductivity is a resistance, $R_{\text{c, macro}}$ for flow out from the macropores introduced.

$$\Gamma_{\text{wm, c}} = \frac{-4\pi M_{\text{c}}(\psi - \psi_{3,\text{ c}})}{R_{\text{c, macro}} \ln(\pi M_{\text{c}} r_{\text{c, macro}}^2)} \tag{1.18}$$

The pressure at a given position in the macropore depends on the water level in the macropore

$$\psi_{3,\text{ c}} = z_{\text{c, macro}} - z \tag{1.19}$$

where $z_{\text{c, macro}}$ is the water level en the macropore. If the macropore is empty is $z_{\text{c, macro}} = z_{\text{c, bottom}}$ where $z_{\text{c, bottom}}$ is the z-coordinate of the bottom of the macropore. As a consequence of equation (1.19), we have for macropores which ends in drains:

$$\psi_{3,\text{ c}} = z_{\text{drain}} - z \tag{1.20}$$

where z_{drain} is the z-coordinate of the drain.

All the considerations above are for the transfer of water between a macropore class and the matrix. To calculate the total transfer between the macropores and the matrix it is necessary to sum up the contributions from each of the macropore classes. Thus the sink the macropores contributes to in the maxtrix flow is

$$\Gamma_{\text{wm, macro}} = \sum_{c=1}^{NC} \Gamma_{\text{wm, c}} \tag{1.21}$$

where NC is the number of macropore classes.

1.2.2 Macropore interaction with surface water

When the surface is ponded, water can directly enter the macropores without first entering the soil matrix. The rate is calculated very roughly and based on Poisseuilles law (e.g. Hillel, 1998). In the assumption made here only gravity drives the flow. The vertical flow in a macropore can be computed as:

$$Q_{\text{infiltration}} = \frac{\pi r_{\text{c, macro}}^4 \rho_w g(l + H_{\text{pond}})}{8l\mu} \approx \frac{\pi \rho_w g r_{\text{c, macro}}^4}{8\mu} \tag{1.22}$$

where μ is the dynamic viscosity, ρ_w the density of water, g the gravitational acceleration, l the distance from the surface to the water level in the macropore class (or the bottom of the macropore if it is empty) and H_{pond} is the ponding depth. The infiltration rate into the macropore class is:

$$i_{\text{c, macro}} = \frac{\pi M_{\text{c}} \rho_w g r_{\text{c, macro}}^4}{8\mu} \tag{1.23}$$

The total infiltration into macropores is the sum of the infiltration into the different macropore classes

$$i_{\text{macro}} = \sum_{c=1}^{NC} i_{\text{c, macro}} \tag{1.24}$$

In the numerical model in a timestep of size Δt the implemented routine allows no more water for infiltration than present at the surface on the start of the timestep. Furthermore there can not infiltrate more water into a macropore class as there is space for in the start of the timestep. If all water is infiltrated in the timestep, the water is distributed between the classes proportional to the area density, M_{c} of the classes.

1.3 Finite Volume Method

1.3.1 Mesh

In Daisy2D, the domain, Ω is divided into N non-overlapping polygons, also denoted control volumes or cells. In Daisy2D it should be possible to choose be-

tween grids consisting of only rectangular cells or meshes consisting of trapezoids with two vertical faces. Figure 1.1 shows a grid only consisting of rectangular cells. The domain Ω in the figure is in divided into 3 subdomains, each consisting of a number of cells. Each subdomain is characterized by different hydraulic properties. The grid shown in figure 1.2 consists of trapezoids (where most of them also are rectangles). Only in the proximity of the drainpipe (see figure 1.3), the cells are not rectangular.

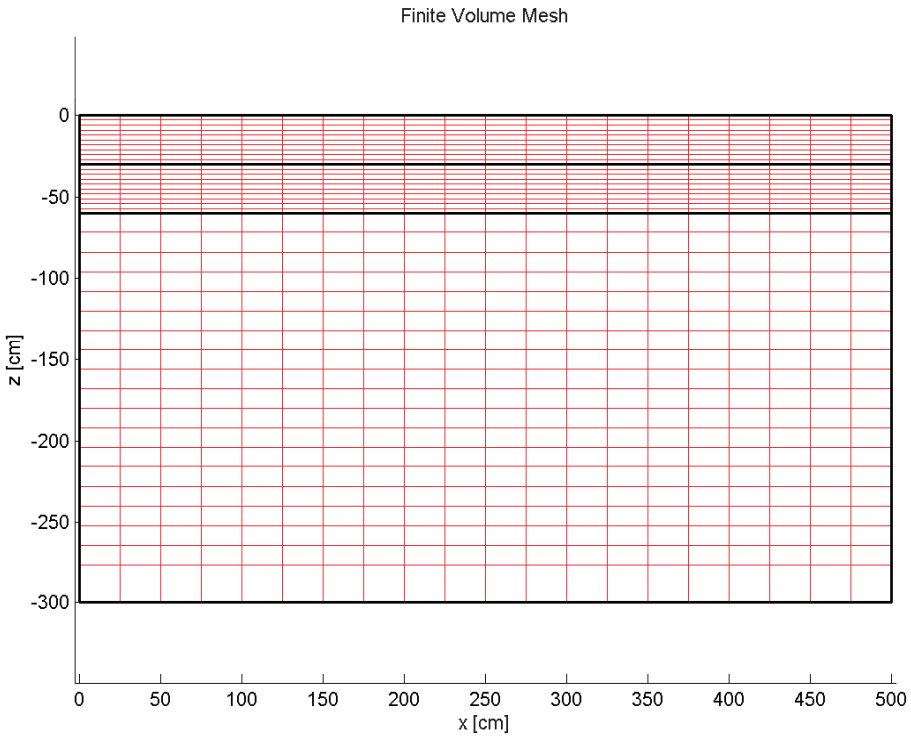

Figure 1.1: Example of grid consisting of rectangular cells.

The quadrilateral (rectangular or trapezoid) cells are denoted Q_i where $i = 1, 2, \cdots, N$. $|Q_i|$ denotes the area of Q_i, and ∂Q_i is the boundary of Q_i i.e. the edges (or faces) of Q_i. All internal edges e_{ij} are labeled by indices, i and j of the adjacent cells that shares face. The grid is constructed such that only whole faces are shared ($e_{ij} = Q_i \cap Q_j$). The length of e_{ij} is $|e_{ij}|$ and the unit normal vector pointing from $Q_i$into Q_j and orthogonal to e_{ij} is denoted $\bar{\mathbf{n}}_{ij}$. σ_i contains cell indices of cells sharing faces with cell i. σ_i' contain indices of cell faces of cell i which are placed on $\partial\Omega$, i.e. it is not shared with another cell. σ_i' is divided into two subsets, $\sigma_i'^D$ and $\sigma_i'^N$ of boundary cell faces with a Dirichlet and Neumann boundary condition, respectively.

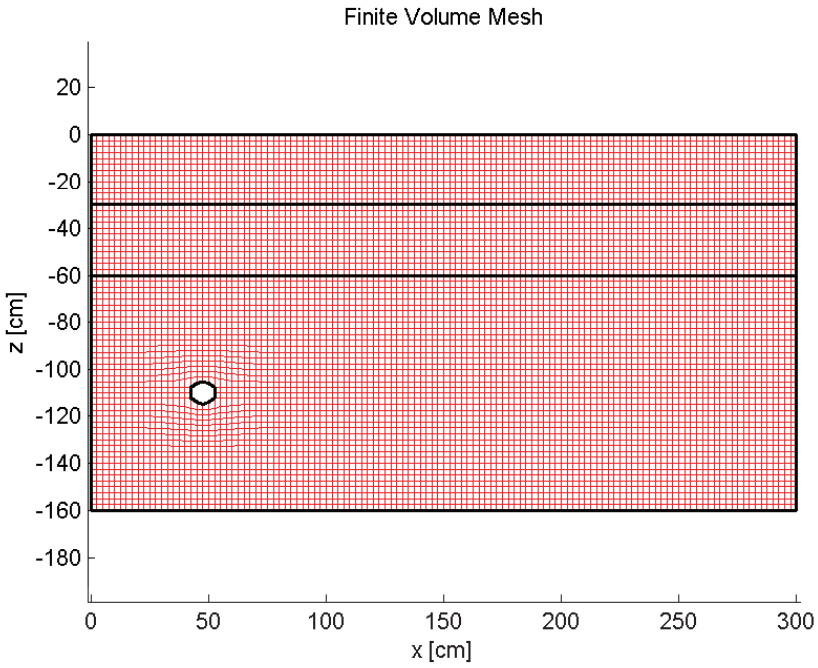

Figure 1.2: Example of grid consisting of trapezoids.

1.3.2 Cell mass-balances

Richards equation is integrated over control volume (here a cell), Q_i. By applying the divergence theorem by Green-Gauss, we obtain

$$\int_{Q_i} \frac{\partial \theta_{\mathrm{m}}}{\partial t} d\Omega = \int_{\partial Q_i} (\mathbf{K}(\psi)\nabla(\psi + z)) \cdot \bar{\mathbf{n}} dl - \int_{Q_i} \Gamma_{\mathrm{wm}} d\Omega \qquad (1.25)$$

where $\bar{\mathbf{n}}$ is the outwarded unit normal and ∂Q_i the boundary of Q_i. The cell averages of θ_{m} and ψ are denoted θ_i and ψ_i. θ_i and ψ_i, $i = 1, 2, \cdots N$ where N is the number of cells that are collected in the vectors $\boldsymbol{\theta}$ and $\boldsymbol{\psi}$. Discretization of equation (1.25) based on a grid consisting of quadrilaterals yield

$$|Q_i| \left(\frac{d\theta_{\mathrm{m}}}{dt} \right)_i = \sum_{j \in \sigma_i} D_{ij}(\boldsymbol{\psi}) + \sum_{j \in \sigma_i} G_{ij}(\boldsymbol{\psi}) + \sum_{j' \in \sigma_i'} B_{ij'}(\boldsymbol{\psi}) - S_i(\boldsymbol{\psi}) \qquad (1.26)$$

where:

- $D_{ij}(\boldsymbol{\psi})$ describe the diffusive transport between internal borders
- $G_{ij}(\boldsymbol{\psi})$ describe the gravitational transport between internal boundaries

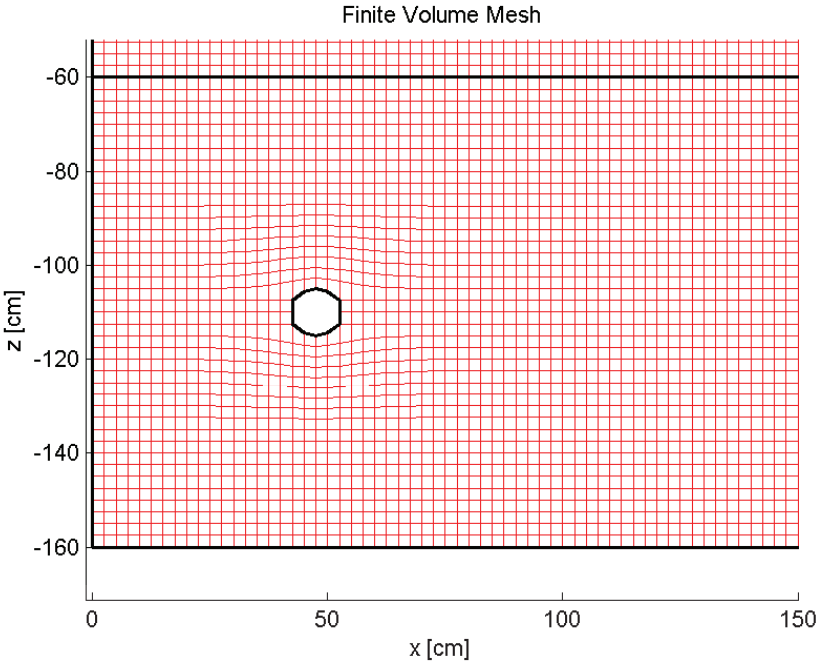

Figure 1.3: Close picture of grid near the drain pipe.

- $B_{ij'}(\boldsymbol{\psi})$ describe flux for external boundaries $j' \in \sigma_i'$
- $S_i(\boldsymbol{\psi})$ is the integrated sink term (point and area distributed sinks) in the cell.

The diffusive transport from cell i to cell j can be calculated as

$$D_{ij}(\boldsymbol{\psi}) = |e_{ij}|(\mathbf{K}(\boldsymbol{\psi}) \cdot (\nabla\psi)_{ij}) \cdot \bar{\mathbf{n}}_{ij} \tag{1.27}$$

For evaluating equation (1.27) it is necessary to estimate the gradient $(\nabla\psi)_{ij}$. $(\nabla\psi)_{ij}$ is evaluated by a different method for meshes with rectangular cells than for the more general and complicated case with meshes consisting of trapezoid cells. The gravitational transport from cell i to cell j can be calculated as

$$G_{ij}(\boldsymbol{\psi}) = |e_{ij}|(\mathbf{K}(\boldsymbol{\psi}) \cdot ([0\ 1]^T)) \cdot \bar{\mathbf{n}}_{ij} \tag{1.28}$$

The boundary flux term is split into the contribution from boundaries with Neumann and Dirichlet condition respectively:

$$\sum_{j' \in \sigma_i'} B_{ij'}(\boldsymbol{\psi}) = \sum_{j' \in \sigma_i'^N} B^N_{ij'}(\boldsymbol{\psi}) + \sum_{j' \in \sigma_i'^D} B^D_{ij'}(\boldsymbol{\psi}) \tag{1.29}$$

For the boundaries with Neumann conditions we have

$$B^N_{ij'}(\boldsymbol{\psi}) = -q_{\mathrm{m},ij'}|e_{ij'}| \tag{1.30}$$

where $q_{\mathrm{m},ij'}$ is the size of the Darcy flux, perpendicular to the cell face and positive for flux out from cell i. The easiest way to implement Dirichlet boundary conditions is simply to force ψ_i to the value that ψ has on the face with Dirichlet conditions. Conflicts can arise if cell i has more than one face with a Dirichlet condition. Instead, the Dirichlet boundary condition is implemented as if the midpoint of the Dirichlet face was a neighbor cell. Similar to an interior cell face, a diffusive and a gravitational contribution can be calculated:

$$B^D_{ij'}(\boldsymbol{\psi}) = D^D_{ij'}(\boldsymbol{\psi}) + G^D_{ij'}(\boldsymbol{\psi}) \tag{1.31}$$

where

$$D^D_{ij'}(\boldsymbol{\psi}) = |e_{ij'}|(\mathbf{K}(\psi_i) \cdot (\nabla\psi)_{ij'}) \cdot \bar{\mathbf{n}}_{ij'} \tag{1.32}$$

$$G^D_{ij'}(\boldsymbol{\psi}) = |e_{ij'}|(\mathbf{K}(\psi_i) \cdot ([0\ 1]^T)) \cdot \bar{\mathbf{n}}_{ij'} \tag{1.33}$$

where the pressure associated with cell i has been used for calculating the hydraulic conductivity. The sink term used in equation (1.6) can be divided into two parts

$$\Gamma_{\mathrm{w1}} = \Gamma_{\mathrm{wma}} + \Gamma_{\mathrm{wmp}}\delta(x_p - x)\delta(z_p - z) \tag{1.34}$$

where Γ_{wma} is the contribution from a area distributed sink and Γ_{wma} is the contribution from a point sink. (x_p, z_p) are the coordinates of the point sink which shall be placed in the interior of a cell(not on the cell faces). δ is the Dirac delta function. Thus, the contribution from the sink terms to a cell yields

$$S_i(\boldsymbol{\psi}) = \Gamma_{\mathrm{wma}}|Q_i| + \Gamma_{\mathrm{wmp}} \tag{1.35}$$

Area distributed sinks are typically extraction from roots or (in Daisy2D) water flow between the soil matrix and macro pore domain. The point sinks can be tile drains or drip irrigation systems (point sources). Both Γ_{wma} and Γ_{wmp} can be dependent on the solution (ψ).

1.3.3 Rectangular cells

For the situation with a mesh consisting of rectangular cells, only matrix pressure in the four neighbor cells (see figure 1.4) are applied for calculating the fluxes through the faces of the cell (five point stencil). In the present section we will only evaluate the gradient for the "eastern" cell face of cell i. The theory can easily be applied for the 3 remaining directions. The distances necessary for evaluating the flux from a cell to the cell placed east of the cell are shown in figure 1.5.

The value of ψ in the midpoint of the eastern cell (ψ_E) can be expressed by a Taylor expansion of the value of ψ at the midpoint of the cell face:

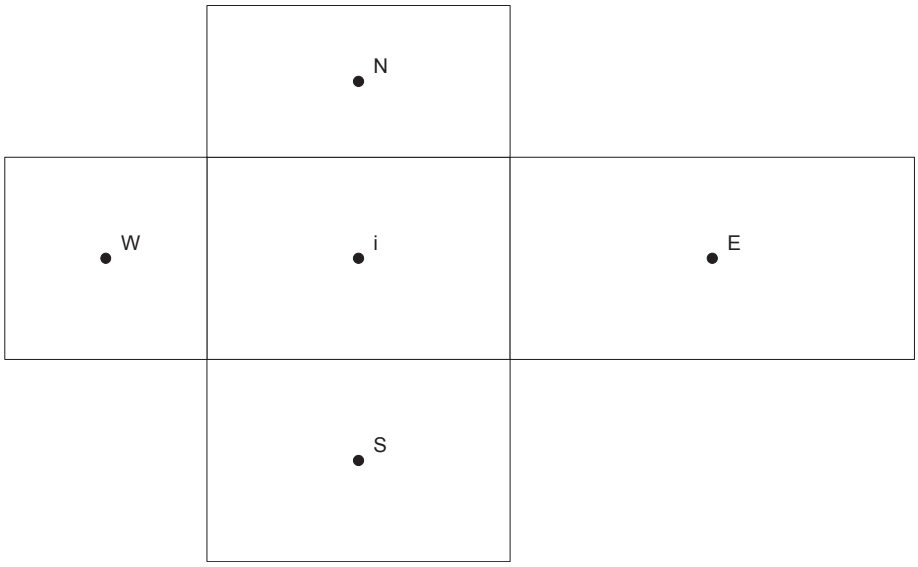

Figure 1.4: Cell i and the neighbor cells it share faces with.

$$\psi_E = \psi(x + \delta x^+) = \sum_{k=0}^{m} \frac{1}{k!} \left(\frac{d^k \psi}{dx^k} \right)_f (\delta x^+)^k + R^+ \tag{1.36}$$

where m is the order of the Taylor expansion and R^+ is the Lagrange remainder. Similar can ψ_i be computed

$$\psi_i = \psi(x - \delta x^-) = \sum_{k=0}^{m} \frac{1}{k!} \left(\frac{d^k \psi}{dx^k} \right)_f (-\delta x^-)^k + R^- \tag{1.37}$$

It can be assumed that $R^+ - (-1)^{m+1} R^- \approx 0$. Thus if a Taylor expansion of first order ($m = 1$) is chosen we get

$$\left(\frac{d\psi}{dx} \right)_f (\delta x^+ + \delta x^-) \approx \psi_E - \psi_i \tag{1.38}$$

If a higher order Taylor expansion is chosen we get

$$\left(\frac{d\psi}{dx} \right)_f (\delta x^+ + \delta x^-) \approx \psi_E - \psi_i - \epsilon_{Ei} \tag{1.39}$$

where the correction term can be calculated as

$$\epsilon_{Ei} \approx \sum_{k=2}^{m} \frac{1}{k!} \left(\frac{d^k \psi}{dx^k} \right)_f \left[(\delta x^+)^k - (-\delta x^-)^k \right] \tag{1.40}$$

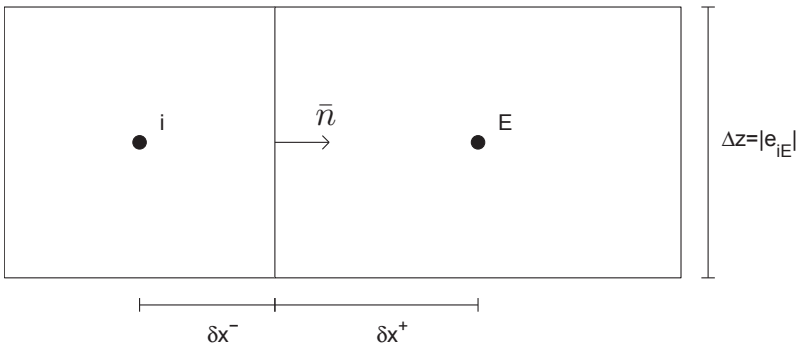

Figure 1.5: Distances used for calculation of flux between cell i and its "eastern" neighbor.

It can be seen that a second order precision is obtained with $m = 1$ and $\delta x^+ = \delta x^-$. $m = 1$ is chosen for the relative simple model for rectangular cells. The width and height of cell i are denoted $(\Delta x)_i$ and $(\Delta z)_i$ respectively, thus $\delta x^- = \frac{(\Delta x)_i}{2}$, $\delta x^+ = \frac{(\Delta x)_E}{2}$ and $|e_{iE}| = (\Delta z)_i = (\Delta z)_E$. The outwarded unit normal, $\vec{\mathbf{n}}_{iE} = [1\ 0]^T$. By applying equation (1.27), the diffusive transport through the cell eastern face is:

$$D_{iE}(\boldsymbol{\psi}) = (K_{xx})_{iE} \frac{2(\Delta z)_i}{(\Delta x)_E + (\Delta x)_i} (\phi_E - \phi_i) \tag{1.41}$$

The gravitational transport from cell i to cell E is:

$$G_{iE}(\boldsymbol{\psi}) = 0 \tag{1.42}$$

If the eastern cell face of cell i belongs to the boundary of Ω (no eastern neighbor), $B_{iE'}$ shall be calculated. If the cell face has a Neumann boundary condition we have

$$B^N_{iE'}(\boldsymbol{\psi}) = -q_{iE'}(\Delta z)_i \tag{1.43}$$

where $q_{iE'}$ is the magnitude of the flux transported out from through the cell face. If the cell face have a Dirichlet boundary condition:

$$D^D_{iE'}(\boldsymbol{\psi}) = (K_{xx})_i \frac{2(\Delta z)_i}{(\Delta x)_i} (\psi_{E'} - \psi_i) \tag{1.44}$$

where $\psi_{E'}$ is the value of ψ in the midpoint on the eastern cell face of cell i. The gravitational part gives:

$$G^D_{iE'}(\boldsymbol{\psi}) = 0 \tag{1.45}$$

1.3.4 Conductivity at cell faces

The conductivity at the cell faces between adjacent cells (as used in equations (1.27)) are in Daisy calculated by either the arithmetic, geometric or harmonic mean. For steady state flow speaks physical arguments for applying the harmonic mean:

$$\frac{1}{K_{ij}} = \frac{1}{2}\left[\frac{1}{K(\psi_i)} + \frac{1}{K(\psi_j)}\right] \tag{1.46}$$

Simulation have shown that using the harmonic average can have the effect that water practically not can be transported in some cases with sharp gradients in the pressure potentials which can occurs in situations with evaporation and layered soil. Of that reason is the arithmetic mean chosen as default:

$$K_{ij} = \frac{1}{2}\left[K(\psi_i) + K(\psi_j)\right] \tag{1.47}$$

1.3.5 Upper boundary condition

The upper boundary condition describes how much of the applied water and surface water that infiltrates into the soil. For instance if the rate of the applied water exceeds the amount of water that can infiltrate into the soil, (the infiltrability) water is stored on the surface.

In the start of each of the iterations, within the time step, the infiltrability is calculated using Darcy's law (based on the pressure at surface in the last time step and the pressure in the surface cell.) If the amount of available water (surface water + applied water in the current time step) exceeds the amount of water that can infiltrate into the soil as calculated with the infiltrability, a Dirichlet (pressure) boundary condition is applied. If the amount of water which can infiltrate into the soil, as calculated with the infiltrability exceeds the amount of available water then a Neumann (flux) boundary condition is applied. The upper boundary can at a given time consists of parts with Dirichlet and parts with Neumann condition.

Surface flow

In order to take care of the surface water in simulations with a rectangular soil domain, a very simple surface flow module is developed.

In Daisy2D the surface flow model is executed after each time step. In a later version more physical based model can be included, for instance a solver of the Saint-Venant equations (see for example Chow *et al.*, 1988). In the present *0D* model is the surface water distributed so the resulting water level is equal for the whole surface. The water over a predefined level (detention storage) is removed.

1.3.6 Aquitard boundary condition

As in the existing one-dimensional Daisy it is possible to simulate the existence of an aquitard below the lower boundary of the soil domain. The aquitard is described by a thickness, a hydraulic conductivity and the pressure potential in the aquifer just below the bottom of the aquitard.

In start of the iteration loop, inside each time step, the flow across the lower boundary is estimated using Darcy´s law where the pressure in the boundary cells and the properties of the aquitard are required. The aquitard is then implemented as a Neumann boundary condition.

1.3.7 Tile drains

It is possible to simulate a (user defined) number of tile drains. Tile drains removes water when the matrix pressure potential in the soil around the drain is positive. The actual pressure in a drain pipe depends on position in the drain system, the hydraulic radius, etc, etc. An often applied simplification codes for variably saturated flow is to regard the pressure in the drain pipe as atmospheric.

When the soil in the drain point is unsaturated ($\psi < 0$) the solution corresponds to the solution for an undrained soil. If the soil is saturated ($\psi > 0$) the drains removes water from the soil matrix hence $\psi = 0$.

In the numerical model, the drain pipe is described as a point. The drain points shall be placed in the interior of a cell and cannot be placed at cell edges.

For obtaining a numerical stable solution it is in the beginning of a new iteration in the time step tested if the mean value of the matrix pressure in the drain cell and its eastern and western neighbors (if they exists) exceeds 0. If the mean value is positive the pressure in the drain cell is forced to zero. After each time step a mass balance for each of the drain cells is made to calculate the amount of drained water.

Test simulations show that the code both is able to turn on the drain when the soil is getting wetter and turn of the drain when the soil is getting drier. Figure 1.6 shows the results from a simulation with an aquitard boundary condition and a drain. The upper boundary has a no flux condition, thus the only supply of water is through the aquitard. As it can be observed, the matrix pressure potential in the drain is 0.

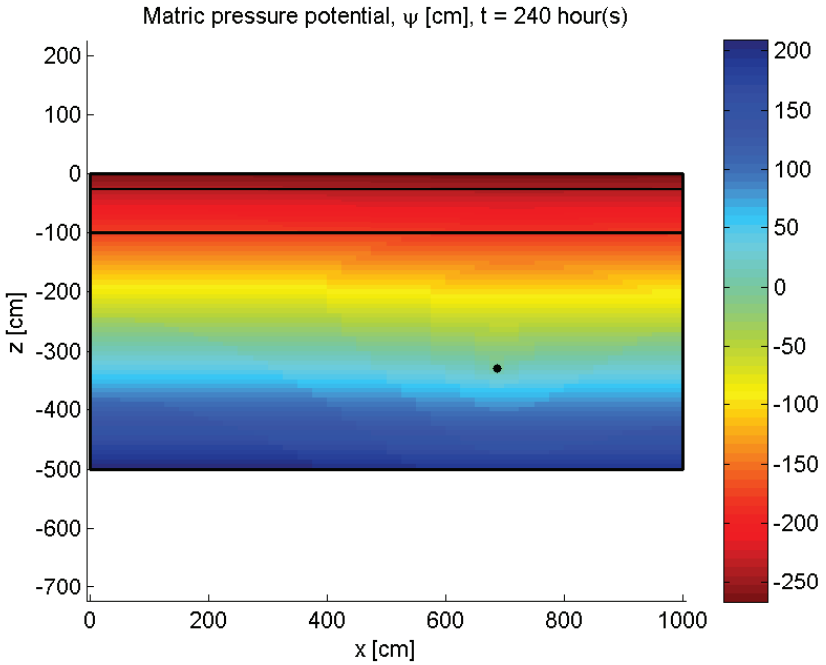

Figure 1.6: Matrix pressure potential in a drained soil. The drain is indicated with a dot. The lower boundary is formed by an aquitard condition.

1.3.8 Drip irrigation

1.3.9 Iteration scheme

Equation (1.26) describes how the matrix pressure potential in a given cell depends on the matrix pressure potential in the neighboring cells. By assembling equation (1.26) for $i = 1, 2 \cdots N$, the problem can be written as a ordinary differential equation (ODE) on the form:

$$\mathbf{Q}\frac{d\boldsymbol{\theta}}{dt} = \mathbf{E}(\boldsymbol{\psi})\boldsymbol{\psi} + \mathbf{F}(\boldsymbol{\psi}) \tag{1.48}$$

where $\mathbf{Q}$ is a diagonal matrix with $Q(i,i) = |Q_i|$ and $\theta_\mathrm{m} = \theta_\mathrm{m}(\psi)$. $\mathbf{E}(\boldsymbol{\psi})\boldsymbol{\psi}$ is the assembly of D_{ij} and $D^D_{ij'}$ and G_{ij}, $G^D_{ij'}$, $B^N_{ij'}$ and S_i are assembled in $\mathbf{F}(\boldsymbol{\psi})$. The equation is solved in the time domain using the backward Euler method:

$$\mathbf{Q}\frac{\boldsymbol{\theta}^{n+1,m+1} - \boldsymbol{\theta}^n}{\Delta t} = \mathbf{E}(\boldsymbol{\psi}^{n+1,m})\boldsymbol{\psi}^{n+1,m} + \mathbf{F}(\boldsymbol{\psi}^{n+1,m}) \tag{1.49}$$

In order to get rid of θ_m at iteration step $m+1$, the mixed formulation by Celia *et al.* (1990) is applied. In the mixed formulation, the water content at time step $n+1$ and iteration step $m+1$ is approximated by a Taylor expansion:

$$\begin{aligned} \theta_\mathrm{m}^{n+1,m+1} &= \theta_\mathrm{m}^{n+1,m} + \frac{d\theta_\mathrm{m}}{d\psi}\,|^{n+1,m}\,(\psi^{n+1,m+1} - \psi^{n+1,m}) \\ &= \theta_\mathrm{m}^{n+1,m} + C^{n+1,m}(\psi^{n+1,m+1} - \psi^{n+1,m}) \end{aligned} \tag{1.50}$$

where $C = \partial\theta_\mathrm{m}/\partial\psi$ is the specific water capacity function. The time derivative of θ_m can then be approximated as:

$$\begin{aligned} \frac{\partial\theta_\mathrm{m}}{\partial t} &\approx \frac{\theta_\mathrm{m}^{n+1,m+1} - \theta_\mathrm{m}^n}{\Delta t} = \frac{\theta_\mathrm{m}^{n+1,m+1} - \theta_\mathrm{m}^{n+1,m}}{\Delta t} + \frac{\theta_\mathrm{m}^{n+1,m} - \theta_\mathrm{m}^n}{\Delta t} \\ &\approx C^{n+1,m}\frac{\psi^{n+1,m+1} - \psi^{n+1,m}}{\Delta t} + \frac{\theta_\mathrm{m}^{n+1,m} - \theta_\mathrm{m}^n}{\Delta t} \end{aligned} \tag{1.51}$$

Thus, the iterative scheme is

$$\begin{aligned} &\left(\frac{1}{\Delta t}\mathbf{Q}\mathbf{C}(\boldsymbol{\psi}^{n+1,m}) - \mathbf{E}(\boldsymbol{\psi}^{n+1,m})\right)\boldsymbol{\psi}^{n+1,m+1} = \\ &\mathbf{F}(\boldsymbol{\psi}^{n+1,m}) + \frac{1}{\Delta t}\mathbf{Q}\mathbf{C}(\boldsymbol{\psi}^{n+1,m})\boldsymbol{\psi}^{n+1,m} + \frac{1}{\Delta t}\mathbf{Q}\left(\boldsymbol{\theta}^n - \boldsymbol{\theta}^{n+1,m}\right) \end{aligned} \tag{1.52}$$

where $\mathbf{C}$ is a diagonal matrix with $C(i,i) = C_i$.

In the MATLAB-prototype it is possible to choose simulations with a constantly or dynamically size of the time steps, Δt. For the last choice, the size of Δt depends on how difficult it is to obtain a solution. A procedure based on same principles is described in detail in Mollerup (2001). In Daisy2D the current Daisy method will be applied.

1.3.10 Matrix solution technique

In the prototype, for solving the large matrix system of the type $\mathbf{Ax} = \mathbf{b}$ (see equation (1.52)), the MATLAB backslash operator (also called leftdivision) is used. For description of the applied sparse matrix solver is refereed to Mollerup (2001).

1.3.11 Hydraulic properties

In the Daisy2D it shall be possible to choose between the existing models for the soil hydraulic properties in Daisy. In the prototype, the retention characteristics are described with the model by van Genuchten (1980):

$$\theta_{\mathrm{m}} = \begin{cases} \theta_r + \frac{\theta_s - \theta_r}{[1+|\alpha\psi|^n]^m} & \text{for } \psi < 0 \\ \theta_s & \text{for } \psi \geq 0 \end{cases} \tag{1.53}$$

where α, n and m are empirical parameters, θ_s and θ_r are the saturated and the residual water content, respectively. By combination with the hydraulic conductivity model by Mualem (1976) and choosing $m = 1 - 1/n$, the hydraulic conductivity can be calculated as

$$K = K_s S_e^{1/2}[1 - (1 - S_e^{1/m})^m]^2 \tag{1.54}$$

where K_s is the hydraulic conductivity at saturation and S_e is the effective saturation defined as

$$S_e = \frac{\theta_{\mathrm{m}} - \theta_r}{\theta_s - \theta_r} \tag{1.55}$$

The retention model by van Genuchten has been adapted to a large class of soils.

1.4 Verification

The FVM-code is verified by comparing solutions obtained by FVM with quasi-analytical solutions for one-dimensional infiltration by Philip.

1.4.1 Infiltration Model of Philip

Philip (1957b) showed that the infiltration depth as function of time and saturation can be written as a power series in $t^{\frac{1}{2}}$. The coefficients are then functions of soil water content, θ_{m}. From the expression for the infiltration depth, as function of water content and time, it is relatively easy to derive that the cumulative infiltration, also can be written as a power series in $t^{\frac{1}{2}}$. The assumptions for the theory, is a one-dimensional vertical flow into a homogenous soil semi-infinite soil column, initially with uniform water content. The cumulative infiltration is expressed as

$$I = \sum_{n=1}^{+\infty} A_n t^{\frac{n}{2}} \tag{1.56}$$

where $A_1 = S$ is the often refereed sorptivity as defined in Philip (1969). The coefficients are found by solving a set of successive integro-differential equations. One drawback of the power series theory is that the theory only describes the infiltration process well for short to intermediate times. The power series is "practical convergent" for $t < t_{\text{grav}}$. Where t_{grav} is the characteristic time of the infiltration process

$$t_{\text{grav}} = \left(\frac{S}{K_0 - K_i} \right)^2 \tag{1.57}$$

where $K_i = K(\theta_i)$ and $K_0 = K(\theta_0)$ is the hydraulic conductivity corresponding to the initial water content, θ_i and the water content at the soil surface, θ_0. For ponded conditions at the soil surface we have $K_0 = K_s$.

The soil parametrization, which is applied for the test simulations, is the G.E. silt loam (van Genuchten, 1980) where $K_s = 4.96$ cm/day, $\theta_s = 0.396$ cm^3/cm^3, $\theta_r = 0.131$ cm^3/cm^3, $\alpha = 0.00423$ cm^{-1} and $n = 2.06$.

A constant size of Δt= 1/60 day has been applied in the FVM test simulations. For all simulations the initial condition is h_i=-200 cm, corresponding to $\theta_i = 0.332$ cm^3/cm^3 is chosen.

Vertical falling-head infiltration

Initially, it was shown that the power series solution can be applied for non-saturated or just saturated conditions at the soil surface (see Philip, 1955, 1957b,a). Philip (1958) later expanded the theory to cover ponding situations with constant positive pressure at the soil surface. Later it was shown (Mollerup and Hansen, 2007) that the power series solution also can be applied for a falling-head condition, where the ponding depth is dependent on the amount of infiltrated water. The pressure at the soil surface is then

$$H = H_0 - I \tag{1.58}$$

where H_0=20 cm is the initial ponding depth.

In the FVM simulations, both the vertical and horizontal discretisation, $\Delta z = \Delta x$ is 1 cm. The lower boundary was placed at $z = 600$ cm with a free drainage (gravity flow) condition. For the scenario is t_{grav}=3.34 days and the time at which the pond empties, t_p =2.6022 days is computed by applying the iteration procedure as proposed in Mollerup and Hansen (2007). In FVM-simulation, the pond empties at approximately t =2.5833 days. I.e. t_p is approximately 0.7% higher for the power series solution than for the similar FVM results obtained with a rather rough discretization in time. Minor errors can be expected in the power series solution as only the first 4 terms are calculated. For constant-head simulation the first 6 terms are calculated. Philip (1957b) found that normally only first two or three terms are necessary for a for practical use sufficient correct solutions.

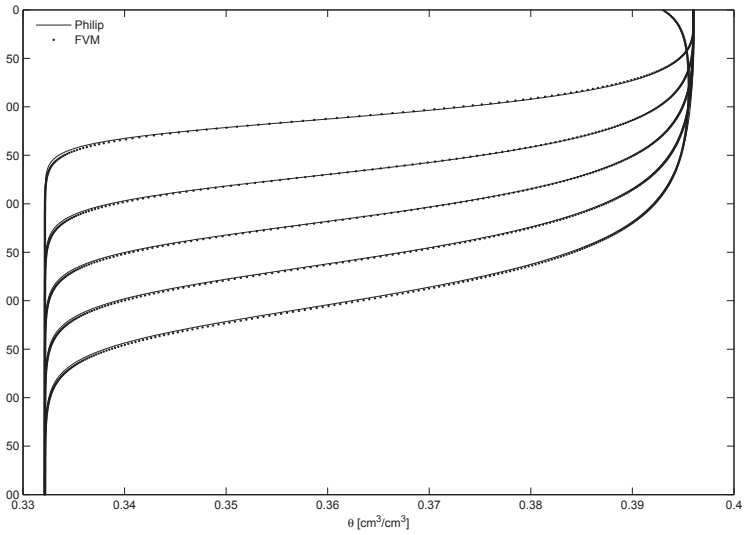

Figure 1.7: Analytical and FVM solution for vertical falling head infiltration. The solution is shown for $t = 1/5,\ 2/5,\ 3/5,\ 4/5$ and $1 \cdot t_{\mathrm{p}}$.

In figure 1.7, the wetting profiles as calculated by applying FVM and the power series theory are shown. The wetting profiles are shown for $t = 1/5,\ 2/5,\ 3/5,\ 4/5$ and $1 \cdot t_{\mathrm{p}}$. As it can be observed, the solutions are almost identical except for $t = t_{\mathrm{p}}$ (2.6022 days) where the effects of the slightly earlier emptying ponded water in the FVM simulation instantly effects the water content profiles.

Horizontal constant-head infiltration

For also insuring that horizontal flows are simulated correctly a simulation with a horizontal oriented column is made. For the FVM simulation, the column has height of 1 cell and a width of 800 cells with $\Delta x = \Delta z$ =1 cm. The left boundary condition is H =20 cm and the initial condition is h_n =-200 cm. Vertical constant-head infiltration can analytically be calculated as:

$$I = A_1 \sqrt{(t)} \tag{1.59}$$

where A_1 is identical to the A_1 calculated for vertical infiltration with constant-head (and falling-head) conditions. Contrary to vertical infiltration, equation (1.59) is applicable also for longer periods. Figure 1.8 shows the water content profiles at $t = 1/5,\ 2/5,\ 3/5,\ 4/5$ and $1 \cdot t_{\mathrm{grav}}$. as calculated with FVM and the power series theory. As it can be seen are the solutions almost identical.

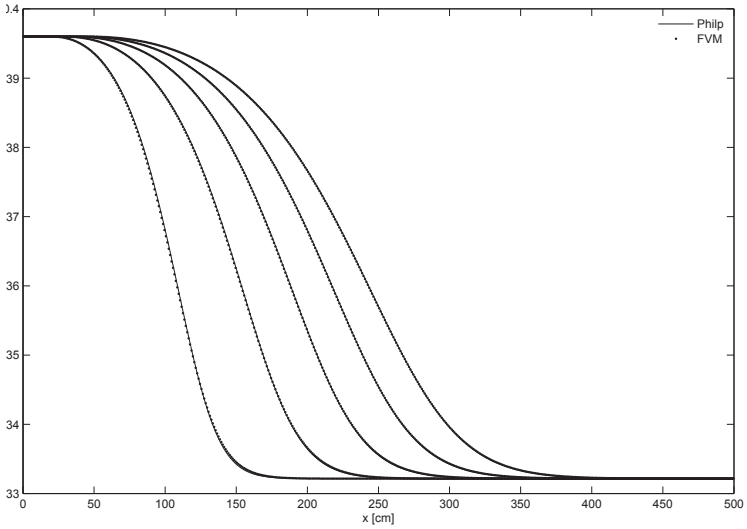

Figure 1.8: Analytical and FVM solution for horizontal infiltration. The solution is shown for $t = 1/5,\ 2/5,\ 3/5,\ 4/5$ and $1 \cdot t_{\text{grav}}$.

1.4.2 Vertical constant-head infiltration in a wide column

Until now all the verification simulations are made for a grid consisting of only 1 cell in the direction perpendicular to the flow direction. Also the size of the cells was equal. In the wide column experiment the cell height varies with the depth. The soil column consists of 3 horizons (A, B and C). The A-horizon is 25 cm depth with Δz =1 cm, the B-horizon is 75 cm depth with Δz =3 cm, and the C-horizon is 400 cm depth with Δz =8 cm. The soil column have a width of 200 cm with Δx =20 cm. Figure 1.9 shows the mesh and figure 1.10 shows a upper part of the mesh.

In the simulation is the ponding depth constantly $H = 20$ cm. Figure 1.11 shows the water content after 1 day. As it can be observed, the water do not vary with the x-coordinate for a given depth, i.e. there is no indication of unintended exchange of water between internal vertical cell boundaries. Also here (not shown) comparisons with a power series solution shown fine agreement

1.4.3 Other simulations

Also a simulation with a Neumann (flux) condition at the upper boundary and a simulation with a non-zero sink term have been conducted. The simulations showed mass-balances with negligible errors.

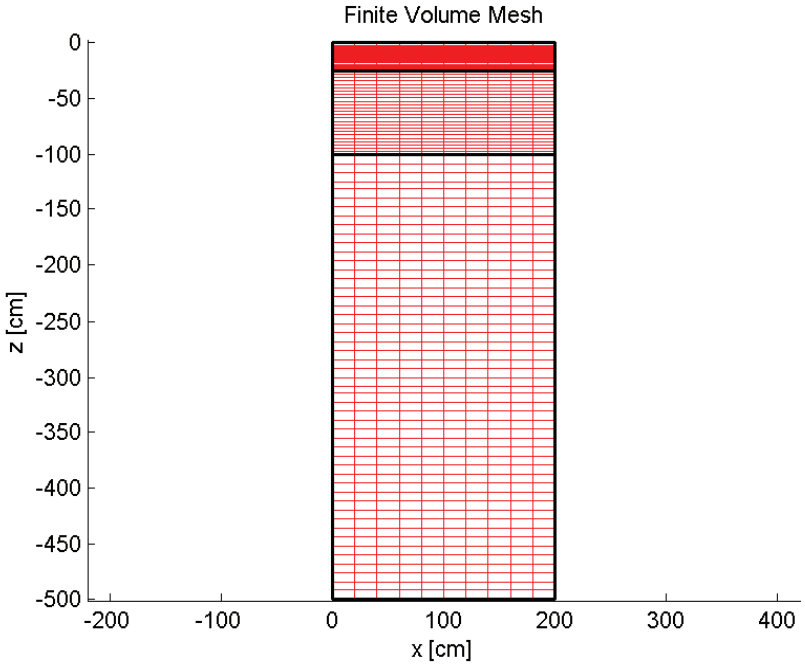

Figure 1.9: Mesh for the wide column simulation.

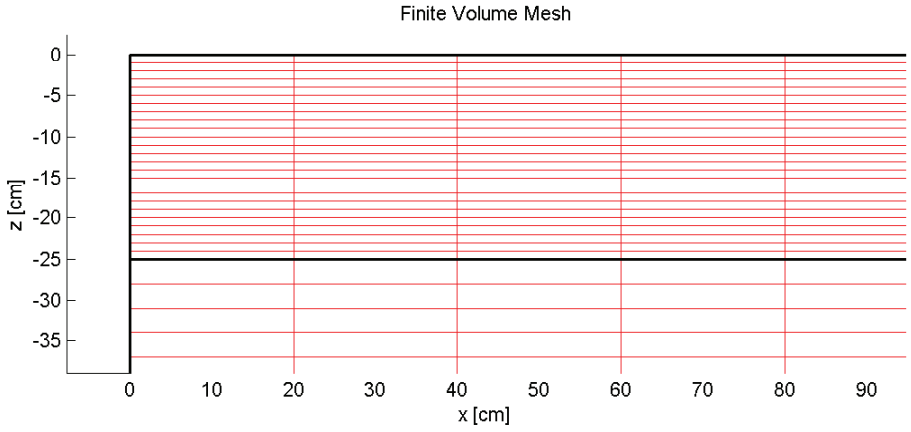

Figure 1.10: Upper left part of mesh used for the wide column simulation.

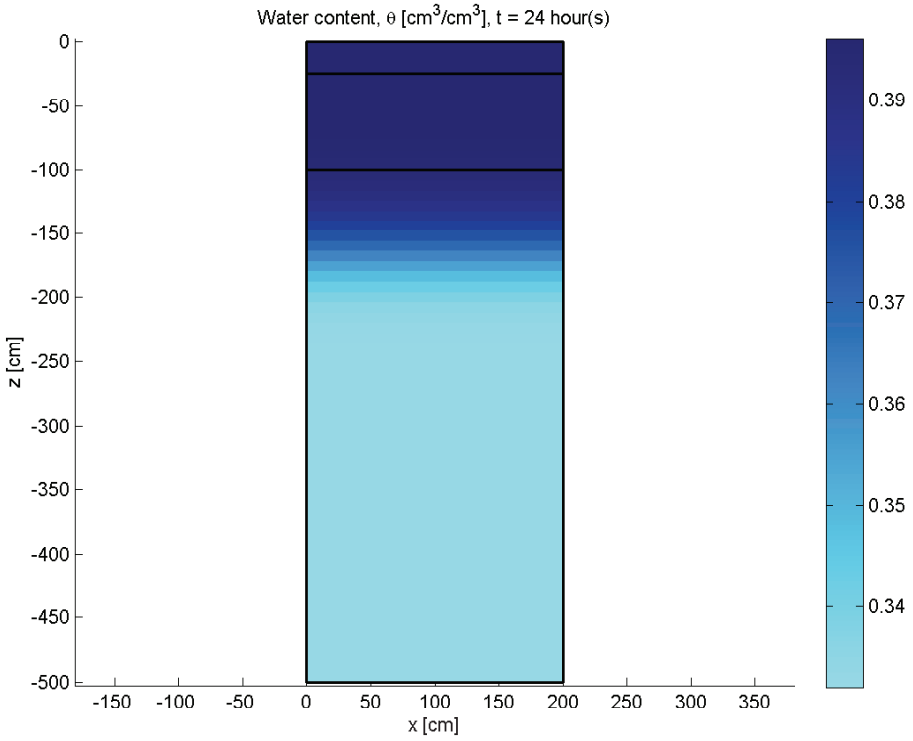

Figure 1.11: Water distribution after 1 day in the wide column simulation.

Chapter 2

Solute movement

2.1 2-domain matrix transport

For describing the solute movement, the soil matrix as solved by Richard' equation (equation (1.7)) the water is divided into two domains, a primary and a secondary domain:

$$\theta_{\mathrm{m}} = \theta_1 + \theta_2 \tag{2.1}$$

where θ_1 and θ_2 are the water content in the primary and the secondary domain, respectively. The primary part representing the flow in the smallest pores is always filled first. When the matrix water content, θ_{m} exceeds a certain limit, θ_{lim} the secondary domain start to be filled, i.e θ_{lim} is maximum value of θ_1. Thus, the primary part of θ_{m} can be expressed as

$$\theta_1 = \min(\theta_{\mathrm{m}}, \theta_{\mathrm{lim}}) \tag{2.2}$$

The secondary domain representing the flow in the largest pores is emptied first. The secondary part of θ_{m} can then expressed as

$$\theta_2 = \max(0, \theta_{\mathrm{m}} - \theta_{\mathrm{lim}}) \tag{2.3}$$

The fluxes as computed by Darcys equation are divided into two; a part representing the fluxes in the primary domain, $\mathbf{q}_1$ and a part representing the fluxes in the secondary domain, $\mathbf{q}_2$:

$$\mathbf{q}_{\mathrm{m}} = \mathbf{q}_1 + \mathbf{q}_2 \tag{2.4}$$

Similarly is the hydraulic conductivity matrix divided into a primary and a secondary part.

$$\mathbf{K}_{\mathrm{m}} = \mathbf{K}_1 + \mathbf{K}_2 \tag{2.5}$$

where $\mathbf{K}_1$ can be calculated

$$\mathbf{K}_1 = \mathbf{K}(\theta_1) \tag{2.6}$$

i.e. using the hydraulic conductivity function as used for the water movement computations, but with θ_1 instead of θ. Thus $\mathbf{K}_2$ can be calculated as:

$$\mathbf{K}_2 = \begin{cases} \mathbf{0} & \text{for } \theta_2 = 0 \\ \mathbf{K}(\theta_\mathrm{m}) - \mathbf{K}(\theta_\mathrm{lim}) & \text{for } \theta_2 \geq 0 \end{cases} \tag{2.7}$$

As a consequence of Darcy's equation can the fluxes $\mathbf{q}_1$ and $\mathbf{q}_2$ be calculated as

$$\mathbf{q}_1 = \frac{\|\mathbf{K}_1\|_2}{\|\mathbf{K}\|_2}\mathbf{q} \tag{2.8}$$

$$\mathbf{q}_2 = \frac{\|\mathbf{K}_2\|_2}{\|\mathbf{K}\|_2}\mathbf{q} \tag{2.9}$$

The associated Darcy velocity can be calculated as $\mathbf{v}_1 = \mathbf{q}_1/\theta_1$ and $\mathbf{v}_2 = \mathbf{q}_2/\theta_2$. It should be remarked that when there is water in the secondary domain is the associated velocity, $\mathbf{v}_2$ often considerably larger than $\mathbf{v}_1$.

The solute concentration is similarly divided into a part associated with the primary water, C_1 and a part associated with the secondary water, C_2. The exchange of solutes between the primary and the secondary domain is driven by the concentration differences. The transfer of solutes from the primary domain to the secondary domain can be regarded as a sink in the primary domain, $\Gamma_{\mathrm{s1}\to\mathrm{s2}}$ or a source in the secondary domain, $-\Gamma_{\mathrm{s2}\to\mathrm{s1}}$

$$\Gamma_{\mathrm{s1}\to\mathrm{s2}} = -\Gamma_{\mathrm{s2}\to\mathrm{s1}} = \begin{cases} \alpha_{1\to2}(C_1 - C_2) & \text{for } C_1 \geq C_2 \\ \alpha_{2\to1}(C_1 - C_2) & \text{for } C_1 < C_2 \end{cases} \tag{2.10}$$

The rates for moving solutes from C_1 to C_2, $\alpha_{1\to2}$ is not necessarily equal to the rate for moving solute from C_2 to C_1, $\alpha_{2\to1}$.

The mass balance for the solute can be expressed as:

$$\begin{aligned} \frac{\partial(\rho_b C_a)}{\partial t} + \frac{\partial(\theta_1 C_1)}{\partial t} + \frac{\partial(\theta_2 C_2)}{\partial t} + \frac{\partial(\theta_\mathrm{mp} C_\mathrm{mp})}{\partial t} \\ = -\nabla\cdot\mathbf{j}_1 - \nabla\cdot\mathbf{j}_2 - \nabla\cdot\mathbf{j}_\mathrm{mp} - \Gamma_\mathrm{s} \end{aligned} \tag{2.11}$$

where ρ_b is the soil bulk density and C_a is the concentration in the adsorbed phase. θ_mp is the volumetric water content in the macropore domain and C_mp is the concentration. $\mathbf{j}_1$, $\mathbf{j}_2$ and $\mathbf{j}_\mathrm{mp}$ are the fluxes in the the primary, secondary and macroporous domain. Γ_s is the net sink term of the solute.

2.2 Solute movement in the primary domain: Advection-dispersion equation

Three physical processes can contribute to movement of solutes in the primary part of the soil water:

- advection
- molecular diffusion
- hydrodynamic dispersion (only in connection with advection)

Advection (or bulk flow) is the process where the dissolved chemical moves with the soil solution. The flux of solute can be described as:

$$\mathbf{j}_1 = \mathbf{q}_1 C_1 \tag{2.12}$$

The Molecular diffusion is a result of the Brownian motion (random walk) of the molecules. A process related to the movement of the water is the hydrodynamic dispersion, which is a consequence of the fact that flow is not uniform, because the flow paths move around obstacles and air, but also because of variation in pore size and the non-uniform velocity distribution inside the pores. Mathematically the hydrodynamical dispersion process can be described as a diffusion process. The movement by diffusion like processes can be expressed as:

$$\mathbf{j}_1 = -\theta_1 \mathbf{D} \nabla C_1, \quad \mathbf{D} = \begin{bmatrix} D_{xx} & D_{xz} \\ D_{zx} & D_{zz} \end{bmatrix} \tag{2.13}$$

where $\mathbf{D}$ is the dispersion tensor (or matrix). The consequence is that the solute tries to move from areas with high concentration to areas with lower concentration. The elements in $\mathbf{D}$ are often calculated as:

$$\begin{aligned} D_{xx} &= \alpha_L \frac{v_{1,x}^2}{|\mathbf{v}_1|} + \alpha_T \frac{v_{1,z}^2}{|\mathbf{v}_1|} + D^* \\ D_{zz} &= \alpha_L \frac{v_{1,z}^2}{|\mathbf{v}_1|} + \alpha_T \frac{v_{1,x}^2}{|\mathbf{v}_1|} + D^* \\ D_{xz} &= D_{zx} = (\alpha_L - \alpha_T) \frac{v_{1,x} v_{1,z}}{|\mathbf{v}_1|} \end{aligned} \tag{2.14}$$

where D^* is the molecular diffusion. The rest of the terms are arising from the hydrodynamic dispersion. α_L is called the longitudinal dispersion and α_T the transversal dispersion. The calculation of the dispersion tensor is based on $\mathbf{v}_1$ and not $\mathbf{v} = \mathbf{q}/\theta$.

The molecular diffusion can be calculated as:

$$D^* = \tau D_0 \tag{2.15}$$

where D_0 is the diffusion coefficient for the solute in free water and τ is the tortuosity factor. As an example Millington and Quirk (1961) suggested:

$$\tau = \frac{\theta_1^{7/3}}{\theta_s} \tag{2.16}$$

Also here, the value is based on θ_1 and not the the total matrix water content θ_m. If we are using equation (2.16) and expressing the mean velocity in the

pores associated with solute movement by $\mathbf{q}_1$ and θ_1, the elements of $\theta_1\mathbf{D}$ can be expressed as:

$$\begin{aligned}\theta_1 D_{xx} &= \alpha_L \frac{q_{1,x}^2}{|\mathbf{q}_1|} + \alpha_T \frac{q_{1,z}^2}{|\mathbf{q}_1|} + D_0 \frac{\theta_1^{10/3}}{\theta_s} \\ \theta_1 D_{zz} &= \alpha_L \frac{q_{1,z}^2}{|\mathbf{q}_1|} + \alpha_T \frac{q_{1,x}^2}{|\mathbf{q}_1|} + D_0 \frac{\theta_1^{10/3}}{\theta_s} \\ \theta_1 D_{xz} &= \theta_1 D_{zx} = (\alpha_L - \alpha_T) \frac{q_{1,x} q_{1,z}}{|\mathbf{q}_1|}\end{aligned} \tag{2.17}$$

The solute movement can be expressed as a sum of the advection and the diffusion process:

$$\mathbf{j}_1 = \theta_1 C_1 \mathbf{v}_1 - \theta_1 \mathbf{D} \nabla C_1 = C_1 \mathbf{q}_1 - \theta_1 \mathbf{D} \nabla C_1 \tag{2.18}$$

The mass balance of dissolved solutes in the primary domain yields:

$$\frac{\partial(\theta_1 C_1)}{\partial t} = -\nabla \cdot \mathbf{j}_1 - \Gamma_{s1} \tag{2.19}$$

where Γ_{s1} is the sink term which remove solutes from the primary water domain. The removed (or added) solute can be absorbed, moved to the secondary domain (Γ_{s1} as expressed by equation (2.10) or the macropore domain or be subject to chemical or biological reduction.

The boundary conditions to the equation specifies a combination of C_1 and its derivative on the boundary. Also here, the *Dirichlet* boundary condition (specified concentration) and the *Neumann boundary condition*, where the flux through the boundary is specified, are common. The Dirichlet boundary condition is:

$$C_1 = C_{1,0} \tag{2.20}$$

where $C_{1,0}$ is the predescribed concentration. The Neumann boundary condition is:

$$\bar{\mathbf{n}} \cdot (C_1 \mathbf{q}_1 - \theta_1 \mathbf{D} \nabla C_1) = \bar{\mathbf{n}} \cdot \mathbf{j}_1 = j_1 \tag{2.21}$$

where j_1 is the size of the flux, positive for outward flux. As boundary condition for the ingoing flow $j_1 = \bar{\mathbf{n}} \cdot \mathbf{q}_1 C_{1,0} = q_1 C_{1,0}$ is often used where $C_{1,0}$ is the concentration of the flow. As lower boundary condition is $j_1 = \bar{\mathbf{n}} \cdot \mathbf{q}_1 C_1 = q_1 C_1$ often used. In both cases it is assumed that the diffusion crossing the border is zero.

Summarized, the problem to be solved for determination of the concentration of solute in Ω is:

$$\begin{cases} \theta_1 \frac{\partial C_1}{\partial t} + C_1 \frac{\partial \theta_1}{\partial t} = -\nabla \cdot (C_1 \mathbf{q}_1 - \theta_1 \mathbf{D} \nabla C_1) - \Gamma_{s1} & \text{in } \Omega \\ \bar{\mathbf{n}} \cdot (C_1 \mathbf{q}_1 - \theta_1 \mathbf{D} \nabla C_1) = j_1 & \text{on } \partial\Omega_1 \\ C_1 = C_{1,0} & \text{on } \partial\Omega_2 \end{cases} \tag{2.22}$$

where $\partial\Omega_1$ is the part of the boundary with Neumann condition, and $\partial\Omega_2$ is the part of the boundary with Dirichlet boundary conditions. Also here it is not necessary that $\partial\Omega_1$ and $\partial\Omega_2$, respectively, are coherent.

2.3 Numerical solution

The basic principles behind the finite volume modeling of the solute transport are very similar to the numerical solution of the water movement equation (Richards' equation). But there are some differences. One of the major differences is that the advection diffusion equation is considered as linear inside each timestep. I.e. the coefficients in the equation in each of the timesteps are independent of the concentrations in the current timestep. This simplification can be done when the size of the sources are dependent only on the concentrations in the previous timstep. Similar are adsorption added as sink/source term. Thus different from the water movement simulation, the Picard iterations loop used inside each timestep can be avoided.

2.3.1 Stabilization methods

There are often a lot of numerical problems involved with the solving of the convection diffusion problem especially when the problems are dominated by convection. The numerical solutions have often unexpected oscillations in that situation. There have been developed a lot of more or less complicated methods to reduce the problems. Three of the methods are *upstream weighting*, *streamline diffusion*, and *timestep reduction*.

Upstream weighting

When steep concentration fronts occur, numerical oscillations can raise. A method to stabilize the system is to apply upstream weighting for the advective solute movement. For advective transport between two cells is the concentration at the face between the cells normally calculated as the average concentration of the two cells. For fully upstream weighting is the concentration at the cell face equal to the upstream concentration.

In Daisy2D it is possible to set a parameter, $0 \leq \alpha \leq 1$ where $\alpha = 1$ corresponds to a fully upstream weighting and $\alpha = 0.5$ corresponds to setting the cell face concentration to the average concentration of the two cells. It is not recommended to apply an $\alpha < 0.5$.

$\mathbf{P_e}$ and $\mathbf{C_r}$ numbers

There are two different numbers which are important for the stability. The *Peclet number*:

$$\mathrm{P_e} = v_1 \Delta x / D \tag{2.23}$$

where v is the velocity, Δx is the space increment and D is the diffusion coefficient (including molecular diffusion and hydrodynamic dispersion). The *Courant number* is defined as:

$$\mathrm{C_r} = v_1 \Delta t / \Delta x \tag{2.24}$$

Theoretical stability investigations are rather complicated, especially in a two or three-dimensional space with heterogeneous soil. Most of the theoretical stability considerations are done for one-dimensional flow with uniform velocity. The classical constraints for stability for the standard Crank-Nicholson-Galerkin (Finite Element Method) is $\mathrm{P_e} \leq 2$ and $\mathrm{C_r} \leq 1$, Perrochet and Bérod (1993).

It can easily be concluded that keeping the Courant number lower than one is just a question of sufficiently small timesteps. But is it possible to make a mesh which under all circumstances prevents that the Peclet number raises over 2?. The Peclet number for the flow in the x-direction is:

$$\begin{aligned}(\mathrm{P_e})_x = \frac{q_{1,x}\Delta x}{\theta_1 D_{xx}} &= \frac{q_{1,x}\Delta x}{\alpha_L \frac{q_{1,x}q_{1,x}}{|\mathbf{q}|} + \alpha_T \frac{q_{1,z}q_{1,z}}{|\mathbf{q}|} + D_0 \frac{\theta_1^{10/3}}{\theta_s}} \\ &< \frac{q_{1,x}\Delta x}{\alpha_T \frac{q_{1,x}q_{1,x}+q_{1,z}q_{1,z}}{|\mathbf{q}_1|}} = \frac{q_{1,x}\Delta x}{\alpha_T |\mathbf{q}_1|} \leq \frac{\Delta x}{\alpha_T}\end{aligned} \tag{2.25}$$

where it is assumed that $\alpha_L \geq \alpha_T$. The same procedure can of course be used to evaluate $(\mathrm{P_e})_z$. It can then be concluded that the maximum Peclet number is lower than $\Delta x/\alpha_T$. If the longitudinal dispersivity is 5 cm and the transversal is 1/10 of the longitudinal and the maximum allowed $\mathrm{P_e}$ is 2 can it be concluded that the maximum side length of the elements shall be approximately 1 cm. This will result in a very fine mesh.

Besides the upstream weighting method it is possible to choose between 2 stabilizing methods:

1. Introducing extra diffusion in the streamline direction so $\mathrm{P_e C_r} \leq \gamma$. Where γ is the performance index.
2. Varying the size of Δt so $\mathrm{P_e C_r} \leq \gamma$.

It is of course also possible to deselect any stabilizing methods. The last stabilizing method is straight forward, but the first deserves its own subsection:

Streamline diffusion

For practical situation are there often stability so long $\mathrm{P_e C_r} \leq \gamma$ where $2 \leq \gamma \leq 10$ (Perrochet and Bérod, 1993) which under all circumstances is less restrictive than keeping both $\mathrm{P_e} \leq 2$ and $\mathrm{C_r} \leq 1$. γ is called the *performance index*.

In the streamline diffusion is according to Perrochet and Bérod (1993) added

some additional longitudinal dispersion to prevent that P_eC_r raises over the chosen performance index. The additional longitudinal dispersion, $\bar{\alpha}_L$ is calculated as:

$$\bar{\alpha}_L = \begin{cases} \frac{|\mathbf{v}_1|\Delta t}{\gamma} - \alpha_L - \frac{D^*}{|\mathbf{v}_1|}, & \text{for } \alpha_L + \frac{D^*}{|\mathbf{v}_1|} < \frac{|\mathbf{v}_1|\Delta t}{\gamma} \\ 0, & \text{for } \alpha_L + \frac{D^*}{|\mathbf{v}_1|} \geq \frac{|\mathbf{v}_1|\Delta t}{\gamma} \end{cases} \tag{2.26}$$

Stability tests

To investigate the stability of the numerical model is a simple system modeled. The situation here is a one-dimensional column, horizontal column with steady-state water flow with pore velocity v. There is no secondary water, θ_2 thus $v_1 = v$. The diffusion, D (both molecular diffusion and hydrodynamic dispersion) is given. For the present test is the solute non-adsorping. For a scenario with linear adsorping (constant retardation factor) the adsorption have a stabilizing effect, thus for linear adsorping solutes the model is expected to be more stable. The advection-dispersion equation in one dimension can be written as:

$$\frac{\partial C_1}{\partial t} = D\frac{\partial^2 C_1}{\partial x^2} - v\frac{\partial C_1}{\partial x} \tag{2.27}$$

where $v = q/\theta$. The initial condition is a zero concentration in the whole column:

$$C_1(x, 0) = 0 \tag{2.28}$$

At the left boundary is the solute flux constant.

$$\left(-D\frac{\partial C_1}{\partial x} + vC_1\right)\Big|_{x=0} = vC_{1,0} \tag{2.29}$$

The solution can then according to van Genuchten and Alves (1982) be written as:

$$\begin{aligned} C1(x,t) = &\frac{1}{2}C_{1,0}\,\mathrm{erfc}\left[\frac{x-vt}{2(Dt)^{1/2}}\right] + \left(\frac{v^2t}{\pi D}\right)\exp\left[-\frac{(x-vt)^2}{4Dt}\right] \\ &- \frac{1}{2}C_{1,0}(1 + \frac{vx}{D} + \frac{v^2t}{D})\exp(vx/D)\,\mathrm{erfc}\left[\frac{x+vt}{2(Dt)^{1/2}}\right] \end{aligned} \tag{2.30}$$

For the simulations is made a water flow situation with steady state flow with the chosen pore water velocity $v = 1$ cm/hour. $C_{1,0}$ is for the simplicity chosen to 1 and $D = 0.05$ cm^2/hour. For the Daisy simulations is the virtual soil column 10 cm wide and 1 cm high. On the domain is generated a regular mesh with 100 equally large elements, each with $\Delta x = 0.1$ cm. With Δt chosen to 1 hour are $C_r = 10$ and $P_e = 2$, i.e. $P_eC_r = 20$. The numerical parameter, ω is set to $1/2$, i.e. a Crank-Nicholson scheme.

In figure 2.1 is the analytical solution compared with numerical solutions with and without upstream weighting corresponding to $\alpha = 1$ and $\alpha = 0.5$, respectively. Streamline diffusion and timestep reduction has not been applied. As it

can be observed, are the wiggles significantly smaller when applying upstream weighting. The only drawback seems to be slightly more numerical diffusion compared with the numerical solution for $\alpha = 0.5$. In the following cases up-

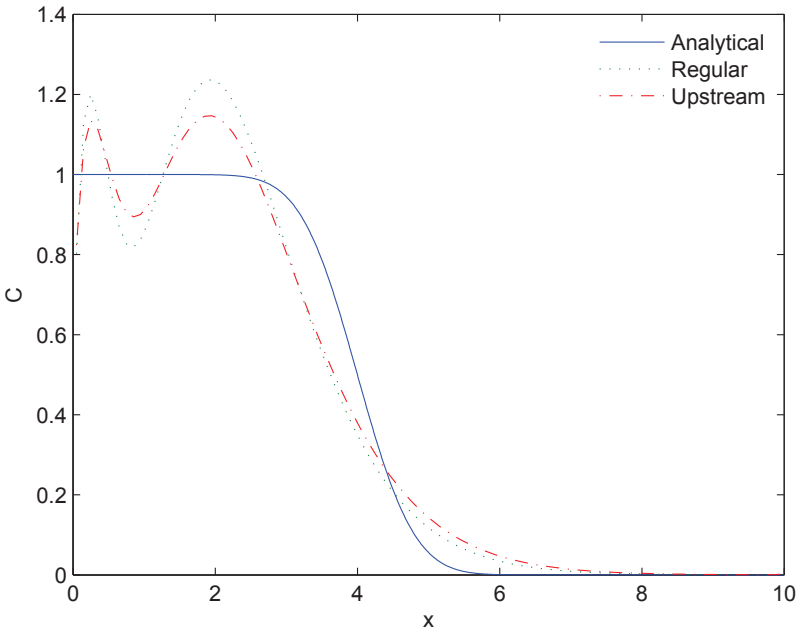

Figure 2.1: Analytical solution compared with numerical solution with regular weighting ($\alpha = 0.5$) and upstream weighting ($\alpha = 1.0$). The solutions are shown as concentration as function of x after simulation of 4 hours. For the actual case are $v = 1$ cm/hour, $D = 0.05$ cm^2/hour. For the numerical simulations are $\Delta t = 1$ hour and $\Delta x = 0.1$ cm, i.e. $\mathrm{P_e} = 2$ and $\mathrm{C_r} = 10$.

stream weighting has not been applied ($\alpha = 0.5$).

In figure 2.2 is the analytical solution shown. Besides is the numerical solution shown for the cases: no stabilization, timestep reduction and streamline diffusion. For both the timestep reduction and streamline diffusion method is the performance index, $\gamma = 10$ chosen. For the simulation without any stabilization are the wiggles significant. The wiggles are smaller for the simulation with streamline diffusion. By comparing with the analytical solution can the additional diffusion be observed. The additional diffusions effectively reduced the $\mathrm{P_e}$-number from 20 to 10. The remaining graph shows the simulation with the timestep reduction stabilizing method where the size of Δt is changed so $\mathrm{P_e C_r} \leq 10$. Here the size of the timestep is reduced from $\Delta t = 1$ hour (no stabilization) to 0.5 hour. Effectively the $\mathrm{C_r}$-number is reduced from 10 to 5,

i.e. for the computation is used 2 times so many timesteps (or approximately 2 times so long CPU-time). Compared with the numerical solution without stabilization are wiggles reduced, but have also smaller wavelength.

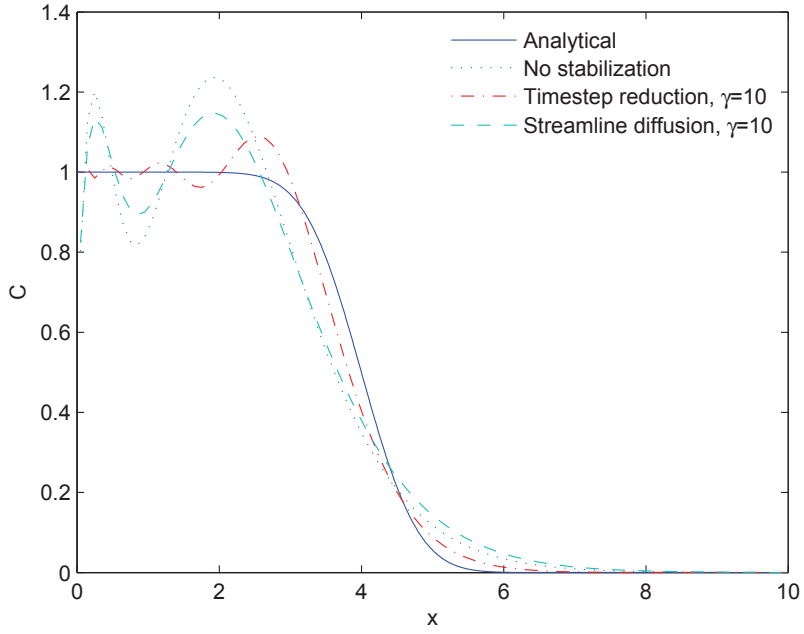

Figure 2.2: Analytical solution compared with different numerical solutions. The solutions are shown as concentration as function of x after simulation of 4 hours. For the numerical solution without stabilization are $P_e = 2$ and $C_r = 10$.

In figure 2.3 is the analytical and numerical solutions shown. The numerical solutions are computed using different performances indexes. The performance index, γ is changed applying timestep reduction. It can be observed that the wiggles are significant for $\gamma = 10$, but for $\gamma = 5$ (and lower) the size of the wiggles seems to be acceptable for most purposes.

In figure 2.4 is the analytical solution shown. Also the numerical solutions for varying performances indexes are shown. The performance index, γ is changed applying streamline diffusion. The wiggles are reduced when using a low value of γ, but compared with the analytical solution, the steepness of the front is reduced dramatically.

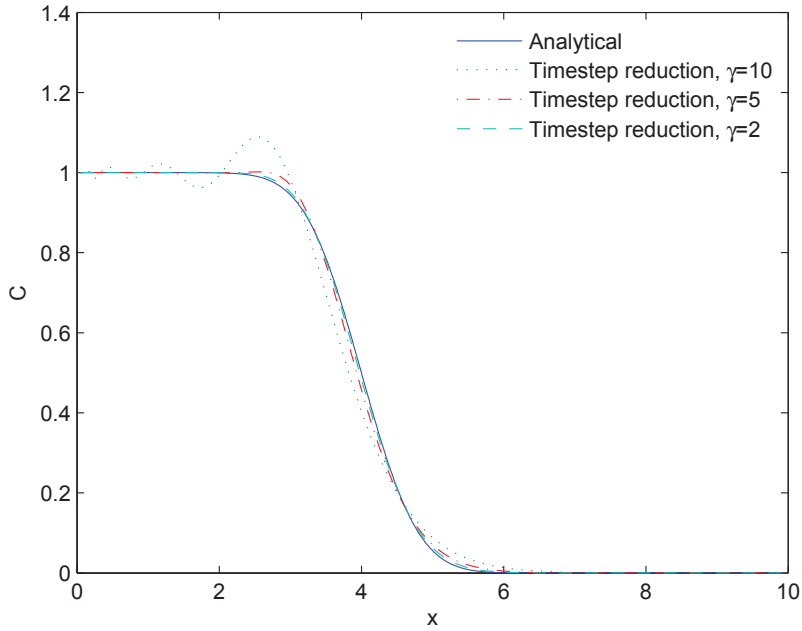

Figure 2.3: Analytical solution compared with different numerical solutions obtained using timestep reduction with varying performance index. For the simulation are $v = 1$ cm/hour and $D = 0.05$ cm^2/hour. For the numerical simulations is $\Delta x = 0.1$ cm and Δt is ranging from $1/10$ hour ($\gamma = 2$) to $1/2$ hour ($\gamma = 10$).

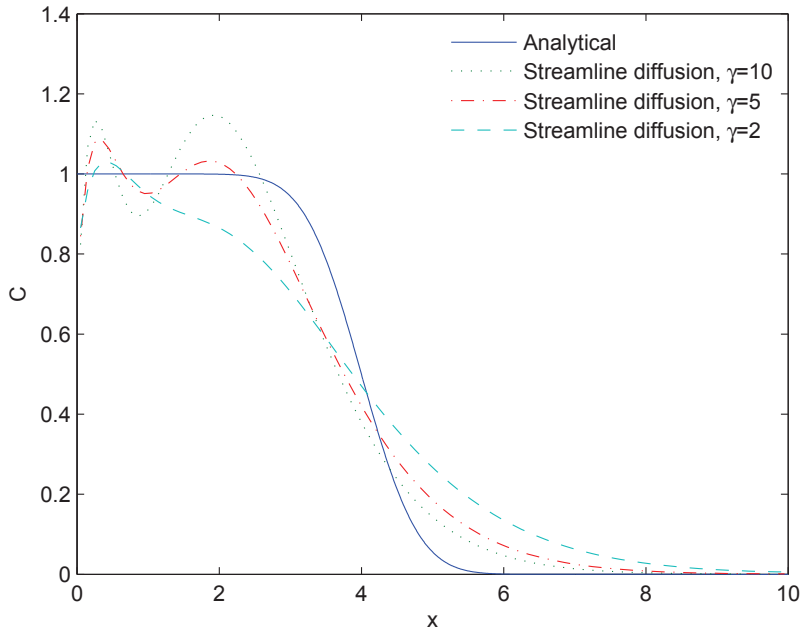

Figure 2.4: Analytical solution compared with numerical solutions obtained using streamline diffusion with varying performance index. For the analytical solution are $v = 1$ cm/hour and $D = 0.05$ cm^2/hour. For the numerical simulations are $\Delta x = 0.1$ cm and $\Delta t = 1$ hour.

2.3.2 Upper boundary condition

The upper boundary condition describes the movement of solute applied at the surface that moves into the soil. It also describes the movement of solutes out from the domain if the water is flowing out at the upper boundary.

If the soil surface not is ponded, the flux into the soil is moved by advection into the domain, with the water. If the surface is ponded with water containing a solute, the solute is also moved solely by advection. A little more accurate description could have been obtained if the boundary condition was implemented as a Dirichlet condition which also allowed the solute to be moved by dispersion and diffusion into the soil. It is assessed that the error is insignificant.

When the water moving out of the domain. No solute is following the water. This is for most solutes a good boundary condition - at least for evaporation processes. For a situation with liquid water is leaving the soil through the upper boundary the description is not appropriate, but at present Daisy is not intended for that kind of scenarios. Summarized the upper boundary condition can be expressed as:

$$\left(-\theta_1 D_{zz}\frac{\partial C_1}{\partial z} + q_z C_1\right)\Big|_{z=z_{\text{surf}}} = \begin{cases} q_{\text{out}} C_{\text{surf}}, & q_{\text{out}} < 0 \\ 0, & q_{\text{out}} > 0 \end{cases} \tag{2.31}$$

where z_{surf} is the z-coordinate of the soil surface, q_z is the flow (positive upwards) and q_{out} is the flux out of the domain (negative for flux into the domain). C_{surf} is the concentration of the surface water.

Numerically all the types of upper boundary conditions is implemented as explicit Neumann conditions, i.e. the solute movement over the boundary is independent of the solute concentrations in the domain.

2.3.3 Lower boundary condition

The lower boundary condition describes the movement of solute through the lower boundary. If the water has a free drainage condition, there is a flux condition for the solute when the solute is moved out of the domain by advection. If there is specified a groundwater table or aquitard boundary condition, i.e. pressure (Dirichlet) conditions for the water flow, also the solute movement have a Dirichlet condition with a specified concentration at the boundary. For a specified steady-state water flux (mostly used for testing purposes), it is possible both to chose specified concentration (Dirichlet) and flux boundary conditions.

Numerically the Neumann boundary conditions is implemented, either implicit or explicit - implicit when the water flux is outwarded from the lower boundary and the concentration associated with the flux is given by the concentration inside the domain - explicit when the water moves into the domain and the

associated concentration is the concentration outside the domain.

The Dirichlet boundary condition is implemented as an explicit Neumann boundary condition. Based on the solution in the previous timestep the flux is calculated with the given concentration on the boundary. The method is different from the method used for the water movement, but prevents an extra iteration loop inside each timestep with following increased computational times. In the water movement simulations, the iteration loop was under all circumstances necessary since the equation is non-linear. But with very large concentration gradients (and following large movement by diffusion and dispersion processes) and small cells at the boundary some numerically problems can occur. To prevent this kind of instability, the size of the timesteps can be lowered if also timestep reduction is chosen as stabilizing method to prevent to high P_eC_r-numbers. If timestep reduction is chosen, the timestep is reduced so:

- For diffusion into the cell, only half of the volume of the concentration difference between border and cell can be transported by diffusion over the boundary into the cell in a timestep.
- For diffusion out from the cell, only half of the volume of the concentration difference between cell and border can be transported by diffusion over the boundary out from the cell in a timestep.

To prevent to large computational times, the timestep can not be lower than a chosen a minimum value. If the instabilities are high and produce negative concentrations at the cells at the boundary, the computations in the timestep are repeated and the solute is only moved by advection over the boundary. This can happen if the minimum value of the size of the timesteps is chosen to high.

2.3.4 Verification: One-dimensional flow with retardation and degradation

There are developed a lot of analytical solutions for the one-dimensional convective-dispersive equation, see for example van Genuchten and Alves (1982). The equations are developed for situations where the diffusion is constant and the water flow is steady state (i.e. $\partial\theta_1/\partial t = 0$ and constant $\mathbf{q}$). The secondary water content, $\theta_2 = 0$ and all the adsorption processes are going through the primary water to the sorped phase. These conditions are seldom fulfilled in the 'real life' where both the water content and the flux are time-dependent. For testing the solute transport model is a situations with steady state water movement simulated.

If the adsorption process is very fast, the amount of adsorbed solute can be expressed with a adsorption isotherm which is a relationship between adsorbed (C_a) and dissolved concentration, C_1. The bulk density is assumed to be constant through time. The two first terms of the left hand side of equation (2.11)

can be rewritten as:

$$\rho_b \frac{\partial C_a}{\partial t} + \frac{\partial (C_1 \theta_1)}{\partial t} = \rho_b \frac{\partial C_a}{\partial C_1} \cdot \frac{\partial C_1}{\partial t} + \theta_1 \frac{\partial C_1}{\partial t} + C_1 \frac{\partial \theta_1}{\partial t} = \theta_1 R \frac{\partial C_1}{\partial t} + C_1 \frac{\partial \theta_1}{\partial t} \tag{2.32}$$

where R often in the literature is called the *Retardation factor*:

$$R = \frac{\rho_b}{\theta_1} \cdot \frac{\partial C_a}{\partial C_1} + 1 \tag{2.33}$$

The most simple adsorption isotherm is the linear adsorption where $C_a = K_d C_1$ and as a consequence $R = 1 + \frac{\rho_b K_d}{\theta_1}$.

Zero or first order kinetics are included in the model. In zero order kinetics, the velocity of the reaction is independent of the concentration and in 1.st order kinetics the reaction velocity is proportional to the concentration. Thus the advection dispersion equation yields:

$$R\theta_1 \frac{\partial C_1}{\partial t} + C_1 \frac{\partial \theta_1}{\partial t} = -\nabla \cdot (C_1 \mathbf{q}_1 - \theta_1 \mathbf{D} \nabla C_1) - \theta_1 \mu_l C_1 + \rho_b \mu_s \tag{2.34}$$

where the second last term represents a first order production in the liquid phase. μ_l is the rate constant. An often-used term is the half-life. In a batch experiment the half-life is the time required for the mass of reacting materiel to decrease to half the original mass. The reaction half-life can be calculated as $t_{1/2} = ln(2)/\mu_l$. The equation can be used for many chemical processes, and for radioactive decay. The last term on the right hand side of equation (2.34) represents a zero order removal from the solid to the liquid phase. μ_s is the rate constant for the zero order process. In van Genuchten and Alves (1982) is considered a one-dimensional case with degradation of both zero and first order. The governing differential equation can then be expressed as:

$$R \frac{\partial C_1}{\partial t} = D \frac{\partial^2 C_1}{\partial x^2} - v \frac{\partial C_1}{\partial x} - \mu C_1 + \gamma \tag{2.35}$$

where μ is the rate constant for first order decay in the liquid and γ represents the similar rate constant for zero-order production in the liquid phase. For the simulation, the initial condition is

$$C1(x, 0) = C_{1,\mathrm{i}} \tag{2.36}$$

and the upper boundary condition is

$$\left(-D \frac{\partial C_1}{\partial x} + v C_1 \right) \Big|_{x=0} = \begin{cases} v C_{1,0}, & 0 < t \leq t_0 \\ 0, & t > t_0 \end{cases} \tag{2.37}$$

The solution is

$$C_1 = \begin{cases} \frac{\gamma}{\mu} + (C_{1,\mathrm{i}} - \frac{\gamma}{\mu})A(x,t) + (C_{1,0} - \frac{\gamma}{\mu})B(x,t), 0 < t \leq t_0 \\ \frac{\gamma}{\mu} + (C_{1,\mathrm{i}} - \frac{\gamma}{\mu})A(x,t) + (C_{1,0} - \frac{\gamma}{\mu})B(x,t) - C_{1,0}B(x,t-t_0), t > t_0 \end{cases} \tag{2.38}$$

where $A(x,t)$ and $B(x,t)$ can be calculated as

$$\begin{aligned} A(x,t) = &\exp(-\mu t/R)\cdot \\ &\left\{1 - \frac{1}{2}\operatorname{erfc}\left[\frac{Rx - vt}{2(DRt)^{1/2}}\right] - \left(\frac{v^2 t}{\pi DR}\right)^{1/2} \exp\left[-\frac{(Rx-vt)^2}{4DRt}\right]\right. \\ &\left. + \frac{1}{2}\left(1 + \frac{vx}{D} + \frac{v^2 t}{DR}\right)\exp(vx/D)\operatorname{erfc}\left[\frac{Rx+vt}{2(DRt)^{1/2}}\right]\right\} \end{aligned} \tag{2.39}$$

$$\begin{aligned} B(x,t) = &\frac{v}{v+u}\exp\left[\frac{(v-u)x}{2D}\right]\operatorname{erfc}\left[\frac{Rx-ut}{2(DRt)^{1/2}}\right] + \\ &\frac{v}{v-u}\exp\left[\frac{(v+u)x}{2D}\right]\operatorname{erfc}\left[\frac{Rx+ut}{2(DRt)^{1/2}}\right] + \\ &\frac{v^2}{2\mu D}\exp\left[\frac{vx}{D} - \frac{\mu t}{R}\right]\operatorname{erfc}\left[\frac{Rx+vt}{2(DRt)^{1/2}}\right] \end{aligned} \tag{2.40}$$

with

$$u = v\sqrt{1 + \frac{4\mu D}{v^2}} \tag{2.41}$$

For comparing the analytical solution with the Daisy solution is chosen an situation with $v = 10$ cm/day, $D = 5$ cm^2/hour, $\gamma = 0.2$ hour $^{-1}$ and $\mu = 0.5$ hour $^{-1}$. For the simulation is Δx=1 cm. The length of the timesteps, Δt is 1/10 day. In figure 2.5 is the Daisy solution compared with the above described analytical solution. As it can be seen are the solutions in practise coincident.

2.4 Solute movement in the secondary domain: Advection

The heterogeneities are normally relatively small in the secondary domain. And when $\theta_2 \neq 0$ are the movement by advection relatively large compared to the movement by molecular diffusion. As a consequence is diffusion-like processes (diffusion and dispersion) in the secondary domain negligible. Thus the solute movement is modeled as a purely advection process:

$$\mathbf{j}_2 = \mathbf{q}_2 C_2 \tag{2.42}$$

The mass balance of dissolved solutes in the secondary domain yields:

$$\frac{\partial(\theta_2 C_2)}{\partial t} = -\nabla \cdot \mathbf{j}_2 - \Gamma_{\mathrm{s2}} \tag{2.43}$$

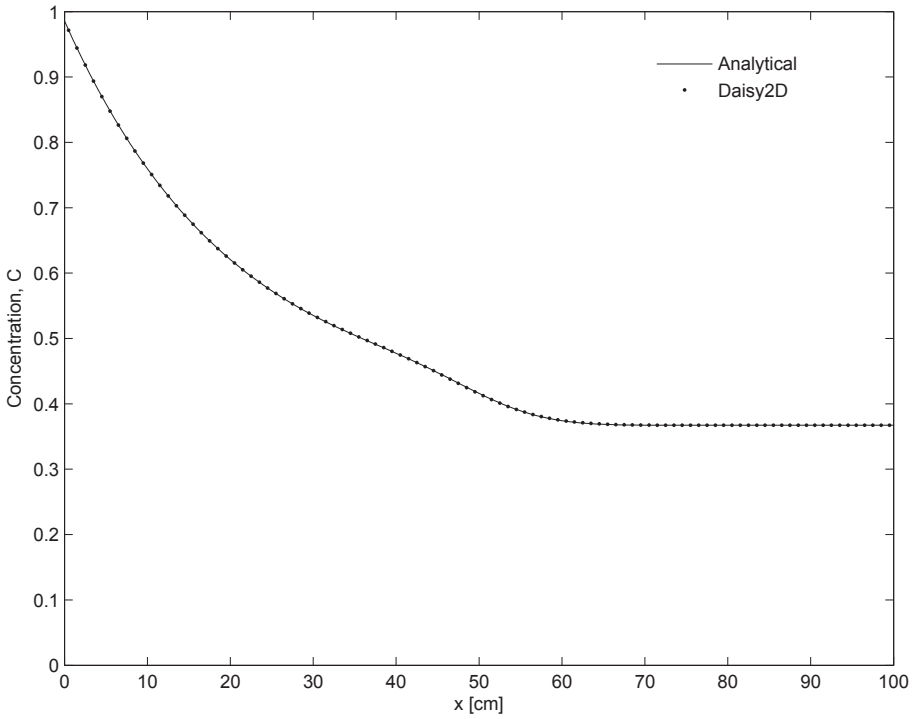

Figure 2.5: Comparison between analytical and Daisy simulation of a process with adsorption, zero order production and first order degradation.

where Γ_{s2} is the sink term which remove solutes from the secondary water domain. The removed (or added) solute can be absorbed, moved to the primary domain (Γ_{s1} as expressed by equation (2.10) or to the macropore domain or be subject to chemical or biological reduction.

Chapter 3

Heat transfer

3.1 Theory

Two physical processes can contribute to heat transfer movement in the matrix part (non macroporous part) of soil:

- conduction
- convection

Mathematical the transport can be expressed as:

$$\mathbf{q}_h = -K_H \nabla T + C_w \rho_w T \mathbf{q}_{\mathrm{m}} \tag{3.1}$$

where T is the temperature, K_H is the thermal conductivity, C_w the specific heat storage of water, ρ_w the density of water and $\mathbf{q}_{\mathrm{m}}$ is the water flux vector for matrix flux. Both K_H and C_w are calculated as in the existing 1D Daisy

The conservation of heat can be expressed as

$$\frac{\partial H}{\partial t} = -\nabla \cdot \mathbf{q}_h \ + S_h = \nabla \cdot (K_H \nabla T - C_w \rho_w T \mathbf{q}_{\mathrm{m}}) + S_h \tag{3.2}$$

where H is the heat content of the soil, t the time and S_h is a heat source. If water is added to the domain by drip irrigation with an amount of S_i the associated added heat is $C_w \rho_w S_i T_i$ where T_i is the temperature of the irrigation water which at the moment is the same as T, i.e. $T_i = T$. For water removed from the soil with a rate of S_w, the corresponding amount of heat is $C_w \rho_w S_w T$. In the model heat can also be added directly without exchanging water.

The left hand side of equation (3.2) can be written as

$$\frac{\partial H}{\partial t} = \frac{\partial (C_s T)}{\partial t} = C_s \frac{\partial T}{\partial t} + T \frac{\partial C_s}{\partial t} \tag{3.3}$$

where C_s is the specific heat capacity of the soil (including water).

The boundary conditions specifies a combination of the the temperature and its derivative on the boundaries. Actual in form of specified heat flux $K_H \nabla T - C_w \rho_w T \mathbf{q}_\mathrm{m}$ (*Neumann boundary condition*) or specified temperature T_0 (*Dirichlet boundary condition*). Summarized, the problem to be solved for determination of the temperatures in Ω is:

$$\begin{cases} C_s \frac{\partial T}{\partial t} + T \frac{\partial C_s}{\partial t} = \nabla \cdot (K_H \nabla T - C_w \rho_w T \mathbf{q}_\mathrm{m}) + S_h & \text{in } \Omega \\ \bar{\mathbf{n}} \cdot (C_w \rho_w T \mathbf{q}_\mathrm{m} - K_H \nabla T) = q_h & \text{on } \partial\Omega_1 \\ T = T_0 & \text{on } \partial\Omega_2 \end{cases} \tag{3.4}$$

where $\partial\Omega_1$ is the part of the boundary with Neumann condition, and $\partial\Omega_2$ is the part of the boundary with Dirichlet boundary conditions. Also here it is not necessary that $\partial\Omega_1$ and $\partial\Omega_2$, respectively, are coherent. $\bar{\mathbf{n}}$ is the outwarded unit normal to the boundary and q_h is the size of the heat movement out of the boundary.

3.2 Numerical solution of Heat transfer equation

The basic principles behind the finite volume modeling of the heat transfer is almost equal to the numerical solution of the equation for the solute movement (advection-dispersion equation).

But there are some differences. In Dasisy2D is made the assumption that the thermal conductivity is equal in all direction. This makes the implementation easier than the advection-dispersion equation where the hydrodynamic dispersion are dependent on the direction. Furthermore the heat movement by conduction is so dominant over the movement caused by convection that numerical instabilities under normal conditions not is expected. Thus different from the implementation of the advection-dispersion equation there is not implemented made any stabilizing methods, except for the boundary conditions (see later).

The partial differential equation (PDE) describing the heat transfer (see equation (3.4)) is considered linear inside each timestep where the values from the beginning of the timestep is used. For frost/thaw processes both the conductivity for heat and the heat capacity is temperature dependent. But the changes during a typical timestep very small. Following are the errors, considering the PDE linear for each timestep small. As a consequence of the quasi linearity are Picard iterations inside each timestep avoided.

3.2.1 Upper boundary conditions

The upper boundary condition describes the transfer of heat energy between the atmosphere and the soil.

In Daisy is the upper boundary condition of Dirichlet type, i.e the surface is forced to have a specific temperature. Except when snow is covering the surface the soil temperature is approximated with the air temperature. For snow covered surfaces are the soil temperature estimated as in the existing Daisy.

At first the upper boundary was implemented in a similar manner as used for the Dirichlet boundary conditions for solute movement. For the heat simulations, the temperature is with the method given exactly at the boundaries. But with the relatively large timesteps intended to be used in the heat simulations the method is sometimes unstable.

Instead a more simple and stable method is applied. In the implementation, the boundary temperature is set in the the nodal points in the upper boundary cells. Then the specified temperature is given a half cell lower than wanted. The tradeoff compared to the other method is small since the uncertainties in the heat simulations are under all circumstances large. And reducing the CPU-costs by using large timesteps when possible is important.

3.2.2 Lower boundary condition

The lower boundary condition describes the transfer of heat energy through the lower boundary. It is possible to choose between 2 boundary conditions: A flux conditions where no energy is transferred through the boundary or as in Daisy 1D a forced temperature with a annual oscillation.

The forced temperature is implemented in a similar manner as for the upper boundary condition. For a no fluxcondition nothing has to be done.

Bibliography

Celia, M. A., Bouloutas, E. T., and Zarba, R. L. (1990). A general mass-conservative numerical solution for the unsaturated flow equation. *Water Resour. Res.*, **26**(7), 1483–1496.

Chow, V. T., Maidment, D. R., and Mays, L. W. (1988). *Applied Hydrology*. McGraw-Hill.

Hillel, D. (1998). *Environmental Soil Physics*. Academic Press, London, UK.

Millington, R. J. and Quirk, J. P. (1961). Permeability of porous solids. *Trans. Faraday Soc.*, **57**, 1200–1207.

Mollerup, M. (2001). *Numerical Modelling of Water and Solute Movement in Tilled Topsoil*. Ph.D. thesis, The Royal Veterinary and Agricultural University, Tåstrup, Denmark.

Mollerup, M. and Hansen, S. (2007). Power series solution for falling-head ponded infiltration. *Water Resour. Res.*, **43**. W03425, doi:10.1029/2006WR004928.

Mualem, Y. (1976). A new model for predicting the hydraulic conductivity of unsaturated porous media. *Water Resour. Res.*, **12**(3), 513–522.

Perrochet, P. and Bérod, D. (1993). Stability of the standard Crank-Nicolson scheme applied to the diffuion-convection equation: some new insights. *Water Resources Research*, **29**(9), 3291–3297.

Philip, J. R. (1955). Numerical solution of equations of the diffusion type with diffusivity concentration-dependent. *Transaction of the Faraday Society*, **51**(7), 885–892.

Philip, J. R. (1957a). Numerical solution of equations of the diffusion type with diffusivity concentration-dependent. II. *Australian Journal of Physics*, **10**, 29–42.

Philip, J. R. (1957b). The theory of infiltration: 1. the infiltration equation and its solution. *Soil Sci.*, **83**, 345–357.

Philip, J. R. (1958). The theory of infiltration: 6. effect of water depth over soil. *Soil Sci.*, **85**, 278–286.

Philip, J. R. (1969). Theory of infiltration. *Advances in hydroscience*, pages 215–296.

van Genuchten, M. T. (1980). A closed-form equation for predicting the hydraulic conductivity of unsaturated soils. *Soil Sci.*, **44**.

van Genuchten, M. T. and Alves, W.-J. (1982). *Analytical Solutions of the one-dimensional convective-dispersive solute transport equation*. United States Department of Agriculture.

Annex 3.2 Daisy 2D code development

A major requirement for every programming project involving Daisy for the last 10 years has been that the added functionality of the project should me merged into the mainstream code. When individual project requirements conflicted, such as when they specified different models for the SAME process, both models would be implemented as a user selectable choice. When the program framework didn't allow this, the program framework would have to be modified to allow it. This approach is significantly more expensive to implement than to branch the mainstream code for each project. However, the advantage to the individual projects is even more significant, each project will benefit from improvements made in all the other projects.

The major requirement to Daisy in SAFIR is the 2D transport of water and solutes in the soil. This requirement goes against the existing framework in one major way, and also requires a generalisation in other areas. The main conflict was that Daisy was organised so the transport code was close to the turnover code. This has been changed to all transport functionality now are part of the SAME selectable "Movement" component. This component also contains the discretization, which has been generalized so the discretization framework now in theory can handle 1, 2 or 3 dimensions. Only 1D and a simple 2D discretization have been implemented so far. The old, 1D functionality of Daisy is available if the user chooses the "vertical" Movement model. A new 2D model named "rectangle" supporting a simple, rectangular grid of vertical and horizontal lines has been implemented as a proof-of-concept of the new framework.

A stand-alone prototype for coupled 2D transport has also been developed, and needs to be integrated in the new Daisy framework. Heat and solute transport has not yet been developed for anything but the old 1D solution, but they have been ported to the new framework so the "vertical" model now has functionality nearly identical to the old code.

Annex 3.3 The stomata-photosynthesis model and the sunlit-shadow radiation model in DAISY

Introduction

Photosynthesis is the conversion of CO_2 to organic compounds in the presence of light. The chloroplasts of a plant cell are the seat of photosynthesis and they are present only in the cells of the green parts of the plant. Photosynthesis can be conveniently treated as three separate components: 1) light reactions, in which radiant energy is absorbed and used to generate the high energy compounds ATP and NADPH; 2) dark reactions, which include the biochemical reduction of CO_2 to sugars using high energy compounds generated in the light reactions; and 3) supply of CO_2 from the ambient air to the site of reduction in the chloroplast.

Plants can be classified into at least three major groups on the basis of the biochemical pathway by which they fix CO_2, the C_3, C_4, and CAM. The latter will not be described in this context. The C_4 photosynthesis differs from C_3 in several biochemical and physiological properties and C_4 plants lack several features of C_3 plants that are associated to photorespiration. Both C_3 and C_4 plants use the enzyme ribulose biphosphate carboxylase (RuBP or Rubisco) for the primary fixation of CO_2; however, the Rubisco reaction is compartmented differently and.

The sun/shade radiation model in Daisy is inspired by the sun/shade model of de Pury and Farquhar (1997). The sun/shade model of de Pury and Farquhar (1997) is a single-layer model which describes the sun and shaded leaves separately. In the sun/shade model of de Pury and Farquhar (1997) the angel of incidence on leaves is not considered. Instead the partitioning between the sunlit and shaded fractions of the canopies is changed every time step. In Daisy, the canopy is divided in several layers with equal leaf area index. The cumulative absorbed irradiance (from the top of the canopy) in the sun/shade model is calculated for each canopy layer.

A number of mechanistic models of photosynthesis and stomatal conductance at the leaf level has been developed and widely used that derive from the C_3 photosynthesis model of Farquhar et al. (1980) and the empirical stomatal conductance model of Ball et al. (1987). Boegh et al. (1987) and Collatz et al. (1991) have implemented these two models combined with the leaf energy balances for both C_3 and C_4 plants. These interacting models are solved by a numerical method, the Newton Raphsons method. There are two models, based on the Farquhar-Ball-Collatz models, for C_3 and for C_4 plants implemented in the DAISY code, the FC-C3 and the FC-C4 model, respectively.

Absorbed irradiance of the canopies

Each plant community has a unique spatial pattern for displaying photosynthetic surfaces and to capture photosynthetic active radiation (PAR). The photosynthetic quantum flux, *I*, is often the major factor determining the rate of carbon dioxide (CO_2) assimilation of individual leaves. Only about 50% of global radiation is PAR.

eq. 1

$$I_{(Total,0)} = \omega \; c \; R_{total} \,,$$

c: Fraction of radiation which is PAR (0.5).
ω: Conversion factor to convert daylight from units W m^{-2} to mol m^{-2} s^{-1} (ε = 46 10^{-6} mol s^{-1} W^{-1} (McCree, 1981)).
R_{total}: Global radiation [W m^{-2}].
$I_{(Total,0)}$: Total PAR per unit ground area above the canopy (mol $m^{-2}s^{-1}$).

In the sun-shade model, irradiance absorbed by sunlit leaves is calculated as absorbed beam plus absorbed diffuse and scattered beam (total PAR). The irradiance absorbed by shaded leaves is calculated as absorbed diffuse and absorbed scattered beam. Diffuse and scattered radiations are assumed isotropic and beam radiation is unidirectional. If the global diffuse radiation is given in the climate input file, the diffuse PAR above the canopy, $I_{(d,0)}$, is given by:

eq. 2

$$I_{d,0} = \omega \; c \; R_d \,,$$

R_d: Global diffuse radiation [W m^{-2}].
$I_{(d,0)}$: Diffuse PAR per unit ground area above the canopy (mol $m^{-2}s^{-1}$).

and the photosynthetic quantum flux *I* for beam PAR above the canopy, $I_{(b,0)}$, is given by:

eq. 3

$$I_{b,0} = \left(R_{total} - R_d \right) c \; \omega \,,$$

Diffuse radiation model (DifRad)

If the global diffuse radiation is not given as an input driving variable, the diffuse radiation model (DifRad) in DAISY calculates the fraction of the total PAR that is diffuse PAR by the principles described de Pury and Farquhar (1997). It is furthermore assumed, that the fraction of the total PAR that is diffuse, equals the fraction of total global radiation that is diffuse. Direct beam PAR calculated from extra-terrestrial PAR is given by:

eq. 4

$$I_{b\_optimal} = \alpha^m R_{ex} \sin\beta \,,$$

$I_{b\_optimal}$: Beam PAR under a cloudless sky [W m^{-2}].
α: Atmospheric transmission coefficient of PAR (0,72)
m: Optical air mass [unit less].
R_{ex}: Extraterrestrial radiation [W m^{-2}].
β: solar elevation angle [radians].
where the optical air mass is given by:

eq. 5

$$m = \frac{P}{P_0 \sin\beta} \,,$$

P: Atmospheric pressure [Pa].
P_0: Atmospheric pressure at sea level (1.013 10^5 Pa).

The diffuse PAR under a cloudless sky is given by:

eq. 6

$$I_{d\_optimal} = f_a\left(1-\alpha^m\right)I_e \sin\beta,$$

$I_{d\_optimal}$: Diffuse PAR under a cloudless sky [W m^{-2}].
f_a: Forward scattering coefficient of PAR in atmosphere (0,426).

An expression for the fraction of diffuse radiation (f_d) of the total attenuated radiation for cloudless skies is then given by:

eq. 7

$$f_d = \frac{I_{d\_optiaml}}{I_{d\_optiaml} + I_{b\_optiaml}},$$

f_d: fraction of diffuse radiation under a cloudless sky [unit less].
$I_{d\_optimal}$: Diffuse PAR under a cloudless sky [W m^{-2}].

At nighttime the sinus function of the solar elevation angle, sin β, becomes negative and then it is assumed that all radiation is diffuse by setting f_d = 1.0. The global diffuse radiation is then given by eq. 8, which is used to calculated the diffuse and beam PAR according to:

eq. 8

$$R_d = f_d\ R_{\text{total}},$$

R_d: Global diffuse radiation [W m^{-2}].
R_{total}: Global radiation [W m^{-2}].

This model was originally developed for the decrease of short wave radiation. Short wave radiation has different scattering and absorption than PAR but, as assumed by de Pury and Farquhar (1997), it is assumed in the DifRad model that the process is similar for PAR.

Distribution of irradiance in the canopy

Absorption of *I* depends i.e. on leaf orientation, leaf arrangement in the canopy, sun elevation in the sky, changes in spectral distribution of *I* through the canopy, and multiple reflections of *I* within the canopy. To describe the penetration of diffuse, beam and scattered PAR in the canopy it is assumed that the decrease of *I* down into a canopy is analogous to absorption of light by chlorophyll or other pigments in a solution, which is described by Beer's law (Nobel, 1991).

The sunlit leaf area fraction (or the sun fleck penetration), $f_{sun,\,i}$, of canopy layer, *i*, is given by:

eq. 9

$$f_{(sun,i)} = \exp\left(-k_b L_i\right),$$

L_i: Cumulative leaf-area index from top of canopy to layer *i* (unit less, L = 0 for *i* = 0 (top), $L = L_c$ for *i* = *n* (bottom)).
k_b: Extinction coefficient of beam radiation (unit less).

The extinction coefficient of beam radiation is given by:

eq. 10

$$k_b = \begin{cases} \dfrac{0.5}{\sin\beta}, & \sin\beta > 0{,}0625 \\ 8.0, & \sin\beta \le 0{,}0625 \end{cases},$$

β: The solar elevation (radiance).

However, when the sinus function to the solar elevation is close to zero, k_b may reach unrealistic values. Therefore k_b has a maximum value when the sinus function returns zero, negative values, or larger the 0.0625 which corresponds to about 4°.

The penetration of sun fleck in the canopy at two different development stages is shown in Figure 1. Increasing leaf area index through the canopy layers decrease the penetration of sun fleck.

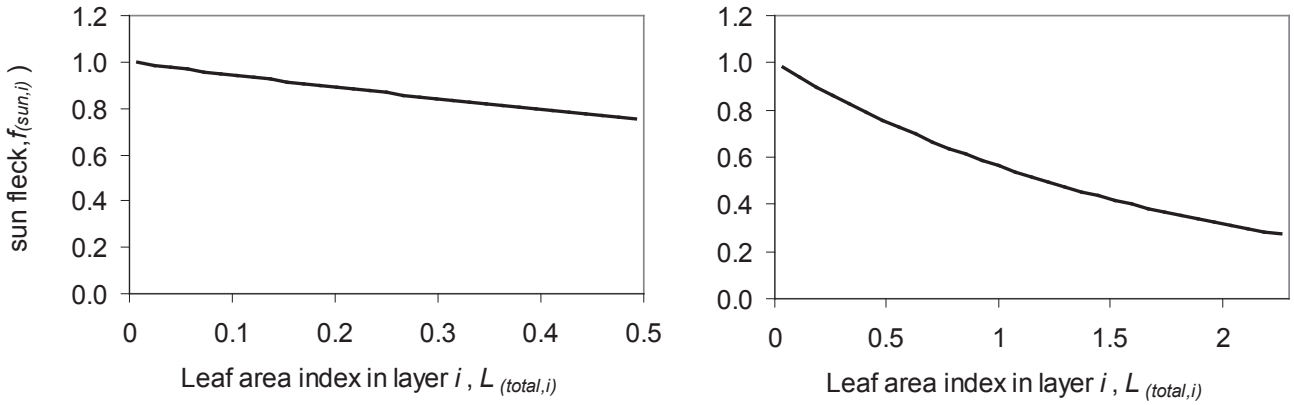

Figure 1. The sun fleck penetration in the canopy layers given by **eq. 9** and **eq. 10** (using sin β = 0.87) at two different leaf area index of the total canopy (L_c). Left: L_c = 0.5. Right: L_c = 2.3.

The sunlit leaf area index, $L_{(sun,i)}$, of canopy layer, i, is then given by:

eq. 11

$$L_{(sun,i)} = \left[\exp\left(-k_b L_{i-1}\right) - \exp\left(-k_b L_i\right)\right] / k_b,$$

L_i: Cumulative leaf-area index from top of canopy to layer i (unit less, L = 0 for i = 0 (top), $L = Lc$ for $i = n$ (bottom)).

While the shaded leaf area index, $L_{(sh,i)}$, in the canopy layer is:

eq. 12

$$L_{(sh,i)} = L_i - L_{(sun,i)},$$

$L_{(sun,i)}$: Cumulative leaf area index of sunlit fraction in canopy layer i (unit less).
$L_{(sh,i)}$: Cumulative leaf area index of shaded fraction in canopy layer i (unit less).

The cumulative sunlit and total leaf area indexes in the canopy layers, at two leaf area index of the canopy, are shown in Figure 2. In the early stage of crop development, where the total leaf area index is low (top, Figure 2) all the leaves in the canopy are sunlit. However, at later development stage, where the total leaf area index is increased the shaded fractions of the leaves increases (bottom, Figure 2).

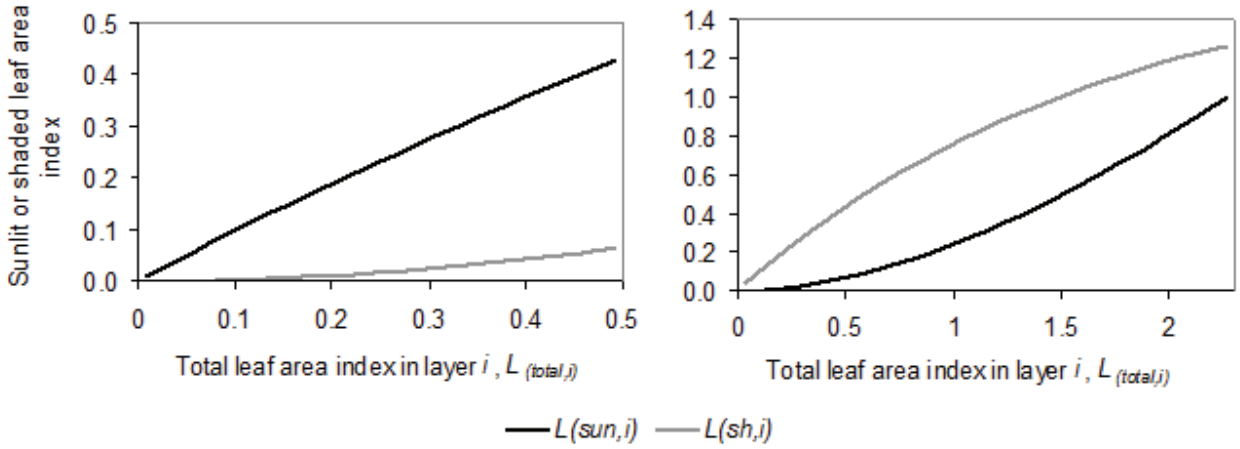

Figure 2. The cumulative sunlit leaf area index, $L_{(sun,i)}$ and shaded leaf area index, $L_{(sh,i)}$ as function of total leaf area index, $L_{(total,i)}$, through the canopy layers given by **eq. 11** and **eq. 12** at two different leaf area index of the total canopy (L_c). Left: $L_c = 0.5$. Richt: $L_c = 2.3$.

Sunlit leaves

Both sunlit leaves and shaded leaves absorb diffuse and scattered diffuse irradiance. The total absorbed irradiance is the sum of absorbed direct beam irradiance, the diffuse irradiance and the scattered beam irradiance for the sunlit fraction. The cumulative (from top of the canopy to the actual layer) direct absorbed beam (without scattering) irradiance, $I_{(b,i)}$, is given by:

eq. 13

$$I_{(b,i)} = I_{(b,0)}\left(1-\sigma\right)\left[1-\exp\left(-k_b L_i\right)\right],$$

σ: Leaf scattering coefficient of PAR (unitless, σ = 0,15 for wheat (de Pury & Farquhar, 1997)).
$I_{(b,0)}$: Beam quantum flux per unit ground area above the canopy (mol $m^{-2}s^{-1}$).
L: Cumulative leaf-area index from top of canopy (unit less, $L = 0$ when $i = 0$ (top), $L = L_c$ when $i = 30$).

The cumulative (from top of the canopy to the actual layer) quantum flux of scattered beam irradiance, $I_{(bs,i)}$, is given by:

eq. 14

$$I_{(bs,i)} = I_{(b,0)}\left[\left(1-\rho_{cb}\right)\left[1-\exp\left(-\left(k_b^{'}+k_b\right)L_i\right)\right]\frac{k_b^{'}}{k_b^{'}+k_b}-\left(1-\sigma\right)\frac{\left[1-\exp\left(-2k_b L_i\right)\right]}{2}\right]$$

$k_b^{'}$: Modified extinction coefficient of beam radiation due to scattering (unit less).
ρ_{cb}: Canopy reflection coefficient for diffuse PAR (ρ_{cb} = 0,029 (de Pury & Farquhar, 1997)).

The modified extinction coefficient of beam radiation due to scattering is affected by the leaf scattering.

eq. 15

$$k_b^{'} = k_b\sqrt{\left(1-\sigma\right)},$$

The cumulative (from top of the canopy to the actual layer) quantum flux of diffuse irradiance, $I_{(d,i)}$, is given by:

eq. 16

$$I_{(d,i)} = I_{(d,0)}\left(1-\rho_{cd}\right)\left[1-\exp\left(-\left(k_d^{'}+k_b\right)L_i\right)\right]\frac{k_d^{'}}{k_d^{'}+k_b},$$

$I_{(d,0)}$: Diffuse quantum flux per unit ground area above the canopy (mol $m^{-2}s^{-1}$).
k'_d: Extinction coefficient of diffuse and scattered PAR radiation (unit less, k'_d: = 0,719 (de Pury & Farquhar, 1997)).
ρ_{cd}: Canopy reflection coefficient for diffuse PAR (ρ_{cd} = 0,036 (de Pury & Farquhar, 1997)).
L_i: Cumulative leaf-area index from top of canopy to layer *i* (unit less, L = 0 for *i* = 0 (top), *L* = L_c for *i* = *n* (bottom)).

The cumulative (from top of the canopy to the actual layer) quantum flux of irradiance absorbed by sunlit leaves, $I_{(sun,i)}$, and that absorbed by shaded leaves, $I_{(sh,i)}$, are calculated separately by assuming that diffuse, scattered diffuse, and scattered beam irradiance reach all leaves.

For the sunlit leaves the total quantum flux in each canopy layer is calculated as the sum of eq. 13, eq. 14, and eq. 16:

eq. 17

$$I_{(sun,i)} = I_{(b,i)} + I_{(bs,i)} + I_{(d,i)},$$

$I_{(bs,i)}$: Scattered beam quantum flux per unit ground area in the canopy (mol $m^{-2}s^{-1}$).
$I_{(b,i)}$: Direct beam quantum flux per unit ground area in the canopy (mol $m^{-2}s^{-1}$).
$I_{(d,i)}$: Diffuse quantum flux per unit ground area in the canopy (mol $m^{-2}s^{-1}$).

The absorbed irradiances of the sunlit fractions in the canopy layers, at two different leaf area index of the canopy, L_c, are shown in Figure 3. It is seen that for the sunlit fraction of the leaves the most dominating type of irradiance which is absorbed is the direct beam fraction even at high leaf area index. However, the sunlit leaf area fraction decrease through the canopy layers which is not shown in Figure 3. The diffuse and scattered radiation remains relatively small through the canopy in this example. If the shaded fraction increases, as during cloudy conditions, then the diffuse and scattered radiation also increases.

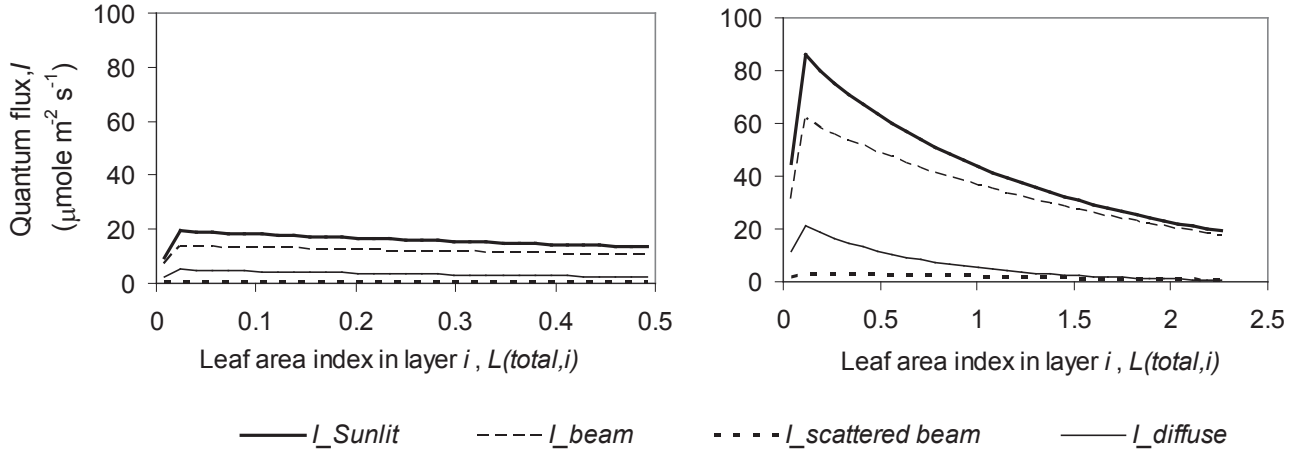

Figure 3. The absorbed quantum flux of the sunlit fractions, $I_{(sun,i)}$, as a function of the cumulative leaf area index, $L_{i)}$ in the canopy layers given by **eq. 13** - eq. **17** at two different leaf area index of the total canopy (L_c). Left: L_c = 0.5. Right: L_c = 2.3.

Shaded leaves

The irradiance absorbed by the shaded leaf area of the canopy is calculated as the difference between the total irradiance absorbed by the canopy, $I_{(total,i)}$, (eq. 18) and the irradiance absorbed by the sunlit leaf area, $I_{(sun,i)}$ (eq. 17). The total quantum flux absorbed by the canopy, $I_{(total,i)}$, is given by:

eq. 18

$$I_{(total,i)} = (1-\rho_{cb})\, I_{(b,0)} \left(1-\exp\left(-k_b' L_i\right)\right) + (1-\rho_{cd})\, I_{(d,0)} \left(1-\exp\left(-k_d' L_i\right)\right),$$

The quantum flux absorbed by the shaded leaf area, $I_{(sh,i)}$ is then given by:

eq. 19

$$I_{(sh,i)} = I_{(total,i)} - I_{(sun,i)},$$

The absorbed quantum flux of the total, sunlit and shaded parts are shown in Figure 4.

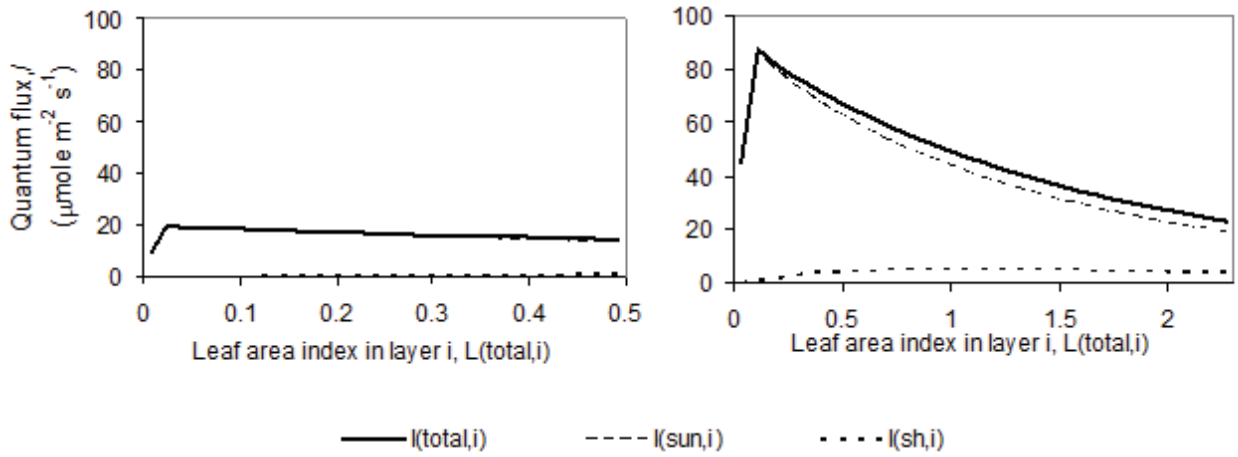

Figure 4. The actual quantum flux of absorbed irradiances (total, sunlit and shaded) as a function of the total leaf area index in each canopy layer, L_i, at two different leaf area index of the total canopy (L_c). Top: $L_c = 0.5$. Bottom: $L_c = 2.3$.

Photosynthesis and stomata conductance model

A number of mechanistic models of photosynthesis and stomata conductance at the leaf level has been developed and widely used (e.g. Boegh et al., 2002; Leuning, 1995; Collatz et al., 1991; Sellers et al., 1996) that derive from the C_3 photosynthesis model of Farquhar et al. (1980) and the empirical stomatal conductance model of Ball et al. (1987). These interacting models are solved by a numerical method, the Newton Raphsons method, described by Collatz et al. (1991).

The majority of plant uses the C_3 pathway including all the temperate cereals (wheat, barley, etc) root crops (e.g. potato and sugar beet), and leguminous species (beans, etc.). Another pathway, the C_4 pathway, is important in certain agricultural (and natural) systems. The C_4 pathway is important for agricultural crops like corn, sugar cane, and certain grasses for pasture as Sudan grass.

There are two Farquhar-Ball-Collatz models of photosynthesis for C_3 and for C_4 plants implemented in the DAISY code, the FC-C3 and the FC-C4 model, respectively.

Stomatal sub-model

Complex physiological mechanisms adjust the opening of stomata in response to changes in environmental conditions which affect the stomatal conductance of leaves and the canopy. The stomatal response to environmental and physiological factors is modeled according to the empirical model developed by Ball et

al. (1987). The model describes stomatal conductance, g_s, as linearly related to CO_2 assimilation rate, A, and relative humidity, h_s, and CO_2 partial pressure, ρ_s, at the leaf surface. To improve the description of stomatal behavior at low CO_2 concentrations, ρ_s is replaced with ρ_s minus the CO_2 compensation point, Γ^*, according to Leuning (1995). The stomatal conductance, g_s, for the sunlit or shaded fraction, f, and canopy layer, i, (noted as $_{(f,i)}$) is given by:

eq. 20

$$g_{s(f,i)} = \begin{cases} wsf\ m \dfrac{A_{(f,i)} P_{tot} h_{s(f,i)}}{\left(\rho_{s(f,i)} - \Gamma^*_{(f,i)}\right)} + b_{(f,i)} & A_{(f,i)} > 0 \\ \\ b_{(f,i)} & A_{(f,i)} \le 0 \end{cases},$$

wsf: Water stress factor (unit less, $wsf = 1$).
m: Empirical vegetation constant ($m = 9$ for wheat, m = 11 for soybean unitless).
$b_{(f,i)}$: Stomatal intercept factor, $b_{(f,i)} = b\ L_{(f,i)}$ ($b = 0.01$ mol m^{-2} s^{-1}).
$L_{(f,i)}$: Cumulative leaf area index (unit less).
h_s: The relative humidity at the leaf surface calculated by eq. 21 (unit less).
$\Gamma^*_{(f,i)}$: CO_2 compensation point of photosynthesis (Pa).
$A_{(f,i)}$: The net photosynthesis rate (mol m^{-2} s^{-1}).
$\rho_{s(f,i)}$: The leaf surface partial CO_2 pressure (Pa).
P_{tot}: The atmospheric pressure (100000 Pa).

The stomata conductance for the influx of CO_2 and the simultaneous efflux of water are directly linked to two vegetation-dependent coefficients (m, b). The two vegetation-dependent coefficients, m and b, have been parameterized by Wang and Leuning (1998) and Ball and Berry (1982) for wheat and soybean, respectively. The water stress factor, wsf, may be given as a function of ABA.

The stomatal model is merged with diffusion equations for water vapor flux through leaf boundary layer and stomata. The humidity at the leaf surface, h_s, is given, according to Collatz et al. (1991), by solving the following quadratic (eq. 21) by the second root:

eq. 21

$$\frac{w_{sf}\ mP_{tot}A_{(f,i)}}{\rho_{s(f,i)} - \Gamma^*_{(f,i)}}\ h_{s(f,i)}{}^2 + \left(b_{(f,i)} + g_{bw(f,i)} - \frac{w_{sf}\ mP_{tot}A_{(f,i)}}{\rho_{s(f,i)} - \Gamma^*} \right) h_{s(f,i)} + \left(\frac{-e_a}{e_{l\_sat}}\ g_{bw(f,i)} - b_{(f,i)} \right) = 0,$$

$g_{bw(f,i)}$: Leaf boundary-layer conductance of water (mol m^{-2} s^{-1}).
e_a: Actual vapor pressure in the air (Pa).
e_{l_sat}: Saturated vapor pressure at the leaf surface given by eq. 24 (Pa).

where the actual air vapor pressure, e_a, is given by:

eq. 22

$$e_a = h_a\ e_{a\_sat},$$

h_a: The relative humidity of the air (mol mol^{-1}).

The saturated vapor pressure, e_{sat}, at the leaf surface or in the air, is according to the code of Collatz et al. (1991):

eq. 23

$$e_{sat} = \exp\left(54.8781919 - \frac{6790.4985}{T_a + 273.15} - 5.02808 \ln\left(T_a + 273.15\right) \right),$$

T_a: Air temperature (°C).

The CO_2 partial pressure in the leaf interior, ρ_i, for C_3 and C_4 plants, are given by Collatz et al. (1991) and Collatz et al. (1992), respectively:

eq. 24

$$\rho i_{(f,i)} = \rho_a - P_{tot}\ A_{(f,i)} \frac{1.6 g_{b(f,i)} + 1.4 g_{s(f,i)}}{g_{s(f,i)} g_{b(f,i)}}, \qquad \text{for } C_3$$

$$\rho_{i(f,i)} = \rho_a\ - P_{tot}\ A_{(f,i)} \frac{1.6}{g_{s(f,i)}}, \qquad \text{for } C_4$$

$\rho_{i(f,i)}$: CO_2 partial pressure in leaf interior (Pa).
$A_{(f,i)}$: Net rate of photosynthesis (mol m^{-2} s^{-1}).
$g_{s(f,i)}$: Stomatal conductance of leaves given by eq. 20 (mol m^{-2} s^{-1}).
$g_{b(f,i)}$: Leaf boundary-layer conductance (mol m^{-2} s^{-1}).
ρ_a: The air partial CO_2 pressure (35 Pa).

Photosynthesis of C_3 leaves

Leaf assimilation (or gross photosynthetic) rate of C_3 leaves is described as the minimum of two limiting rates, w_c and w_e, which are functions that describe the assimilation rates as limited by the efficiency of the photosynthetic Rubisco capacity, w_c, the amount of PAR absorbed, w_e. Thus, the net leaf photosynthetic rate, A, is given by:

eq. 25

$$A_{(f,i)} = \min\left\{ w_{c(f,i)} \ ; w_{e(f,i)} \right\} - R_{(f,i)},$$

$A_{(f,i)}$: Net photosynthesis (mol m^{-2} s^{-1}).
$R_{(f,i)}$: Leaf respiration (mol m^{-2} s^{-1}) given by eq. 34.
$w_{c(f,i)}$: Rubisco limited rate of assimilation (mol m^{-2} s^{-1}).
$w_{e(f,i)}$: Light limited rate of assimilation (mol m^{-2} s^{-1}).

The transition from one limitation to another appears to be somewhat gradual in reality, it is more correct to estimate A by solving the following quadratic (eq. 26) by the first root (Collatz et al., 1991):

eq. 26

$$\beta A_{(f,i)}^{\ 2} - \left(w_{c(f,i)} + w_{e(f,i)}\right) A_{(f,i)} + w_{c(f,i)} w_{e(f,i)} = 0\,,$$

β: Empirical curvature constant (0.95).

β is an empirical constants that describing the transition between limitations, and are typical close to one (Collatz et al., 1991). Solving eq. 26, the net photosynthetic rate is given by:

eq. 27

$$A_{(f,i)} = \frac{\left(w_{c(f,i)} + w_{e(f,i)}\right) - \sqrt{\left(w_{c(f,i)} + w_{e(f,i)}\right)^2 - 4\beta w_{e(f,i)}\, w_{c(f,i)}}}{2\beta} - R_{(f,i)}\,,$$

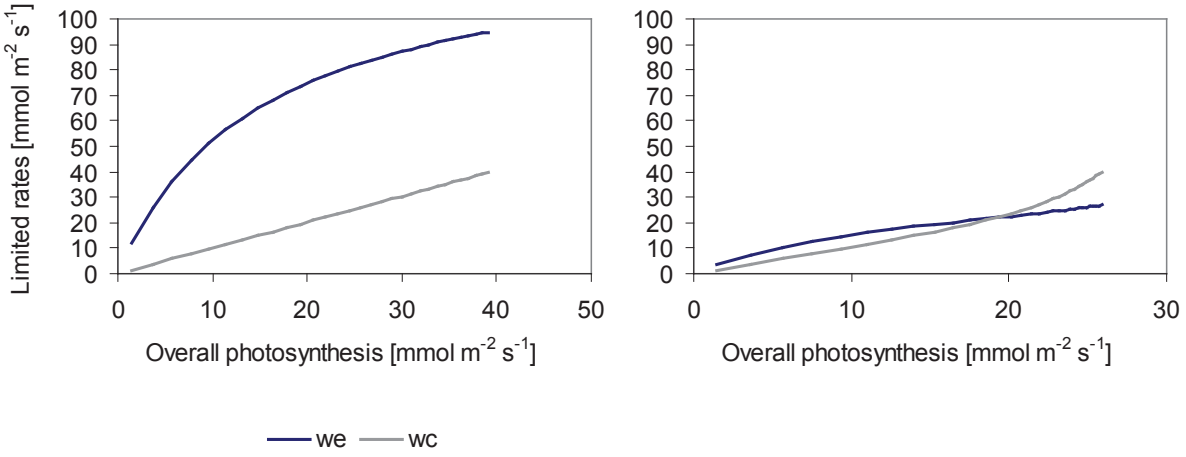

Figure 5. Relation between the light limited rate, w_e, and the Rubisco limited rate, w_c, as a function of the overall photosynthesis (A+R) with the parameter settings: T_a = 25 °C, ρ_i = 25 Pa, and V_{max25} = 90 µmol m^{-2} s^{-1}. Left: $I_{total,i}$ = 1500 µmol m^{-2} s^{-1}, Right: $I_{total,i}$ = 400 µmol m^{-2} s^{-1}.

Figure 5 shows the relation between the light limited rate, w_e, and the Rubisco limited rate, w_c, as a function of the overall photosynthesis. When the quantum light flux is high, w_c limits the photosynthesis (Fig. 5 left). On the contrary, when the quantum light flux is low, w_e limits the photosynthesis (Fig. 5 right). The assimilation rate limited by the efficiency of the photosynthetic Rubisco capacity, w_c, is given by:

eq. 28

$$w_{c(f,i)} = V_{m(f,i)} \frac{\rho_{i(f,i)} - \Gamma^*}{\rho_{i(f,i)} + K_{cl}}\,,$$

$V_{m(f,i)}$: Photosynthetic Rubisco capacity (mol m^{-2} s^{-1}).
$\rho_{i(f,i)}$: CO_2 partial pressure in leaf interior (Pa).
Γ^*: CO_2 compensation point of photosynthesis (3.69 Pa at 25 °C (de Pury and Farquhar, 1997)).

where the parameter K_{cl} is given by:

eq. 29

$$K_{cl} = K_c\left(1+\frac{O_2}{K_o}\right),$$

K_c: Michaelis-Menten constant of Rubisco for CO_2 (40.4 Pa at 25 °C (de Pury and Farquhar, 1997)).
K_o: Michaelis-Menten constant of Rubisco for O_2 (24800 Pa at 25 °C (de Pury and Farquhar, 1997)).
O_2: O_2 partial pressure in leaf interior (20.5 10^3 Pa (de Pury and Farquhar, 1997)).

and V_m is the maximum catalytic capacity of Rubisco per unit leaf area (Farquhar et al., 1980).

The light limited rate of photosynthesis, w_e, is given by:

eq. 30

$$w_{e(f,i)} = J_{(f,i)}\frac{\rho_{i(f,i)}-\Gamma^*_{(f,i)}}{\left(\rho_{i(f,i)}+2\Gamma^*_{(f,i)}\right)},$$

$J_{(f,i)}$: Rate of electron transport (mol m^{-2} s^{-1}).

The rate of electron transport, J, depends on the absorbed irradiance, I_{le}, and an empirical constant, θ. The constant θ describes the non-linear curvature of leaf electron transport responds to irradiance (Farquhar et al., 1980). The rate of electron transport J is estimated by solving the following quadratic (eq. 31) by the small root:

eq. 31

$$\theta J_{(f,i)}{}^2 - \left(I_{le(f,i)}+J_{m(f,i)}\right)J_{(f,i)} + I_{le(f,i)}J_{m(f,i)} = 0,$$

$I_{le(f,i)}$: PAR effectively absorbed (mol m^{-2} s^{-1}).
$J_{(f,i)}$: Rate of electron transport (mol m^{-2} s^{-1}).
$J_{m(f,i)}$: Potential rate of electron transport (mol m^{-2} s^{-1}).
θ: Empirical constant, curvature of leaf responds to irradiance (0.7 (de Pury and Farquhar, 1997)).

where the potential rate of electron transport, J_m, is given by:

eq. 32

$$J_{m(f,i)} = 2.1\ V_{m(f,i)},$$

The photosynthetic active radiation (PAR) effectively absorbed by the leaf, I_{le}, is given by Collatz et al. (1991):

eq. 33

$$I_{le(f,i)} = I_{(f,i)}\alpha,$$

α: Fraction of PAR effectively absorbed (unit less, 0.08 (Collatz et al., 1991)).
$I_{(f,i)}$: Absorbed irradiance given by eq. 17 and eq. 19 (mol m^{-2} s^{-1}).

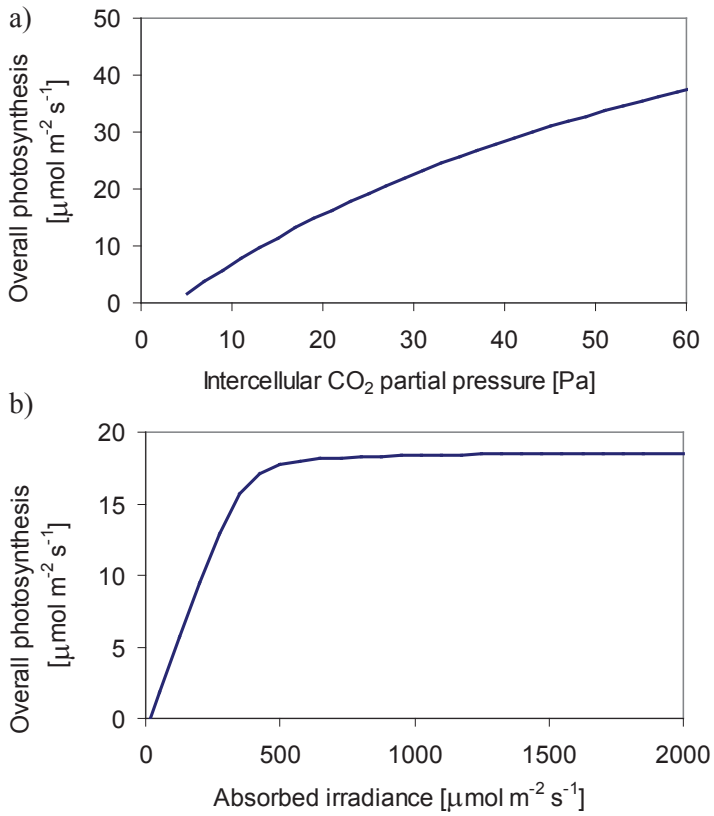

Figure 6. The effect of a) the intercellular partial pressure of CO_2 and b) the absorbed quantum flux of leaf C_3 photosynthesis. The parameter settings: The temperature T = 25 °C, and $V_{max}25$ = 90 µmol m^{-2} s^{-1} in eq. **42**. In a): The absorbed irradiance (quantum flux density) by the leaf $I_{total,0}$ = 1500 µmol m^{-2} s^{-1}, in b): The parameters of the intercellular partial pressure of CO_2 ρ_i = 25 Pa.

The plot of photosynthesis in Figure 6 is plotted against the intercellular partial pressure of CO_2 in the absence of stomata limitations, and the absorbed quantum flux density.

A central process in cellular metabolism is respiration, the oxidation of sugar to CO_2 and water. With respiration, cells obtain the useful chemical energy, adenosine triphosphate (ATP), from sugar in order to maintenance life and growth. The leaf respiration rate, R is proportional to the photosynthetic Rubisco capacity (de Pury & Farquhar, 1997):

eq. 34

$$R_{(f,i)} = V_{m(f,i)} 0.0089 ,$$

$R_{(f,i)}$: Leaf respiration per unit leaf area (mol m^{-2} s^{-1}).

Figure 7 compare the Farquhar leaf respiration calculated by eq. 34 with the overall respiration calculated in Daisy for different crop components. In Daisy the respiration is divided in maintenance and growth respiration. The overall respiration calculated by eq. 34 is comparable to the total respiration of all the contribution for growth and maintenance respiration in Daisy. Therefore the net photosynthesis equilibrated with stomata conductance is calculated by eq. 25. The net photosynthesis is thereafter re-calculated by adding the respiration given by eq. 34 and subtracting the overall respiration which is the sum of growth and maintenance respiration for root, storage organ, leaf and stem compartment.

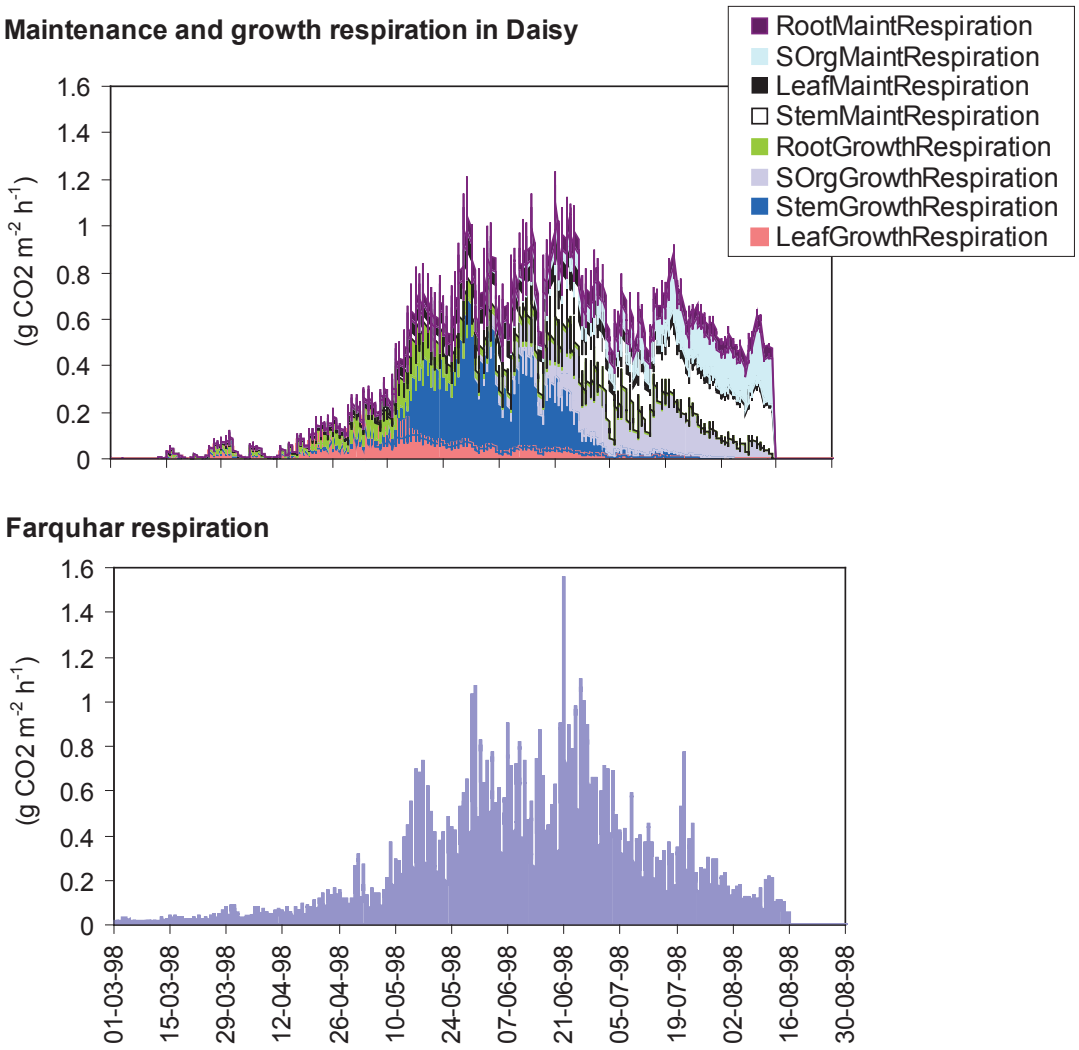

Figure 7. Top: The maintenance and growth respiration calculated by different crop components in Daisy. Bottom: Farquhar "leaf respiration" calculated by eq. **34**.

Photosynthesis of C_4 plants

The photosynthetic model of C_4 plants is based on the model developed by Collatz et al. (1992) and predicts photosynthesis as a function of temperature, photosynthetic active quantum flux density, CO_2 pressure and relative humidity at the leaf surface. The important adjustable parameters in the C_4 model are the capacities of Rubisco and PEP carboxylase to fix CO_2 which can be estimated from leaf photosynthetic responses to light and CO_2. The C_4 photosynthesis model link the C_3 photosynthesis in the bundle sheath chloroplast with a carbon pump driven by the activity of PEP carboxylase in the mesophyll leaf cells. Carbon derived from intercellular CO_2 is fixed into C_4 acids in the mesophyll, transported to the bundle sheath cells and released as CO_2. Leakage of inorganic carbon from the bundle sheath cells to the intercellular spaces occurs because there is a large gradient in CO_2 concentration created by the pump. The steady state balance of these transport processes, the net leaf photosynthetic rate, A, is given by:

eq. 35

$$A_{(f,i)} = \min\left\{ w_{c(f,i)}; w_{e(f,i)}; w_{s(f,i)} \right\} - R_{(f,i)},$$

$A_{(f,i)}$: Net photosynthesis (mol m^{-2} s^{-1}).
$R_{(f,i)}$: Leak of CO_2 from the bundle sheath (mol m^{-2} s^{-1}).

$w_{c(f,i)}$: CO_2 limited rate of assimilation (mol m^{-2} s^{-1}).
$w_{e(f,i)}$: Light limited rate of assimilation (mol m^{-2} s^{-1}).
$w_{s(f,i)}$: Rubisco limited rate of assimilation (mol m^{-2} s^{-1}).

At rate limiting light intensities, the efficiency of CO_2 fixation with respect to absorbed light (quantum yield) determines the rate of photosynthesis. The light dependent rate is given by:

eq. 36

$$w_{e(f,i)} = a_{abs} \alpha \, I_{(f,i)},$$

a_{abs}: Leaf absorbtivity to PAR (a_{abs} = 0.86 (Collatz et al., 1992)).
α: Initial slope of photosynthetic light response (α = 0.04 mol mol^{-1} (Collatz et al., 1992)).
$I_{(f,i)}$: Absorbed irradiance given by eq. 17 and eq. 19 (mol m^{-2} s^{-1}).

At low CO_2 concentrations, empirical studies show that net photosynthesis, A, increases linearly from the compensation point (near zero Pa) to rate saturation which occur at an intercellular CO_2 partial pressure of about 10 Pa. Thus, the CO_2 limited flux given by Collatz et al. (1992):

eq. 37

$$w_{c(f,i)} = k_T \frac{\rho_{i(f,i)}}{P_{tot}},$$

k_T: Initial slope of photosynthetic CO_2 response (0.6 mol m^{-2} s^{-1} (Collatz et al., 1992)).
$\rho i_{(f,i)}$: CO_2 partial pressure in leaf interior (Pa).
P_{tot}: The atmospheric pressure (100000 Pa).

Empirical observations show when w_c and w_e are not limiting, then the rate of assimilation approaches a rate, w_s, that is largely independent of CO_2 and light. The rate under these conditions is controlled by the capacity for CO_2 fixation by Rubisco:

eq. 38

$$w_{s(f,i)} = V_{m(f,i)},$$

$V_{m(f,i)}$: Photosynthetic capacity per unit leaf area given by eq. 52 (mol m^{-2} s^{-1}).

The transition from one limitation to another appears to be somewhat gradual and therefore the photosynthesis is estimated by solving the following quadratics (eq. 39 and eq. 40) by the first root:

eq. 39

$$\theta M_{(f,i)}^{\ 2} - \left(w_{s(f,i)} + w_{e(f,i)} \right) M_{(f,i)} + w_{s(f,i)} w_{e(f,i)} = 0,$$

$M_{(f,i)}$: The flux determined by Rubisco and light (mol m^{-2} s^{-1}).
θ: Curvature parameter (0.83 (Collatz et al., 1992)).

where the curvature parameter, θ, gives a gradual transition between the light limited and Rubisco limited flux. The limitation on the overall rate M and the CO_2 limited flux, w_c, the likewise expressed as a quadratic:

eq. 40

$$\beta A_{(f,i)}^2 - A\left(M_{(f,i)} + w_{c(f,i)} \right) + M_{(f,i)} w_{c(f,i)} = 0,$$

$A_{(f,i)}$: The flux determined by M and CO_2 (mol m^{-2} s^{-1}).
β: Curvature parameter (0.93 (Collatz et al., 1992)).

where the curvature parameter, β, gives a gradual transition between M and the CO_2 limited flux.

Photosynthetic capacity

Rubisco is the most abundant protein in leaves of C_3 plants, constitution up to half the total leaf protein. For this reason it plays a crucial role in the nitrogen economy of plants. To estimate photosynthetic active nitrogen (N) the non-functional and critical limits of N is estimate. The non-functional N is considered structural N, and not used in photosynthesis. The N content above critical is considered luxury N uptake, and also not used in photosynthesis. Hence, the photosynthetic active Rubisco nitrogen, N_p, is given by:

eq. 41

$$N_p = \begin{cases} N_a - N_n, & 0 < (N_a - N_n) < (N_c - N_n) \\ N_c - N_n, & (N_a - N_n) > (N_c - N_n), \\ 0, & 0 > (N_a - N_n) \end{cases}$$

$N_{p:}$ Photosynthetic active Rubisco associated nitrogen (mol m^{-2}).
N_a: Actual leaf nitrogen (mol m^{-2}).
N_c: Critical (luxury) leaf nitrogen (mol m^{-2}).
$N_{n,}$: Non-functional (structural) leaf nitrogen (mol m^{-2}).

where the actual leaf nitrogen content in the canopy, N_a, is given by the crop production component in DAISY. The critical, N_c, and non-functional, N_n, limits are given by the CropN component in DAISY.

The Rubisco N distribution with depth in the canopy layer $N_{p(f,i)}$ can be defined by different functions. An example could be the exponential distribution given by Boegh et al. (2002) as described in section 0.

The maximum leaf Rubisco capacity in each layer, V_{maxi}, at 25 °C is given by:

eq. 42

$$V_{\max 25(f,i)} = \chi_n N_{p(f,i)},$$

$V_{max25,i}$: The maximum leaf Rubisco capacity at 25 °C (mol m^{-2} s^{-1}).
χ_n: Ratio of measured Rubisco capacity to leaf nitrogen (0.116 mol mol^{-1} s^{-1} for wheat (Boegh et al., 2002)).

The canopy photosynthetic capacity in the canopy is described as a function of the Rubisco N distribution:

eq. 43

$$V_{m(f,i)} = V_{\max(f,i)} N_{p(f,i)},$$

$V_{max(f,i)}$ The maximum leaf Rubisco capacity at leaf temperature given by eq. 52 (mol m^{-2} s^{-1}).

The partitioning of leaves into sunlit and shaded fractions is continually changing throughout the day. The calculation of the photosynthetic capacity is affected by these separate fractions.

Sunlit leaves

The photosynthetic capacity of the sunlit leaf fraction, $V_{mSun,i}$, of each canopy layers is given by:

eq. 44

$$V_{m(sun,i)} = L_{(sun,i)} V_{\max(sun,i)} \left[\frac{1 - \exp\left(-k_n - k_b L_{(sun,i)}\right)}{k_n + k_b L_{(sun,i)}} \right],$$

k_b: Extinction coefficient of beam radiation (unit less, given by eq. 10).
$V_{m(sun,i)}$: The canopy photosynthetic capacity in sunlit leaves layer i (mol m^{-2} s^{-1}).
$V_{max(sun,i)}$: The maximum leaf Rubisco capacity in sunlit leaves at temperature T_a given by eq. 52 (mol m^{-2} s^{-1}).

Shaded leaves

Photosynthetic capacity of the shaded leaf fraction, V_{mSh}, of each canopy layers is given by:

eq. 45

$$V_{m(sh,i)} = V_{m(total,i)} - V_{m(sun,i)},$$

$V_{m(sun,i)}$: The Rubisco photosynthetic capacity to leaf nitrogen in the sunlit leaf fraction (mol m^{-2} s^{-1}).
$V_{m(sh,i)}$: The Rubisco photosynthetic capacity to leaf nitrogen in the shaded leaf fraction (mol m^{-2} s^{-1}).

Figure 8 show the different fractions of the photosynthetic capacity in the canopy together with the nitrogen distribution.

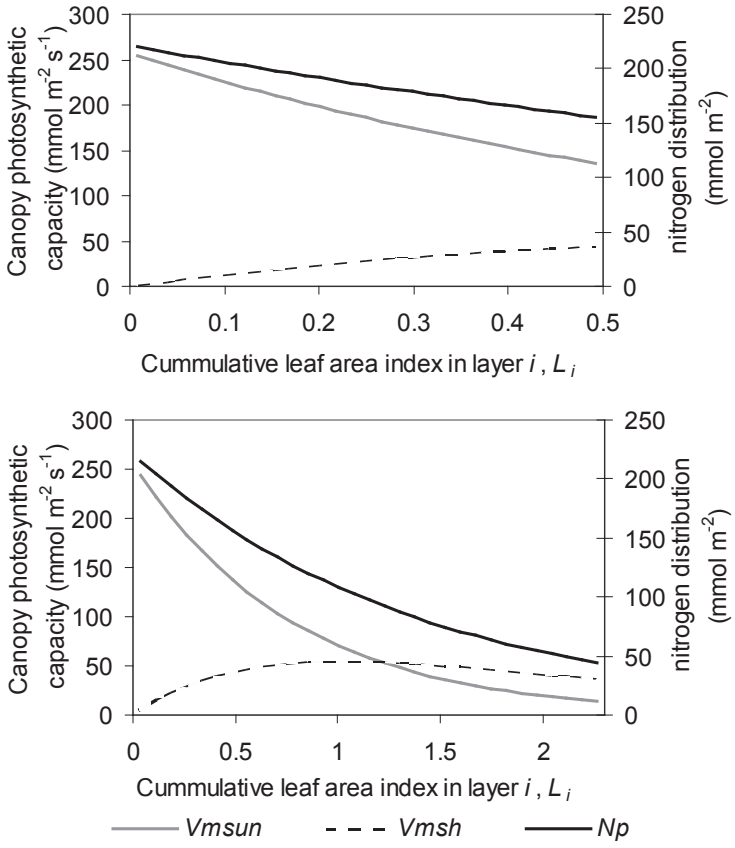

Figure 8. The canopy photosynthetic capacity distributions (left axis) and the nitrogen distribution of Rubisco N (right axis) in the canopy layers. L_c = 2.3 and N_C = 64.3 mg g^{-1}.

Canopy nitrogen distribution sub-model (N-dist)

The maximum leaf Rubisco capacity in each layer is defined as function of photosynthetic active nitrogen. The distribution of photosynthetic active nitrogen in the canopy can be described by different functions. An example could be the Ndist exp model which is an exponential distribution according to Boegh et al., (2002):

eq. 46

$$N_{p,(f,i)} = N_{p,(f,0)} \exp\left(-k_n L_{(f,i)}\right),$$

k_n: Coefficient of leaf nitrogen allocation in a canopy (0,713 (Boegh et al., 2002)).
$L_{(f,i)}$: Cumulative leaf-area index.
$N_{p(f,i)}$: Photosynthetic active Rubisco associated nitrogen distribution (mol m^{-2}).
$N_{p,(f,0)}$: Photosynthetic active Rubisco associated nitrogen in the top of the canopy (mol m^{-2}).

where the photosynthetic active nitrogen (Rubisco N) in the top of the canopy, $N_{p,(f,0)}$, is given by:

eq. 47

$$N_{p,(f,0)} = \frac{k_n N_p}{1 - \exp\left(-k_n L_{(f,i)}\right)},$$

N_p: Photosynthetic active Rubisco associated nitrogen (mol m^{-2}) given by eq. 41.

Figure 9 show the distribution of photosynthetic active nitrogen (Rubisco N) in the canopy where the $N_{p,C}$ = 248 mmol m^{-2} and $N_{p,0}$ = 221 mmol m^{-2}.

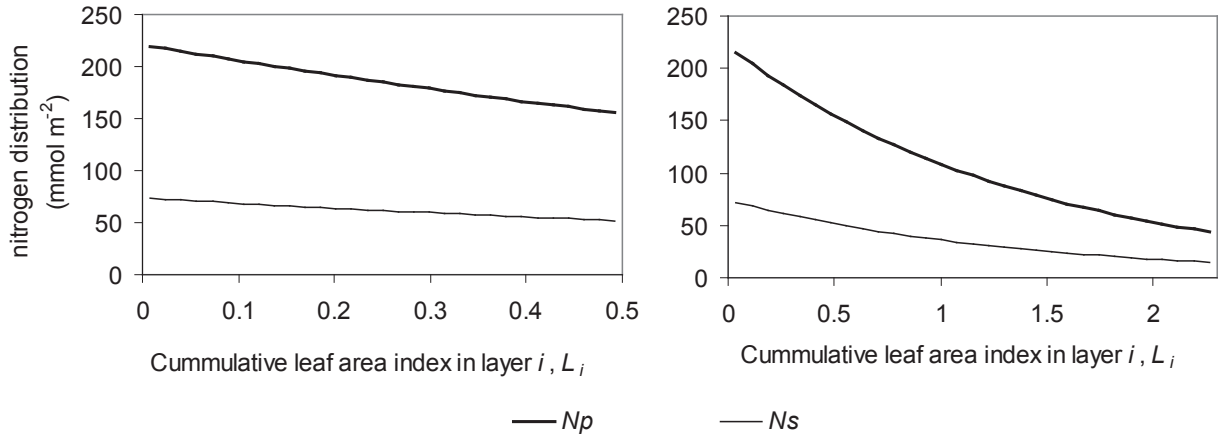

Figure 9. The nitrogen distribution of Rubisco N (left axis) as a function of the cumulative leaf area index in the canopy layers (L_i) with $N_{p,c}$ = 248 mmol m^{-2}. Left: L_c = 0.5. Right: L_c = 2.3.

Temperature dependencies

Several of the photosynthetic- and stomatal-parameters depend on the temperature of the leaf. For C_3 plants this includes the parameters K_c, K_o, Γ^*, V_m, and J_m. For C_4 plants it concerns the parameters Γ^*, k_T and V_m.

k_T

The pseudo-first order rate constant with respect to CO_2, k_T, is given by (Collatz et al., 1992):

eq. 48

$$k_T = kQ_{10k}^{\left((T_a-25)/10\right)}, \qquad \text{for } C_4$$

T_a: Air temperature (°C).

k_T: The pseudo-first order rate constant with respect to CO_2 (mol m^{-2} s^{-1}).
k: Rate constant (0.6 mol m^{-2} s^{-1}).
Q_{10k}: The Q_{10} parameter of k (1.8).

K_c, K_o, and Γ*

For the C_3 photosynthesis model, the parameters K_c, K_o, and Γ^* are adjusted for the effect of temperature by the Arrhenius function (de Pyry and Farquhar, 1997). For the C_4 photosynthesis model, only the Γ^* is used in the model and adjusted by the Arrhenius function:

eq. 49

$$k_{T,x} = k_{25,x} \exp\left(\frac{E_{a,x}(T_a - 25)}{298R\left(T_a + 273\right)}\right), \qquad \text{for } C_3 \text{ and } C_4$$

$k_{T,x}$: Parameter x at T °C.
$k_{25,x}$: Parameter x at 25 °C.
$E_{a,x}$: Activation energy for parameter x ($x = K_c, K_o, \Gamma^*$).
T_a: Air temperature (°C).

Activation energies of the model parameters adjusted for temperature dependencies by eq. 49 and values at 25 °C are listed in Table 1 and defined as default values in the Daisy model.

Table 1 Activation energies and values at 25 °C of the model parameters adjusted for temperature dependencies by **eq. 49** listed in de Pury & Farquhar (1997).

Parameter	E_a (J mol^{-1})	k_{25} (Pa)
Γ^*	29000	3.69
K_o	36000	24800
K_c	59400	40.4

J_m

The parameter J_m, for calculation of the electron-transport limited rate of photosynthesis, is also adjusted by temperature according to de Pury & Farquhar (1997). However, for temperatures below 10 C° the temperature function is reduced with a linear function. Below 4 C° $J_m = 0$:

eq. 50

$$j_m = J_{m_{25}} \exp\left[\frac{\left(T_a + 273{,}15 - 298\right)E_{a,Jm}}{R\left(T_a + 273{,}15\right)298}\right] \frac{\left[1 + \exp\left(\frac{S298 - H}{R298}\right)\right]}{1 + \exp\left(\frac{S\left(T_a + 273{,}15\right) - H}{R\left(T_a + 273{,}15\right)}\right)}$$

eq. 51

$$J_{m_T} = \begin{cases} j_m, & T_a \geq 10\,^{\circ}C \\ j_m\left(\dfrac{T_a - 4}{6}\right), & 4 < T_a < 10\,^{\circ}C, \quad \text{for } C_3 \\ 0, & T_a \leq 4\,^{\circ}C \end{cases}$$

T_a: Air temperature (°C).
J_{m25}: J_m at 25 °C is given by 2.1 $V_{max25(f,i)}$ (de Pury and Farquhar, 1997).
R: Universal gas constant (8.314 J mol^{-1} K^{-1}).
H: Curvature parameter of J_m (220000 J mol^{-1} (de Pury and Farquhar, 1997)).
S: Electron transport temperatures response parameter (710 J mol^{-1} K^{-1} (de Pury and Farquhar, 1997)).
$E_{a,Jm}$: Activation energy for J_m (37000 J mol^{-1} (de Pury and Farquhar, 1997)).

Vm

In the C_3 photosynthesis model, the maximum photosynthetic Rubisco capacity is adjusted for the temperature dependency by a function defined by Harley et al. (1992) and partly by Bernacchi et al. (2001):

eq. 52

$$V_{m(f,i)} = V_{\max 25(f,i)} \frac{\exp\left(C_{V\max} - \dfrac{E_{a,V\max}}{R\left(T_a + 273{,}15\right)}\right)}{1 + \exp\left(\dfrac{Sv\left(T_a + 273{,}15\right) - E_{da,V\max}}{R\left(T_a + 273{,}15\right)}\right)}, \qquad \text{for } C_3$$

$V_{max25(f,i)}$: The maximum leaf Rubisco capacity given by eq. 42 (mol m^{-2} s^{-1}).
$E_{a,Vmax}$: Activation energy for V_{max} (65330 J mol^{-1} (Bernacchi et al., 2001)).
$E_{da,Vmax}$: Deactivation energy for V_{max} (202900 J mol^{-1} (Harley et al., 1992)).
$C_{,Vmax}$: Temperature scaling constant for V_{max} (26,350, (Bernacchi et al., 2001)).
S_v: Entropy term for V_{max} (650 J mol^{-1} K^{-1} (Harley et al., 1992)).

In the C_4 photosynthesis model, the effect of temperature on the photosynthetic Rubisco capacity is given by Collatz et al. (1992):

eq. 53

$$V_{m(f,i)} = \frac{V_{\max 25} Q_{10Vm}^{\left((T_a - 25)/10\right)}}{\left[1 + \exp\left(0.3\left(T_a - 40\right)\right)\right]\left[1 + \exp\left(0.2425\left(15 - T_a\right)\right)\right]}, \quad \text{for } C_4$$

T_a: Air temperature (°C).
$V_{max25(f,i)}$: The maximum leaf Rubisco capacity given by eq. 42 (mol m^{-2} s^{-1}).
Q_{10Vm}: The Q_{10} parameter of V_m (2.4).

The effect of temperature on the leaf C_3 parameters are show in Figure 10 together with the effect of temperature on the overall photosynthesis.

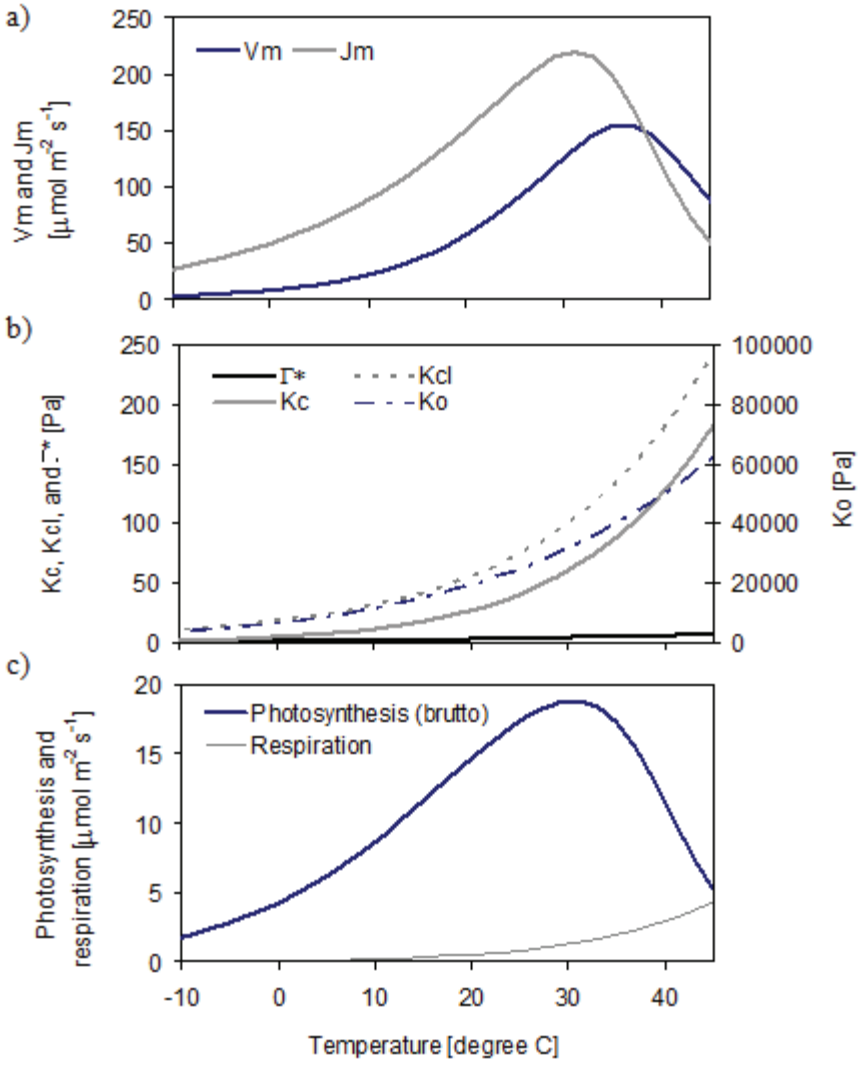

Figure 10. The effect of temperature on leaf C_3 photosynthesis parameters: a) J_m and V_m, b) K_c, K_o, K_{cl} given by eq. **29**, and Γ^*, c) the overall photosynthesis and respiration calculated by Farquhar. The intercellular partial pressure of CO_2 is 25 Pa, the absorbed irradiance (quantum flux density) by the leaf is 1500 µmol m^{-2} s^{-1} and V_{max} is 90 µmol m^{-2} s^{-1} in eq. **42**.

Calculation procedure of the photosynthesis-conductance model

There is a strong interaction between the photosynthesis and the stomatal sub-models in this system. The Daisy code is constructed to obtain a numerical solution, using an initial guess for the stomatal conductance ($g_s = (L_{i-1} - L_i)/5$ mol s^{-1} m^{-2}), and the CO_2 partial pressure in the leaf interior ($\rho_i = 0.5\rho_a = 17.5$ Pa), the code calculates the leaf temperature, photosynthesis, g_s and ρ_i by iterations using the Newton-Raphson method until ρ_i is stable. Newton-Raphson Method states that if $x = r$ is an approximation to $f(x) = 0$, then a better solution is given by:

eq. 54

$$r^{new} = r - \frac{f(r)}{f'(r)},$$

When estimating ρ_i, the function $f(x)$ is given by:

eq. 55

$$f\left(x\right)=\rho_{i(f,i)}\left(t\right)-\rho_{i(f,i)}\left(t-1\right),$$

$\rho_{i(f,i)}$: CO_2 partial pressure in leaf interior in the sunlit or shaded fraction, f, in canopy layer i (Pa).
t: Time step (hour).

where ρ_i for C_3 plants is calculated using eq. 24. The derivates of f follows:

eq. 56

$$f'\left(x\right)=-P_{tot}\left(1.6\frac{1}{g_{s(f,i)}\left(t\right)}+1.4\frac{1}{g_{b(f,i)}\left(t\right)}\right)dx-1,$$

$g_{s(f,i)}$: Stomatal conductance of leaves (mol m^{-2} s^{-1}).
$g_{b(f,i)}$: Leaf boundary-layer conductance (mol m^{-2} s^{-1}).

where dx for C_3 plants is given by:

eq. 57

$$dx=V_{m(f,i)}\frac{K_{cl}+\Gamma*}{\left(\rho_{i(f,i)}+K_{cl}\right)^2},\qquad \text{if } w_c<w_e$$

$$dx=3J_{m(f,i)}\frac{\Gamma*}{\left(\rho_{i(f,i)}+2\Gamma*\right)^2},\quad \text{if } w_c\geq w_e$$

$V_{m(f,i)}$: Photosynthetic capacity per unit leaf area in the sunlit or shaded fraction, f, in canopy layer i (mol m^{-2} s^{-1}).
$\rho_{i(f,i)}$: CO_2 partial pressure in leaf interior in the sunlit or shaded fraction, f, in canopy layer i (Pa).
K_{cl}: The effective Michaelis-Menten coefficient CO_2 (Pa).
Γ^*: CO_2 compensation point of photosynthesis (Pa).

Then the Newthon-Rapson solution to $\rho_{i(f,i)}(t)$ is then given by:

eq. 58

$$\rho_{i(f,i)}\left(t\right)=\rho_{i(f,i)}\left(t-1\right)-\frac{\left(\rho_{i(f,i)}\left(t\right)-\rho_{i(f,i)}\left(t-1\right)\right)}{-P_{tot}\left(1.6\frac{1}{g_{s(f,i)}\left(t\right)}+1.4\frac{1}{g_{b(f,i)}\left(t\right)}\right)dx\left(t\right)-1},\quad \text{for } C_3$$

Which is used to calculate the partial pressure of CO_2 in stomata. For C_4 plants, the same consideration can be done giving:

eq. 59

$$\rho_{i(f,i)}\left(t\right)=\rho_{i(f,i)}\left(t-1\right)-\frac{\left(\rho_{i(f,i)}\left(t\right)-\rho_{i(f,i)}\left(t-1\right)\right)}{-P_{tot}\left(1.6\frac{1}{g_{s(f,i)}\left(t\right)}\right)dx\left(t\right)-1},\qquad \text{for } C_4$$

where the *dx* for C_4 plants is given by:

eq. 60

$$dx(t) = \frac{k_T\left(A_{f,i} - M_{f,i}\right)}{\left(2\beta\ A_{f,i}\right) - M_{f,i} - wc_{f,i}}, \qquad \text{for } C_4$$

k_T: Initial slope of photosynthetic CO_2 response (k = 0.6 mol m^{-2} s^{-1} (Collatz et al., 1992)).

References

Ball,J.T. and Berry,J.A., 1982. The Ci/Cs ratio: A basis for predicitong stomatal control of photosynthesis. In: pp. 88-92.

Ball,J.T., Woodrow,I.E. and Berry,J.A., 1987. A model predicitng stomatal conductance and its contribution to the control of photosynthesis under different environmental conditions. In: I.Biggins (Editor), Progress in Photosynthesisi Research. Martinus Nijhoff Publishers, Netherlands, pp. 221-224.

Bernacchi,C.J., Singsaas,E.L., Pimentel,C., Portis,A.R. and Long,S.P., 2001. Improved temperature response functions for models of Rubisco-limited photosynthesis. Plant Cell and Environment, 24(2): 253-259.

Boegh,E. and Soegaard,H., 2004. Remote sensing based estimation of evapotranspiration rates. International Journal of Remote Sensing, 25(13): 2535-2551.

Boegh,E., Soegaard,H., Broge,N., Hasager,C.B., Jensen,N.O., Schelde,K. and Thomsen,A., 2002. Airborne multispectral data for quantifying leaf area index, nitrogen concentration, and photosynthetic efficiency in agriculture. Remote Sensing of Environment, 81(2-3): 179-193.

Collatz,G.J., Ball,J.T., Grivet,C. and Berry,J.A., 1991. Physiological and Environmental-Regulation of Stomatal Conductance, Photosynthesis and Transpiration - A Model That Includes A Laminar Boundary-Layer. Agricultural and Forest Meteorology, 54(2-4): 107-136.

Collatz,G.J., Ribas-Carbo,M. and Berry,J.A., 1992. Coupled Photosynthesis-Stomatal Conductance Model for Leaves of C4 Plants. Australian Journal of Plant Physiology, 19(5): 519-538.

de Pury,D.G.G. and Farquhar,G.D., 1997. Simple scaling of photosynthesis from leaves to canopies without the errors of big-leaf models. Plant Cell and Environment, 20(5): 537-557.

Farquhar,G.D., Caemmerer,S.V. and Berry,J.A., 1980. A Biochemical-Model of Photosynthetic Co2 Assimilation in Leaves of C-3 Species. Planta, 149(1): 78-90.

Harley,P.C., Thomas,R.B., Reynolds,J.F. and Strain,B.R., 1992. Modeling Photosynthesis of Cotton Grown in Elevated Co2. Plant Cell and Environment, 15(3): 271-282.

Leuning,R., 1995. A Critical-Appraisal of A Combined Stomatal-Photosynthesis Model for C-3 Plants. Plant Cell and Environment, 18(4): 339-355.

McCree,K.J., 1981. Photosynthetically active radiation. In: O.L.Lange, P.S.Nobel, C.B.Osmond, and H.Zeigler (Editors), Physiological Plant Ecology. Vol 12A, Encycclopedia of plant physiology. Springer-Verlag, Berlin, pp. 41-55.

Nobel,P.S., 1991. Physicochemical and environmental plant physiology. Academic Press, San Diego.

Sellers,P.J., Randall,D.A., Collatz,G.J., Berry,J.A., Field,C.B., Dazlich,D.A., Zhang,C., Collelo,G.D. and Bounoua,L., 1996. A revised land surface parameterization (SiB2) for atmospheric GCMs .1. Model formulation. Journal of Climate, 9(4): 676-705.

Wang,Y.P. and Leuning,R., 1998. A two-leaf model for canopy conductance, photosynthesis and partitioning of available energy I: Model description and comparison with a multi-layered model. Agricultural and Forest Meteorology, 91(1-2): 89-111.

Annex 3.4 Estimating root density in Daisy

Estimating the root density from root dry matter and size

Per Abrahamsen*, Mikkel Mollerup, and Søren Hansen
University of Copenhagen, LIFE
Department of Agricultural Sciences
Højbakkegård Allé 9, 2630 Taastrup, Denmark

October 28, 2008

Abstract

In this paper we extend an emperical root density distribution based on densely populated homogenious fields to row crops. The row crops are modeled as having a uniform density in the direction parallel to the rows, but variable in the direction perpindicular to the row. In each case how to find the distribution parameters from the root dry matter and the size of the root zone.

1 Densily populated fields

In accordance with Gerwitz and Page (1974), the root density distribution L_z for a crop can be described by

$$L_z = L_0 \, e^{-az} \tag{1}$$

where L_0 is the root density at the soil surface, a is a distribution parameter, and z is the depth below soil surface.

We here assume that the density is uniformly distributed on the horizontal plane, an assumption that fails with e.g. row crops.

The parameters a and L_0 will both vary with time. For a production oriented simulation model like Daisy (Hansen et al., 1991; Abrahamsen and Hansen, 2000), it can be more convenient to specify the density in terms of accumulated root dry matter M_r and total root depth d_c, as described in Hansen et al. (1990) or the following.

We define the root depth at the lowest depth where the root density is at above specified threshold L_m. By inserting this in (1), we get

$$L_m = L_{d_c} = L_0 \, e^{-ad_c} \tag{2}$$

We convert the root mass to root length l_r by assuming the specific root length S_r is a known constant (rather than varying with depth)

$$l_r = S_r \, M_r \tag{3}$$

*Corresponding author. Fax: +4535333384 Email: daisy@dina.kvl.dk

The total root length is also the integral of the root density over the profile

$$l_r = \int_0^\infty L_z \, dz = \int_0^\infty L_0 \, e^{-az} \, dz = \frac{L_0}{a} \tag{4}$$

By inserting the expression we get for L_0 from (4) in (2) we get

$$L_m = l_r \, a \, e^{-ad_c} \tag{5}$$

If we substitute $W = -ad_c$ and isolate the known values on the right side this gives us

$$We^W = -L_m \frac{d_c}{l_r} \tag{6}$$

The solution to this equation with regard to W happens to be the definition of the Lambert-W function (Euler, 1783; Lambert, 1758). The function on the left hand side of the equation is depicted on figure 1.

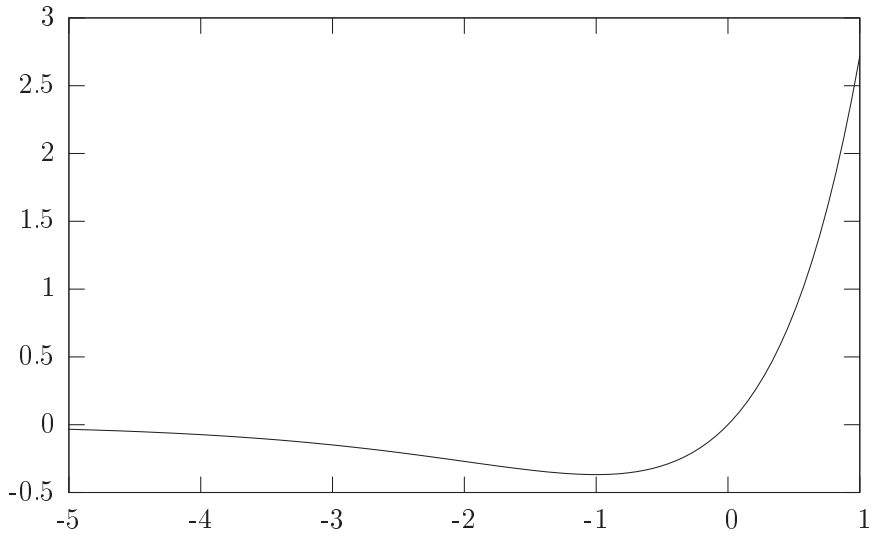

Figure 1: We^W

Since we now know the value for Wm we can find the desired density parameters L_0 and a by substituting back

$$a = -W/d_c \tag{7}$$

$$L_0 = \frac{L_m}{e^{-ad_c}} = L_m e^{ad_c} \tag{8}$$

1.1 Numeric solution to W

We start by dividing the funtions into monotonic intervals by finding the derivative

$$\frac{dW \, e^W}{dW} = e^W + We^W \tag{9}$$

The equation

$$e^W + We^W = 0 \tag{10}$$

has one solution, $W = -1$. The expression $W\,e^W$ is decreasing below -1 and increasing above -1. Thus, $W = 0$ is a global minimum.

Since $\lim_{Q\to-\infty} W\,e^W = 0$ we get a single solution when $-L_m\frac{d_c}{l_r}$ is exactly at the bottom point ($-1e^{-1}$), two when it is above (it is never positive), and none when it is below. The later situation corresponds to the case where there are insufficent root l_r to satisfy the minimal root density L_m within the given root zone d_c.

Both solutions are valid, but represent different distributions.

- The solution for $W < -1$ represents a large a parameter. From (8) we see this also means L_0 is large. Thus, the solution corresponds to a root zone with a high density near the top that decreases rapidly to L_m at the bottom of the root zone, and continues to decrease so only a small contribution to the total root length from below he root zone.
- The solution for $W > -1$ (and thus small values of a and L_0) corresponds to a low root density near the top that decreases slowly, and thus gives a larger contribution to the total root length from below the root zone.

As the total root length increases, pressing W towards 0 or $-\infty$, the difference between the solutions grow. When there is just enough roots to satisfy the contraints at $W = -1$, the two solutions converges to one. As we like our roots to stay mostly within the root zone, we choose the solution for $W < -1$. We can thus find W numerically using Newton's method and an initial guess of -2.

1.2 Limited growth

The distribution in (1) implies a gradual decrease of roots going towards, but never reaching zero. There are two problems with this. The first one is emprical, for some soils it doesn't match what we observe, rather than a gradual decrease, there is sharp decrease at a specific depth, as the roots are unable to penetrate further down **?**. The other one is practical, too large a root zone makes computation impractical.

The way we model the first issue is to divide the root depth into a crop specific and soil independent potential root depth d_c, and soil specific and crop independent maximum root depth d_s. The actual root depth d_a is then the shallowest of these two.

$$d_a = \min(d_c, d_s) \tag{11}$$

We now create a modified root density function L_z^* by defining it to zero below d_a, and a L_z scaled to preserve mass balance above.

$$L_z^* = \begin{cases} k^* L_z & \text{if } z \le d_a \\ 0 & \text{if } z > d_a \end{cases} \tag{12}$$

where

$$k^* = \frac{l_r}{\int_0^{d_a} L_z\,dz} \tag{13}$$

thus solving both problems.

2 Row crops

We can describe a row crop with a two dimensional model by assuming that the plants are densily packed in the row. Our second dimension x is horizontal, ortogonal to the row. The root density at a specific point can be denoted $L_{z,x}$, and we chooce origo so $L_{0,0}$ is the the root density in the top of the row. See figure 2.

TODO: Insert figure here.

Figure 2: Crop row.

We then define the following root dstribution

$$L_{z,x} = L_{0,0}\, e^{-a_z z} e^{-a_x x} \tag{14}$$

where a_z and a_z control the density decrease in the two dimensions.

2.1 Finding the parameters

To find the parameters a_z, a_x and $L_{0,0}$, we assume as before that the root depth and root mass is known, and now additionally that the root radius w_c is known. We define the root zone depth d_c to be the depth right below the row ($x = 0$) where the root density is L_m. As $x = 0$ is the place where (14) predicts the highest density, the average root density at that depth will be well below L_m. Similarily, we define the radius w_c as the horizontal distance from the row where the root density at the surface ($z = 0$)

$$L_m = L_{d,0} = L_{0,r} \tag{15}$$

The total root length on one side of the row (l_R), which we assume is known from our crop model, is the integral of the root density over the half plane

$$\begin{aligned} l_R &= \int_0^\infty \int_0^\infty L_{z,x}\, dz\, dx \\ &= \int_0^\infty \int_0^\infty L_{0,0}\, e^{-a_z z} e^{-a_x x}\, dz\, dx \\ &= \frac{L_{0,0}}{a_z a_x} \end{aligned} \tag{16}$$

Thus (14) can be rewritten

$$L_{z,x} = l_R\, a_z\, a_x\, e^{-a_z z} e^{-a_x x} \tag{17}$$

By using (17) in (15) we get

$$L_m = l_R\, a_z\, a_x\, e^{-a_z d} \tag{18}$$

$$L_m = l_R\, a_z\, a_x\, e^{-a_x r} \tag{19}$$

Thus $e^{-a_z d} = e^{-a_x r}$ or

$$a_x = \frac{d_c}{w_c} a_z \tag{20}$$

By inserting (20) in (19) we get

$$L_m = l_R\, a_z\, \frac{d}{r} a_z\, e^{-a_z d} \tag{21}$$

If we substitute

$$Q = -a_z d \tag{22}$$

and isolate the known values on the right side, this gives us:

$$Q^2\, e^Q = L_m \frac{d\, r}{l_R} \tag{23}$$

The left hand side expression is illustrated in figure 3. Unlike (6), nobody bothered to give the solution to (23) a name.

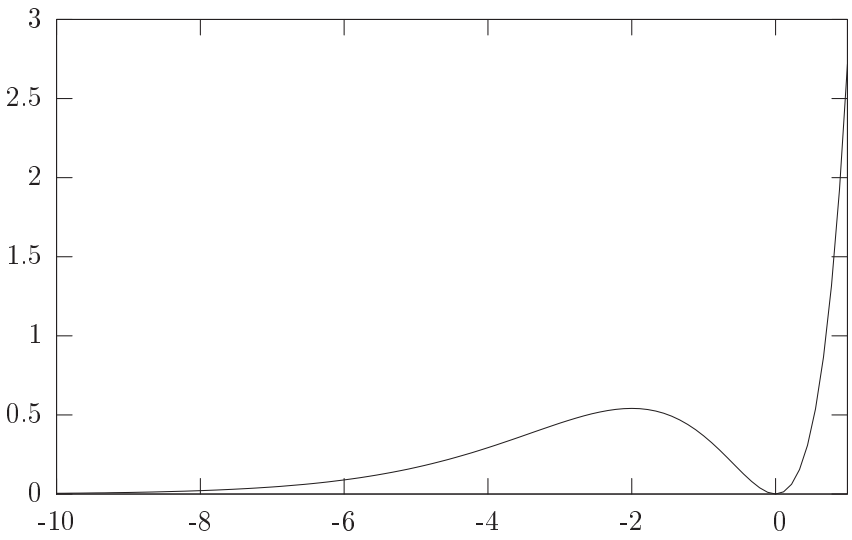

Figure 3: $Q^2 e^Q$

2.2 Numeric solution to Q

We start by dividing the funtions into monotonic intervals by finding the derivative

$$\frac{d(Q^2\, e^Q)}{dQ} = 2Qe^Q + Q^2 e^Q \tag{24}$$

The equation

$$2Qe^Q + Q^2 e^Q = 0 \tag{25}$$

has two solutions, $Q = 0$ and $Q = -2$, and the expression $Q^2\, e^Q$ is increasing below -2, decreasing between -2 and 0, and increasing above 0. Thus, $Q = 0$ is a local (and in this case also global) minimum, and $Q = -2$ is a local maximum.

We are not interested in positive values for Q, they correspond to negative values for a_z, and the simplification in (16) are only valid if $a_z > 0$.

Since $\lim_{Q\to-\infty} Q^2\,e^Q = 0$ we get a single negative solution when $L_m\frac{dr}{l_R}$ is exactly at the top point (2^2e^{-2}), two when it is smaller (it is never negative), and none when it is larger. The later situation corresponds to the case where there are insufficent root l_R to satisfy the minimal root density L_m within the given root zone dr.

Both negative solutions are valid, but represent different distributions.

- The solution for $Q < -2$ represents a large a_z (and thus also a_x) parameter. From (16) we see this also means $L_{0,0}$ is large. Thus, the solution corresponds to a root zone with a high density near the center that decreases rapidly to L_m near the edge of the root zone, and continues to decrease so only a small contribution to the total root length fro outside the root zone.

- The solution for $Q > -2$ (and thus small values of a_x, a_x and $L_{0,0}$) corresponds to a low root density near the center that decreases slowly, and thus gives a larger contribution to the total root length from outside the root zone.

As the total root length increases, pressing Q towards 0 or $-\infty$, the difference between the solutions grow. When there is just enough roots to satisfy the contraints at $Q = -2$, the two solutions converges to one. As we like our roots to stay mostly within the root zone, we choose the solution for $Q < -2$.

We can find Q numerically using Newton's method and an initial guess of -3. From that we can find a_z from (22), a_x from (20), and $L_{0,0}$ from (16).

2.3 Multiple rows

If the rows are close enough, the root systems will overlap as shown on figure 4.

If R is the distance between rows, and we assume an infinite number of identical rows, this can be expressed by the equation

$$L^*_{z,x} = \begin{cases} \sum_{i=0}^{\infty}(L_{z,x+iR} + L_{z,R+iR-x}) & \text{if } x < R/2 \\ 0 & \text{if } x \geq R/2 \end{cases} \tag{26}$$

Using (14) and the rules for geometric serieses we can rewrite the first case to get rid of the sum

$$\begin{aligned} & \sum_{i=0}^{\infty}(L_{z,x+iR} + L_{z,R+iR-x}) \\ = \;& L_{0,0}\,e^{-a_z z}\sum_{i=0}^{\infty}(e^{-a_x(x+iR)} + e^{-a_x(R+iR-x)}) \\ = \;& L_{0,0}\,e^{-a_z z}(e^{-a_x x}\sum_{i=0}^{\infty}e^{-a_x iR} + e^{-a_x(R-x)}\sum_{i=0}^{\infty}e^{-a_x iR}) \\ = \;& L_{0,0}\,e^{-a_z z}(e^{-a_x x} + e^{-a_x(R-x)})\sum_{i=0}^{\infty}e^{-a_x iR}) \\ = \;& L_{0,0}\,e^{-a_z z}(e^{-a_x x} + e^{-a_x(R-x)})\sum_{i=0}^{\infty}((\tfrac{1}{e})^{a_x R})^i \\ = \;& \frac{L_{0,0}\,e^{-a_z z}(e^{-a_x x}+e^{-a_x(R-x)})}{1-\frac{1}{e}^{a_x R}} \end{aligned} \tag{27}$$

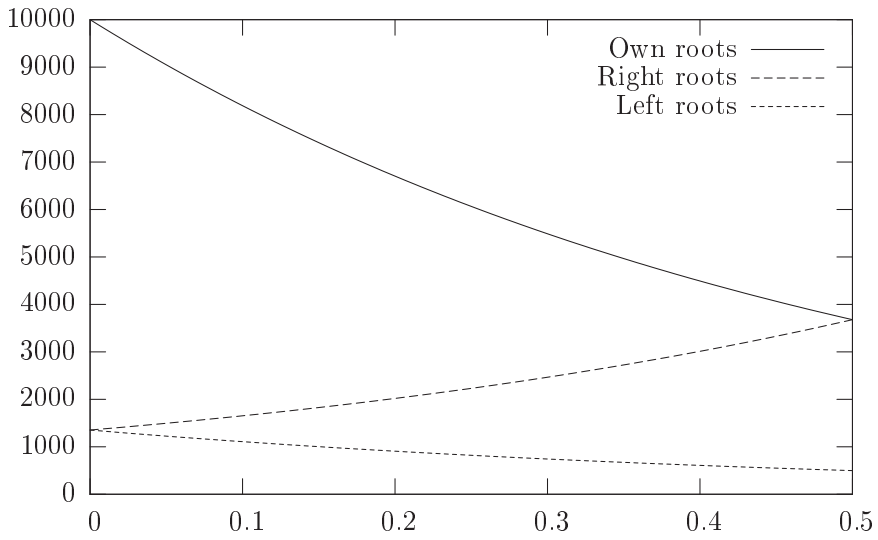

Figure 4: The x-axis represents the distance from a row to the midpoint between it and the row to its right. The y-axis is the root density for roots originating in a specific row. The top line represents the roots from the row itself. The next line the roots from the row to the right. And the last line the roots from the row to the left. In theory, all the rows on the field will contibute some roots to the interval. The root density in the interval will be the sum of all the individual contributions.

2.4 Mapping between the models

We would like to retain our original distribution when ignoring the x dimension. We coudn't do that when looking only at the root system for a single row, as it is infinitely wide and thus has an average density of zero. However, if we look at the roots of single row, we get

$$L_z = \frac{2\int_0^\infty L_{z,x}\,dx}{R} \tag{28}$$

We multiply by two as we assume the two sides of the rows are identical. By integrating to ∞ rather than just $R/2$ we do include roots from outside the row. However, because the system has an infinite number of identical rows, the amount of roots from the crop outside its own row is exactly the same as the amount of roots from other rows inside the row we are examining.

Inserting (14) and (1) in (28) we get

$$\begin{aligned} L_0\,e^{-az} &= \tfrac{2}{R}\int_0^\infty L_{0,0}\,e^{-a_z z}e^{-a_x x}dx \\ &= \tfrac{2L_{0,0}\,e^{-a_z z}}{R}\int_0^\infty e^{-a_x x}dx \\ &= L_{0,0}\,e^{-a_z z}\tfrac{0-1}{-a_x} \\ &= \tfrac{2L_{0,0}}{Ra_x}e^{-a_z z} \end{aligned} \tag{29}$$

So we get

$$a_z = a \tag{30}$$

$$L_{0,0} = \frac{1}{2}a_x R L_0 \tag{31}$$

$$L_0 = \frac{2L_{0,0}}{a_x R} \tag{32}$$

as the equation to use when switching between the one and two dimensional descriptions.

List of symbols

Symbol	Unit	Description
a	m^{-1}	Root density distribution parameter
a_z	m^{-1}	Vertical root density distribution parameter
a_x	m^{-1}	Horizontal root density distribution parameter
d_a	m	Soil limited root depth
d_c	m	Crop potential root depth
d_s	m	Soil maximum root depth
k^*		Soil root limit factor
l_r	$\mathrm{m/m}^2$	Total root length per area
l_R	m/m	Total root length per length of row on one side
L_0	$\mathrm{m/m}^3$	Average root density at soil surface
$L_{0,0}$	$\mathrm{m/m}^3$	Root density in row at soil surface
L_m	$\mathrm{m/m}^3$	Minimal root density
L_z	$\mathrm{m/m}^3$	Root density at soil depth z
L_z^*	$\mathrm{m/m}^3$	Soil limited root density at soil depth z
$L_{z,x}$	$\mathrm{m/m}^3$	Root density at soil depth z and distance x from row
$L_{z,x}^*$	$\mathrm{m/m}^3$	Root density from multiple rows
M_r	$\mathrm{kg/m}^2$	Total root dry matter
Q		Substitution variable
R	m	Distance between rows
S_r	m/kg	Specific root length
W		Lambert-W function
w_c	m	Horizontal root radius
x	m	Horizontal distance from row
z	m	Soil depth

References

Abrahamsen, P., Hansen, S., Mar. 2000. Daisy: An open soil-crop-atmosphere model. Environmental Modelling and Software 15 (3), 313–330.

Euler, L., 1783. De serie lambertina plurimisque eius insignibus proprietatibus. Acta Acad. Scient. Petropol 2, 29–51.

Gerwitz, A., Page, E. R., Aug. 1974. An empirical mathematical model to describe plant root systems. The Journal of Applied Ecology 11 (2), 773–381.

Hansen, S., Jensen, H. E., Nielsen, N. E., Svendsen, H., 1990. Daisy — soil plant atmostphere system model. Tech. Rep. A10, Miljøstyrelsen.
URL `http://www.mst.dk/udgiv/Publications/1990/87-503-8790-1/pdf/87-503-8790-1.PDF`

Hansen, S., Jensen, H. E., Nielsen, N. E., Svendsen, H., 1991. Simulation of nitrogen dynamics and biomass production in winter wheat using the Danish simulation model Daisy. Fertilizer Research 27, 245–259.

Lambert, J. H., 1758. Observations variae in mathesin puram. Acta Helvitica, physico-mathematico-anatomico-botanico-medica 3, 128–168.

Annex 3.5 ABA in Daisy

ABA in Daisy

Per Abrahamsen

October 21, 2008

1 Introduction

ABA is a plant hormom which regulates, among other things, the closing of stomata. By triggering the production of ABA in crops it is sometimes possible to combine a significant reduction in water use, with a moderate reduction in yield. By supporting ABA in Daisy, we hope to be better at predicting when and how such savings can be achieved.

ABA is produced in the root system and has its effect in the canopy. In the present implementation in Daisy transport, storage, and degradation of ABA are all ignored in favor of a system where the ABA concentration in the canopy is solely function of the current water status in the root system.

ABA also has other effects, such as on roth growth and plant phenology, but these are not implemented in Daisy and outside the scope of this paper.

2 ABA production in soil

Let V represent the soil volume we are simulating. The soil volume should as minimum include the entire root zone. For every point in V, Daisy will calculate three values: the volumetric water uptake S, the root density l, and the water potential h.

Based on these values, we have several models for estimating ABA in the stem ($\text{ABA}_{\text{XYLEM}}$) from the conditions in the soil.

2.1 Based on uptake location

The first model is based directly on pot experiments where both $\text{ABA}_{\text{XYLEM}}$ and the water potential (h) is measured. The pots are sufficiently small that the water potential is assumed to be the same everywhere in the pot. From this an empirical relationship ($\text{ABA}_{\text{UPTAKE}}(h)$) between h and $\text{ABA}_{\text{XYLEM}}$ in the pots can be developed. By assuming the same relationship between ABA concentration and uptaken water also holds in a field, we get (1).

$$\text{ABA}_{\text{XYLEM}} = \frac{\int_V S \, \text{ABA}_{\text{UPTAKE}}(h) \, dV}{\int_V S \, dV} \tag{1}$$

The function $\text{ABA}_{\text{UPTAKE}}(h)$ must be supplied by the user.

2.2 Based on production in roots

ABA is produced in the roots with a rate that depends in the water potential ($\text{ABA}_{\text{ROOT}}(h)$). If we assume all the ABA produced ends up in the stem, we can use $\text{ABA}_{\text{ROOT}}(h)$ to find $\text{ABA}_{\text{XYLEM}}$, as in (2).

$$\text{ABA}_{\text{XYLEM}} = \frac{\int_V l \, \text{ABA}_{\text{ROOT}}(h) \, dV}{\int_V S \, dV} \tag{2}$$

The function $\text{ABA}_{\text{ROOT}}(h)$ must be supplied by the user.

2.3 Based on production in soil

Both $S\text{ABA}_{\text{UPTAKE}}(h)$ and $l\text{ABA}_{\text{ROOT}}(h)$ are special cases of calculating the ABA contribution from the soil water potential, root uptake, and root density. We call the generalized function $\text{ABA}_{\text{SOIL}}(S, l, h)$, and the generalized equation for (3).

$$\text{ABA}_{\text{XYLEM}} = \frac{\int_V \text{ABA}_{\text{SOIL}}(S, l, h) \, dV}{\int_V S \, dV} \tag{3}$$

We get (1) by setting $\text{ABA}_{\text{SOIL}}(S, l, h) = S \, \text{ABA}_{\text{UPTAKE}}(h)$ and (2) by setting $\text{ABA}_{\text{SOIL}}(S, l, h) = l \, \text{ABA}_{\text{ROOT}}(h)$.

The function $\text{ABA}_{\text{SOIL}}(S, l, h)$ must be supplied by the user.

2.4 No ABA production

The simplest model for ABA production is to assume no ABA is produced, which also gives the simlest equation ((4)).

$$\text{ABA}_{\text{XYLEM}} = 0 \tag{4}$$

3 ABA effect in canopy

3.1 ABA effect on photosynthesis

The ABA effect on photosynthesis is through a factor (ABA_{COND}) which is multiplied to the stomata conductance. The factor is calculated as decribed in (5).

$$\text{ABA}_{\text{COND}} = e^{-k\text{ABA}_{\text{XYLEM}}} \tag{5}$$

3.2 ABA effect on transpiration

The sun shade open canopy (ssoc) soil vegetation atmosphere (svat) model will use the calculated stomata conductance as part of an energy balance between soil, atmosphere, canopy, dark, and sunlit leaves. The mechanics of the ssoc svat model is outside the scope of this note. As part of this energy balance, transpiration will be estimated. The transpiration will affect ABA production in soil, which again will affect stomata conductance. A one step iteration model is used for finding a solution for both ABA production and stomata conductance.

4 List of symbols

Symbol	Unit	Description
ABA_{COND}	None	ABA effect on stomata conductance.
$\text{ABA}_{\text{ROOT}}(h)$	g ABA/cm ROOT/h	ABA production in roots
$\text{ABA}_{\text{SOIL}}(S, l, h)$	g ABA/cm^3 SOIL/h	ABA contribution from soil
$\text{ABA}_{\text{UPTAKE}}(h)$	g ABA/cm^3 WATER	ABA concentration in water from roots
$\text{ABA}_{\text{XYLEM}}$	g ABA/cm^3 WATER	ABA concentration in xylem
h	hPa	Soil water potential
k	cm^3 WATER/g ABA	Coefficient for calculating ABA_{COND}
l	cm ROOT/cm^3 SOIL	Root density
S	cm^3 WATER/cm^3 SOIL/h	Volumetric water uptake
V	cm^3 SOIL	Soil volume

Annex 3.6 Soil Vegetation Atmosphere Transfer (SVAT) model

A SVAT model simulates the exchange of gases and energy between the canopy-soil-system and the atmosphere. This SVAT model is based on the resistance/conduction concept and considers three sources viz. soil, sunlit and shaded leaves. The SVAT model considers the following surface fluxes:

$$H_{atm} = H_{S\to c} + H_{snl\to c} + H_{shl\to c} \quad (0.1)$$

$$E_{atm} = E_{S\to c} + E_{snl\to c} + E_{shl\to c} \quad (0.2)$$

$$F_{atm} = F_{S\to c} + F_{snl\to c} + F_{shl\to c} \quad (0.3)$$

where H, E, and F denote ecosystem fluxes of sensible heat [W m^{-2}], water vapour [kg m^{-2} s^{-1}], and CO_2 [µmol m^{-2} s^{-1}] respectively. The subscripts describes the pathway of the fluxes; *atm*, *S→c*, *snl→c*, and *shl→c*, are the flux into the atmosphere, the flux from the soil to the canopy air space, the flux from the sunlit leaves to the canopy air space, and the flux from the shaded leaves to the canopy air space. The conceptualization for the exchange of latent heat or water vapour is shown in Fig. 1.

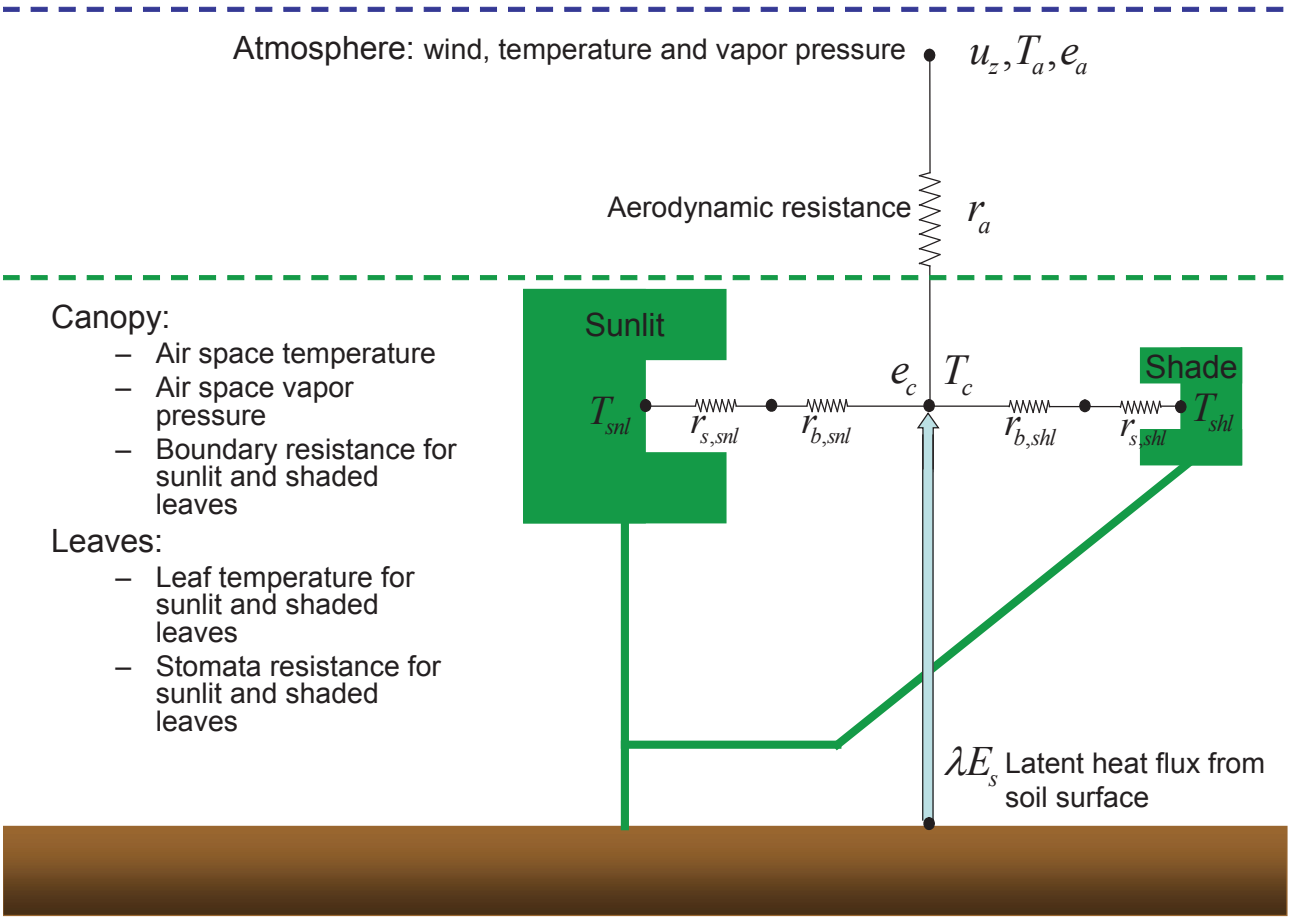

Figur 1 Conceptual model of the exchange of latent heat (water vapour)

Latent heat fluxes [W m^{-2}] are obtained by multiplying the corresponding water vapour flux by the latent heat of vaporization, λ [J kg^{-1}]:

$$\lambda = 3149000 - 2370T_a \quad (0.4)$$

where T_a is the air temperature [K].

The model is based on the principles of conservation of energy and matter, i.e.:

$$R_{abs-soil} - L_{o-soil} = G_{soil} + H_{S\to c} + \lambda E_{S\to c} \qquad (0.5)$$

$$R_{abs-snl} - L_{o-snl} = H_{snl\to c} + \lambda E_{snl\to c} \qquad (0.6)$$

$$R_{abs-shl} - L_{o-shl} = H_{shl\to c} + \lambda E_{shl\to c} \qquad (0.7)$$

where eq. (1.5), eq. (1.6), and eq. (1.7) are energy balances of the soil, sunlit leaves and shaded leaves, respectively. The term on the left side of the equations represents the absorbed radiation of the considered part of the system and G_{soil} is the ground heat flux at the surface. The model considers the absorption of photosynthetically active radiation (PAR), near infrared radiation (NIR), and long-wave thermal radiation separately. Adding the three radiation components in (1.5), eq. (1.6), and eq. (1.7) and subtracting the emission of long-wave radiation from each fraction (L_{o-soil} , L_{o-snl} , and L_{o-shl}) yields the net radiation of canopy-soil system. G_{soil} [W m^{-2}] is estimated by:

$$G_{soil} = \frac{k_h}{z_1}\left(T_S - T_{z1}\right) \qquad (0.8)$$

where T_s and T_{z1} is the soil surface temperature [K] and the soil temperature at the depth z_1 [m], respectively, and k_h is the thermal conductivity of the soil [W m^{-1}]. T_{z1}, z_1, and k_h are obtained from the soil temperature model. For simplicity the values from the beginning of the considered time-step are used.

$E_{S\to c}$ in eq. (1.5) is estimated by the soil water dynamics model and surface model. $E_{S\to c}$ represents the combined evaporation through the soil surface and from water stored at the soil surface. Again, the value from the beginning of the considered time-step is used.

The term $F_{S\to c}$ in eq. (1.3) comprises soil respiration (soil microbial biomass and plant roots) and is obtained from the soil organic matter model and the plant growth model. $F_{snl\to c} + F_{shl\to c}$ comprises photosynthesis of sunlit and shaded leaves in combination with the respiration of the above ground plant biomass. Values are obtained from the photosynthesis model and the plant growth model. The photosynthesis model considers sunlit as well as shaded leaves and in linked to the SVAT through a common dependence of stomata conductance.

Absorption of radiative energy

Shortwave radiation comprises photosynthetically active radiation (PAR) and near infrared radiation (NIR). In the model they each contribute 50% to the solar radiation and they are treated in the same way. They only differ in respect to optical properties, Table 1.

The canopy cover fraction as function of the leaf area index of L_{ai} is estimated as:

$$f_{can} = 1 - \exp\left(-0.5 L_{ai}\right) \qquad (0.9)$$

Shortwave radiation, PAR or NIR, (I_t , W m^{-2}) is divided into a direct beam (I_b , W m^{-2}) and a diffuse (I_d , W m^{-2}) component, i.e.:

$$I_b = \left(1 - f_{dif}\right) I_t \qquad (0.10)$$

$$I_d = f_{dif} I_t \qquad (0.11)$$

where f_{dif} is the diffuse fraction of the global radiation.

Shortwave radiation absorbed by a canopy with a leaf area index of L_{ai} and a spherical leaf distribution is estimated as:

$$I_{abs-can} = I_d\left(1-\rho_{d,c-s}\right)\left(1-\exp\left(-k_d^* L_{ai}\right)\right) + I_b\left(1-\rho_{b,c-s}\right)\left(1-\exp\left(-k_b^* L_{ai}\right)\right) \qquad (0.12)$$

where parameters is obtained from Table 1 and Table 2.

Shortwave radiation absorbed by the sunlit fraction of the canopy is:

$$I_{abs-snl} = I_d\left(1-\rho_{d,c-s}\right)k_d^* F\left(k_d^*+k_b\right) + I_b\left(1-\rho_{b,c-s}\right)k_b^* F\left(k_b^*+k_b\right) + I_b a_b k_b\left(F\left(k_b\right)-F\left(2k_b\right)\right)$$

$$F\left(x\right) = \left(1-\exp\left(-xL_{ai}\right)\right)\Big/ x \quad (0.13)$$

and the sunlit fraction of the leaf area index, L_{ai}, is estimated as:

$$f_{snl} = \frac{1-\exp\left(-k_b L_{ai}\right)}{k_b L_{ai}} \quad (0.14)$$

Shortwave radiation absorbed by the shaded fraction of the canopy is:

$$I_{abs-shl} = I_{abs-can} - I_{abs-snl} \quad (0.15)$$

Shortwave radiation absorbed by the soil is:

$$I_{abs-soil} = I_d\left(1-\rho_{d,c-s}\right) + I_b\left(1-\rho_{b,c-s}\right) - I_{abs-can} \quad (0.16)$$

Table 1. Optical properties of leaves and soil surface.

		PAR	NIR	Long-wave
Leaf absorptance	α	0.80	0.17	
Soil surface reflectance	ρ_s	0.10	0.18	
Leaf emissivity	ε_l			0.98
Soil emissivity	ε_l			0.95

Table 2. Canopy and canopy-soil parameters assuming spherical leaf distribution. L_{ai} is the leaf area index of the canopy

Parameter	Equation
Direct-beam extinction coefficient for black leaves. β = sun elevation angle	$k_b = \frac{0.5}{\sin\beta}$
Direct-beam extinction coefficient	$k_b^* = k_b\sqrt{\alpha}$
Direct-beam canopy reflectance	$\rho_{b,c} = 1-\exp\left(-2\frac{k_b}{1+k_b}\frac{1-\sqrt{\alpha}}{1+\sqrt{\alpha}}\right)$
Direct-beam canopy-soil reflectance	$\rho_{b,c-s} = \frac{\rho_{b,c}+\frac{\rho_{b,c}-\rho_s}{\rho_{b,c}\rho_s-1}\exp\left(-2k_b^*L_{ai}\right)}{1+\rho_{b,c}\frac{\rho_{b,c}-\rho_s}{\rho_{b,c}\rho_s-1}\exp\left(-2k_b^*L_{ai}\right)}$
Diffuse radiation extinction coefficient for black leaves.	$k_d = \frac{-\ln(\tau_d)}{L_{ai}}$ $\tau_d = 2\int_0^{\pi/2}\exp\left(-k_bL_{ai}\right)\sin\psi\cos\psi d\psi$
Diffuse radiation extinction coefficient	$k_d^* = k_d\sqrt{\alpha}$
Diffuse radiation canopy-soil reflectance	$\rho_{b,c-s} = \frac{\rho_{b,c}+\frac{\rho_{b,c}-\rho_s}{\rho_{b,c}\rho_s-1}\exp\left(-2k_d^*L_{ai}\right)}{1+\rho_{b,c}\frac{\rho_{b,c}-\rho_s}{\rho_{b,c}\rho_s-1}\exp\left(-2k_d^*L_{ai}\right)}$

Absorbed long-wave radiation:

$$L_{abs-soil} = \left(1-f_{can}\right)L_i \quad (0.17)$$

$$L_{abs-snl} = f_{can}f_{snl}L_i \quad (0.18)$$

$$L_{abs-shl} = f_{can}\left(1-f_{snl}\right)L_i \quad (0.19)$$

where L_i is the incoming long-wave radiation from the atmosphere. The total (PAR, NIR and long-wave) absorbed radiation by soil, sunlit and shaded leaves can now be estimated as:

$$R_{abs-soil} = I_{abs-soil}^{PAR} + I_{abs-soil}^{NIR} + L_{abs-soil} \quad (0.20)$$

$$R_{abs-snl} = I_{abs-snl}^{PAR} + I_{abs-snl}^{NIR} + L_{abs-snl} \quad (0.21)$$

$$R_{abs-shl} = I_{abs-shl}^{PAR} + I_{abs-shl}^{NIR} + L_{abs-shl} \quad (0.22)$$

The absorbed net radiation for the soil is estimated as:

$$R_{n-soil} = R_{abs-soil} - L_{o-soil} = R_{abs-soil} - \left(1-f_{can}\right)\varepsilon_s\sigma T_s^4 = R_{abs-soil} - \left(1-f_{can}\right)\varepsilon_s\sigma\left(T_a + \left(T_s - T_a\right)\right)^4$$
$$\approx R_{abs-soil} - \left(1-f_{can}\right)\varepsilon_s\sigma T_a^4 - \left(1-f_{can}\right)4\varepsilon_s\sigma T_a^3\left(T_s - T_a\right) \equiv R_{abs-soil}^{Eq} - G_{soil}^R\left(T_s - T_a\right) \quad (0.23)$$

where σ is Stefan-Boltzmann constant (5.67 10^{-8} W m^{-2} K^{-1}), $R_{abs-soil}^{Eq}\left(= R_{abs-soil} - \left(1-f_{can}\right)\varepsilon_s\sigma T_a^4\right)$ is absorbed equilibrium net radiation for the soil [W m^{-2}] and $G_{soil}^R\left(=\left(1-f_{can}\right)4\varepsilon_s\sigma T_a^3\right)$ is soil radiative conductance [W m^{-2} K^{-1}]. Correspondingly, the absorbed net radiation for sunlit and shaded leaves can be written as:

$$R_{n-snl} \approx R_{abs-snl}^{Eq} - G_{snl}^R\left(T_{snl} - T_a\right) \quad (0.24)$$

$$R_{n-shl} \approx R_{abs-shl}^{Eq} - G_{shl}^R\left(T_{shl} - T_a\right) \quad (0.25)$$

where $R_{abs-snl}^{Eq}\left(= R_{abs-snl} - f_{can}f_{snl}\varepsilon_s\sigma T_a^4\right)$ and $R_{abs-shl}^{Eq}\left(= R_{abs-shl} - f_{can}\left(1-f_{shl}\right)\varepsilon_s\sigma T_a^4\right)$ is absorbed equilibrium net radiation for the sunlit and shaded leaves, respectively, and $G_{snl}^R\left(= f_{can}f_{snl}4\varepsilon_s\sigma T_a^3\right)$ and $G_{shl}^R\left(= f_{can}\left(1-f_{snl}\right)4\varepsilon_s\sigma T_a^3\right)$ is soil radiative conductance for sunlit and shaded leaves, respectively.

Sensible heat fluxes

The sensible heat fluxes (H_{atm}, $H_{soil\to c}$, $H_{snl\to c}$, and $H_{shl\to c}$) are estimation of as:

$$H_{atm} = c_p\rho_a g_a\left(T_c - T_a\right) = G_{atm}^H\left(T_c - T_a\right) \quad (0.26)$$

$$H_{soil\to c} = c_p\rho_a g_{soil\to c}^H\left(T_s - T_c\right) = G_{soil\to c}^H\left(T_s - T_c\right) \quad (0.27)$$

$$H_{snl\to c} = c_p\rho_a g_{snl\to c}^H\left(T_{snl} - T_c\right) = G_{snl\to c}^H\left(T_{snl} - T_c\right) \quad (0.28)$$

$$H_{shl\to c} = c_p\rho_a g_{shl\to c}^H\left(T_{shl} - T_c\right) = G_{shl\to c}^H\left(T_{shl} - T_c\right) \quad (0.29)$$

where c_p is the specific heat of air (1005 J kg^{-1} K^{-1}), ρ_a is the density of air [kg m^{-3}], g_a, $g_{soil\to c}^H$, $g_{snl\to c}^H$, and $g_{shl\to c}^H$ are conductances corresponding to the fluxes [m s^{-1}], T_c, T_{snl}, and T_{shl} is canopy air temperature, and temperature of sunlit and shaded leaves, respectively. The estimation of the conductances are given in sections below.

Latent heat fluxes

The latent heat fluxes (λE_{atm}, $\lambda E_{snl\to c}$, and $\lambda E_{shl\to c}$) are estimation of as:

$$\lambda E_{atm} = \frac{c_p\rho_a g_a}{\gamma}\left(e_c - e_a\right) = G_{atm}^w\left(e_c - e_a\right) \quad (0.30)$$

$$\lambda E_{snl\to c} = \frac{c_p\rho_a g_{snl\to c}^w}{\gamma}\left(e^*\left(T_{snl}\right) - e_c\right) = G_{snl\to c}^w\left(e^*\left(T_{snl}\right) - e_c\right) \quad (0.31)$$

$$\lambda E_{shl\to c} = \frac{c_p\rho_a g_{shl\to c}^w}{\gamma}\left(e^*\left(T_{shl}\right) - e_c\right) = G_{shl\to c}^w\left(e^*\left(T_{shl}\right) - e_c\right) \quad (0.32)$$

where γ is psychrometer constant, g_a^w, $g_{snl\to c}^w$, and $g_{shl\to c}^w$ are conductances corresponding to the fluxes [m s^{-1}], T_c, T_{snl}, and T_{shl} is canopy air temperature, and temperature of sunlit and shaded leaves, respectively. $e^*\left(T\right)$ is saturation vapour pressure at the temperature T.The estimation of the conductances are given in sections below.

Introducing the Penman approximation eq. (1.31) and eq. (1.32) can be rewritten:

$$\lambda E_{snl\to c} = G^{w}_{snl\to c}\left(e^{*}\left(T_a\right)+s\left(T_{snl}-T_a\right)-e_c\right) \quad (0.33)$$

$$\lambda E_{shl\to c} = G^{w}_{shl\to c}\left(e^{*}\left(T_a\right)+s\left(T_{shl}-T_a\right)-e_c\right) \quad (0.34)$$

where s is slope of the saturation vapour pressure curve vs. temperature. The estimation of the conductances are given in sections below.

Conservation of energy

Considering the tree components, soil, sunlit and shaded leaves, separately yield tree conservation of energy equations, viz. eq. (1.5), eq. (1.6), and eq. (1.7). These equations may now be rewritten. Introducing eq. (1.23), eq. (1.8), and eq. (1.27), in eq. (1.5) yields:

$$R^{Eq}_{abs-soil} - G^{R}_{soil}\left(T_s - T_a\right) = \frac{k_h}{z_1}\left(T_S - T_{z1}\right) + G^{H}_{soil\to c}\left(T_s - T_c\right) + \lambda E_{soil\to c} \quad (0.35)$$

Similarly, introducing eq. (1.24), eq. (1.28), and eq. (1.33), in eq. (1.6) yields;

$$R^{Eq}_{abs-snl} - G^{R}_{snl}\left(T_{snl} - T_a\right) = G^{H}_{snl\to c}\left(T_{snl} - T_c\right) + G^{w}_{snl\to c}\left(e^{*}\left(T_a\right)+s\left(T_{snl}-T_a\right)-e_c\right) \quad (0.36)$$

And introducing eq. (1.25), eq. (1.29), and eq. (1.34), in eq. (1.7) yields:

$$R^{Eq}_{abs-shl} - G^{R}_{shl}\left(T_{shl} - T_a\right) = G^{H}_{shl\to c}\left(T_{shl} - T_c\right) + G^{w}_{shl\to c}\left(e^{*}\left(T_a\right)+s\left(T_{shl}-T_a\right)-e_c\right) \quad (0.37)$$

Introducing eq. (1.26), eq. (1.27), eq. (1.28), and eq. (1.29), in eq. (1.1) yields:

$$G^{H}_{atm}\left(T_c - T_a\right) = G^{H}_{soil\to c}\left(T_s - T_c\right) + G^{H}_{snl\to c}\left(T_{snl} - T_c\right) + G^{H}_{shl\to c}\left(T_{shl} - T_c\right) \quad (0.38)$$

And introducing eq. (1.30), eq. (1.33), and eq. (1.34), in eq. (1.2) yields:

$$G^{w}_{atm}\left(e_c - e_a\right) = G^{w}_{snl\to c}\left(e^{*}\left(T_a\right)+s\left(T_{snl}-T_a\right)-e_c\right) + G^{w}_{shl\to c}\left(e^{*}\left(T_a\right)+s\left(T_{shl}-T_a\right)-e_c\right) + \lambda E_{soil\to c} \quad (0.39)$$

Determination of state variables and fluxes

Assuming that the state variables $T_s, T_c, T_{snl}, T_{shl}$, and e_c are the only unknown variables then they can be found by solving eq. (1.35) through (1.39). When $T_s, T_c, T_{snl}, T_{shl}$, and e_c are known then the system is determined and the appropriate sensible heat, latent heat, and raditive fluxes can be calculated. However, several of the conductances depend on the unknown state variables. Hence, the equations must be solved in an iterative manner.

Aerodynamic Resistance

Displacement height (d [m]) and roughness length for momentum (z_0 [m]) is according to Shuttleworth and Gurney (1990) estimated as:

$$d = 1.1 h_{veg} \ln\left(1 + \sqrt[4]{c_d L_{ai}}\right) \quad (0.40)$$

$$z_0 = \begin{cases} z_0' + 0.3 h_{veg}\sqrt{c_p L_{ai}} & 0.0 \le c_p L_{ai} < 0.2 \\ 0.3\left(h_{veg} - d\right) & 0.2 \le c_p L_{ai} < 1.5 \end{cases} \quad (0.41)$$

where h_{veg} is vegetation height [m], L_{ai} is leaf area index, c_p is an effective drag coefficient $\left(c_p \approx 0.07\right)$, and z_0' is roughness length for momentum for bare soil.

The roughness length for heat is

$$z_{0h} = z_0 / 7 \quad (0.42)$$

The aerodynamic stability indicator (η) is according to Choudhury (1986) estimated as:

$$\eta = \frac{5\left(z_r - d\right) g \left(T_0 - T_a\right)}{T_a u_z^2} \qquad (0.43)$$

where z_r screen-height [m], g is acceleration due to gravity (9.82 m s^{-2}), T_a and u_z are air temperature (K) and wind speed (m s^{-1}) at screen-height, and T_0 is surface temperature (K). $\eta < 0$ corresponds to a stable atmosphere while $\eta > 0$ corresponds to an unstable atmosphere.

Aerodynamic resistance, r_a [s m^{-1}] between canopy source height (canopy point) and reference (screen) height above the canopy is estimated by:

$$r_a = \begin{cases} \dfrac{1}{\kappa^2 u_z}\left[\ln\left(\dfrac{z_r - d}{z_0}\right) - \psi_*\right]\left[\ln\left(\dfrac{z_r - d}{z_{0h}}\right) - \psi_*\right] & \text{for } \eta \le 0 \\ \dfrac{\ln\left(\dfrac{z_r - d}{z_0}\right)\ln\left(\dfrac{z_r - d}{z_{0h}}\right)}{\kappa^2 u_z \left(1+\eta\right)^{3/4}} & \text{for } \eta > 0 \end{cases} \qquad (0.44)$$

where:

$$\psi_* = \frac{\psi_a - \sqrt{\psi_a^2 - 4\left(1+\eta\right)\eta\left(\ln\left(\dfrac{z_r - d}{z_0}\right)\right)^2}}{2\left(1+\eta\right)}$$

$$\psi_a = \ln\left(\frac{z_r - d}{z_{0h}}\right) + 2\eta \ln\left(\frac{z_r - d}{z_0}\right) \qquad (0.45)$$

When $\psi_* < -5$, then ψ_* is set to -5 (Choudhury, 1986) .

Aerodynamic conductance g_a is estimate as:

$$g_a = \frac{1}{r_a} \qquad (0.46)$$

The aerodynamic conductance depends on the following state variables: vegetation height $\left(h_{veg}\right)$, leaf area index $\left(L_{ai}\right)$, wind speed $\left(u_z\right)$, air temperature $\left(T_a\right)$, and surface temperature $\left(T_0\right)$.

Boundary layer conductance of sunlit and shaded leaves

Diffusivity of heat, D_h [m s^{-1}], water vapor, D_w [m s^{-1}], and CO_2, D_C [m s^{-1}]:

$$D_h = 1.869\ 10^{-5}\left(\frac{101300\ \text{Pa}}{P_{surf}}\right)\left(\frac{T_a}{273.16\ \text{K}}\right)^{1.81}\ \text{m}^2\text{s}^{-1} \quad (0.47)$$

$$D_w = 2.178\ 10^{-5}\left(\frac{101300\ \text{Pa}}{P_{surf}}\right)\left(\frac{T_a}{273.16\ \text{K}}\right)^{1.81}\ \text{m}^2\text{s}^{-1} \quad (0.48)$$

$$D_C = 1.381\ 10^{-5}\left(\frac{101300\ \text{Pa}}{P_{surf}}\right)\left(\frac{T_a}{273.16\ \text{K}}\right)^{1.81}\ \text{m}^2\text{s}^{-1} \quad (0.49)$$

where P_{surf} is air pressure at the surface (101300 Pa unless otherwise specified) and T_a is air temperature (at screen-height) [K]).

Leaf boundary layer conductance for heat, eq. (1.50), water vapor, eq. (1.51), and CO_2, eq. (1.52), due to free convection (Houborg, 2006):

$$g_{lbf}^{H} = D_h \left(\frac{\sqrt[4]{g w_l^3 \nu^{-2} \left(T_l - T_a\right) T_a^{-1}}}{w_l} \right) \quad (0.50)$$

$$g_{lbf}^{w} = \begin{cases} 0.5 g_{lbf}^{H} \left(D_w / D_h\right) & \text{hypostomotous leaves} \\ g_{lbf}^{H} \left(D_w / D_h\right) & \text{amphistomatous leaves} \end{cases} \quad (0.51)$$

$$g_{lbf}^{CO_2} = g_{lbf}^{H} \left(D_C / D_h\right) \quad (0.52)$$

where g is acceleration due to gravity (9.82 m s^{-2}), w_l is leaf width (0.05 m unless otherwise specified), ν is molecular viscosity ($\nu = 1.327\ 10^{-5} \left(101300\ \text{Pa} / P_{surf}\right)\left(T_a / 273.16\ \text{K}\right)^{1.81}$ $m^2 s^{-1}$), and T_l is leaf temperature [K] (sunlit or shaded leaves).

Leaf boundary layer conductance for heat, eq.(1.53), water vapor, eq.(1.54), and CO_2, eq.(1.55), due to forced convection (Houborg, 2006):

$$g_{lbu}^{H} = 0.006 \sqrt{\frac{u_z \exp\left(-k_u L_{ai}\right)}{w_l}} \quad (0.53)$$

$$g_{lbu}^{w} = \begin{cases} 0.5 g_{lbu}^{H} \left(D_w / D_h\right) & \text{hypostomotous leaves} \\ g_{lbu}^{H} \left(D_w / D_h\right) & \text{amphistomatous leaves} \end{cases} \quad (0.54)$$

$$g_{lbu}^{CO_2} = g_{lbu}^{H} \left(D_C / D_h\right) \quad (0.55)$$

where u_z is wind speed (m s^{-1}) at screen-height, k_u parameter describing the vertical variation of wind speed within the canopy ($k_u = 0.5$, Houborg (2006)), and L_{ai} is leaf area index.

Applying the "big leaf" approach, leaf boundary layer conductance is up-scaled to canopy level according to Wang and Leuning (1998). The total boundary conductance at canopy level for heat for sunlit leaves, eq. (1.56) , and shaded leaves, eq. (1.57), due to the combined effect of free and forced convection is:

$$g_{b-snl}^{H} = L_{ai}^{snl} g_{lbf-snl}^{H} + \frac{1 - \exp\left(-\left(0.5 k_u + k_b\right) L_{ai}\right)}{0.5 k_u + k_b} g_{lbu}^{H} \quad (0.56)$$

$$g_{b-shl}^{H} = L_{ai}^{shl} g_{lbf-shl}^{H} + \left[\frac{1 - \exp\left(-0.5 k_u L_{ai}\right)}{0.5 k_u} - \frac{1 - \exp\left(-\left(0.5 k_u + k_b\right) L_{ai}\right)}{0.5 k_u + k_b} \right] g_{lbu}^{H} \quad (0.57)$$

where L_{ai}^{snl} and L_{ai}^{shl} are the leaf area index of sunlit and shaded leaves, respectively; $g_{lbf-snl}^{H}$ and $g_{lbf-shl}^{H}$ are leaf boundary layer conductance for heat of sunlit and shaded leaves, respectively (eq. (1.50), T_l = leaf temperature of corresponding sunlit and shaded leaves); and k_b is extinction coefficient for black leaves in direct-beam irradiance.

g_{b-snl}^{w} and g_{b-shl}^{w} are estimated by eq. (1.56) and eq. (1.57), respectively by substituting the appropriate leaf boundary layer conductances. Similarly, $g_{b-snl}^{CO_2}$ and $g_{b-shl}^{CO_2}$ are estimated.

The boundary layer conductances depend on the following state variables: total leaf area index, $\left(L_{ai}\right)$, sunlit leaf area index, $\left(L_{ai}^{snl}\right)$, shaded leaf area index, $\left(L_{ai}^{shl}\right)$, wind speed $\left(u_z\right)$, air temperature $\left(T_a\right)$, and leaf temperature of sunlit $\left(T_{snl}\right)$ and shaded leaves $\left(T_{shl}\right)$.

The conductance for sensible heat from sunlit and leaf surface into the canopy air is given by eq. (1.58) and eq. (1.59), repectively:

$$g_{snl\to c}^{H} = g_{b-snl}^{H} \quad (0.58)$$

$$g_{shl\to c}^{H} = g_{b-shl}^{H} \quad (0.59)$$

And the conductance for latent heat from the stomata of sunlit and leaf surface into the canopy air is given by eq. (1.60) and eq. (1.61), repectively:

$$g_{snl\to c}^{w} = \frac{g_{b-snl}^{w} g_{s-snl}^{w}}{g_{b-snl}^{w} + g_{s-snl}^{w}} \quad (0.60)$$

$$g_{shl\to c}^{w} = \frac{g_{b-shl}^{w} g_{s-shl}^{w}}{g_{b-shl}^{w} + g_{s-shl}^{w}} \quad (0.61)$$

where g_{s-snl}^{w} and g_{s-shl}^{w} is the bulk stomata conductance for sunlit and shaded leaves, respectively [m s^{-1}].

Soil aerodynamic conductance

The conductance for transport of heat between the soil surface and a height of the canopy point ($g_{soil\to c}^{H}$, [m s^{-1}]) can according to Norman et al. (1995) be estimated as:

$$g_{snl\to c}^{H} = 0.004 + 0.012\,u_s \quad (0.62)$$

where u_s is a wind speed characterizing the conditions in the canopy air space just above the soil surface [m s^{-1}]. u_s is estimatet as:

$$u_s = u_c \exp\left(-a\left(1 - \frac{0.05}{h_{veg}}\right)\right) \quad (0.63)$$

$$a = 0.28\, L_{ai}^{2/3} h_{veg}^{1/3} l_m^{-1/3}$$

where u_c is a wind speed at the top of the canopy [m s^{-1}], L_{ai} is leaf area index, h_{veg} is vegetation height [m], and l_m is mean leaf size [m] given by four times the leaf area divided by the perimeter. If we assume elliptical leaves and that the major axis equals the leaf width w_l [m] and the minor axis equals ½w_l then we get $l_m \approx 1.26 w_l$.

The stability is characterized by the Monin-Obukhov length (L_{mo} [m]):

$$L_{mo} = -\frac{r_a u_*^3 T_a}{\kappa g\left(T_s - T_a\right)} \quad (0.64)$$

where r_a is aerodynamic resistance [s m^{-1}], u_* is friction velocity [m s^{-1}], T_a is air temperature (at screen-height) [K], κ is von Karman's constant ($\kappa = 0.41$), g is acceleration due to gravity (9.82 m s^{-2}), and T_s is surface temperature (K). L_{mo} is positive in stable conditions and negative in unstable conditions.

The friction velocity is:

$$u_* = \frac{\kappa u_z}{\ln\left[\left(z_r - d\right)/z_0\right]} \quad (0.65)$$

where u_z is wind speed (m s^{-1}) at screen-height, z_r screen-height [m], d is displacement height [m], and z_0 is roughness length for momentum [m].

The wind speed at the top of the canopy u_c [m s^{-1}] is estimated as:

$$u_c = \begin{cases} u_z \left[\dfrac{\ln\left[\left(h_{veg} - d\right)/z_0\right]}{\ln\left[\left(z_r - d\right)/z_0\right] + 4.7\left(z_r - d\right)/L_{mo}} \right] & \text{for } L_{mo} \geq 0 \\ u_z \left[\dfrac{\ln\left[\left(h_{veg} - d\right)/z_0\right]}{\ln\left[\left(z_r - d\right)/z_0\right] - \psi} \right] & \text{for } L_{mo} < 0 \end{cases}$$

$$\psi = \ln\left[\left(\frac{1+y}{2}\right)^2 \left(\frac{1+y^2}{2}\right)\right] - 2\arctan\left(y\right) + \frac{\pi}{2} \quad (0.66)$$

$$y = \left(1 - 16\left(\frac{z_r - d}{L_{mo}}\right)\right)^{-0.25}$$

where h_{veg} is vegetation height [m].

The soil aerodynamic conductance depends on the following state variables: vegetation height$\left(h_{veg}\right)$, leaf area index$\left(L_{ai}\right)$, wind speed $\left(u_z\right)$, air temperature$\left(T_a\right)$, and soil surface temperature$\left(T_s\right)$.

Canopy physiological conductance for CO_2 transfer

The Ball-Berry-Leuning model (molar conductance [mol m^{-2} s^{-1}]) is described in the Annex on "The stomata-photosynthesis model and the sunlit-shadow radiation model in DAISY". The model has been modified in order to take into account the effects of ABA. The modified Ball-Berry-Leuning model (molar conductance [mol m^{-2} s^{-1}]) for leaf layer *i* is:

$$g_{s,i}^{'CO_2} = g_0 + m\frac{A_n}{\left(c_s - \Gamma\right)h_s}\exp\left(-\beta_1 c_{ABA}\right) \quad (0.67)$$

where g_0 is a stomatal intercept factor, m is an empirical vegetation constant, A_n is the net leaf photosynthesis rate [mol m^{-2} s^{-1}], c_s is the leaf surface CO_2 concentration [mol m^{-3}], Γ the CO_2 compensation point [mol m^{-3}], h_s is the relative humidity at the leaf surface, β_1 is an empirical constant and c_{ABA} is the ABA concentration in the xylem sap.

The physiological conductance can be converted to [m/s] by:

$$g_{s,i}^{CO_2} = \frac{RT}{P} g_{s,i}^{'CO_2} \quad (0.68)$$

Up-scaling from leaf to canopy yields the stomata conductance for water vapor:

$$g_s^w = \begin{cases} 2\left(D_w / D_C\right) \sum_i^{n_{LAI}} \Delta L_{ai} g_{s,i}^{CO_2} & \text{hypostomotous leaves} \\ \left(D_w / D_C\right) \sum_i^{n_{LAI}} \Delta L_{ai} g_{s,i}^{CO_2} & \text{amphistomatous leaves} \end{cases} \quad (0.69)$$

where n_{LAI} is the number of leaf layers and ΔL_{ai} is the size of the leaf layer.

References

Choudhury, BJ, Reginato, RJ, and Idso, SB (1986). An analysis of infrared temperature observations over wheat and calculation of latent heat flux. Agricultural and Forest Meteorology, 37, 75-88.

Houborg, R (2006) Inferences of key environmental an vegetation biophysical controls for use in regional-scale SVAT modeling using Terra and Agua MODIS and weather prediction data. PhD dissertation, Institute of Geography, University of Copenhagen,

Norman, JM, Kustas, WP, and Humes, KS (1995) Source approach for estimating soil and vegetation energy fluxes in observations of directional radiometric surface temperature. Agricultural and Forest Meteorology, 77, 263-293.

Shuttleworth, WJ and Gurney, RJ (1989). The theoretical relationship between foliage temperature and canopy resistance in sparse crops. Quarterly Journal of the Royal Meteorological Society, 116, 497-519.

Annex 3.7 Detailed description of the processes in the SALTMED

The first version of the SALTMED model has been described in detail in Ragab (2002) with some examples of applications. The SALTMED model includes the following key processes: evapotranspiration, plant water uptake, water and solute transport under different irrigation systems, nitrogen dynamics and dry matter & biomass production. A brief description of the above mentioned processes will be given in the following sections.

1. Evapotranspiration, water uptake and Water & solute flow equations

Evapotranspiration

Evapotranspiration has been calculated using the Penman-Monteith equation according to the modified version of FAO (1998) in the following form:

$$ET_o = \frac{0.408\Delta(R_n - G) + \gamma \frac{900}{T+273} U_2 (e_s - e_a)}{\Delta + \gamma(1 + 0.34U_2)} \qquad (1a)$$

where ET_o is the reference evapotranspiration, (mm day^{-1}), R_n is the net radiation, (MJ m^{-2} day^{-1}), G is the soil heat flux density, (MJ m^{-2} day^{-1}), T is the mean daily air temperature at 2 m height, (^oC), Δ is the slope of the saturated vapour pressure curve, (kPa $^oC^{-1}$), γ is the psychrometric constant, 66 Pa $^oC^{-1}$, e_s is the saturated vapour pressure at air temperature (kPa), e_a is the prevailing vapour pressure (kPa), and U_2 is the wind speed at 2 m height (m s^{-1}) . The calculated ET_o here is for short well-watered green grass. In this formula, a hypothetical reference crop with an assumed height of 0.12 m, a fixed surface resistance of 70 s m^{-1} and an albedo of 0.23 were considered.

In presence of stomata / canopy surface resistance data, one could use the widely used equation Penman-Monteith (1965) in the following form:

$$\lambda E_p = \frac{\Delta R_n + \rho C_p \frac{(e_s - e)}{r_a}}{\Delta + \gamma \frac{(1 + r_s)}{r_a}} \qquad (1b)$$

where rs and ra are the bulk surface and aerodynamic resistances (s m-1).
The r_s can be measured or calculated from environmental and meteorological parameter or from the Leaf water potential and Absicic Acid, ABA.

In the absence of meteorological data (temperature, radiation, wind speed etc.) and if Class A pan evaporation data are available, the SALTMED model can use these data to calculate ET_o according to the FAO (1998) procedure. The model can also calculate the net radiation from solar radiation according to the FAO (1998) procedure if net radiation data is not available.

The crop evapotranspiration ET_c is calculated as:

$$ET_c = ET_o(K_{cb} + K_e) \quad (2)$$

where K_{cb} is the crop transpiration coefficient (known also as basal crop coefficient) and K_e is the soil evaporation coefficient. The values of K_{cb} and K_c, (the crop coefficient) for each growth stage and the duration of each growth stage for different crops are available in the model's database. These data can be used in the absence of measured values. K_e is calculated according to FAO (1998). K_{cb} and K_c are adjusted according to FAO (1998) for wind speed and relative humidity different from 2 m s^{-1} and 45% respectively. The SALTMED model runs with a daily time step and uses K_{cb} and K_e. The latter are not universal and their values differ according to climatic conditions and other factors.

Plant Water Uptake in the Presence of Saline Water

The Actual Water Uptake Rate
The formula adopted in the SALTMED model is that suggested by Cardon and Letey (1992), which determines the water uptake S (d^{-1}) as:

$$S(z,t) = \left[\frac{S_{\max}(t)}{1 + \left(\frac{a(t)h + \pi}{\pi_{50}(t)} \right)^3} \right] \lambda(z,t) \quad (3)$$

where

$\lambda(z) = 5/3L$ for $z \leq 0.2L$ (4)

$= 25/12L * (1 - z/L)$ for $0.2L < z \leq L$ (4a)

$= 0.0$ for $z > L$ (4b)

where $S_{max}(t)$ is the maximum potential root water uptake at the time *t*; *z* is the vertical depth taken positive downwards, $\lambda(z,t)$ is the depth-and time-dependent fraction of total root mass, L is the maximum rooting depth, *h* is the matric pressure head, π is the osmotic pressure head; π_{50} (t) is the time-dependent value of the osmotic pressure at which $S_{max}(t)$ is reduced by 50%, and *a*(t) is a weighing coefficient that accounts for the differential response of a crop to matric and solute pressure. The coefficient *a*(t) equals $\pi_{50}(t)/h_{50}(t)$ where $h_{50}(t)$ is the matric pressure at which $S_{max}(t)$ is reduced by 50%.

The Maximum Water Uptake S_{max} (t). S_{max} (t)is calculated as:

$$S_{max}(t) = ET_o(t) * K_{cb}(t) \quad (5)$$

The values of h_{50} and π_{50} can be obtained from experiments or from literature such as FAO (1992).

The Rooting Depth

The rooting depth was assumed to follow the same course as the crop coefficient K_c. Therefore, it has been described by the following equation:

$$\text{Root depth (t)} = [\text{Root depth}_{min} + (\text{Root depth}_{max} - \text{Root depth}_{min})] * K_c(t) \quad (6)$$

The maximum root depth is available either from direct measurements or from the literature.

The Rooting Width

Compared with rooting depth, there is a very little information in the literature on lateral extent of the rooting systems of field crops over time. Therefore, a simple equation has been suggested as follows:

$$\text{Root width (t)} = [\text{Root width / Root depth}] \text{ ratio} * \text{root depth (t)} \quad (7)$$

The [Root width/Root depth] ratio is dependant on the crop and soil type and other factors. It can be obtained either from experimental data or from the literature. During the growth, new roots enter new grid cells.

The model then calculates the water uptake only from those cells with roots. The model grid cells are identified by 0, 1 or 2 . The value of 0 is associated with cells with no roots and 1 for cells fully occupied with roots and 2 for cells with partial root presence. The model produces a data file showing the two – dimensional root distribution for every day of the simulation.

Relative and Actual Crop Yield

The Relative Crop Yield, RY

Due to the unique and strong relationship between water uptake and biomass production, and hence the final yield, the relative crop yield RY is estimated as the sum of the actual water uptake over the season divided by the sum of the maximum water uptake (under no water and salinity stress conditions) as:

$$RY = \frac{\sum S(x,z,t)}{\sum S_{max}(x,z,t)} \quad (8)$$

where x, z are the horizontal and vertical coordinates of each grid cell that contain roots, respectively.

The Actual Yield, AY

The actual yield, AY is simply obtainable by:

$$AY = RY * Y_{max} \quad (9)$$

where Y_{max} is the maximum yield obtainable in a given region under optimum and stress-free condition. The other option to obtain the actual yield is by calculating the daily biomass production and obtaining the actual yield from the harvest index times the total dry matter (see the relevant section on crop growth and dry matter).

Water and Solute Flow

The water flow in soils was described mathematically by the well-known Richard's equation. It is a partial non-linear differential equation, partial in time and space. It is based on two soil physical principles: Darcy's law and mass continuity. Darcy's law reads:

$$q = -K(h)\frac{\delta H}{\delta Z} \tag{10}$$

Where q is the water flux, *K(h)* is the hydraulic conductivity as a function of soil water pressure head, *Z* is the vertical coordinate directed downwards with its origin at soil surface, and *H* is the hydraulic head which is the sum of the gravity head, Z, and the pressure head, ψ, thus:

$$H = \psi + Z \tag{11}$$

The vertical transient-state flow water in a stable and uniform segment of the root zone can be described by a Richard's type equation as:

$$\frac{\partial\theta}{\partial t} = -\frac{\partial}{\partial z}\left[K(\theta)\frac{\partial(\psi + z)}{\partial z}\right] - S_w \tag{12}$$

where θ is volume wetness; *t* is the time; *z* is the depth; *K (θ)* is the hydraulic conductivity (a function of wetness); ψ is the matrix suction head; and S_w is the sink term representing extraction by plant roots. The movement of solute in the soil system, its rate and direction, depends greatly on the path of water movement, but it is also determined by diffusion and hydrodynamic dispersion. If the latter effects are negligible, solute flow by convection can be formulated (Hillel, 1977) as:

$$J_c = qc = \bar{v}\theta c \tag{13}$$

where J_c is the solute flux density; *q* is the water flux density of the water; *c* the concentration of solute in the flowing water and $\bar{v}$ is the average velocity of the flow. The rate of a diffusion of a solute (J_d) in bulk water at rest is related (by Fick's law) to the concentration gradient as:

$$J_d = D_o\left(\partial c/\partial x\right) \tag{14}$$

where D_0 is the diffusion coefficient. In soil the diffusion coefficient, D_s, is decreased due to the fact that the liquid phase occupies only a fraction of soil volume, and also due to the tortuous nature of the path. It can therefore be expressed according to the following equation:

$$D_s = D_0\theta\xi \tag{15}$$

$$\xi = \theta^{7/3} / \theta_s^{\,2} \tag{16}$$

where ξ is the tortuosity, an empirical factor smaller than unity, which can be expected to decrease with decreasing θ as shown in Equation 16 (Šimůnek and Suarez, 1994). The convection flux generally causes hydrodynamic dispersion too, an effect that depends on the microscopic non-uniformity of flow velocity in the various pores. Thus a sharp boundary between two miscible

solutions becomes increasingly diffuse about the mean position of the front. For such a case, the diffusion coefficient has been found by Bresler (1975) to depend linearly on the average flow velocity $\bar{v}$, as follows:

$$D_h = \alpha \bar{v} \tag{17}$$

where α is an empirical coefficient. By the combination of the diffusion, the dispersion and the convection the overall flux of solute can be obtained as:

$$J = -\left(D_h + D_s\right)\left(\partial c / \partial x\right) + \bar{v}\theta c \tag{18}$$

If one takes the continuity equation into consideration, one-dimensional transient movement of a non-interacting solute in soil can be expressed as:

$$\frac{\partial(\theta c)}{\partial t} = \frac{\partial}{\partial z}\left(D_a \frac{\partial c}{\partial z}\right) - \frac{\partial(qc)}{\partial z} - S_s \tag{19}$$

in which *c* is the concentration of the solute in the soil solution, *q* is the convective flux of the solution, D_a is a combined diffusion and dispersion coefficient, and S_s is a sink term for the solute representing root adsorption/uptake.

Under irrigation from a trickle line source, the water and solute transport can be viewed as two-dimensional flow and can be simulated by one of the following:
1) a "plane flow" model involving the Cartesian co-ordinates x and z. Plane flow takes place if one considers a set of trickle sources at equal distance and close enough to each other so that their wetting fronts overlap after a short time from the start of the irrigation.

2) a "cylindrical flow" model described by the cylindrical co-ordinates r and z.
Cylindrical flow takes place if one considers the case of a single trickle nozzle or a number of nozzles spaced far enough apart so that overlap of the wetting fronts of the adjacent sources does not take place. For a stable, isotropic and homogeneous porous medium, the two-dimensional flow of water in the soil can be described according to Bresler (1975) as:

$$\frac{\partial \theta}{\partial t} = \frac{\partial}{\partial x}\left[K(\theta)\frac{\partial \psi}{\partial x}\right] + \frac{\partial}{\partial z}\left[K(\theta)\frac{\partial(\psi + z)}{\partial z}\right] \tag{20}$$

where *x* is the horizontal co-ordinate; *z* is the vertical-ordinate (considered to be positive downward); K (θ) is the hydraulic conductivity of the soil. Considering isotropic and homogeneous porous media with principal axes of dispersion oriented parallel and perpendicular to the mean direction of flow, the hydrodynamic dispersion coefficient D_{ij} can be defined as follows:

$$D_{ij} = \lambda_T |V| \delta_{ij} + \left(\lambda_L - \lambda_T\right) V_i V_j / |V| + D_s(\theta) \tag{21}$$

where λ_L is the longitudinal dispersivity of the medium; λ_T is the transversal dispersivity of the medium; δ_{ij} is Kronecker delta (i.e., δ_{ij} =1 if i = j and δ_{ij} = 0 if i $\neq$ j) ; V_i and V_j are the *i*th and *j*th components of the average interstitial flow velocity V respectively, $V = (V^2_x + V^2_z)^{1/2}$ and D_s (θ) is the soil diffusion coefficient as defined in Equation 15.

If one considers only two dimensions and substituting D_{ij} , the salt flow equation becomes:

$$\frac{\partial(C\theta)}{\partial t} = \frac{\partial}{\partial x}\left(D_{xx}\frac{\partial C}{\partial x} + D_{xz}\frac{\partial C}{\partial z} - q_x C\right) + \frac{\partial}{\partial z}\left(D_{zz}\frac{\partial C}{\partial z} + D_{zx}\frac{\partial C}{\partial x} - q_z C\right) \qquad (22)$$

In the model, sprinkler, flood and basin irrigation are described by one-dimensional flow equations (e.g. Eqs 12 & 19). Furrow and trickle line source are described by 2-dimensional equations (e.g. Eqs 20 & 22). Trickle point source is described by cylindrical flow equations obtained by replacing x by the radius " r" and rearranging Equations 20 and 22 as given by Bresler (1975) and Fletcher Armstrong and Wilson (1983). The water and solute flow equations were solved numerically using a finite difference explicit scheme (Ragab et al., 1984).

Soil Hydraulic Parameters

Solving the water and solute transport equations require two soil water relations, namely the soil water content - water potential relation and the soil water potential - hydraulic conductivity relation. They were taken according to van Genuchten (1980).

Drainage

The model has two options for drainage. Two options are available, either free drainage or an impermeable layer at the bottom of the soil profile.

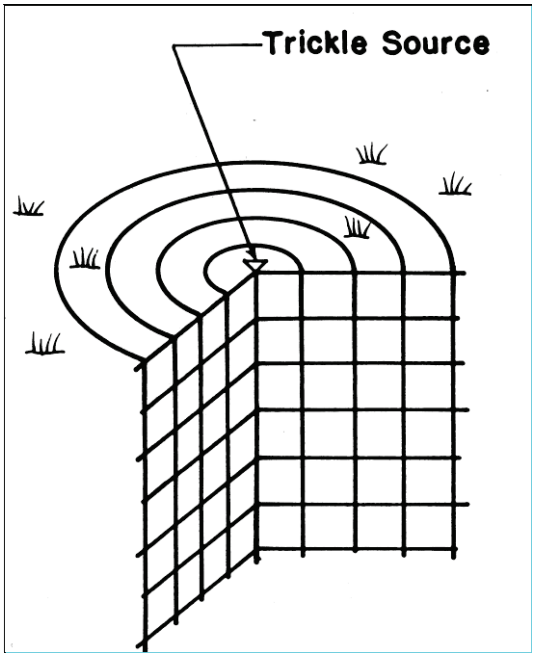

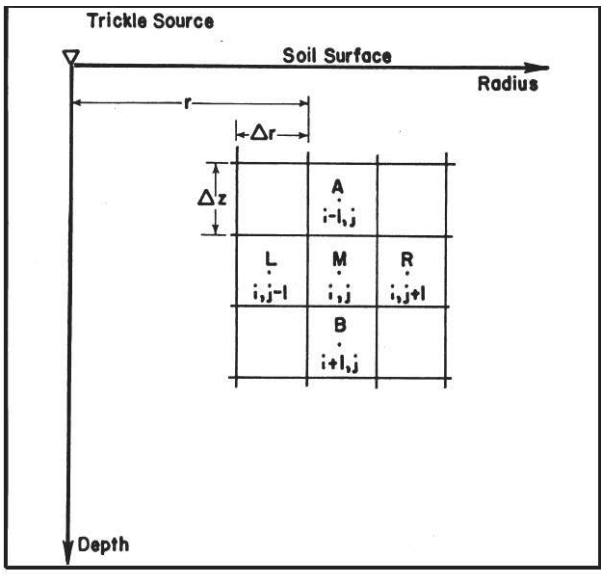

Example of the flow domain under drip irrigation

References

Bresler, E., 1975. Two-dimensional transport of solute during non-steady infiltration for a trickle source. Soil Sci. Soc. Amer. Proc. 39, 604-613.

Cardon, E.G., Letey, J., 1992. Plant water uptake terms evaluated for soil water and solute movement models. Soil Sci. Soc. Am. J. 56, 1876-1880.

FAO, 1998. Crop evapotranspiration, Irrigation and Drainage Paper No 56. Rome, Italy.
FAO, 1992. The use of saline waters for crop production. Irrigation and Drainage Paper No 48. Rome, Italy.
Fletcher Armstrong, C., Wilson, T.V., 1983. Computer model for moisture distribution in stratified soils under tickle source. Transactions of ASAE, 26: 1704-1709.
Hillel. D., 1977. Computer simulation of soil-water dynamics; a compendium of recent work. IDRC, Otawa, Canada, 214pp.
Ragab, R., 2002. A holistic generic integrated approach for irrigation, crop and field management: the SALTMED model. Environmental Modelling and Software, 17, 345-361.
Ragab, R., Feyen, J., Hillel, D., 1984. Simulating two-dimensional infiltration into sand from a trickle line source using the matric flux potential concept. Soil Sci. 137, 120-127.
Šimůnek, J., Suarez, D.L., 1994. Two-dimensional transport model for variably saturated porous media with major chemistry. Water Resources Research, 30, 1115-1133.
Van Genuchten, M. Th., 1980. A closed - form equation for predicting the hydraulic conductivity of unsaturated soils. Soil Sci. Soc. of Am. J. 44, 892-898.

2. Crop Growth and Biomass production

The approach used is very much based on the work of Eckersten and Jansson, 1991.

1- Increase in Biomass Δ q, g/m^2/day = Net Assimilation "NA"

Net Assimilation "NA" = Assimilation " A " – Respiration losses " R"

2- Assimilation rate,"A"per unit of area = E* I* f(Temp)* f(T)*f(Leaf-N) g/m^2/day

where

E = is the photosynthetic Efficiency, g dry matter / MJ (=~2.0)

I is the radiation input: $= Rs\,(1- e^{-k*LAI})$

Rs is global Radiation, MJ/m^2/day, k is extinction coefficient (~=0.6) and

LAI is the leaf area Index (m^2/m^2).

Rs is given in climate data, LAI is interpolated in SALTMED

Assimilation rate,"A"per unit of area = E* I* (stress factors related to Temperature, Transpiration and Leaf Nitrogen content)

References:

Eckersten, H and Jansson, P,.- E. 1991. Modelling water flow, nitrogen uptake and production for wheat. Fertilizer Research 27: 313-329.

3. Calculating the Stomata Conductance from the Absecic Acid, ABA

The modelling approach is based on Tardieu *et al.* (1993).

$gs = gs_{minimum} + \alpha * Exp (ABA * \beta * Exp (\sigma * \Psi_l))$

gs = Stomata conductance, mole/m^2/sec

$gs_{minimum}$ = mimimum Stomata conductance (*default 0.05 mole/m^2/sec)*

ABA = Absecic Acid concentration, daily values
(default 0.5 mmole/m^3)

Ψ_l = Leaf water potential in M pa, daily values,
(default -1.3 Mpa)

α, β, σ are fitting parameters, default values are :

Alpha, α	Beta, β	Sigma, σ
0.184	-2.69	-0.183

ABA and Ψ_l are given as daily values.

References

Tardieu, F, Zhang, J. and Gowing, D. J. G. 1993. Stomatal control by both [ABA] in the xylem sap and leaf water status: a test of a model for droughted or ABA-fed field-grown maize. Plant, Cell and environment .16:413-420.

4. Calculating the stomata Conductance from regression Equation:

The modelling approach for stomatal conductance is based on the multiplicative model described by Jarvis 1976 and modified by Korner et al. (1995).

Based on Jarvis (1967) and Korner (1994)

$g_s = g_{smax} * f(VPD) * f(T) * F(SW) * f(PAR)$

gsmax = Maximum Stomata conductance

f (VPD) is the relative effect of the VPD on stomata conductance
f(T) is the relative effect of the Temperature on stomata conductance
f (SW) is the relative effect of the soil water content on stomata conductance
f(PAR) is the relative effect of the radiation on stomata conductance

The sum of $\sum f(VPD) * f(T) * F(SW) * f(PAR) \leq 1$

f(VPD) = 1- [(VPD min – VPD) / (VPD min- VPD max)]

VPD is calculated on daily basis from Temperature and RH data given as daily values in the input file of the climate data .

VPD min and VPD max are either User input values or can be calculated first from the model code as the first thing before a dynamic run.

$F(T) = 1 - [(T - T\text{minimum}) / (T\text{optimum} - T\text{ minimum})]^2$

T is daily average Temperature given as input in climate data file

Tminimum and Toptimum are user input, C

$f(SW) = 0$ if soil water content, θ is $\leq$ soil water content at wilting point θ_{WP}

$f(SW) = [(\theta - \theta_{WP}) / (\theta_{fc} - \theta_{WP})]$ if $\theta_{WP} < \theta < \theta_{FC}$

$f(SW) = 1$ if $\theta_{FC} < \theta < \theta_{SAT}$

θ is the average Root zone soil water content can be obtained as average values of the fully rooted squares.

θ_{WP}, θ_{FC}, θ_{SAT} are Soil water content at wilting point, at Field Capacity and at saturation (or Porosity) given as input in the soil data base.

$F(PAR) = 1 - \exp(-\alpha * PFD)$

α is a user input $= 0.2$

PFD is Photons flux density micromole /m^2/sec (range : 0-900 , average is 450)

References

Emberson, L.D. Ashmore, M. R., and Cambridge, H.M. 1998. Development of Methodologies for Mapping Level II Critical Levels of Ozone. DETR Report no. EPG 1/3/82. Imperial College of London, London.

Jarvis, P. G. 1976. The iterepretation of the variations in leaf water potential and stomatal conductance found in canopies in the field. Philosophical. Transactions of the Royal Society. B273:593-610.

Körner, C. 1994. Leaf diffusive conductance in the major vegetative types of the globe. In Schulze, E. D., and Calwell, M.M . (Editors), Ecophysiology of Photosynthesis. Ecological Studies, vol.100. Springer Verlaag, Berlin, pp 463-490.

Pleijel, H., Danielsson, H., Vandermeiren, K., Blum, C., Colls, J, and Ojanpera, K. 2002. Stomatal conductance and ozone exposure in relation to potato tuber yield-results from the European CHIP programme. European Journal of Agronomy, 17:303-317.

5. Calculating Soil temperature from Air Temperature:

The top soil layer is the most biologically active layer where most of the organic matter decomposition and mineralization takes place. The microbial activity is affected by soil temperature of this layer. This temperature was found to be correlated to air temperature. The approach used here is to infer the soil temperature of the top layer (ploughing layer) from the air temperature based on the work of Kang et al. (2000) and Zheng et al. (1993).

For air temperature "A" and soil temperature " T ", the relation can be described as:

For $A_j > T_{j-1}(z)$:

$$T_j(z) = T_{j-1}(z) + [A_j - T_{j-1}(z)] * \text{Exp}[-z((\pi / (k_s * p))^{0.5}] * \text{Exp}[-k(LAI_j + litter_j)]$$

For $A_j \leq T_{j-1}(z)$:

$$T_j(z) = T_{j-1}(z) + [A_j - T_{j-1}(z)] * \text{Exp}[-z((\pi / (k_s * p))^{0.5}] * \text{Exp}[-k(litter_j)]$$

A_j is average Air Temperature at day " j " in °C .

This is calculated from Tmin and Tmax given as input in climate data file.

$T_{j-1}(z)$ is Soil temperature at day " j_{-1} " previous day at depth "z " below soil surface, °C

$T_j(z)$ is Soil temperature at day " j " and depth "z " below soil surface, °C

$\text{Exp}[-z((\pi / (k_s * p))^{0.5}]$ is a damping ratio

k_s is the thermal diffusivity as a function of soil water, air and mineral content. $m^2 s^{-1}$

$k_s =$ (thermal conductivity/(bulk density* specific heat capacity)).

P: is period of either diurnal or annual temperature variation, z is in meters

LAI: is calculated already in the model on daily basis, Litter fraction is given as user input.

References

Kang, S., Kim, S., Oh, S. and Lee, D. 2000. Predicting spatial and temporal patterns of soil temperature based on topography, surface cover and air temperature. Forest Ecology and Management 136:173-184.

Marshall, T.J., Holmes, J. W., and Rose, C.W. (editors). 1996. Soil Physics (3rd edition) , 358-376. Cambridge University Press. Cambridge, UK.

Zheng, D., Hunt, Jr., Running, S.W. 1993. A daily soil temperature model based on air temperature and precipitation for continental applications. Climate Research 2: 183-191.

6. Soil Nitrogen dynamics and Nitrogen uptake

This is very much based on SOIL N model of Johnsson *et al.* 1987. The following processes were implemented in SALTMED:

- Mineralization
- Immobilization
- Nitrification
- Denitrification
- Leaching
- Plant N Uptake

Nitrogen input included dry and wet deposition, incorporation of crop residues, manure application, chemical fertilizer application and with irrigation water as fertigtion.

References

Eckersten, H and Jansson, P,.- E. 1991. Modelling water flow, nitrogen uptake and production for wheat. Fertilizer Research 27: 313-329.

Johnsson, H., Bergstrom, L and Jansson, P.-E.. 1987. Simulated nitrogen dynamics and losses in a layered agricultural soil. Agriculture, Ecosystems and Environment, 18:333-356.

Wu, L., McGechan, M., B., Lewis, D. R., Hooda, P. S., and Vinten, A., J., A. 1998. Parameter selection and testing the soil nitrogen dynamics model SOILN. Soil Use and Management, 14: 170-181

Annex 3.8 SALTMED model frames (user Interface) and Examples of outputs

Main input tabs

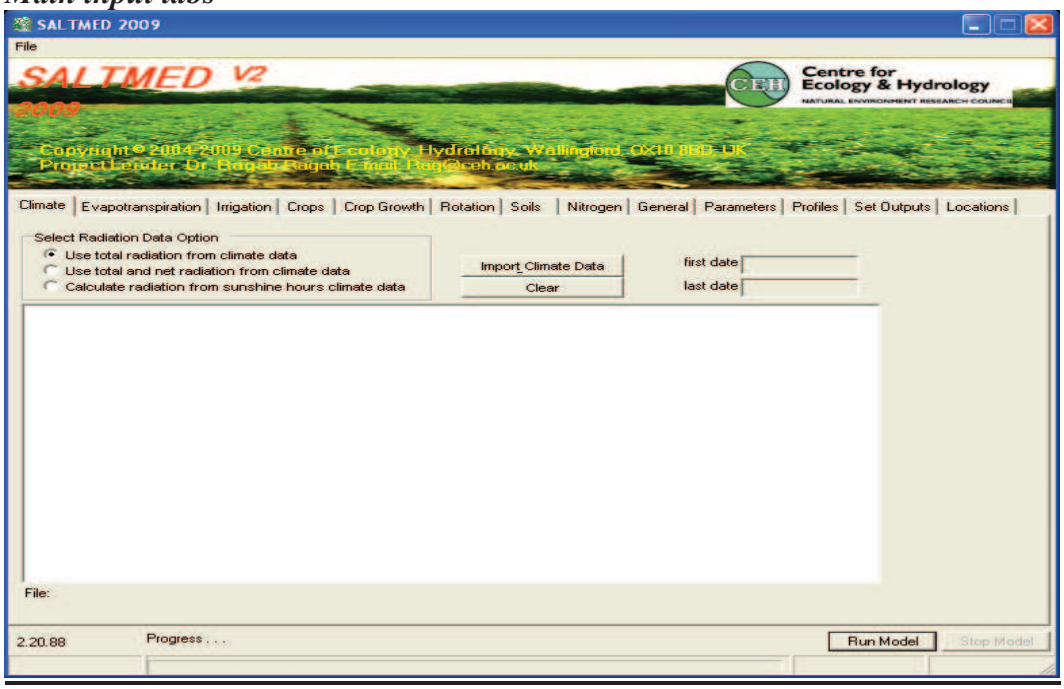

Model input can be saved and uploaded via a text file

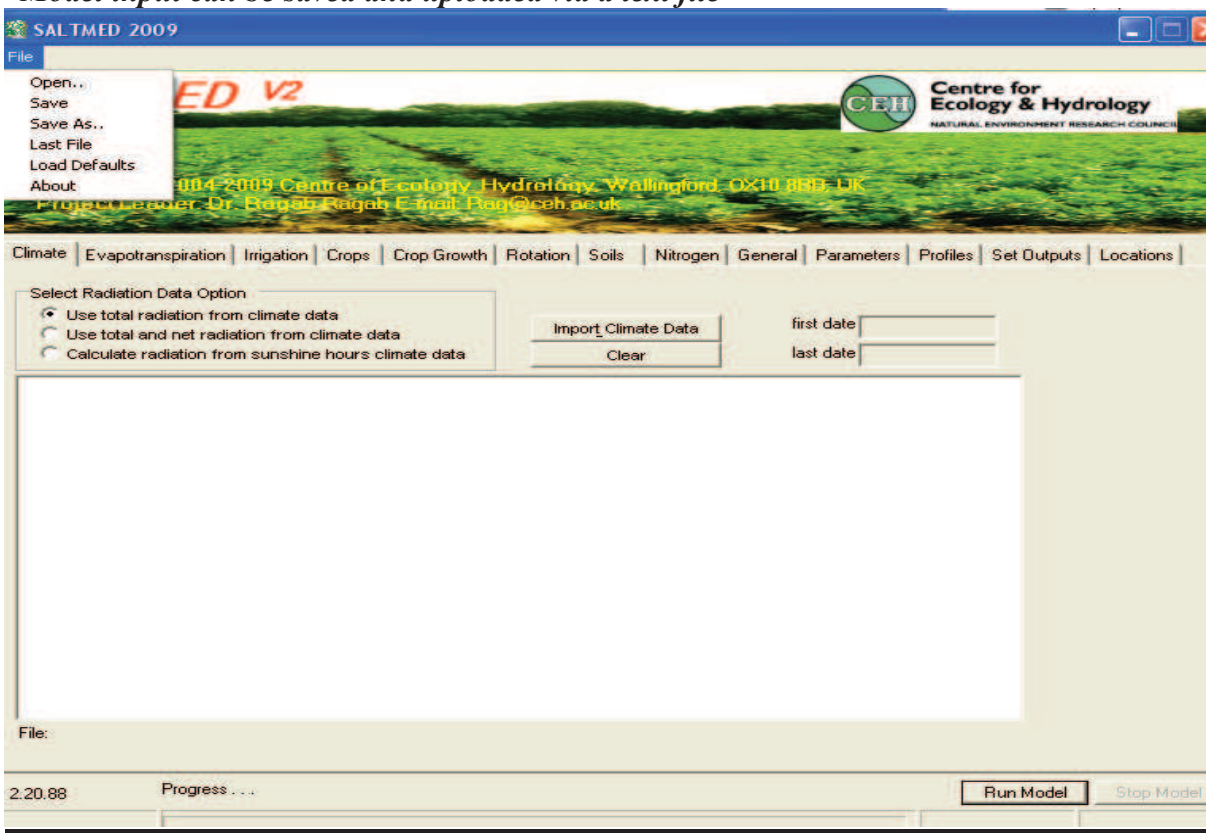

Climate data input

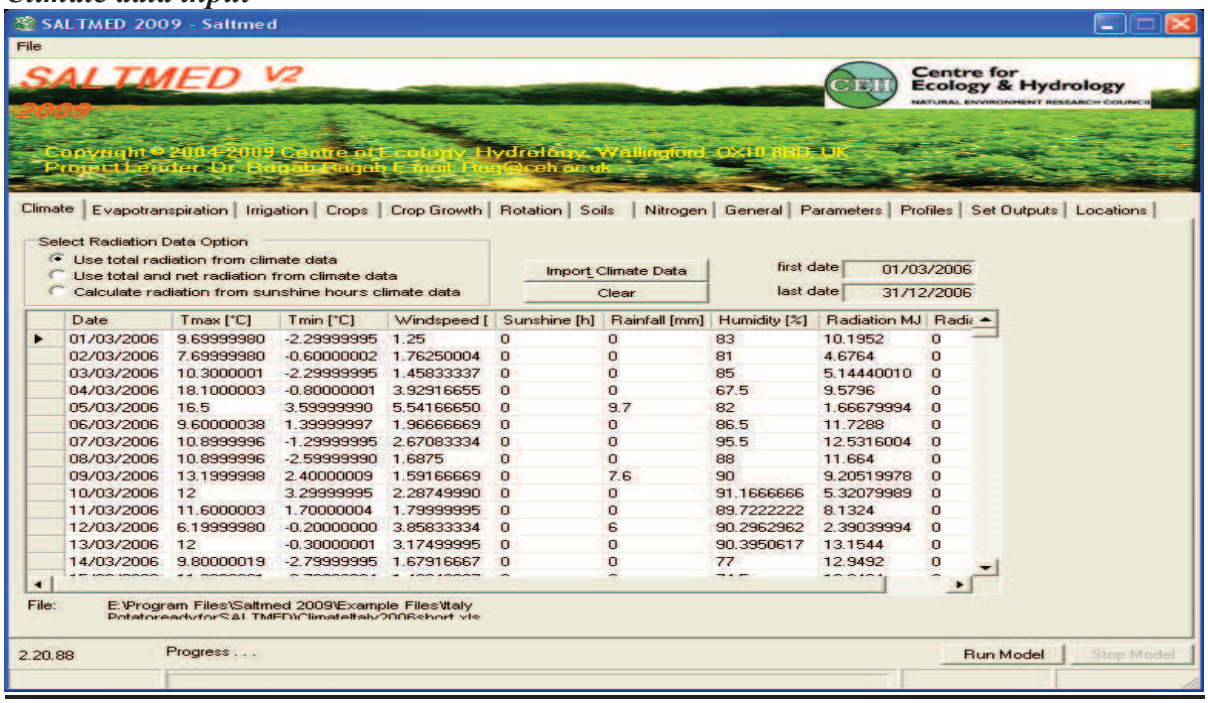

Evapotranspiration calculation options (1)

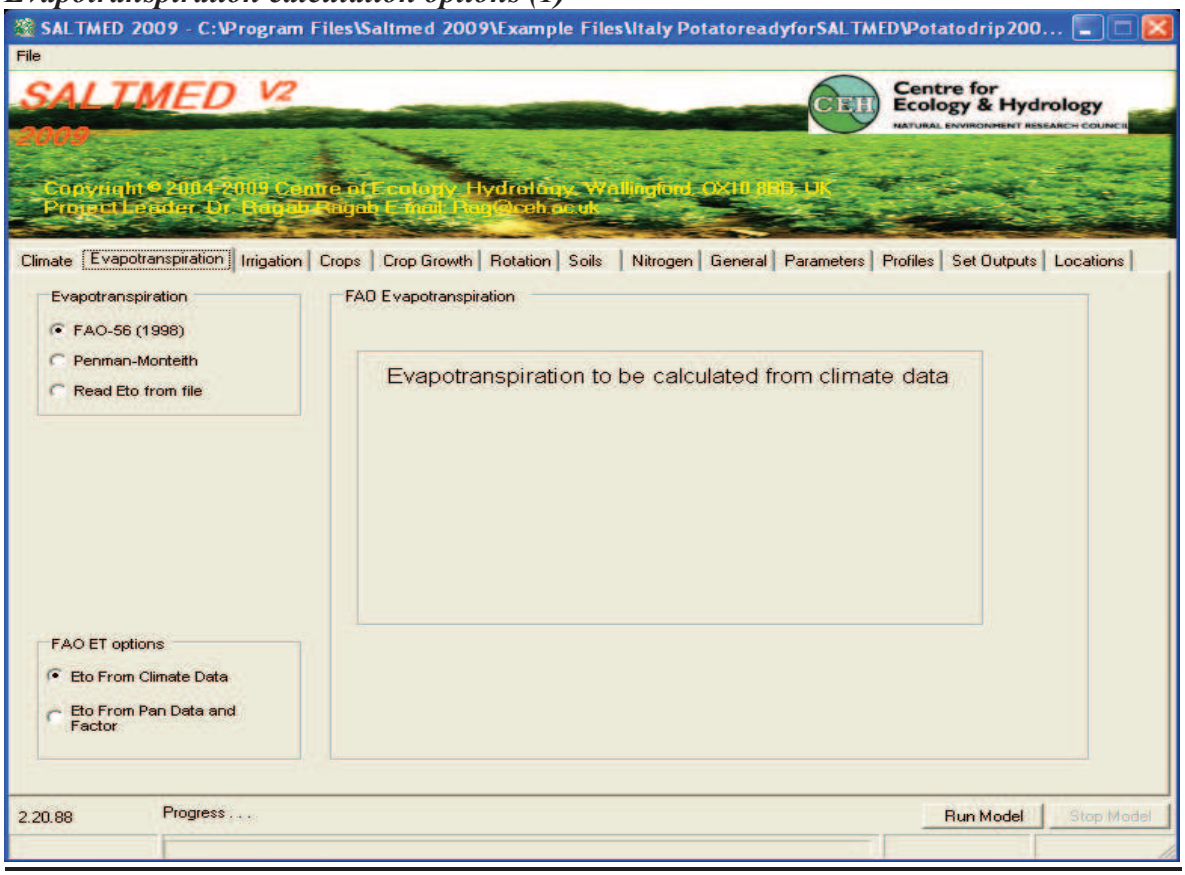

Evapotranspiration calculation options (2)

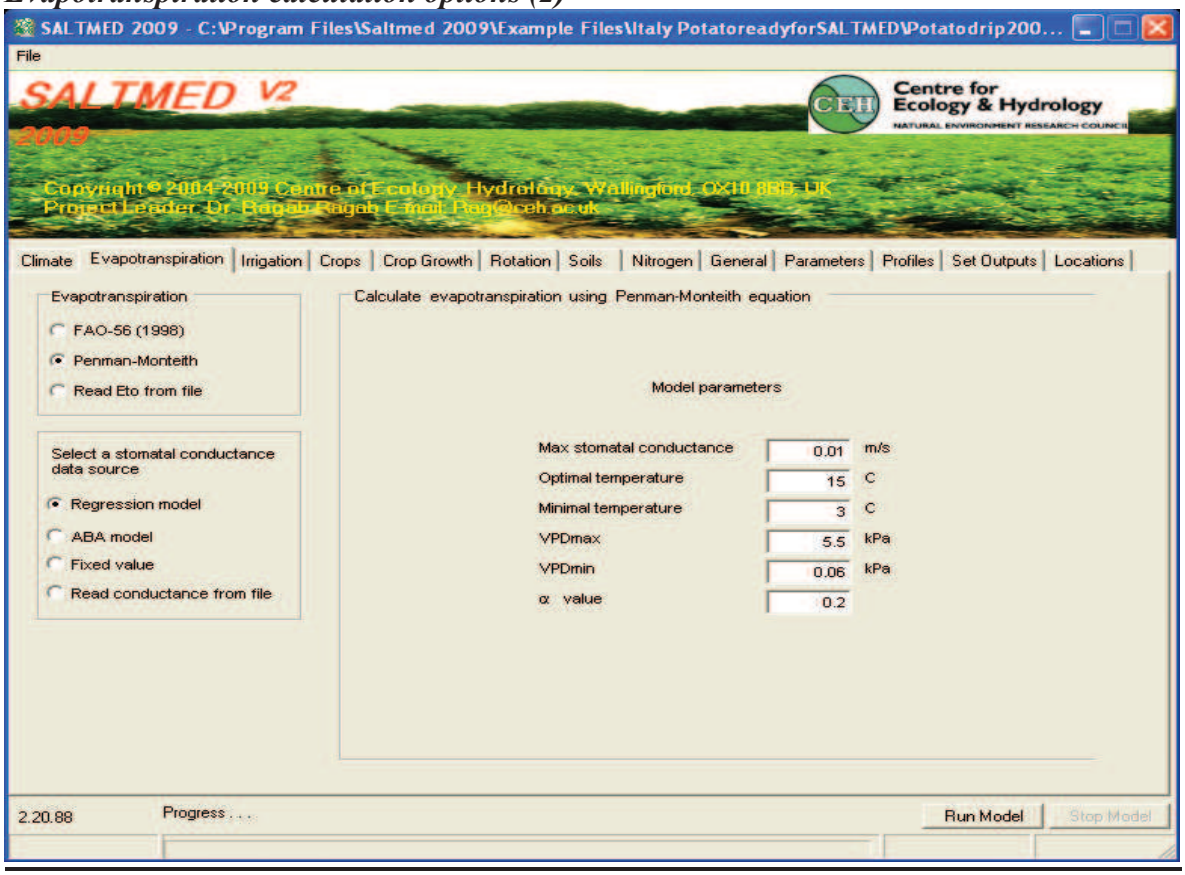

Evapotranspiration calculation options (3)

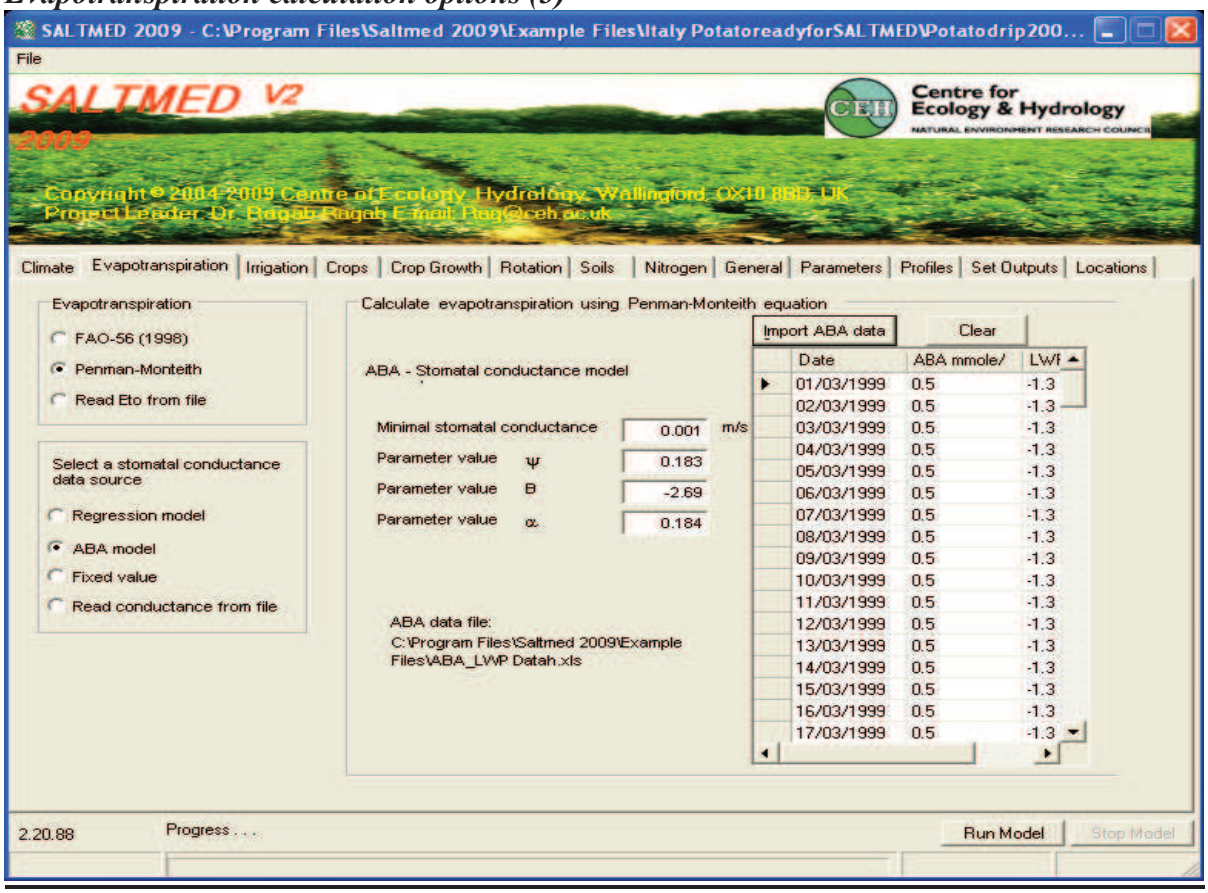

Evapotranspiration calculation options (4)

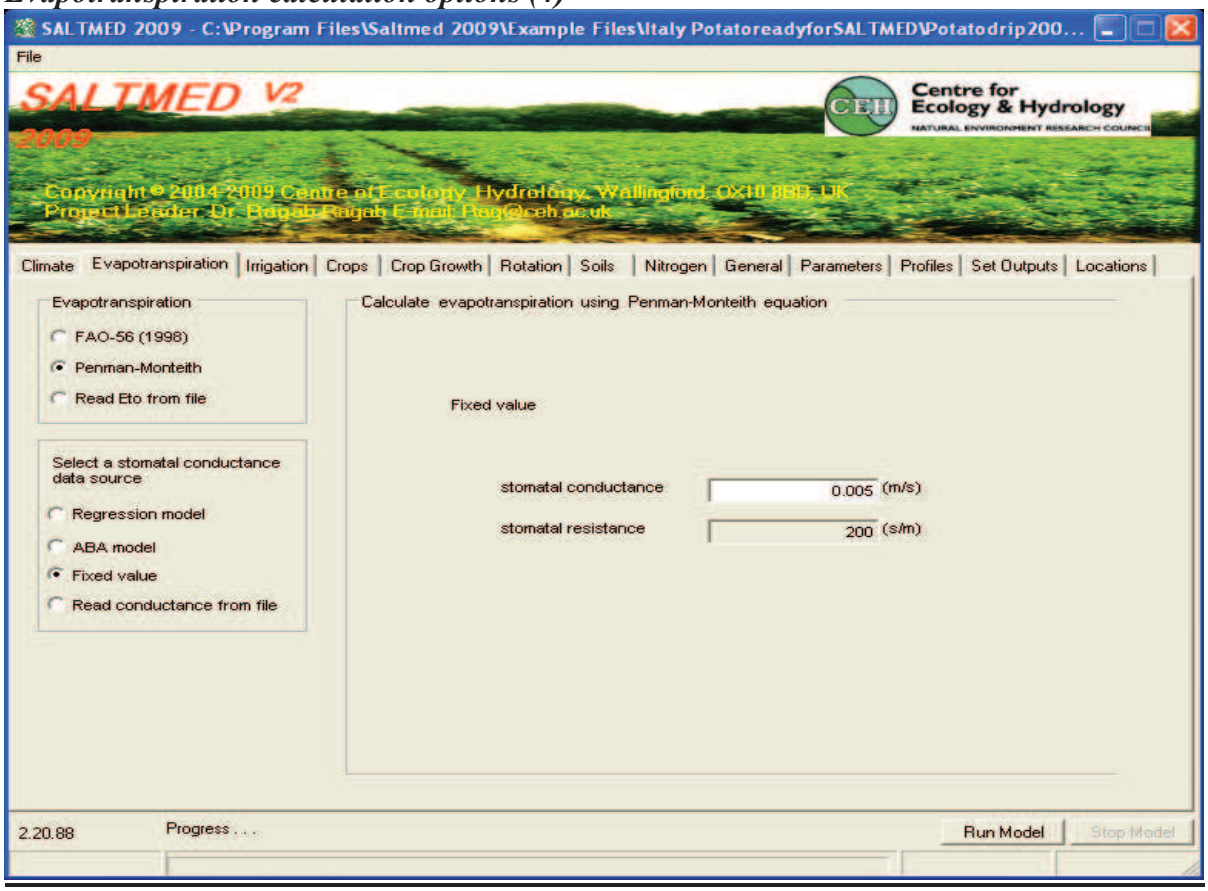

Evapotranspiration calculation options (5)

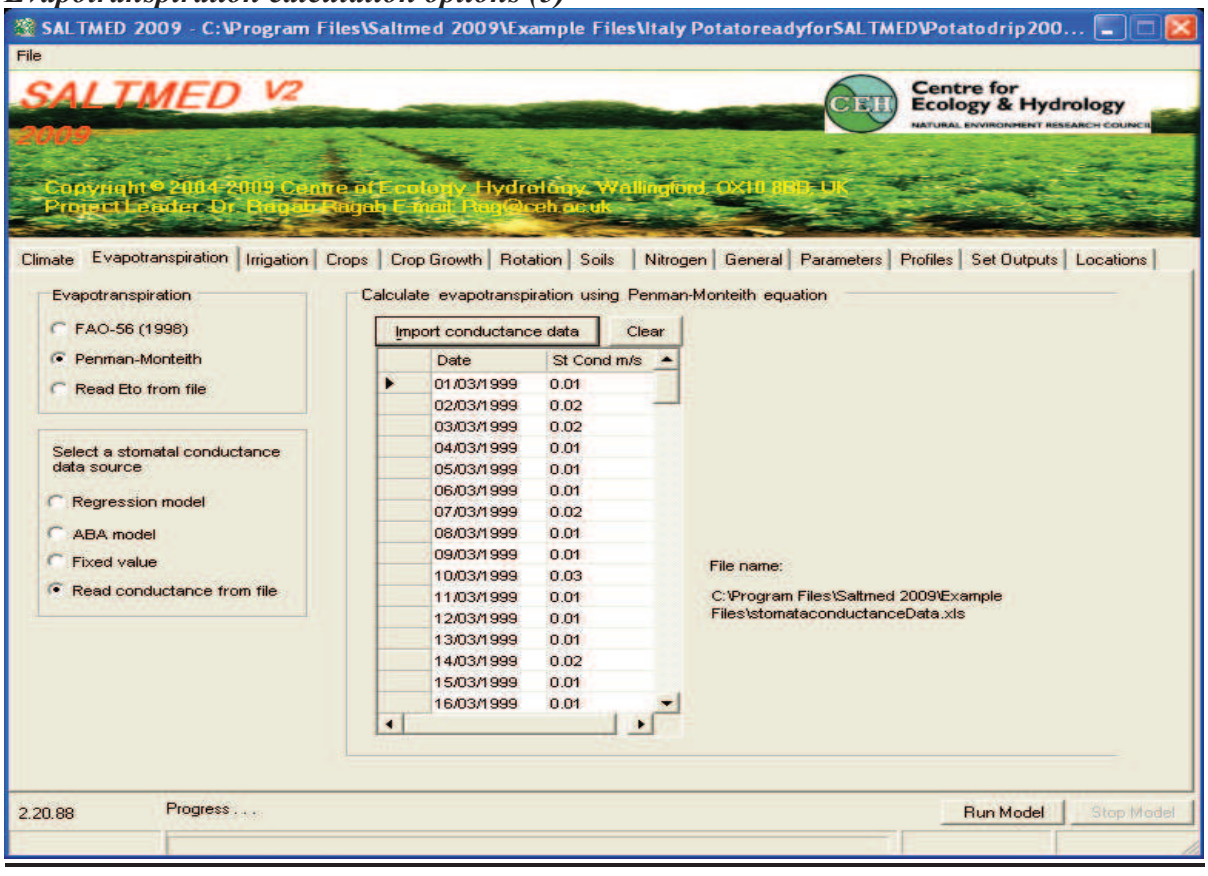

Evapotranspiration calculation options (6)

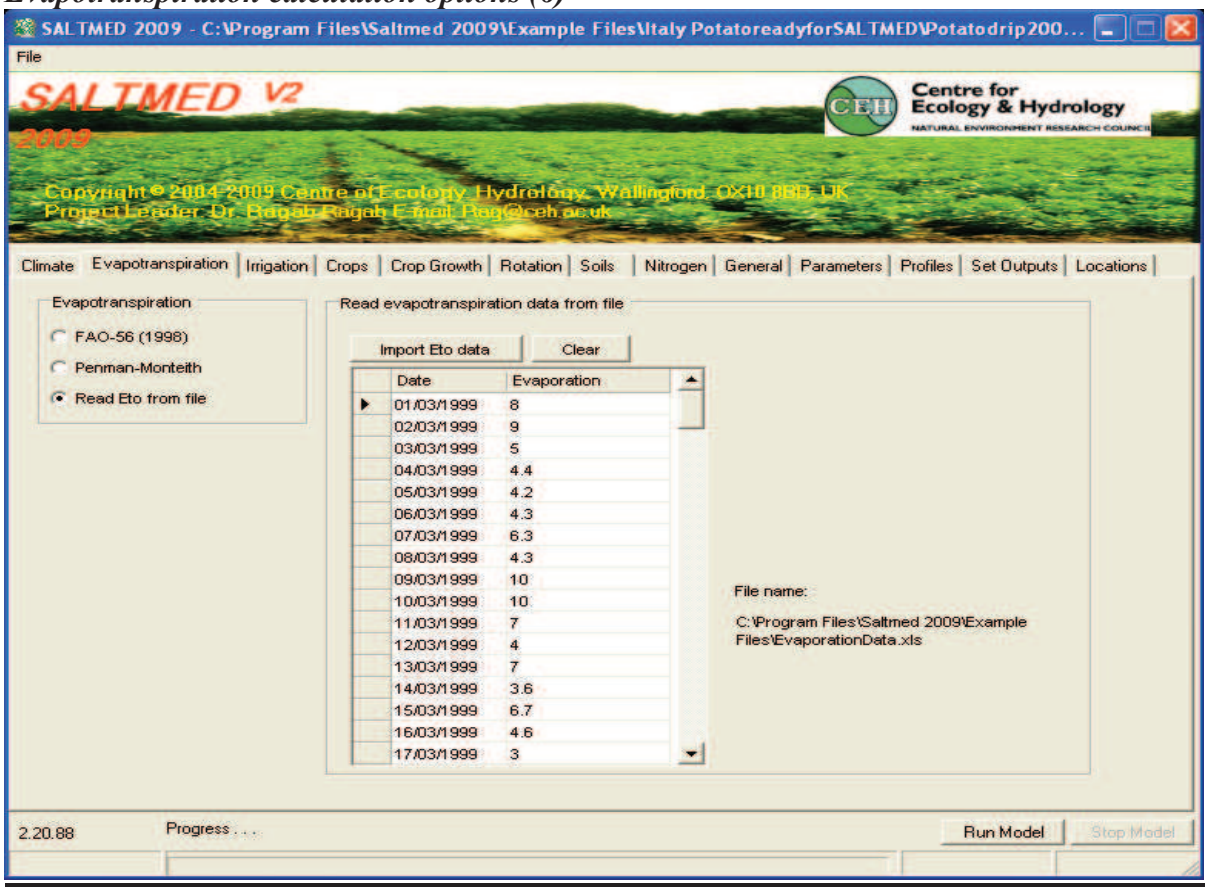

Evapotranspiration calculation options (7)

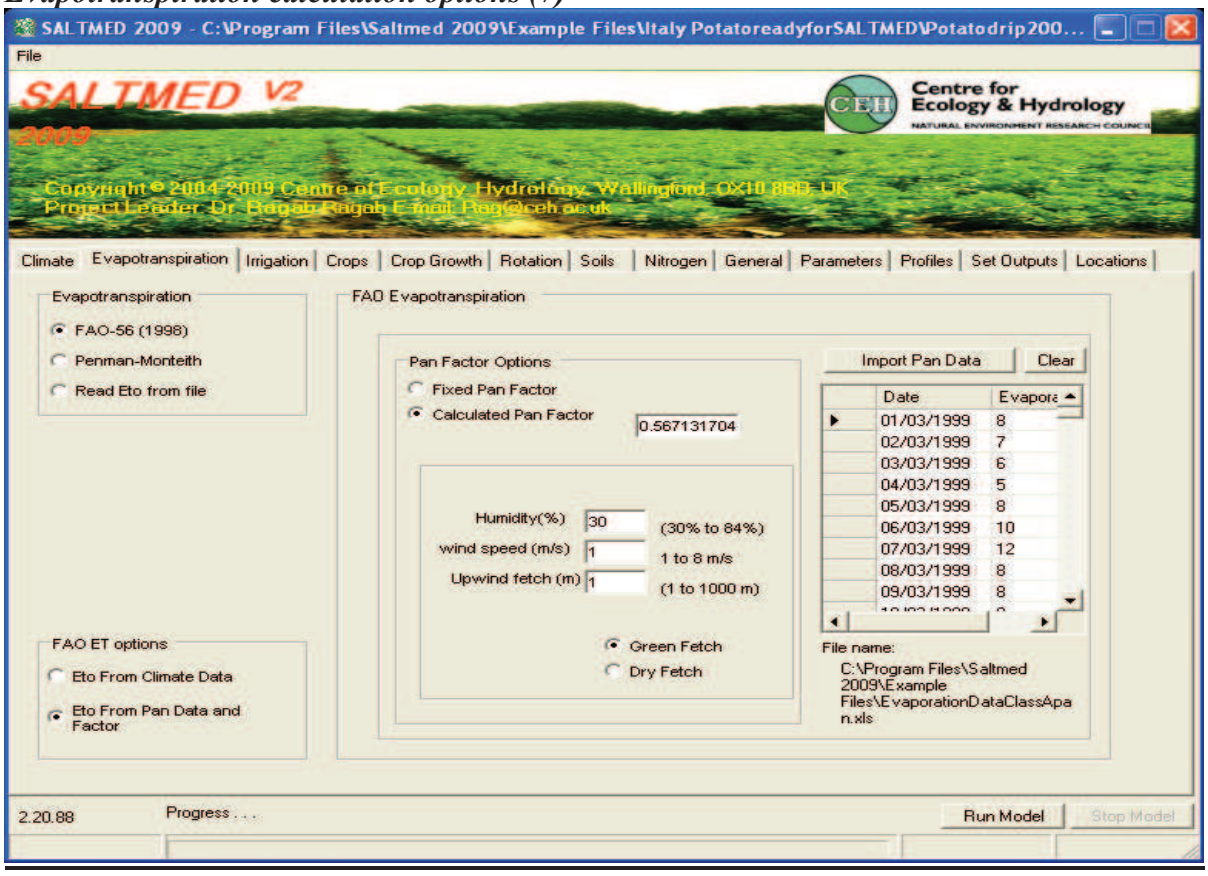

Evapotranspiration calculation options (8)

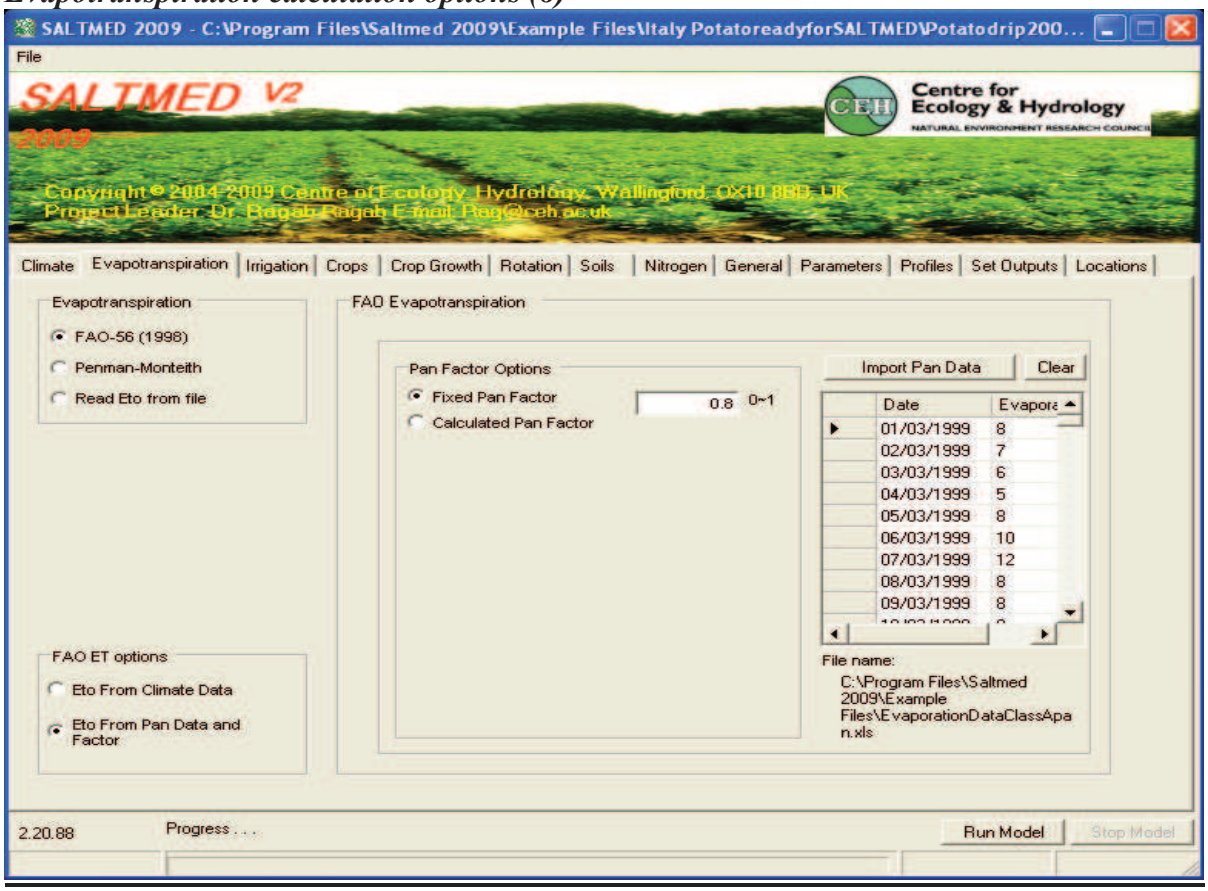

Irrigation input file (drip sub subsurface example)

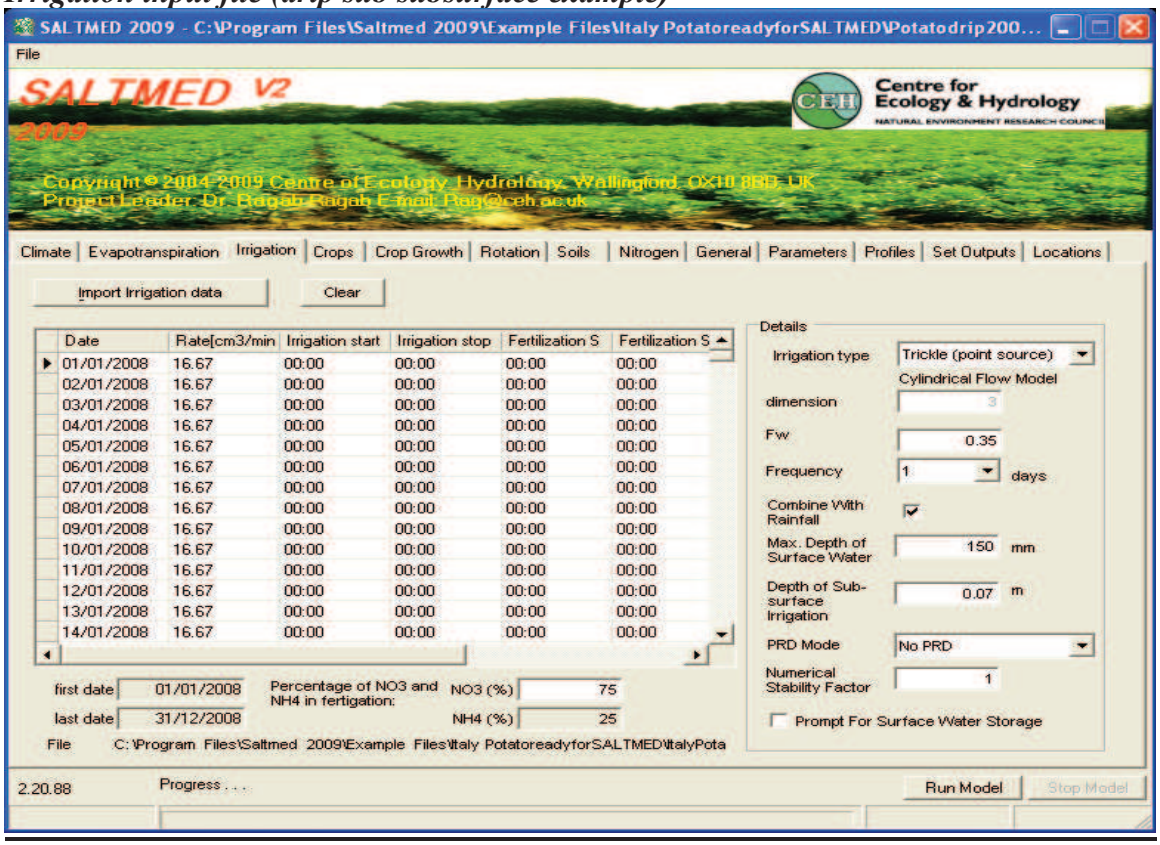

Irrigation input file (drip sub subsurface PRD example)

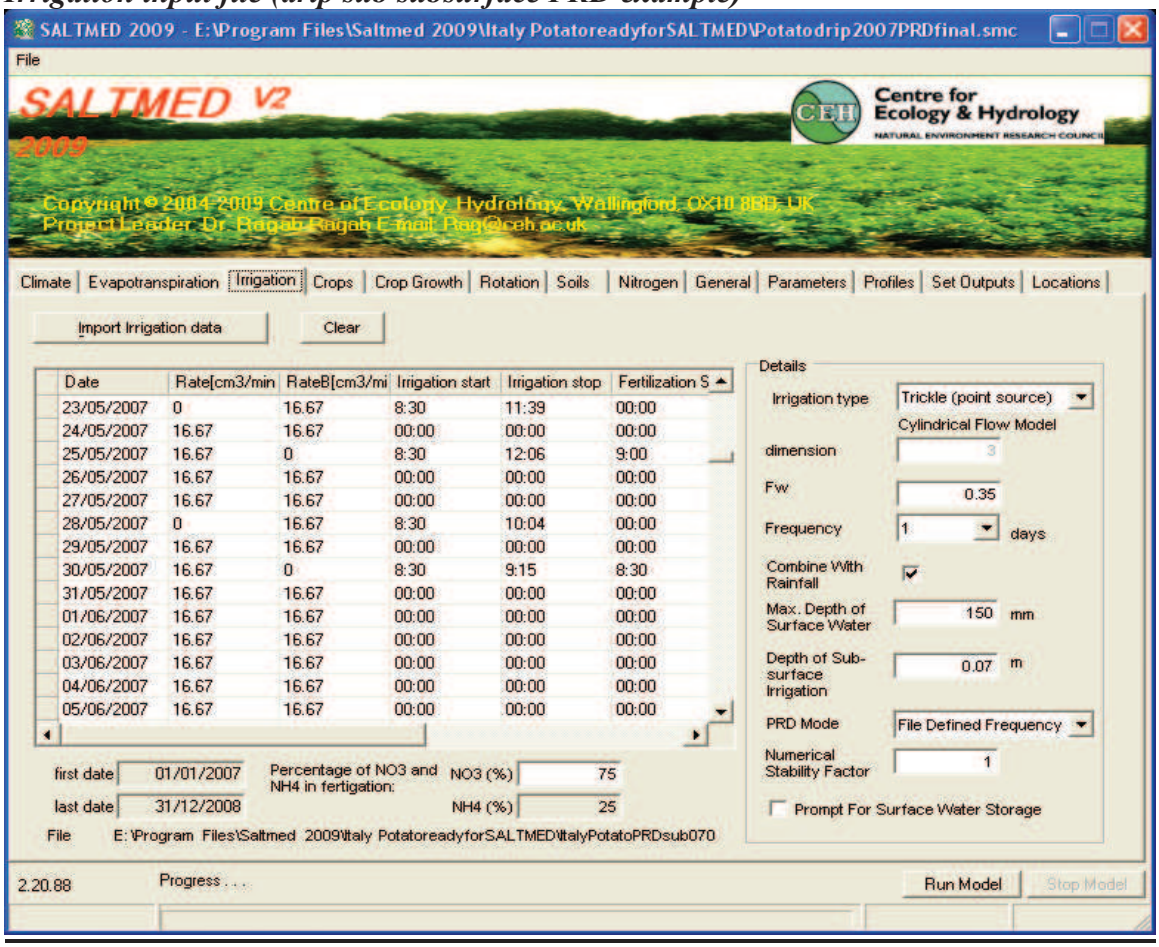

Crop growth input parameters (1)

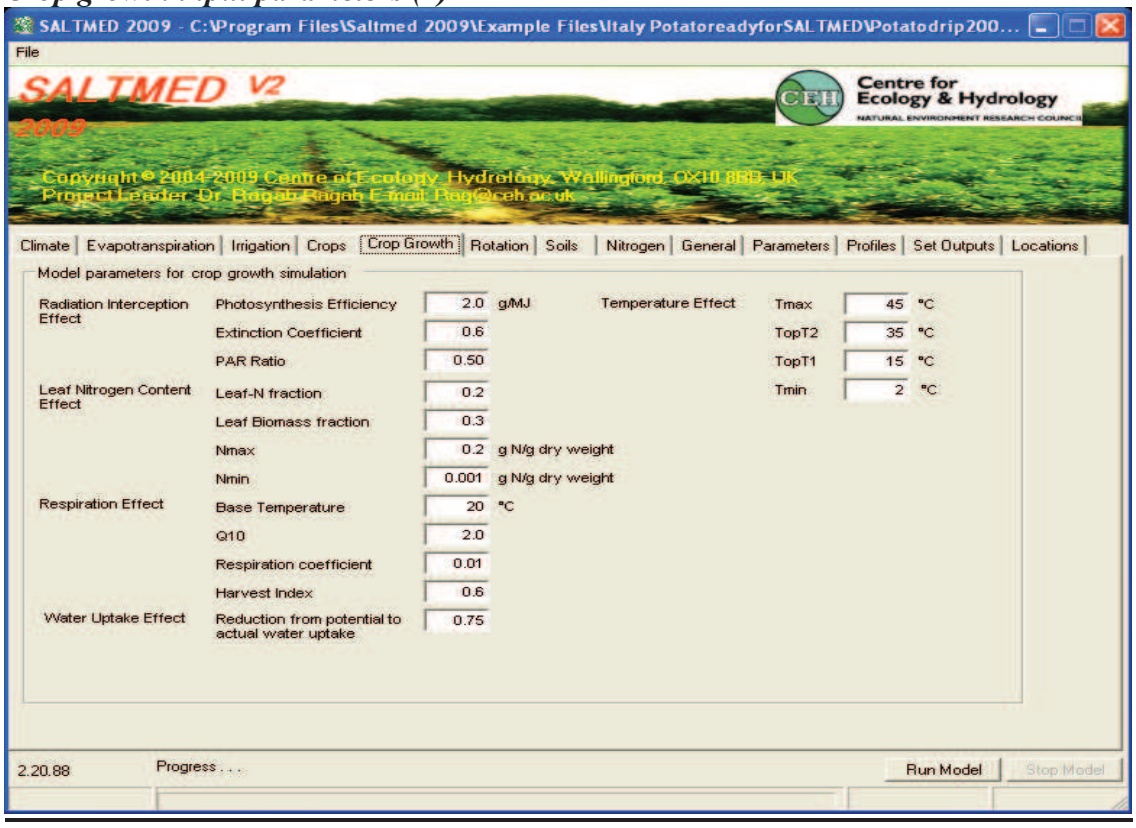

Crop growth input parameters (2)

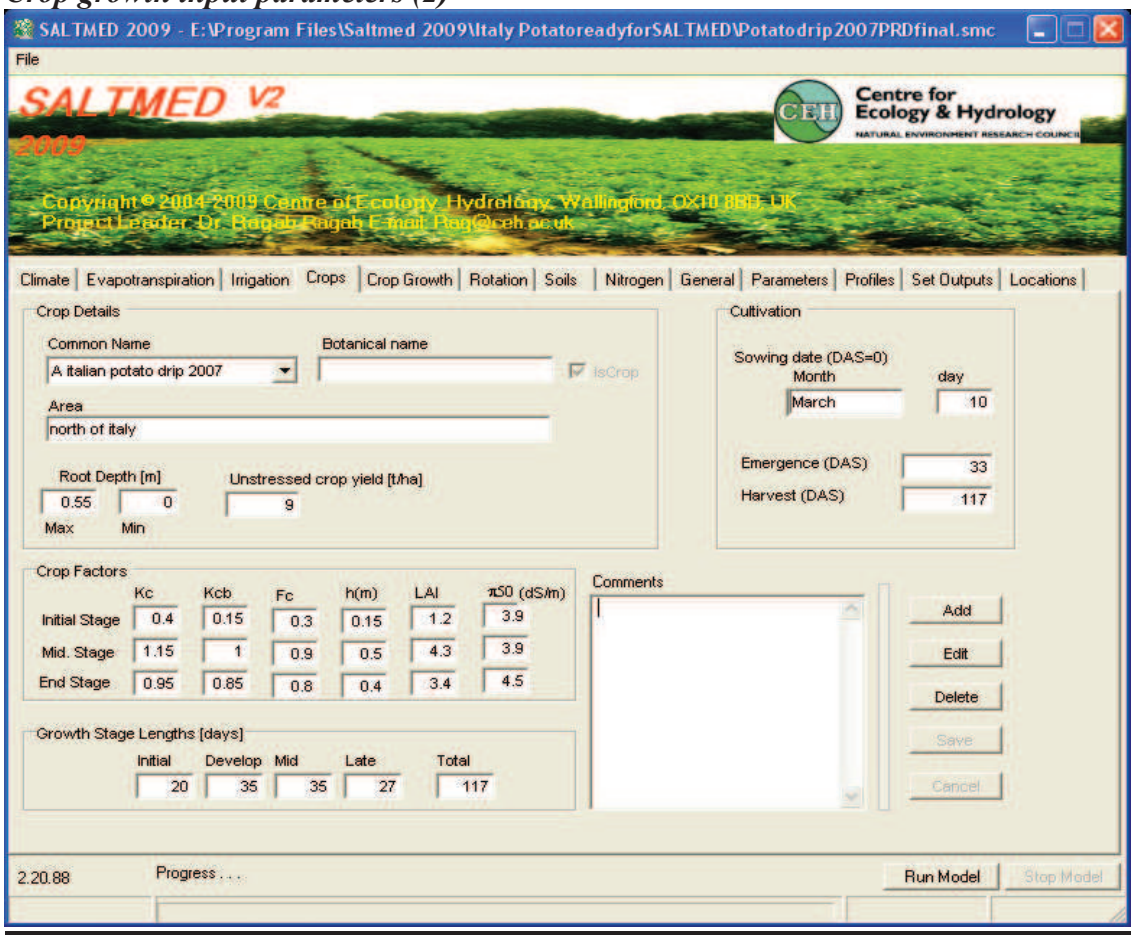

Crop rotation option 1 (no rotation)

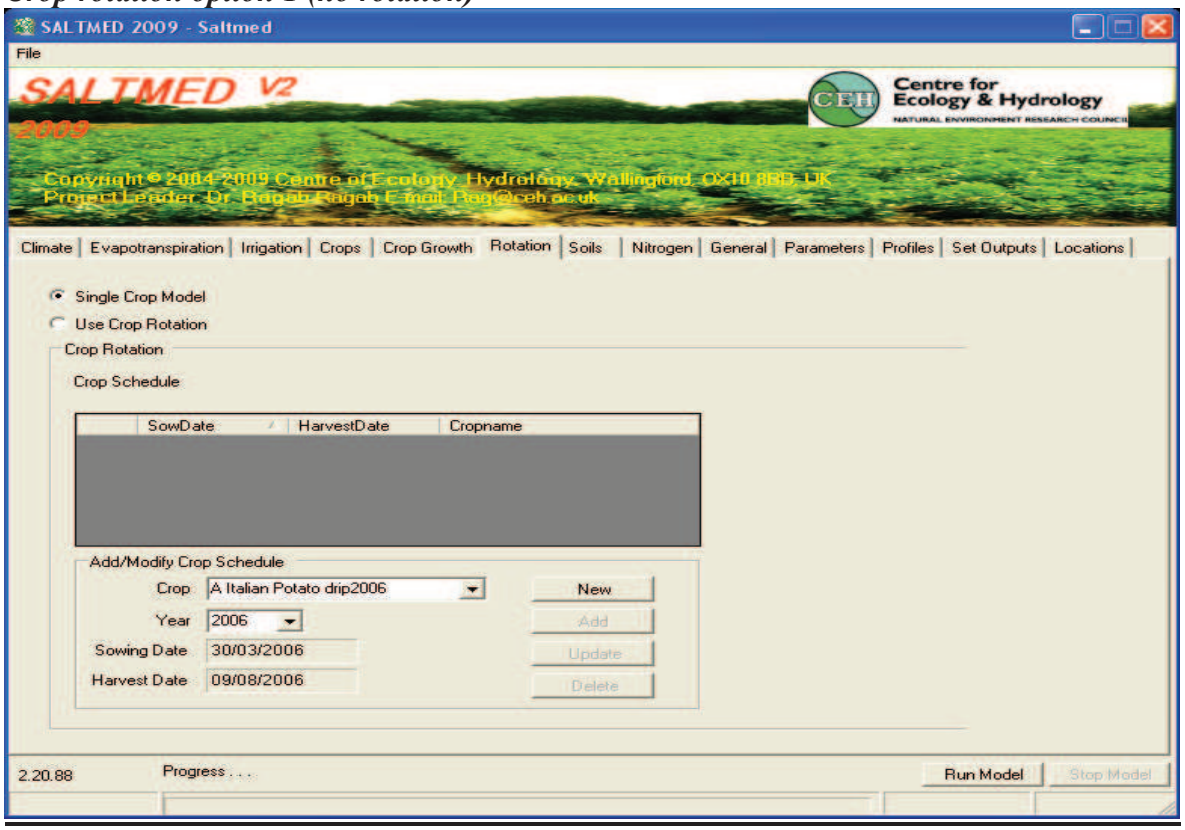

Crop rotation option 2 (rotation)

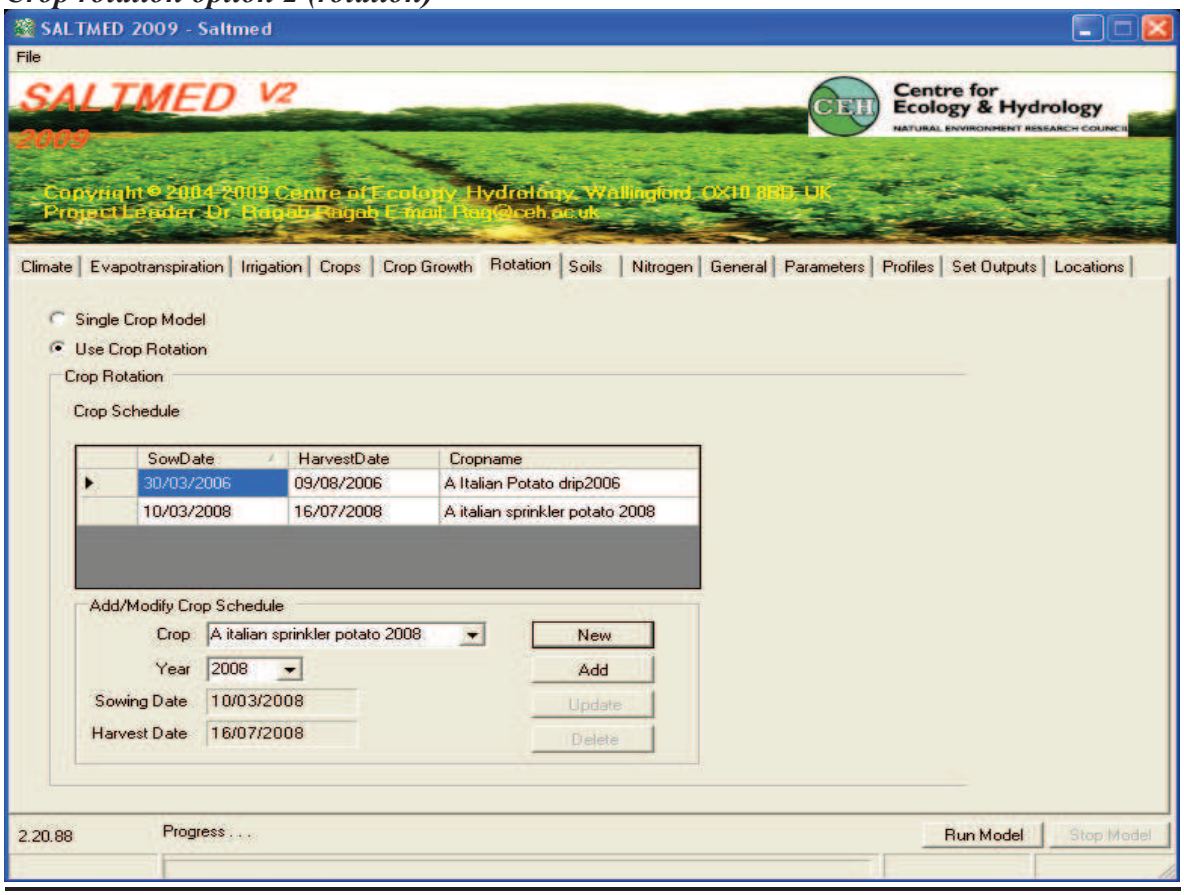

Soil input parameters

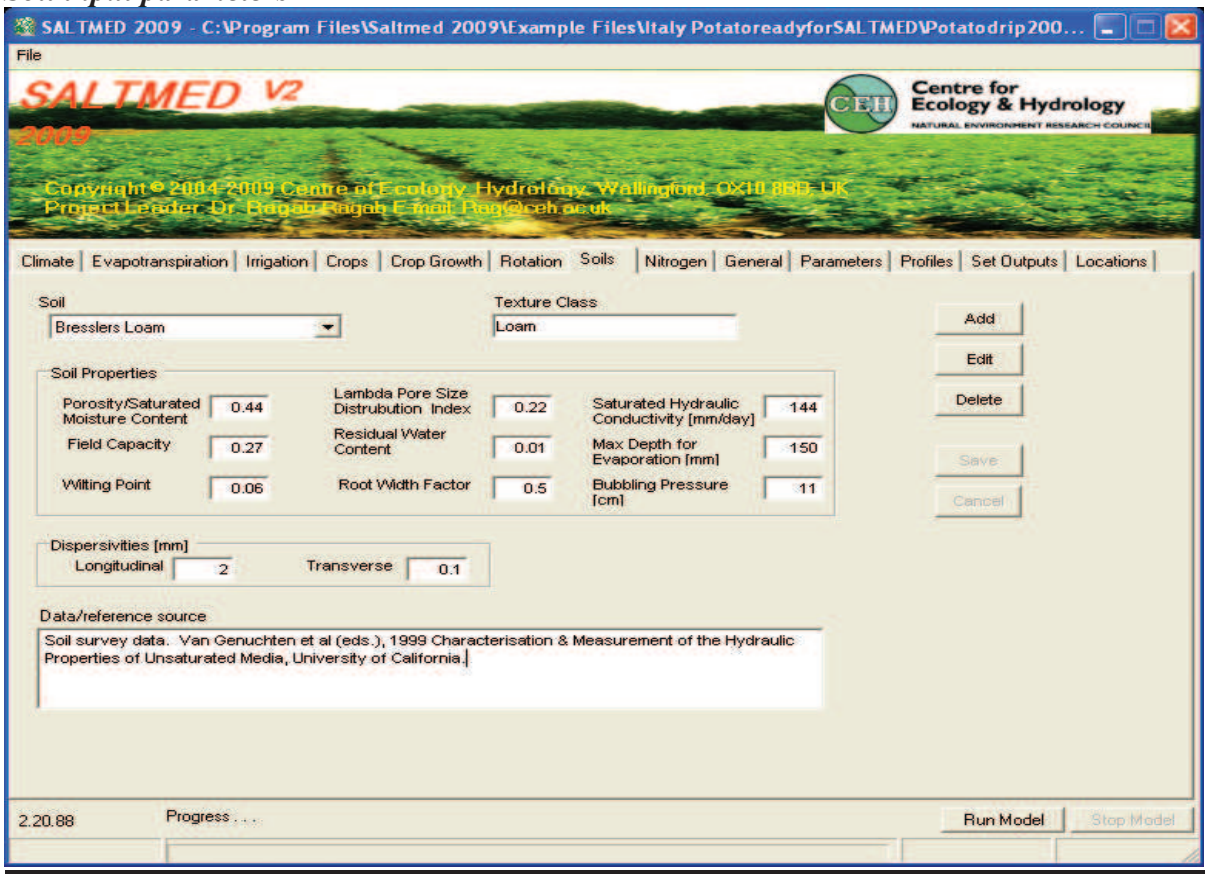

Soil temperature, N-Fertilizer input file, N-mineralization, N-transformation parameters initial N condition and environmental input parameters

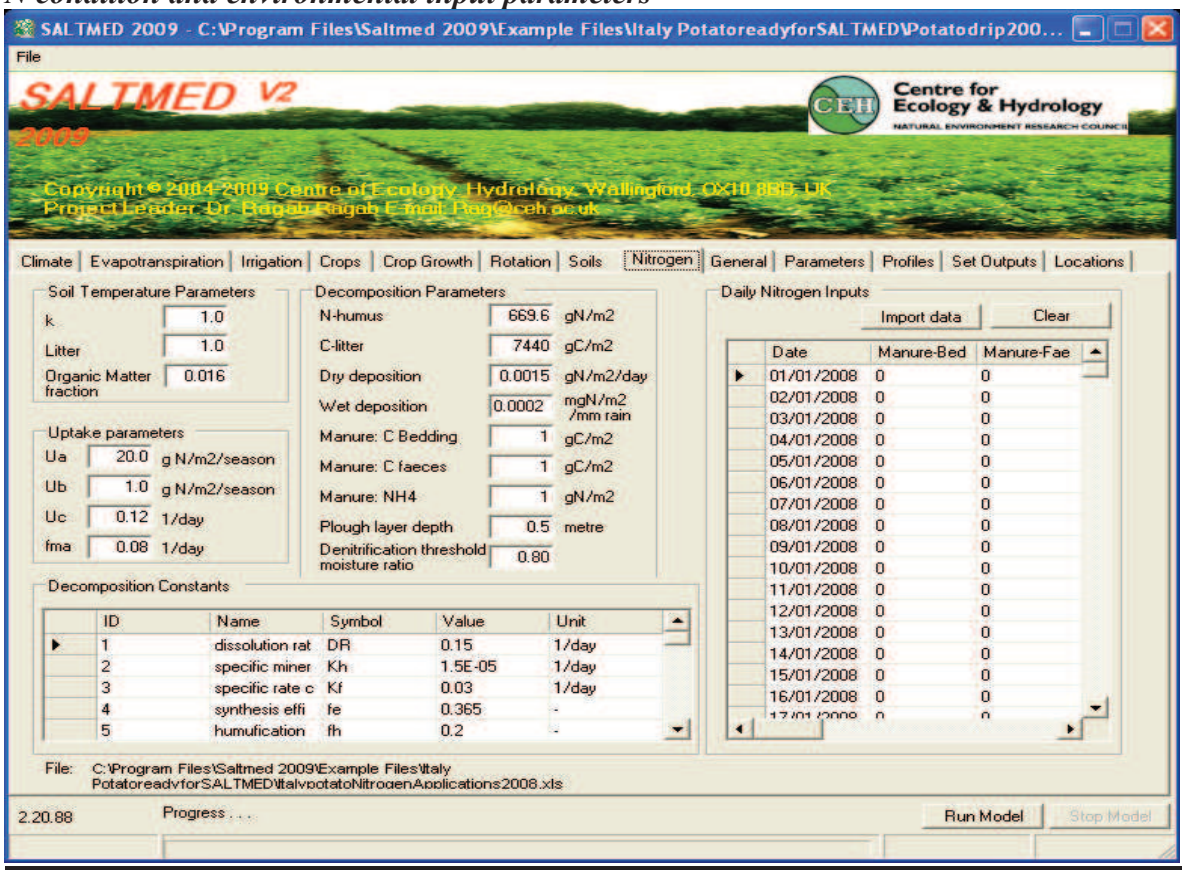

Soil initial condition- input parameters per soil layer

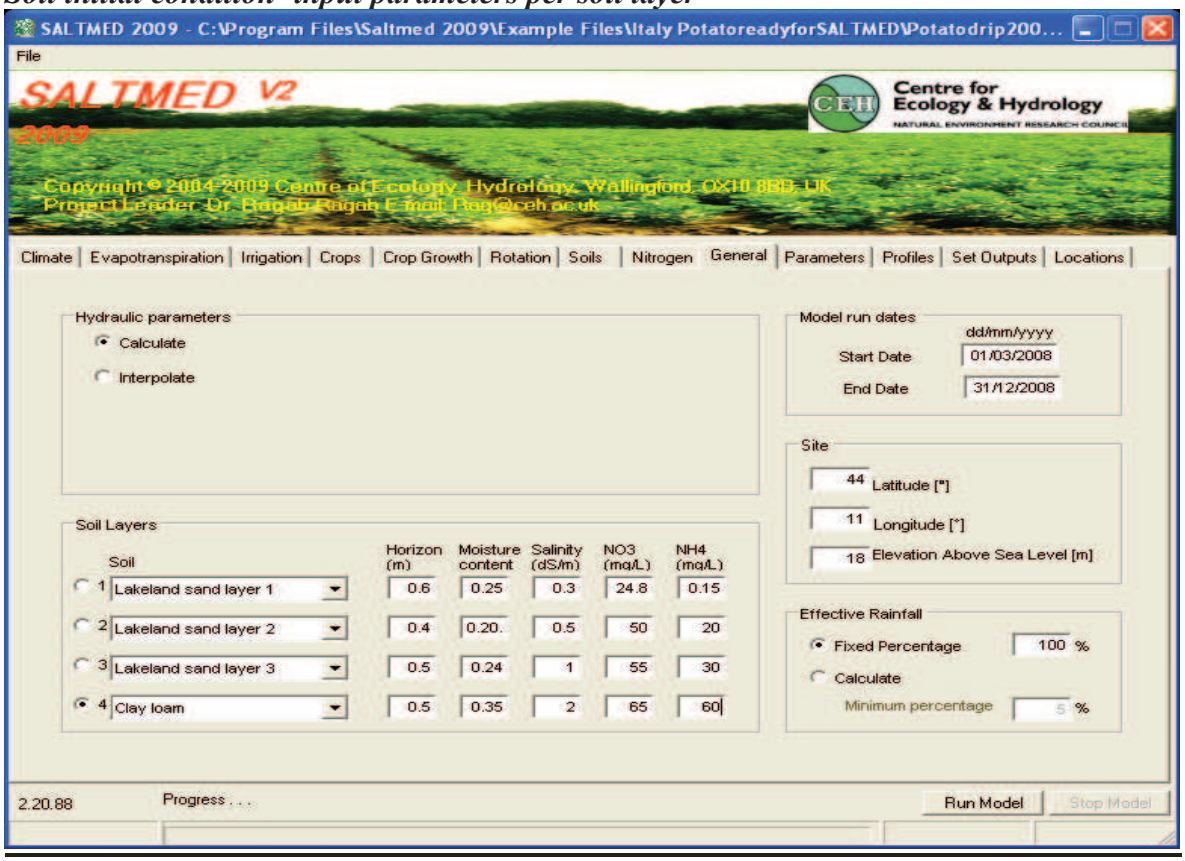

Model input parameters

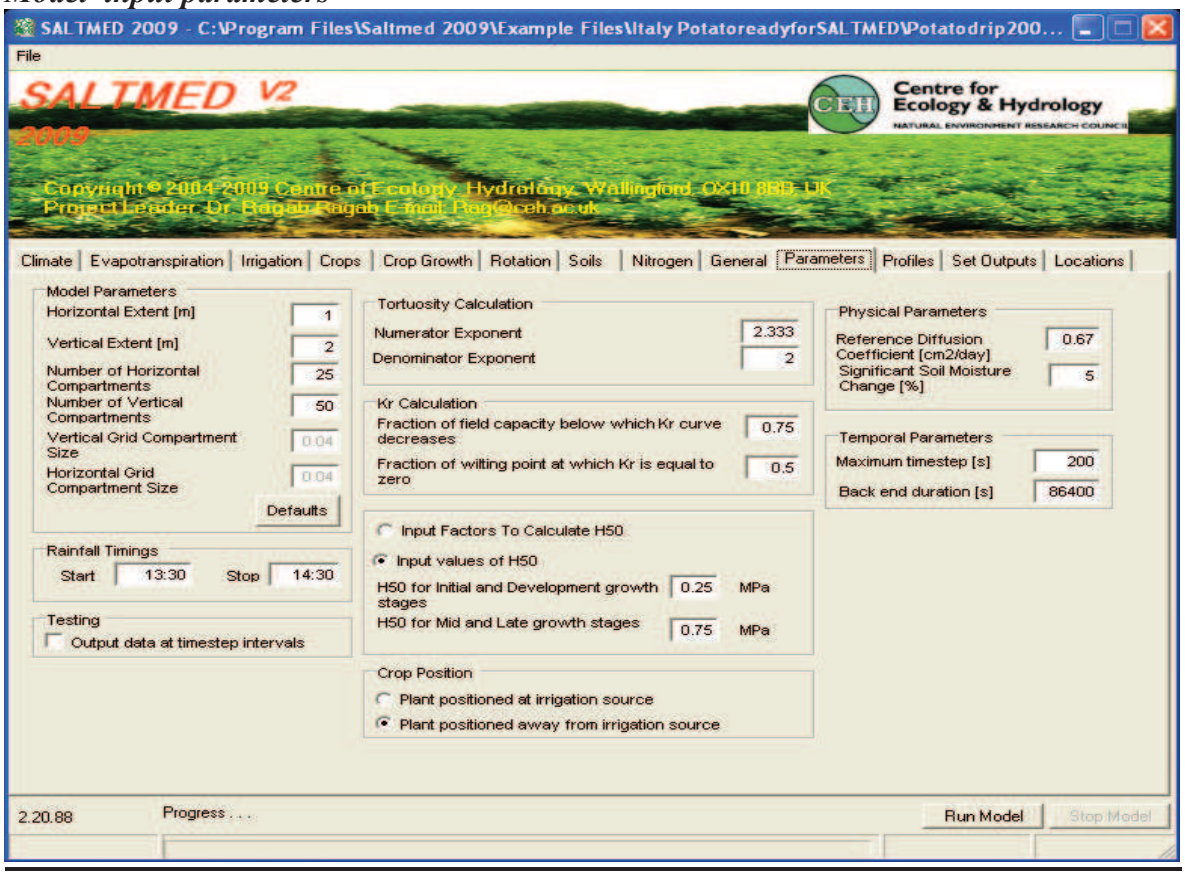

Output specifications for plotting output parameters

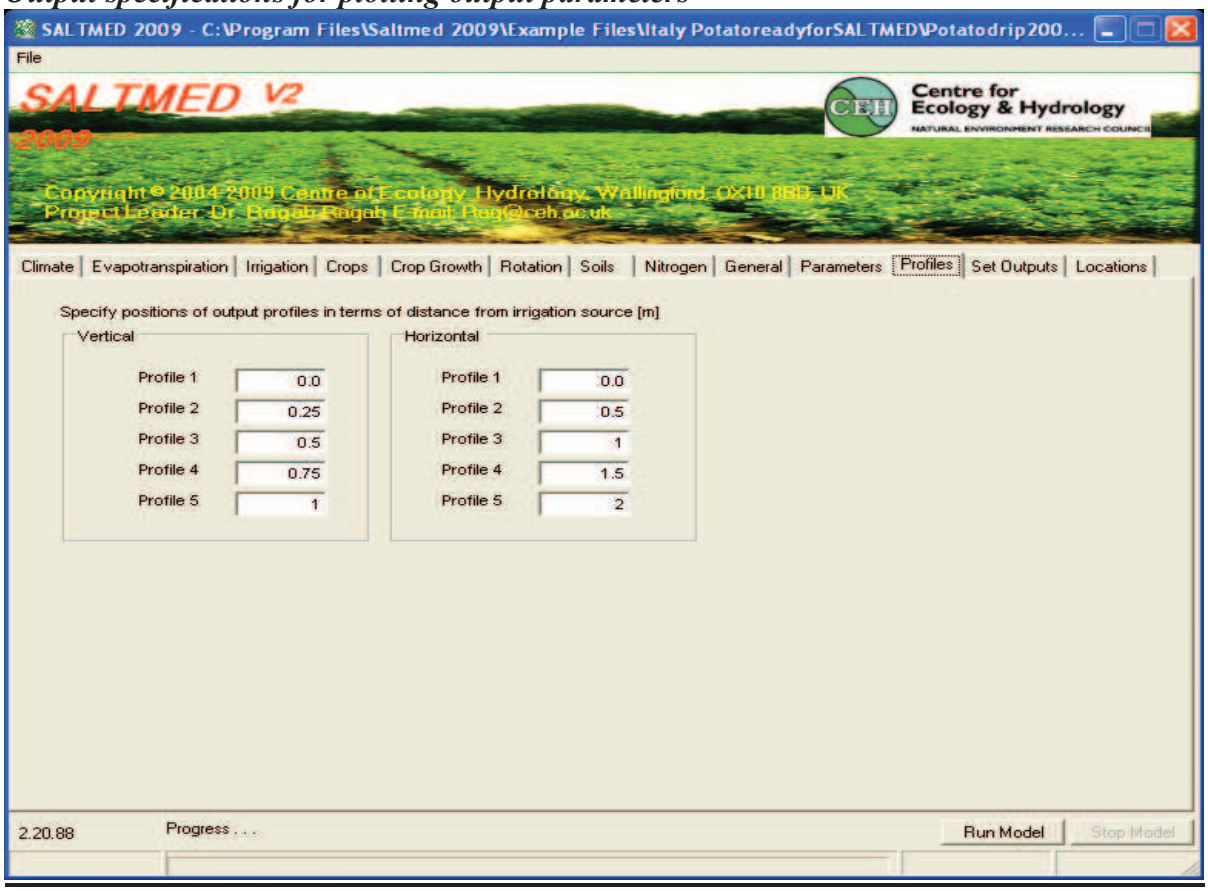

Output selection options

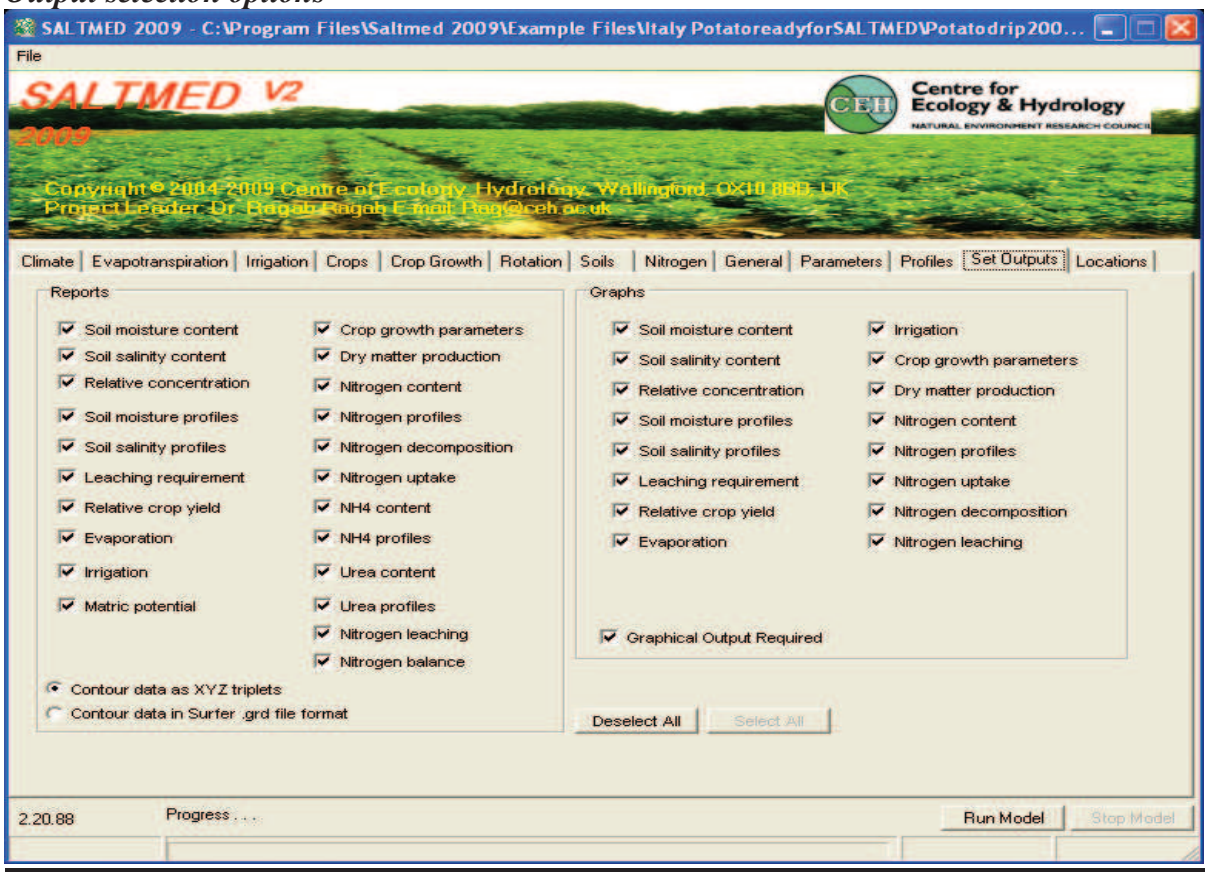

Output selection folder

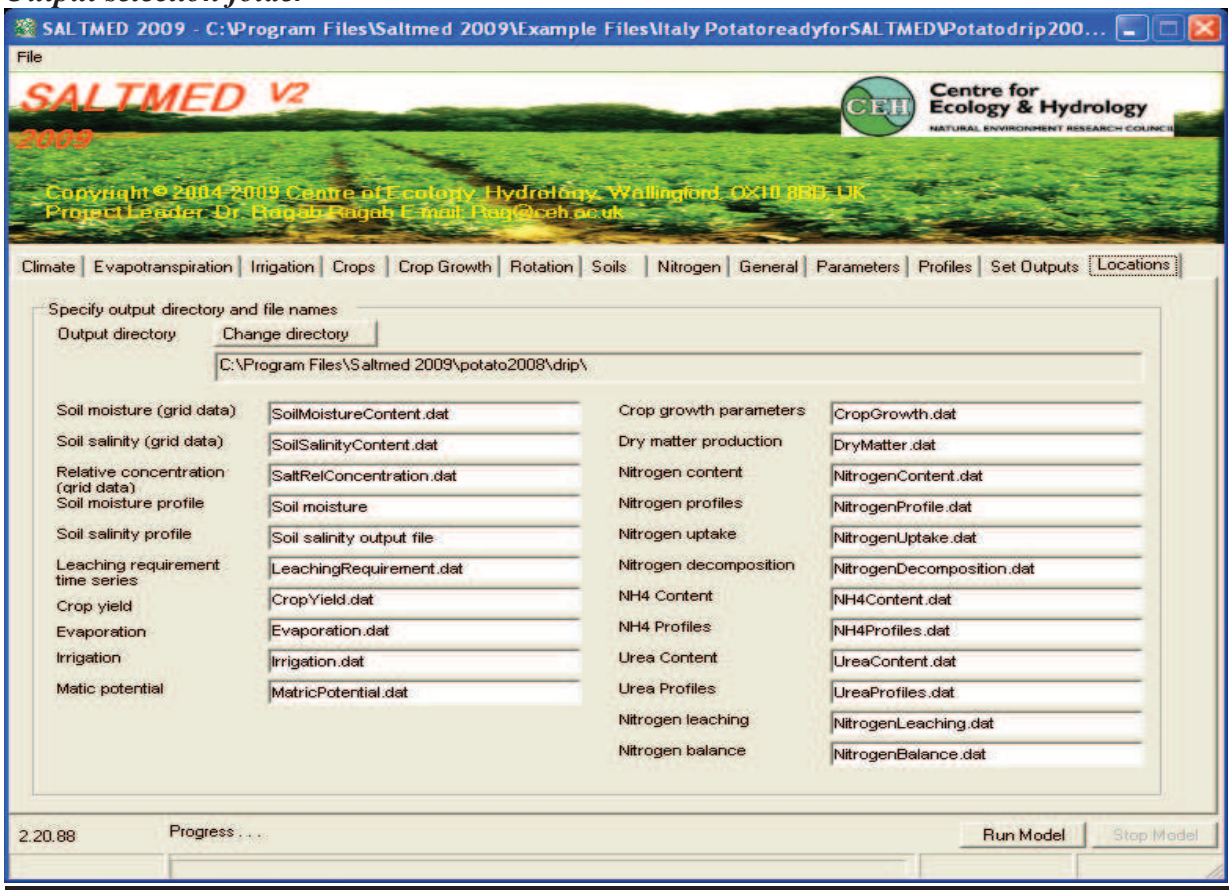

Output example of Dry matter

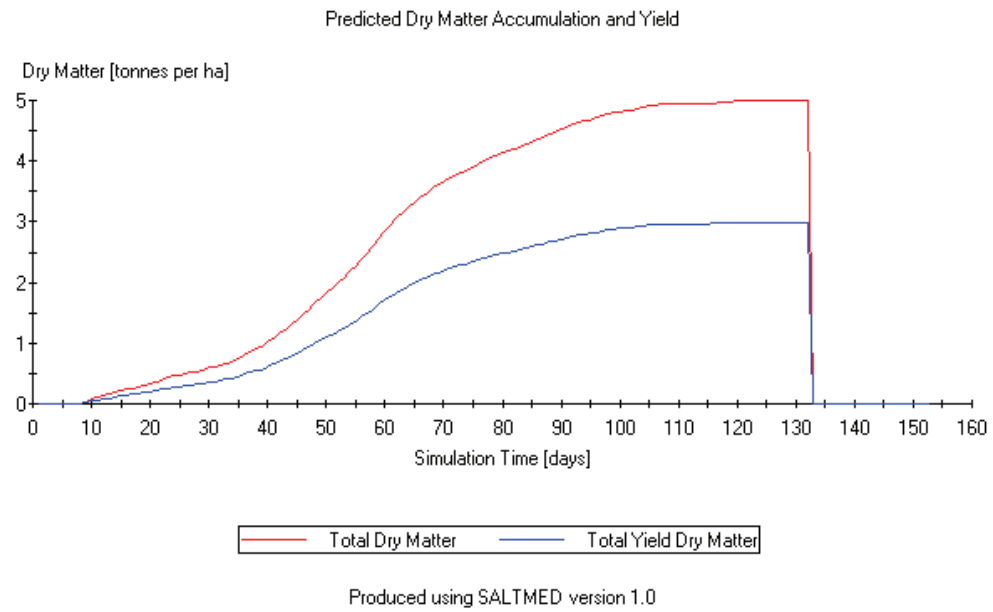

Output example of plant –N uptake

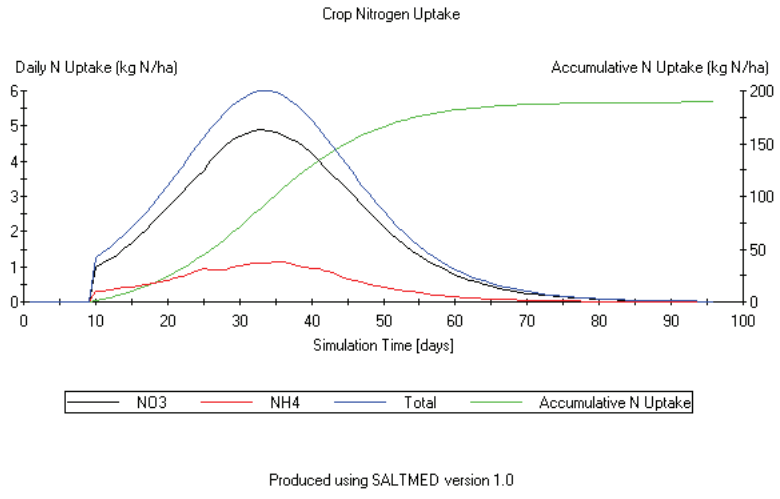

Output example of N-Leaching

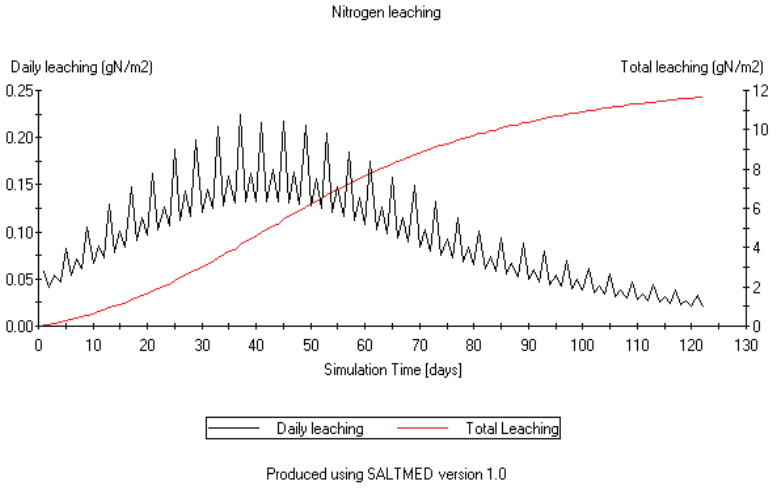

Output example of soil moisture under drip irrigation

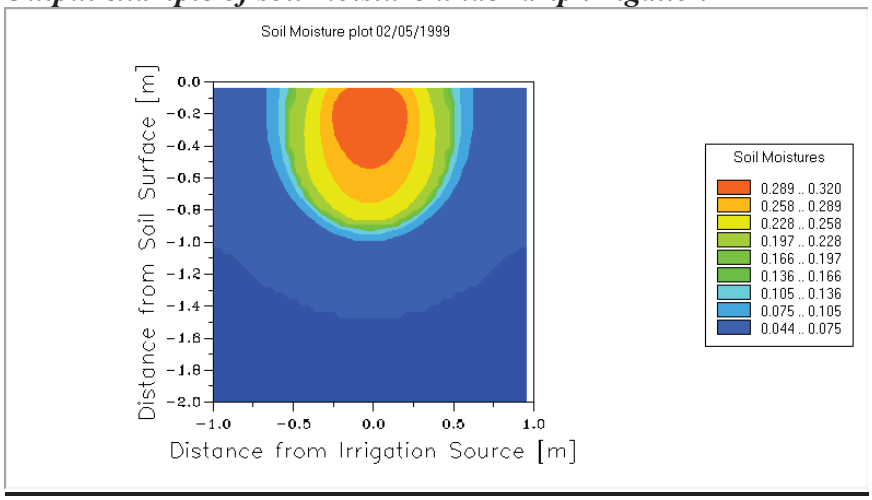

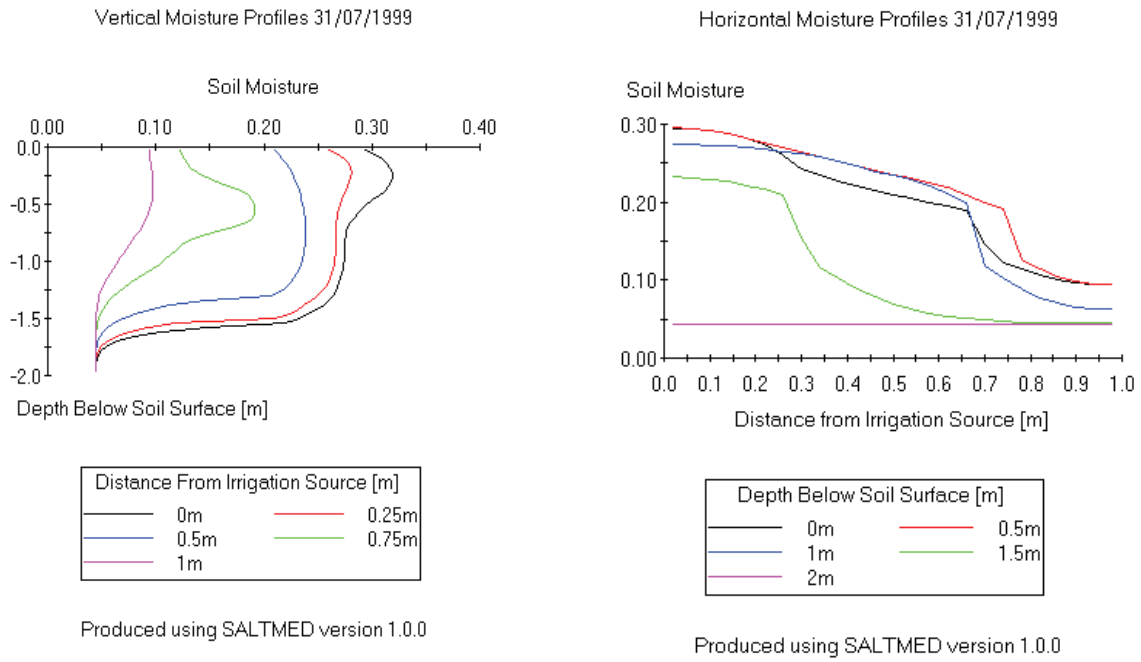

Output example of soil salinity under drip irrigation

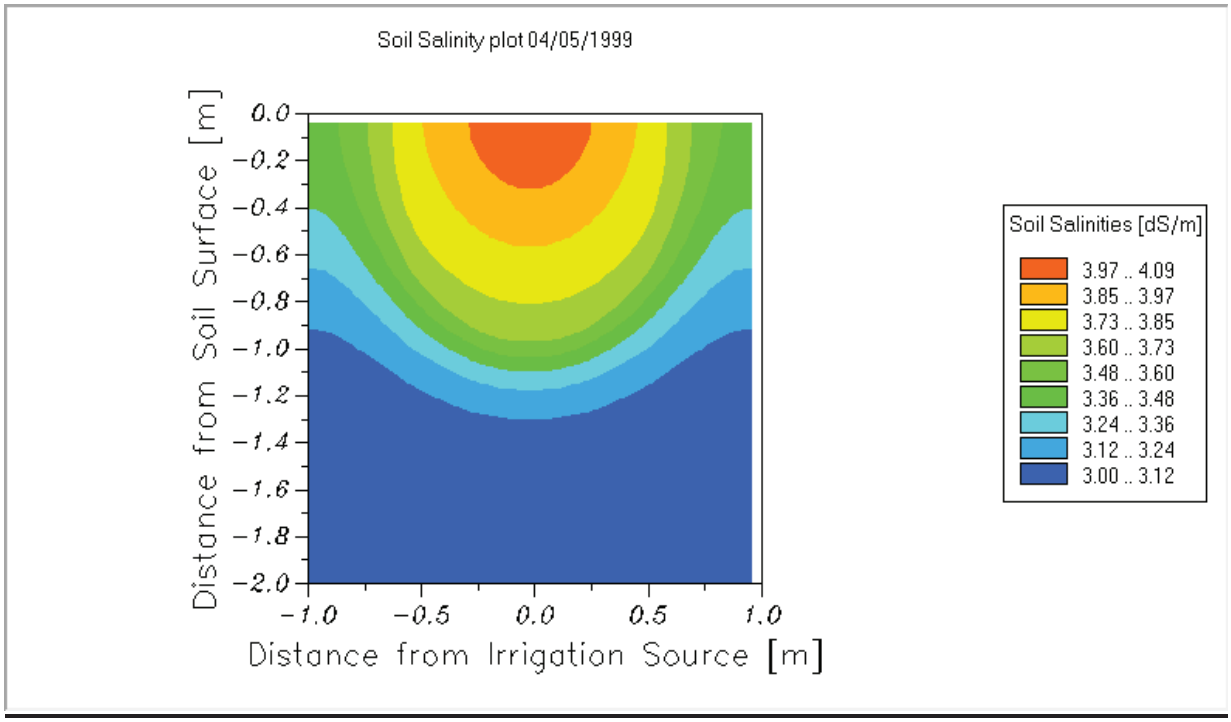

Output example of soil moisture under subsurface drip irrigation

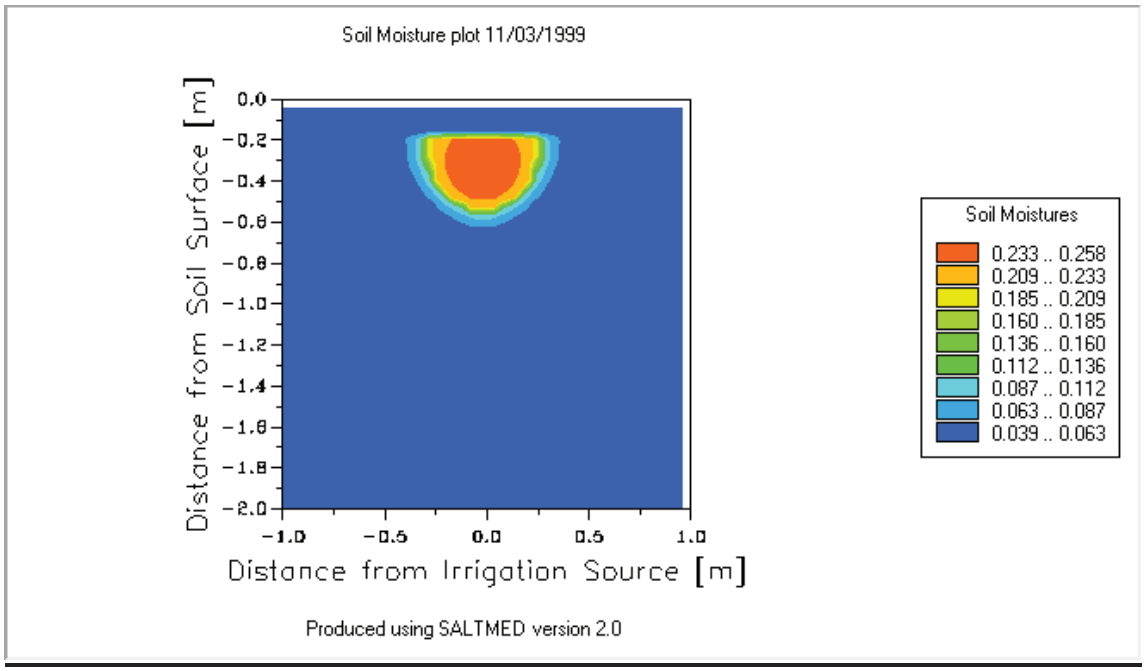

Output example of soil moisture under PRD drip irrigation

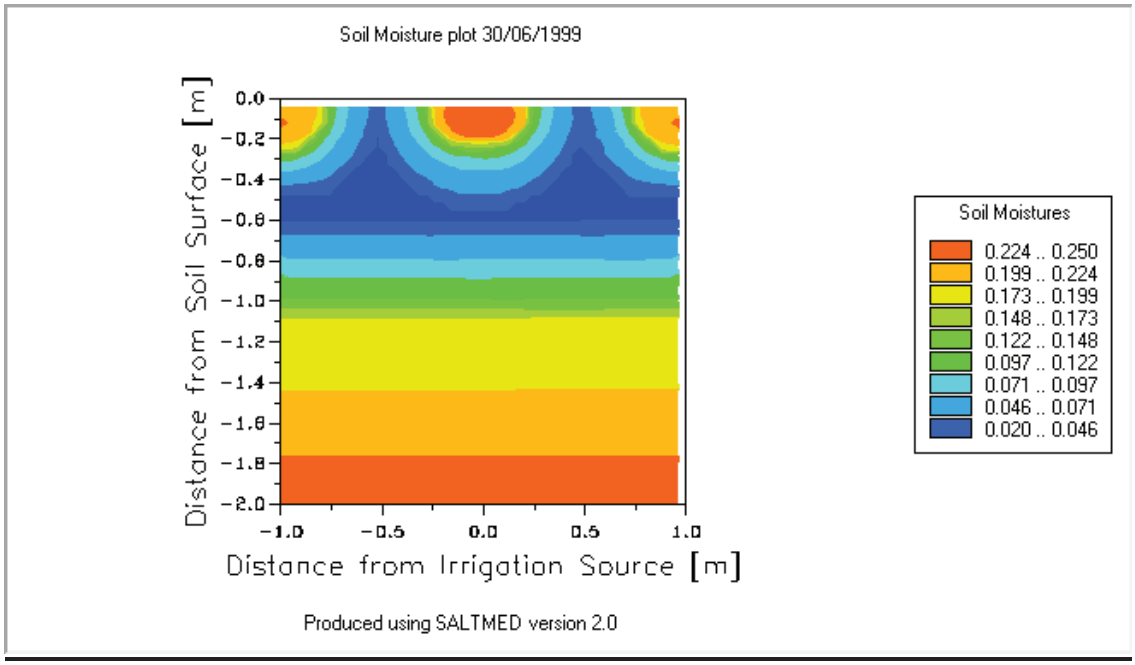

Output example of soil moisture under PRD subsurface drip irrigation

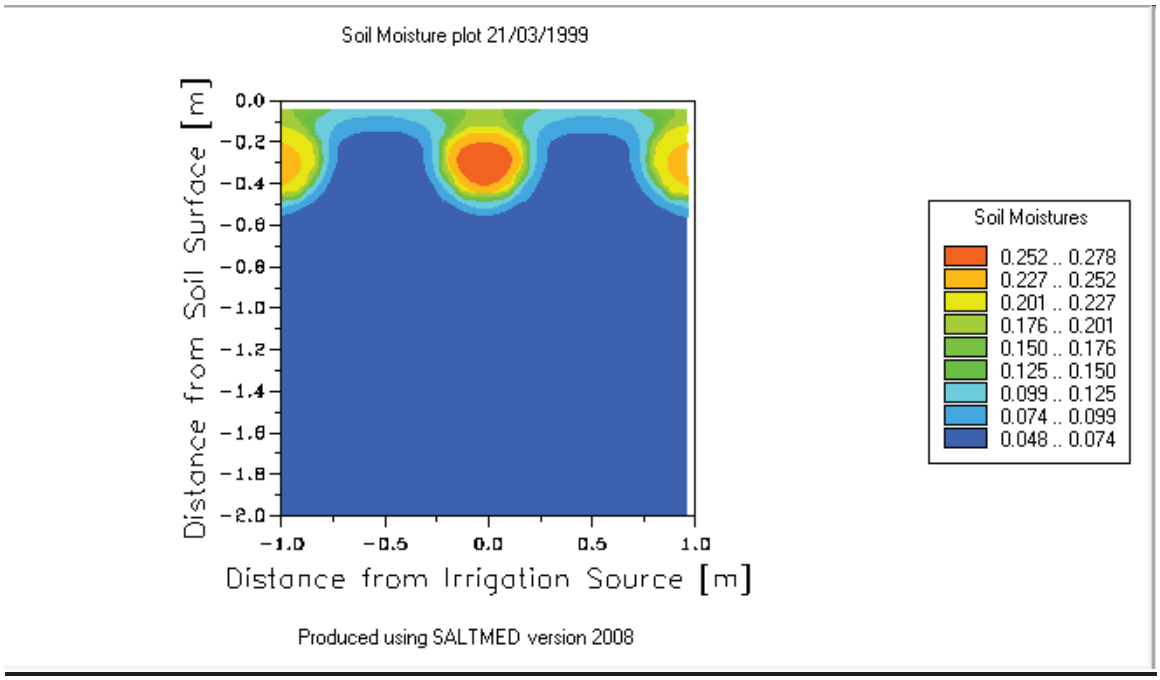

Output example of soil moisture profile under PRD drip irrigation

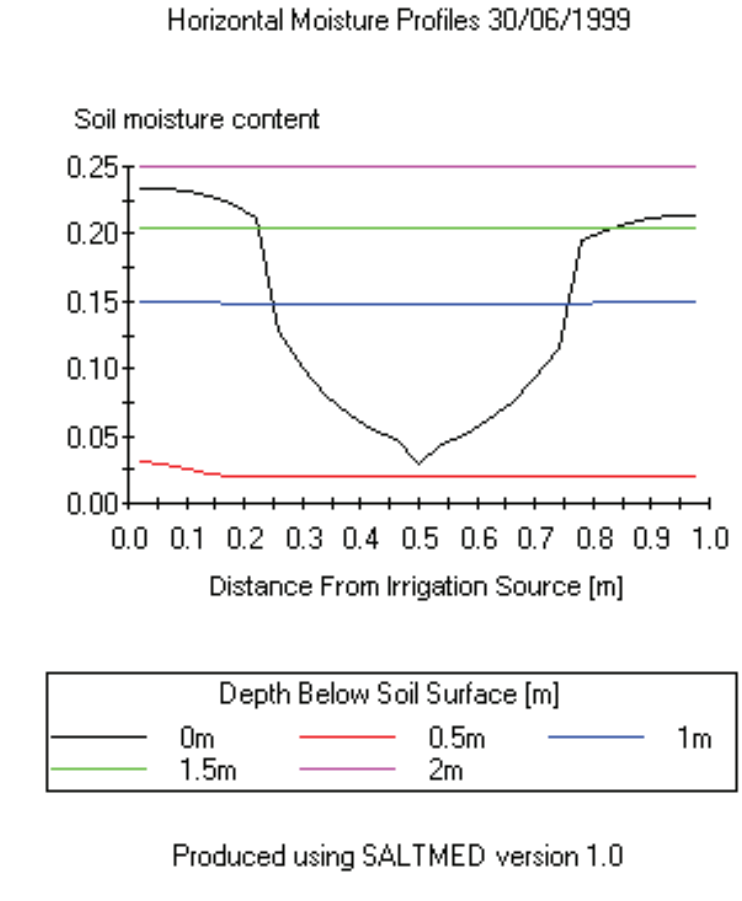

Output example of soil nitrogen profiles

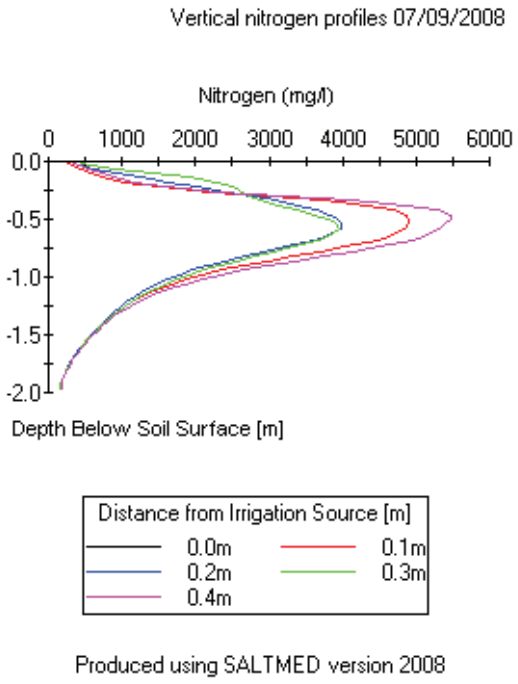

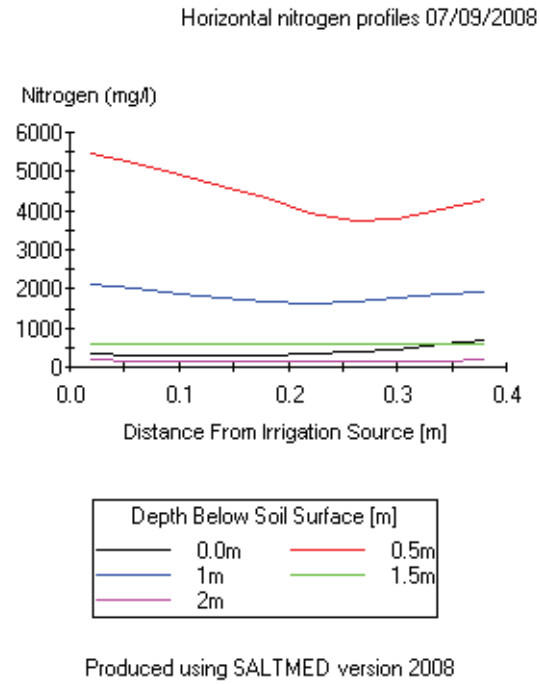

Output example of Evapotranspiration

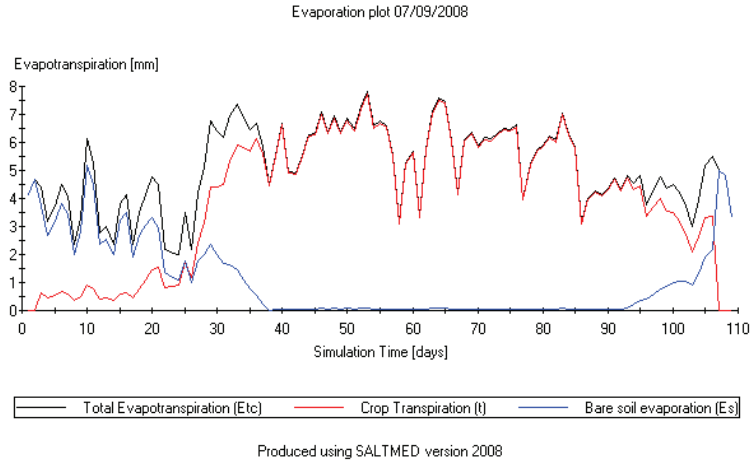

Output example of irrigation+ rainfall

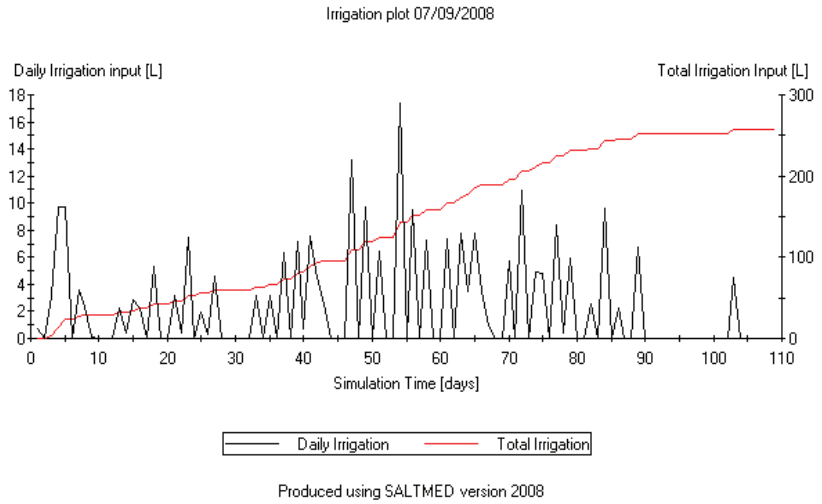

Output example of crop growth parameters

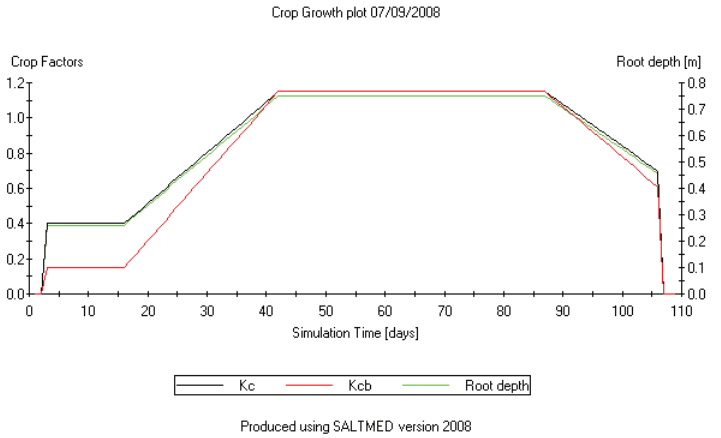

SALTMED MODEL Can be Downloaded at: **http://www.safir4eu.org**

The basis of SALTMED model can be found at:
Special Issu : J. Agric. Water Management,volume 98 (1-2), September, 2005, (Guest Editor, Ragab Ragab)

Annex 3.9 Test of the new Daisy model

by Finn Plauborg[1], Mikkel Mollerup[2], Per Abrahamsen[2], Fulai Liu[3], Bo Vangsø Iversen[1], Mathias N. Andersen[1], Christian R. Jensen[3], Søren Hansen[2]

1. Department of Agroecology and Environment, Faculty of Agricultural Sciences, University of Aarhus, Denmark
2. Dept. of Basic Sciences and Environment, Faculty of Life Sciences, University of Copenhagen, Denmark
3. Dept. of Agriculture and Ecology, Faculty of Life Sciences, University of Copenhagen, Denmark

New processes developed for the Daisy model

Based on several experiments in glasshouse and field conditions in Denmark new process sub-models have been developed for implementation in Daisy. These new sub-models have been reported in scientific journal papers, where the most important are mentioned below.

F. Liu, A. Shahnazari, M.N. Andersen, S.-E. Jacobsen, C.R. Jensen. 2006. Effects of deficit irrigation (DI) and partial root drying (PRD) on gas exchange, biomass partitioning, and water use efficiency in potato. Scientia Horticulturae 109: 113–117.

F. Liu, A. Shahnazari, M.N. Andersen, S.-E. Jacobsen, C.R. Jensen. 2006. Physiological responses of potato (Solanum tuberosum L.) to partial root zone drying: ABA signalling, leaf gas exchange, and water use efficiency. Journal of Experimental Botany 57: 3727-2735.

Shahnazari, F. Liu, M.N. Andersen, S.-E. Jacobsen, C.R. Jensen. 2007. Effects of partial root-zone drying on yield, tuber size and water use efficiency in potato under field conditions. Field Crops Research 100: 117–124.

F. Liu, R. Song, X. Zhang, A. Shahnazari, M.N. Andersen, F. Plauborg, S.-E. Jacobsen, C.R. Jensen. 2008. Measurement and modelling of ABA signalling in potato (Solanum tuberosum L.) during partial root-zone drying. Environmental and Experimental Botany 63, 385-391.

Ahmadi, S.H., Andersen, M.N, Poulsen, R.T., Plauborg, F., Hansen, S. 2009. A Quantitative Approach for Developing More Mechanistic Gas Exchange Models for Field Grown Potato: A New Insight into Chemical and Hydraulic Signalling. Agricultural and Forest Meteorology 149, 1541-1551.

Liu, F., Andersen, M.N., Jensen, C.R. 2009. Capability of the 'Ball-Berry' model for predicting stomatal conductance and water use efficiency of potato leaves under different irrigation regimes. Scientia Horticulturae 122, 346-354.

These studies deals with ABA produced in the root system of potato when the crop is imposed to different deficit regimes, e.g. Partial Root Drying (PRD). The results have been formulation of ABA production functions which have been included into Daisy, Figs. 1 and 2.

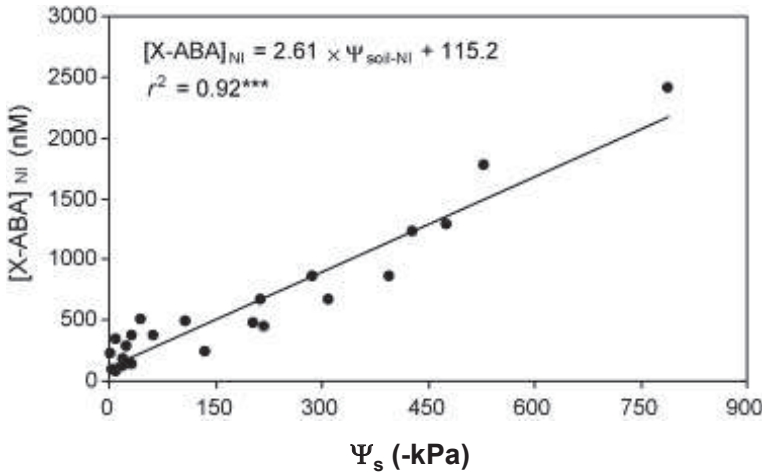

Figure 1. ABA concentration (X-[ABA as a response to soil water potential (Liu et al., 2008).

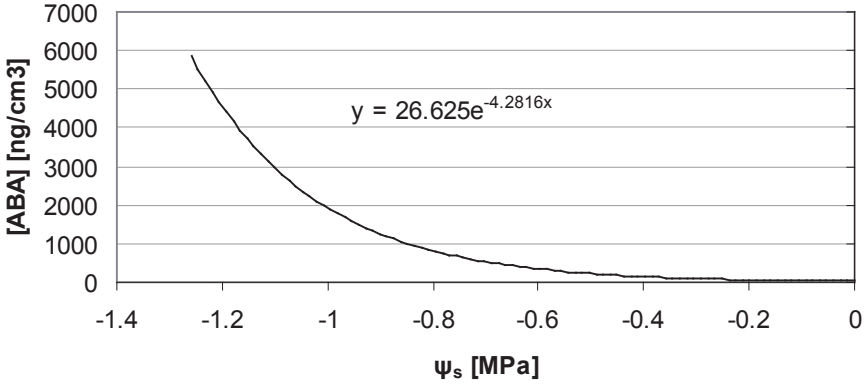

Figure 2. ABA concentration (X-[ABA]) as a response to soil water potential Abrahamsen (pers. comm. 2009).

This response and its effect on gas exchange have lead to formulation of new single leaf models of stomatal conductance (g_s).

Gutschick and Simonneau (2002), Abrahamsen (pers. 2009)

$$g_s = m\, A_n\, h_s/c_s \exp(-\beta\,[ABA]) + g_{s0}$$

with m =17, β= 0.095 [cm^3/ng] and g_{s0}= 0.15 [$mol/m^2/s$]

Liu et al. (2009) $g_s = mA_n \frac{h_s}{C_s} + g_0 \qquad m = m_i e^{-\beta\psi_s}$

Ahmadi et al. (2009)

$$g_s = mA_n{}^{\lambda} \frac{h_s{}^{\alpha}}{c_s} \exp\left(-\beta[ABA]\right)\exp\left(-\delta|\psi_s|\right)$$

$$g_s = \frac{m}{c_s}\exp\left(\lambda A_n\right)\exp\left(\alpha h_s\right)\exp\left(-\beta[ABA]\right)\exp\left(-\delta|\psi_s|\right)$$

Testing the new Daisy model

The above sub-models have been implemented into the comprehensive Daisy model (see D3_2) and testing have been carried out for potatoes in Denmark and fresh tomatoes in Crete, Greece

Results from potatoes in Denmark

The focus of semi-field experiments at Aarhus University was to create comprehensive datasets on gas exchange and soil water dynamics in potatoes imposed to irrigation strategies, Full Irrigation, Deficit Irrigation and Partial Root zone Drying. The findings are fully reported in a coming special issue in Agricultural Water Management, and hence here only some few results are shown. Figure 3 shows the Daisy modelled stomatal conductance (g_s) under predict the field measurements in the late season. Still research is needed to understand this difference, which for the moment is thought to be an effect of nitrogen on photosynthesis maybe not yet well included in the model.

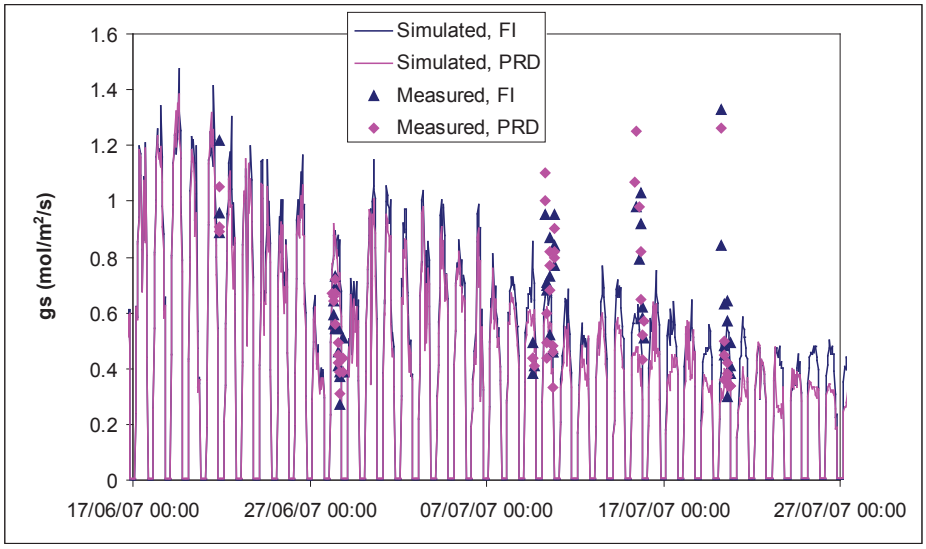

Figure 3. Daisy simulated stomatal conductance (g_s) versus measured in field grown potatoes.

Another discussed still to be further researched is if ABA production functions needs to be soil texture dependent, and morning and afternoon ABA not pictured by the model (Fig. 4) has any relevance. The latter as hardly any production takes place early and late during the day.

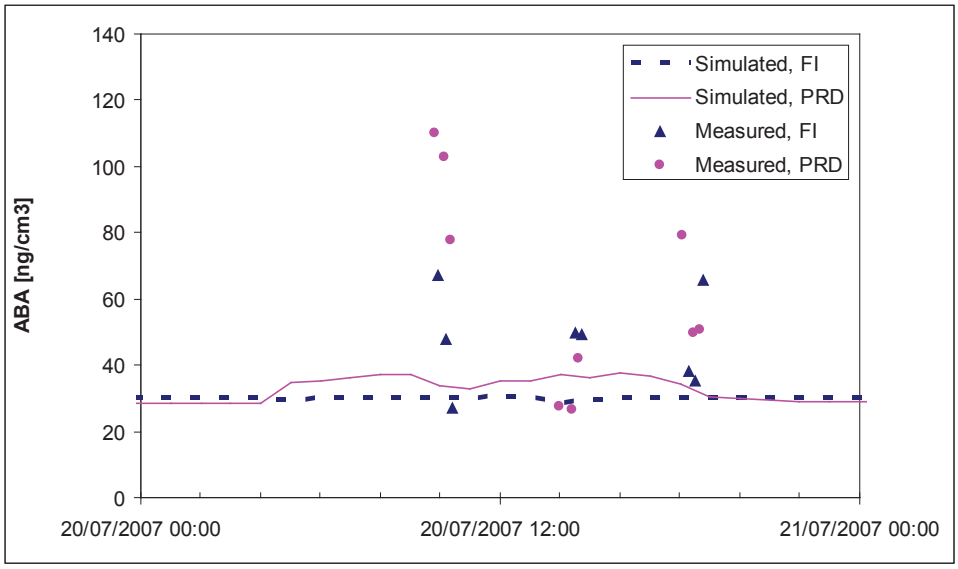

Figure 4. Simulated and measured ABA concentration in the upper leaves of potatoes around 10, 14 and 18 hours 20 July 2007.

Results from fresh tomatoes at Crete, Greece

Data from 2007 was used for calibration and data from 2008 for verification of the Daisy model.

2007 data

Figure 5 shows (top) a good calibration of the Daisy model as measured and simulated dry matter (DM) in fully irrigated fresh tomato fits well although total DM in the harvested tomatoes in the last harvest was 10% over predicted. Measured and simulated leaf area index compares well (middle), as do measured and simulated leaf nitrogen (bottom).

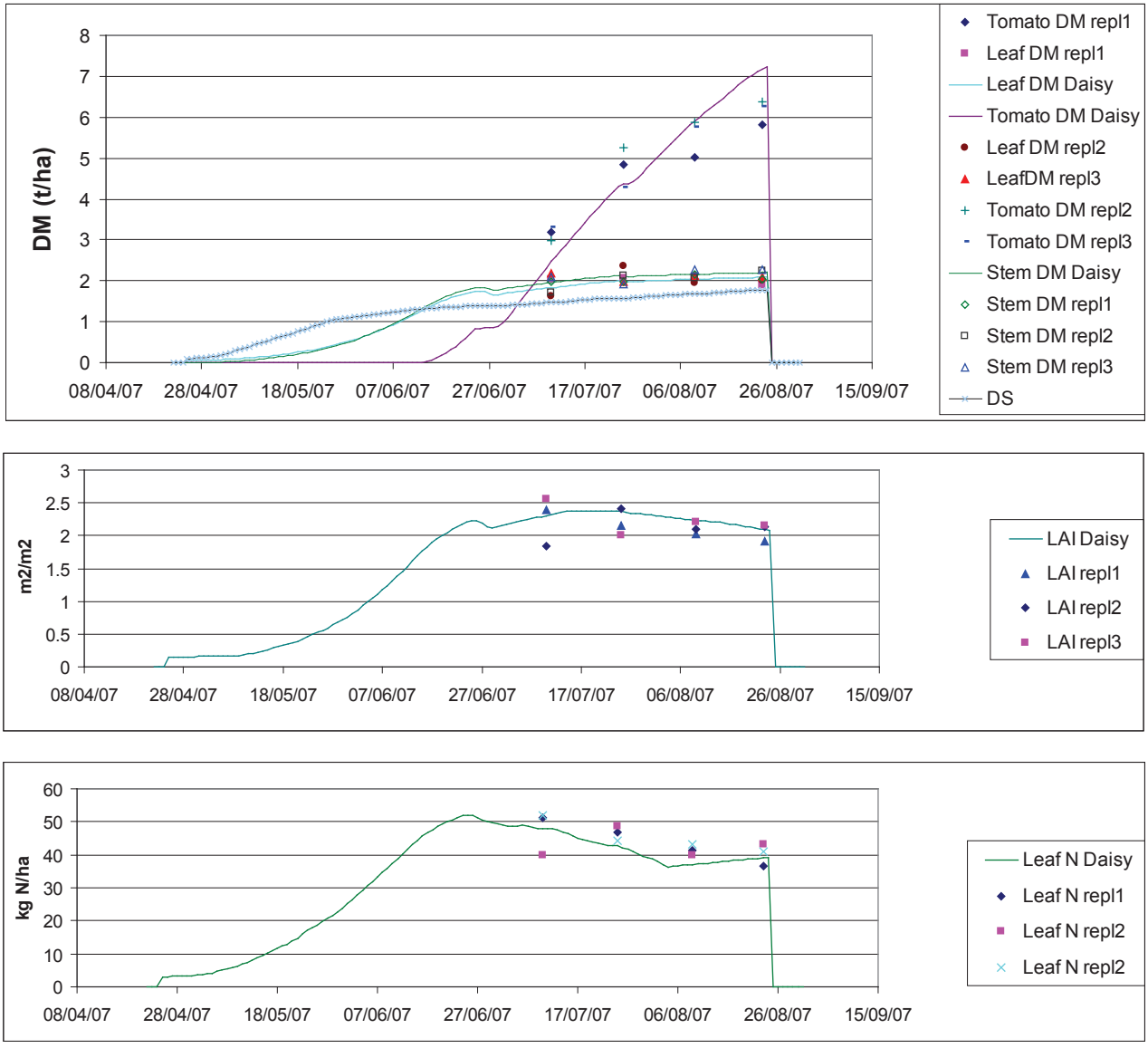

Figure 5. Fully irrigated fresh tomato, measured and simulated: (top) dry matter, (middle) leaf area index, (bottom) leaf nitrogen.

Figure 6 shows the same comparison as in figure 5, but data from the PRD irrigated treatments. The calibration from fully irrigated treatment performs very well and nice comparisons were obtained.

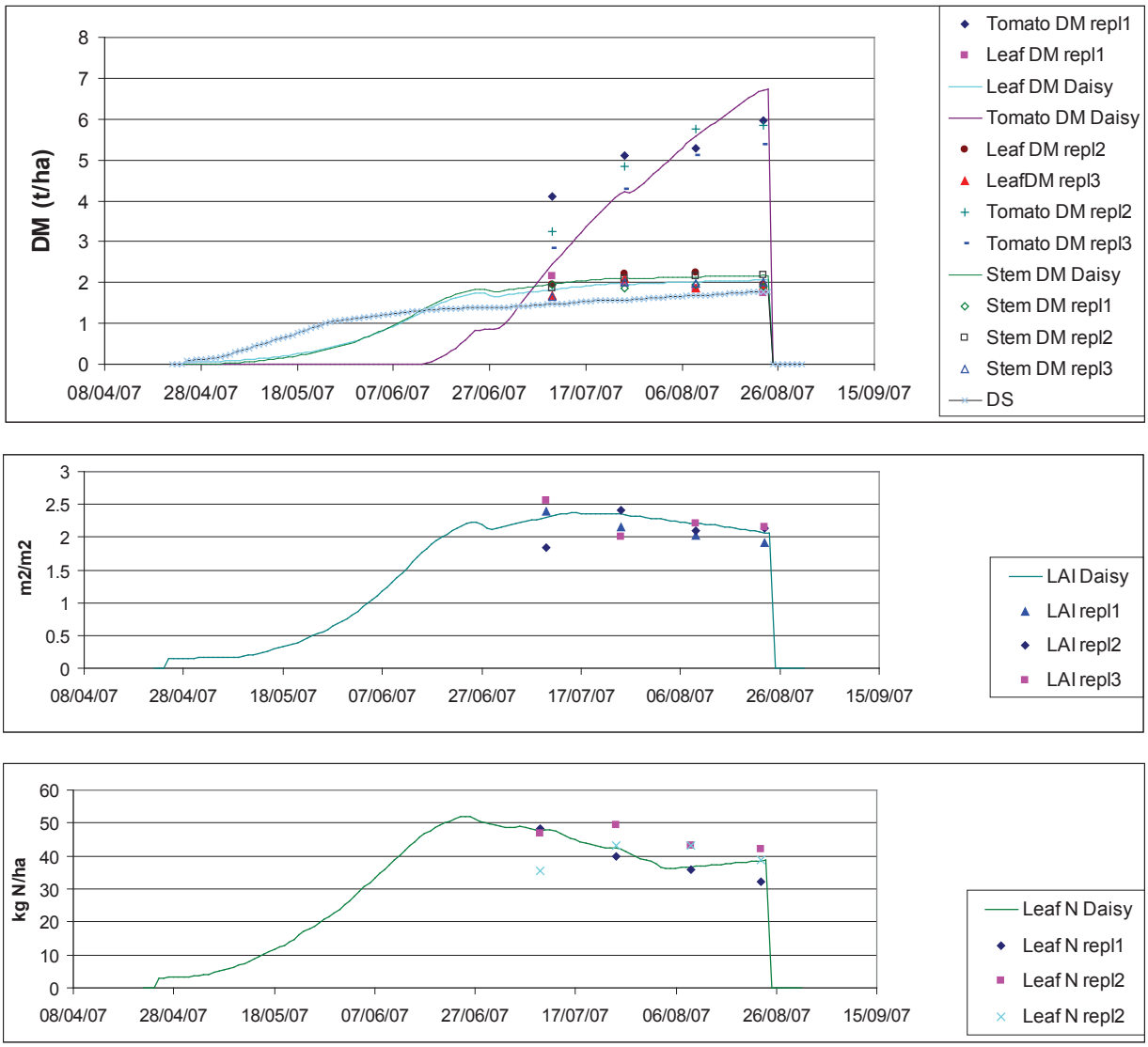

Figure 6. PRD irrigated fresh tomato, measured and simulated: (top) dry matter, (middle) leaf area index, (bottom) leaf nitrogen.

Figure 7 shows measured and simulated soil water content in the centre of the tomato row in depth 0-40 cm (top) fully irrigated, (middle) right side of the tomato in the PRD treatment, and (bottom) the left side of the tomato plant. The hydraulic parameters were not calibrated resulting in a slight over prediction, especially in the fully irrigated treatment. From 7 July the over prediction may be caused by a too low simulated stomatal conductance (cf. Fig. 3) indicating that this model developed in pot experiments needs to be assessed from the field measurements. However a clear response in both measured and simulated soil water content were observed in the PRD treatments.

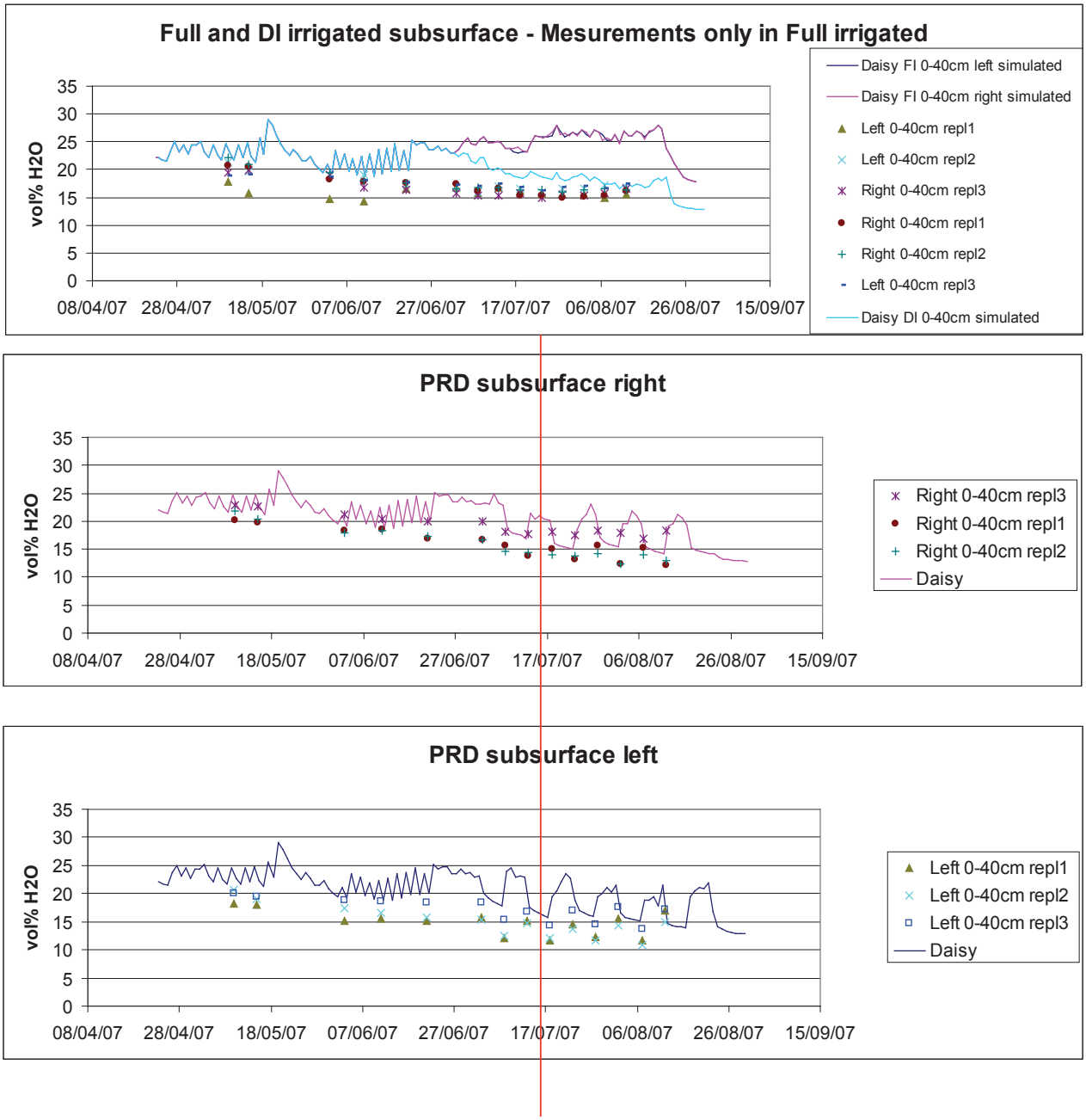

Figure 7. Measured and simulated soil water content. Fully irrigated (top), right site of the tomato plant (middle), and left side (bottom).

Figure 8 shows simulated ABA concentration in the fully, deficit and the PRD treatments. The responses are quite acceptable as the highest concentration of ABA was obtained in the deficit and next the PRD treatments.

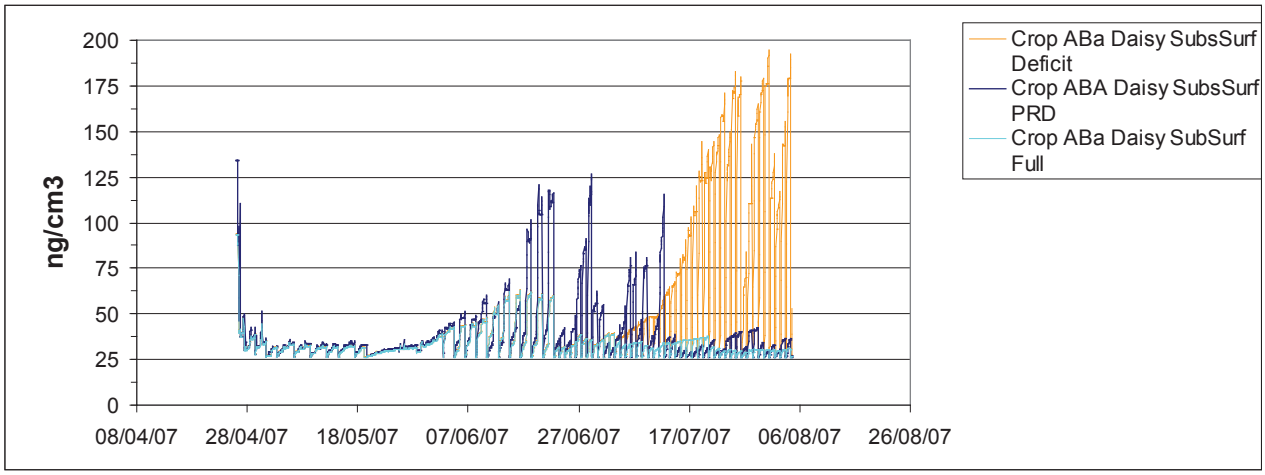

Figure 8. Simulated ABA concentration in the top leaves of tomato in the fully, deficit and PRD treatments.

Figure 9 shows irrigation inputs (green bars) to the fully, deficit and PRD treatments, causing a simulated transpiration (blue bars) slightly higher in fully irrigated compared with the PRD treatment.

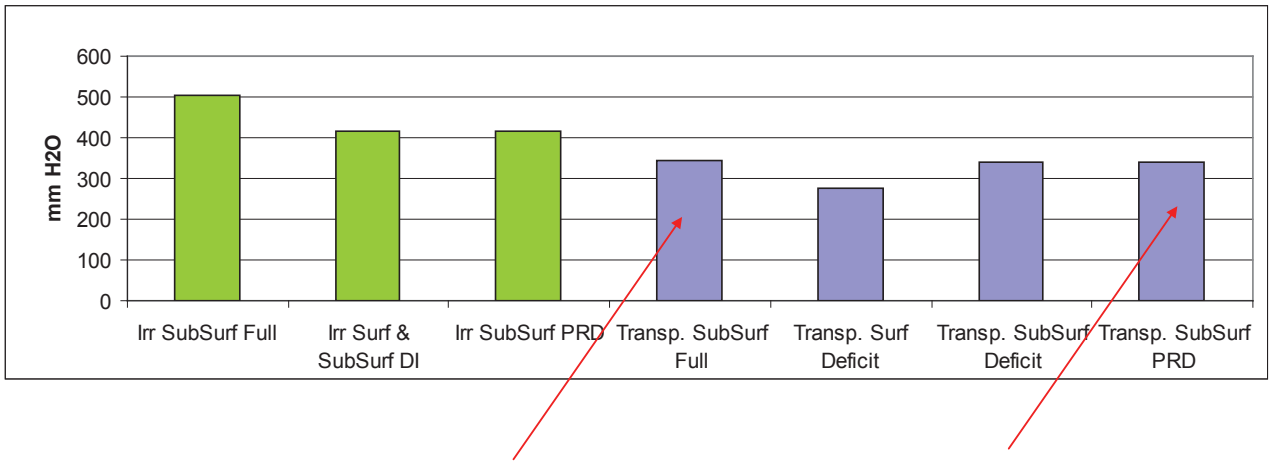

Figure 9. Irrigation input in the 2007 treatments with tomato (green bars). Simulated transpiration in the different treatments (blue bars).

Figure 10 shows tomato dry matter yield in simulated (purple bars) and measured (green bars) in the 2007 tomato experiments.

The above mentioned tendency of over prediction of the tomato yield can be found in both the fully and PRD irrigated treatments, however the trend of lower yield in the PRD treatment was consistent in both measured and simulated data.

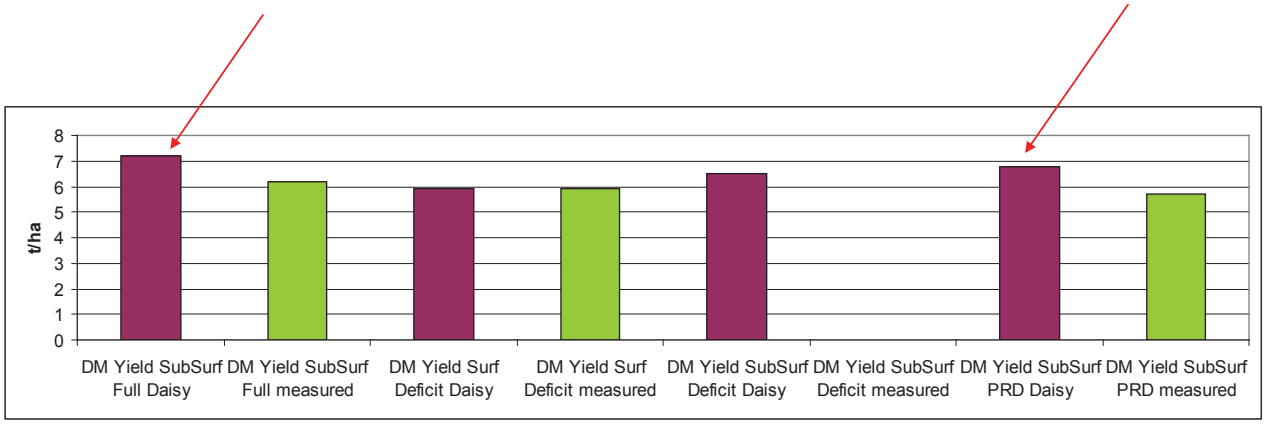

Figure 10. Measured and simulated dry matter yield in the 2007 tomato treatments.

2008 data

Figure 11 shows measured and simulated dry matter (DM) in fully irrigated fresh tomato (top left) and PRD irrigated fresh tomato (top right). Stem and leafs compare well whereas the fruit dry matter was highly over predicted. It seems that the model needs some refinements as the tendency of over prediction was found also in 2007, however the big difference in 2008 may be caused mainly by the observed miss flowering and pollination not captured by the model. Measured and simulated leaf area index compares well (middle left and right), as do measured and simulated leaf nitrogen (bottom left and right).

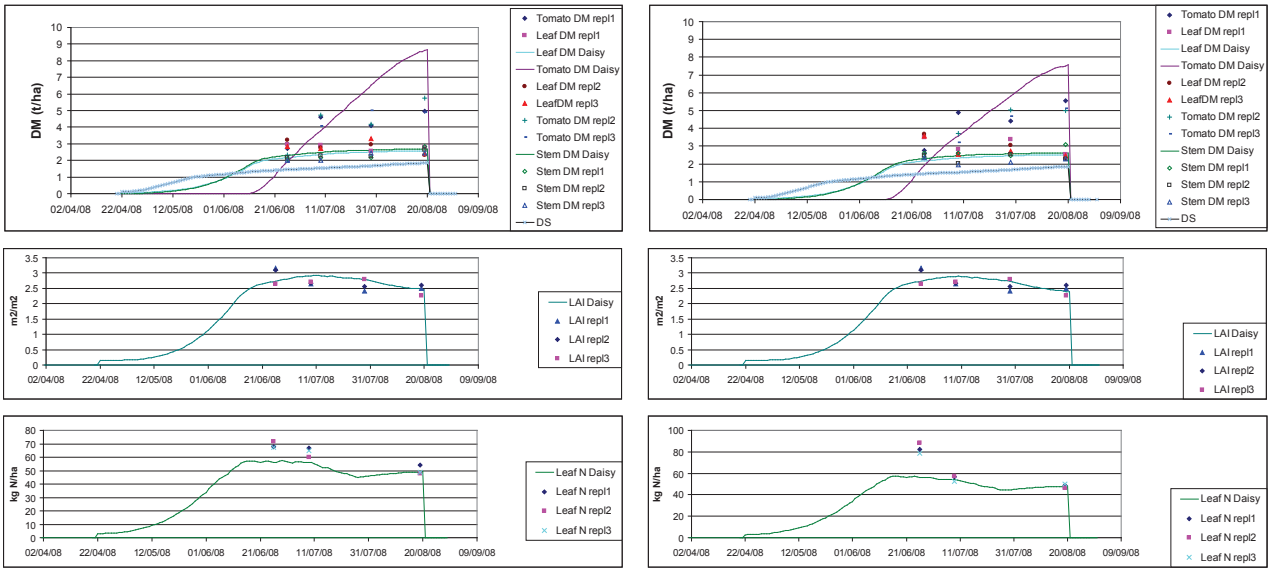

Figure 11. Fully irrigated (left) and PRD irrigated (right) fresh tomato, measured and simulated: (top) dry matter, (middle) leaf area index, (bottom) leaf nitrogen.

Figure 12 shows measured and simulated soil water content in the centre of the tomato row in depth 0-40 cm (top) fully irrigated, (middle) right side of the tomato in the PRD treatment, and (bottom) the left side of the tomato plant. The hydraulic parameters were not calibrated resulting in a slight over prediction, especially in the fully irrigated treatment. From 21 June the over prediction may be caused by a too low simulated stomatal conductance indicating that this model developed in pot experiments needs to be assessed from the

field measurements. However a clear response in both measured and simulated soil water content were observed in the PRD treatments.

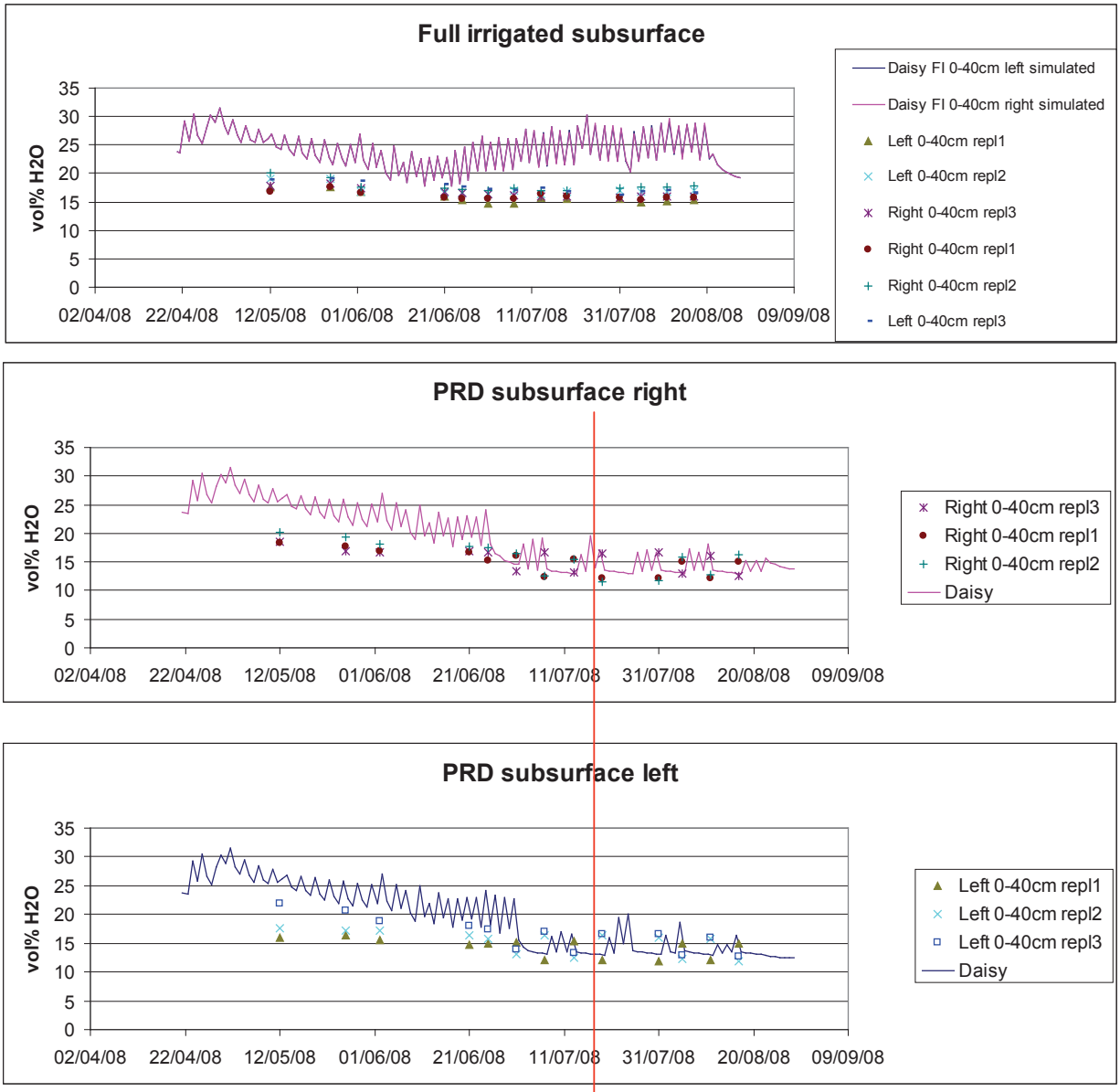

Figure 12. Measured and simulated soil water content. Fully irrigated (top), right site of the tomato plant (middle), and left side (bottom).

Figure 13 shows simulated ABA concentration in the fully and the PRD treatments. The responses are quite acceptable as the highest concentration of ABA was obtained in the PRD treatments.

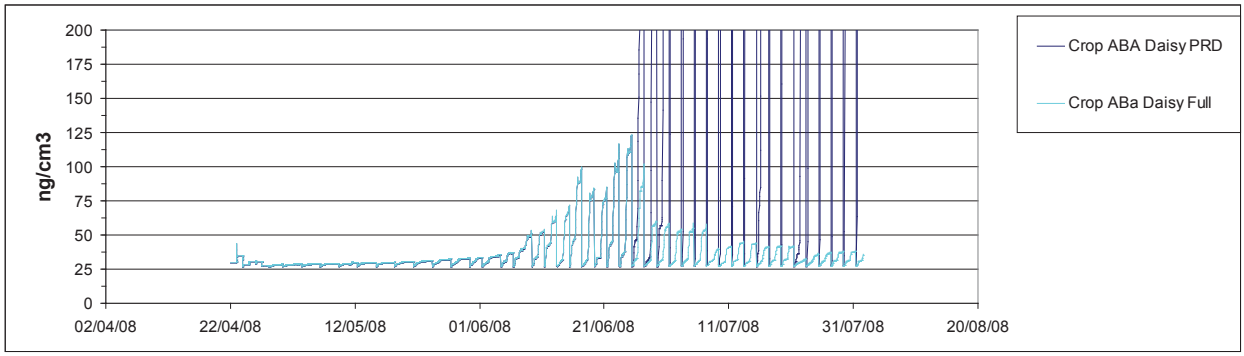

Figure 13. Simulated ABA concentration in the top leaves of tomato in the fully and PRD treatments.

Figure 14 (top) shows 2008 irrigation inputs (green bars) to the fully and PRD treatments, causing a simulated transpiration (blue bars) quite higher in fully irrigated compared with the PRD treatment, and hence an important water saving was achieved. This was obtained without a dramatic decrease in fruit yield. (Fig. 14, bottom).

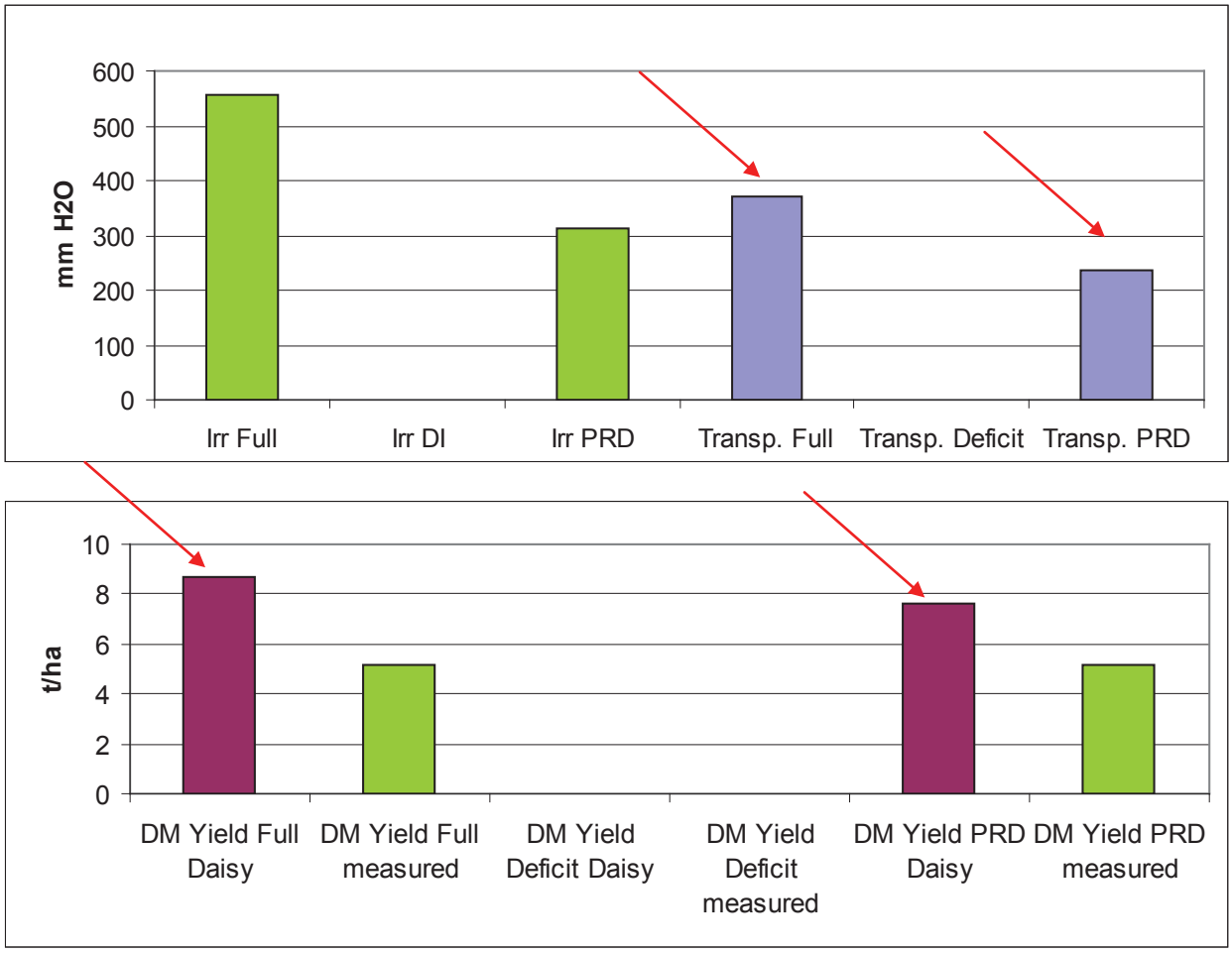

Figure 14. (top) Irrigation input in the 2008 treatments with tomato (green bars). Simulated transpiration in the different treatments (blue bars). (bottom) Tomato dry matter yield in simulated (purple bars) and measured (green bars) in the 2008 tomato experiments.

Conclusions

In the Danish experiments the level of ABA measured in FI and PRD irrigated potatoes differed due to the sampling method, field or glasshouse conditions?

The pot gs model seams not fully valid in field experiments, especially in the middle and late part of the season, however as no measurements were carried out in the Crete experiment further studies is needed to confirm this.

The new Daisy 2D-water soil water flow and leaf gas exchange equations for photosynthesis and stomata conductance seems well implemented in the Daisy model. Calibration of the soil hydraulic parameters may improve the comparisons to measured soil water content.

Increased intrinsic WUE at leaf level in pot potatoes with PRD was not consistently verified at canopy level with the new Daisy for fresh tomatoes, however important trends of water saving without too high yield loss was observed in the PRD treatments.

Further studies are needed to explore if ABA production function and gs models are different in tomatoes compared with potatoes.

Annex 3.10 Some selected simulation results using the SALTMED model

Yield simulation results

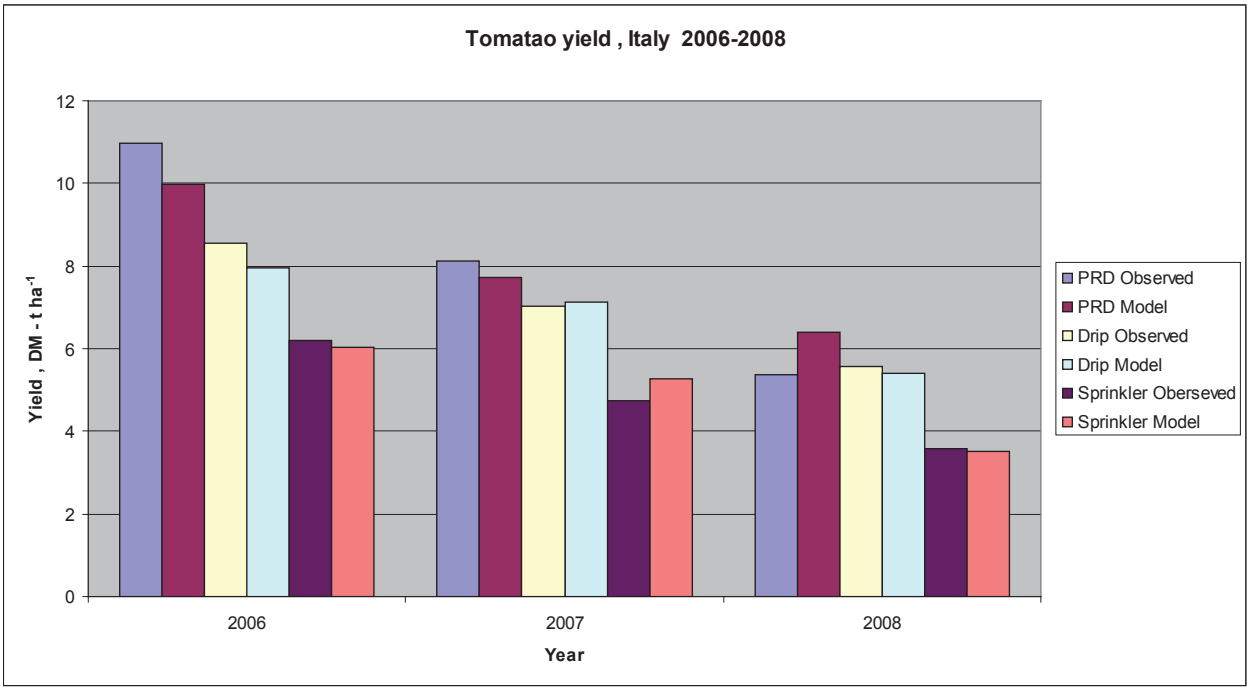

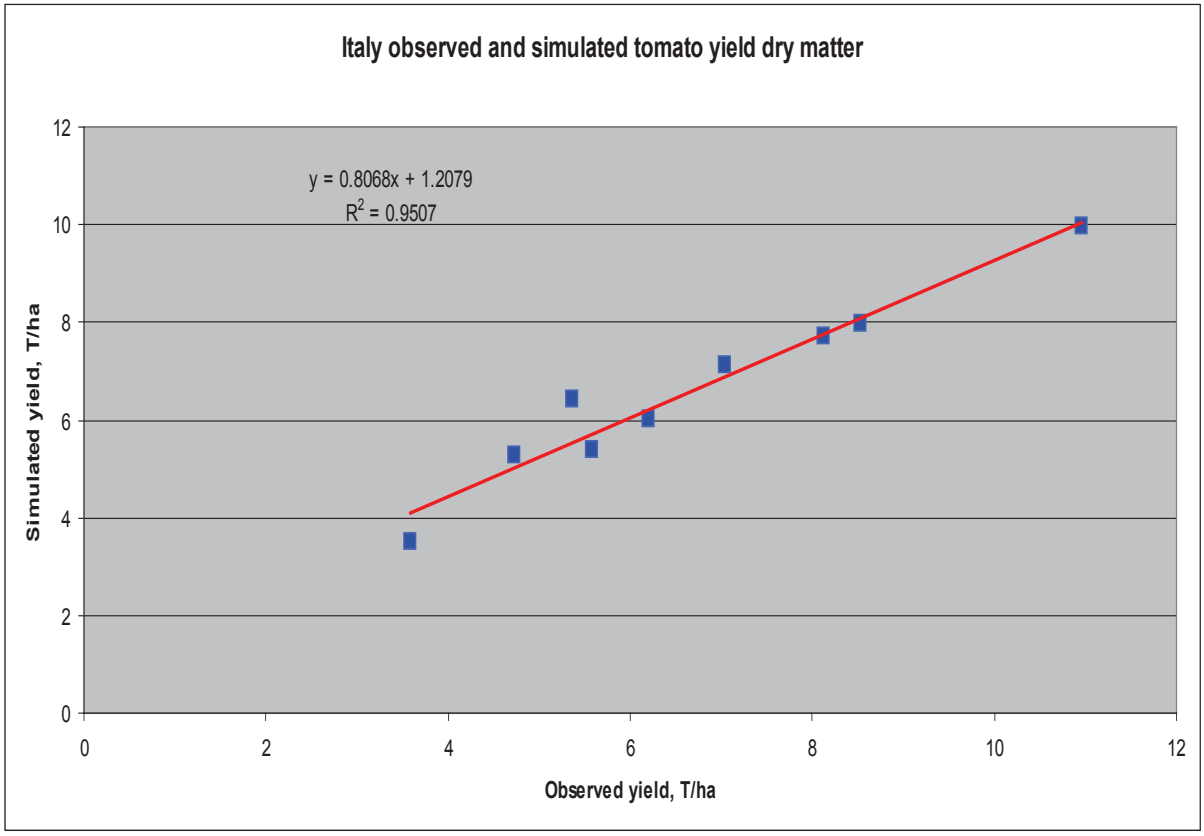

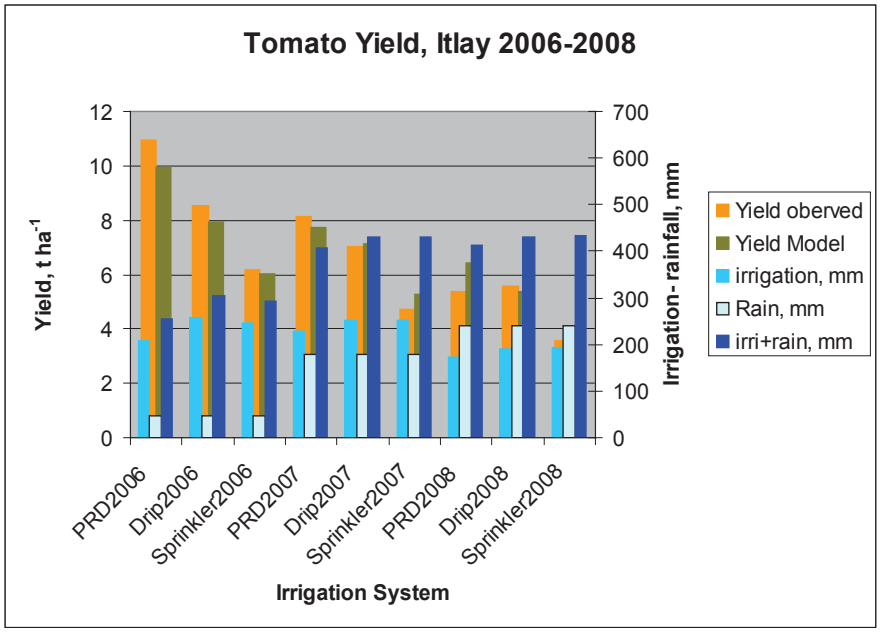
Tomato Yield, Itlay 2006-2008
Yield, t ha-1
Irrigation - rainfall, mm
Irrigation System
PRD2006
Drip2006
Sprinkler2006
PRD2007
Drip2007
Sprinkler2007
PRD2008
Drip2008
Sprinkler2008
Yield oberved
Yield Model
irrigation, mm
Rain, mm
irri+rain, mm

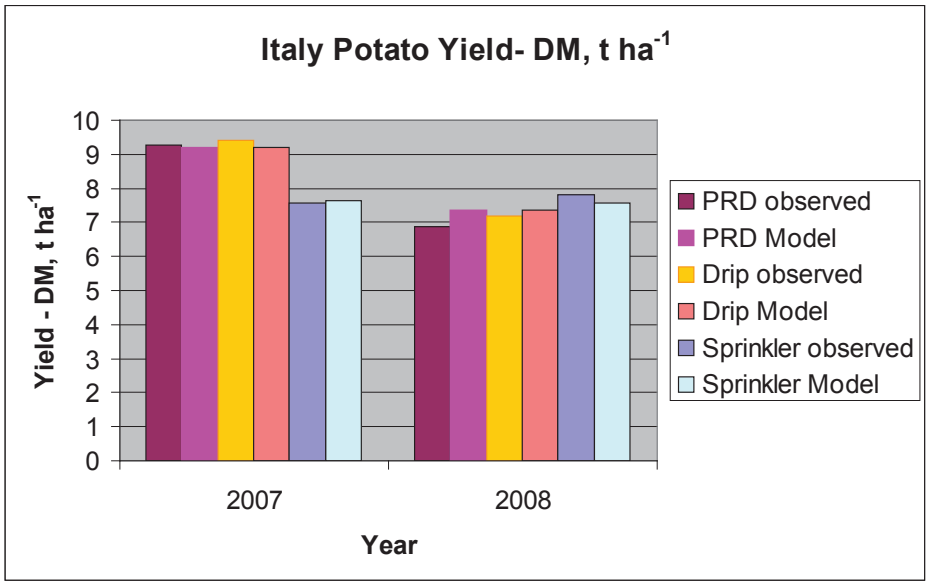
Italy Potato Yield- DM, t ha-1
Yield - DM, t ha-1
Year
2007
2008
PRD observed
PRD Model
Drip observed
Drip Model
Sprinkler observed
Sprinkler Model

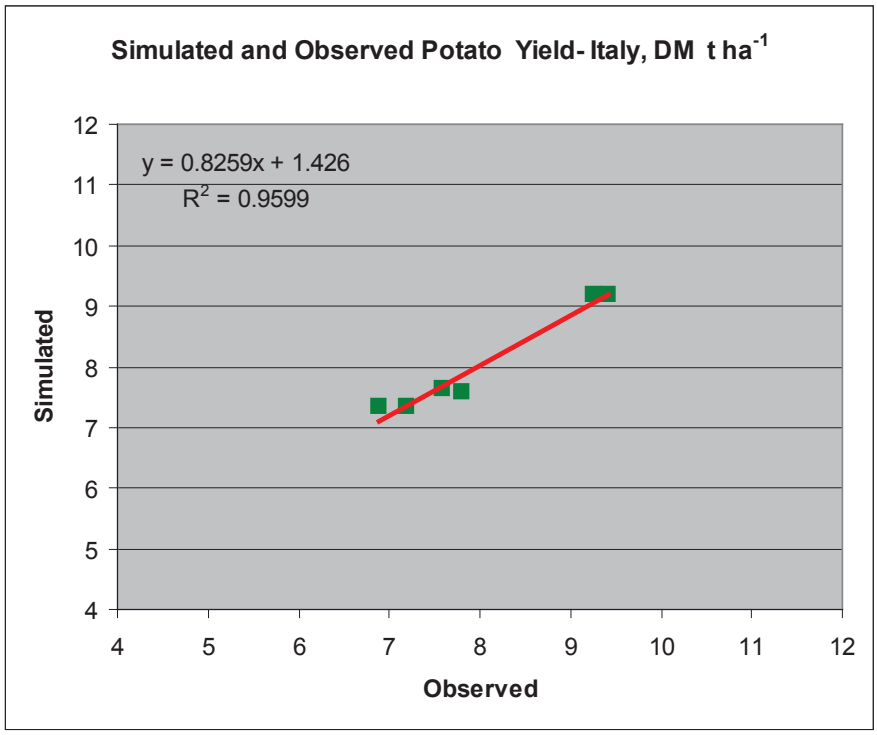
Simulated and Observed Potato Yield- Italy, DM t ha-1
y = 0.8259x + 1.426
R2 = 0.9599
Simulated
Observed
12
11
10
9
8
7
6
5
4
4
5
6
7
8
9
10
11
12

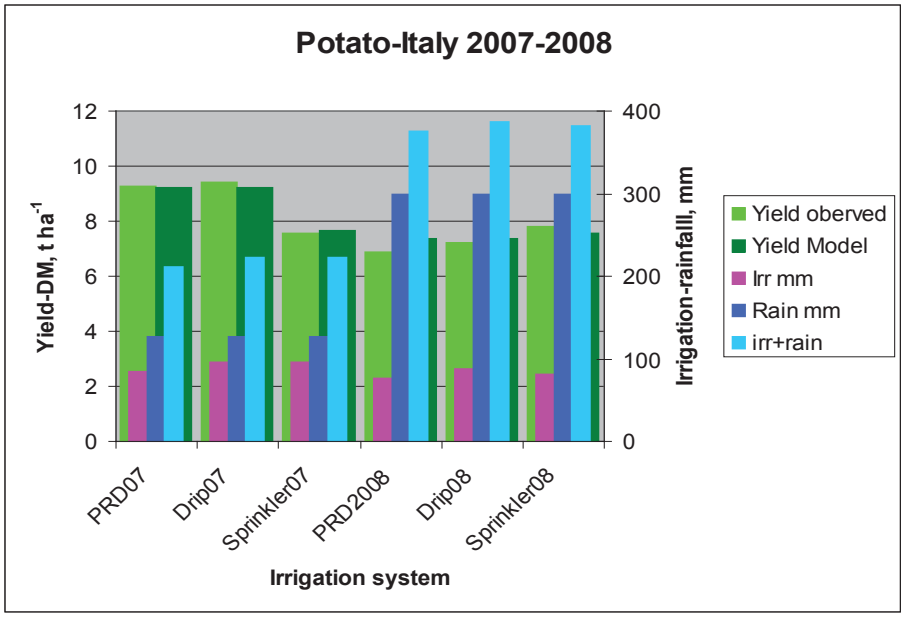
Potato-Italy 2007-2008
Yield-DM, t ha-1
Irrigation-rainfall, mm
Irrigation system
PRD07
Drip07
Sprinkler07
PRD2008
Drip08
Sprinkler08
Yield oberved
Yield Model
Irr mm
Rain mm
irr+rain
0
2
4
6
8
10
12
0
100
200
300
400

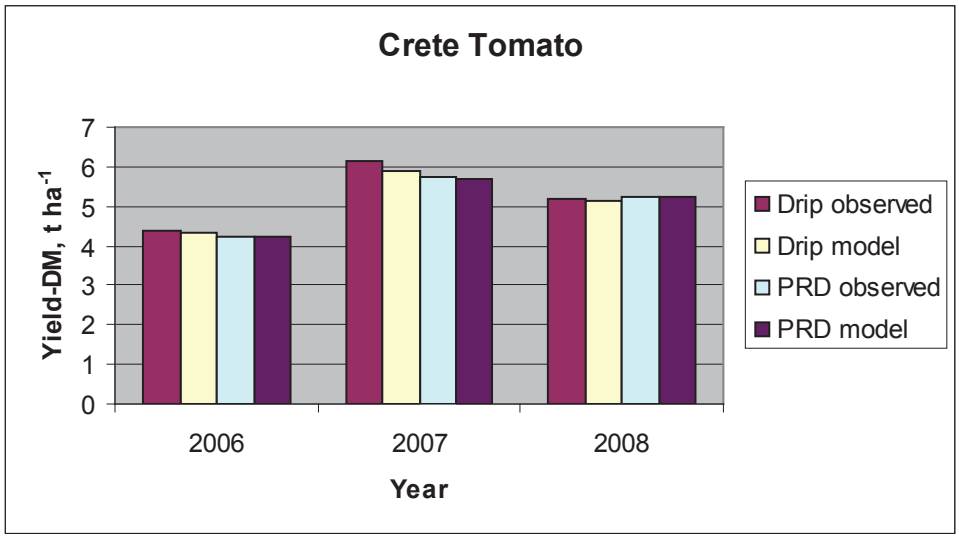
Crete Tomato
Yield-DM, t ha-1
0
1
2
3
4
5
6
7
2006
2007
2008
Year
Drip observed
Drip model
PRD observed
PRD model

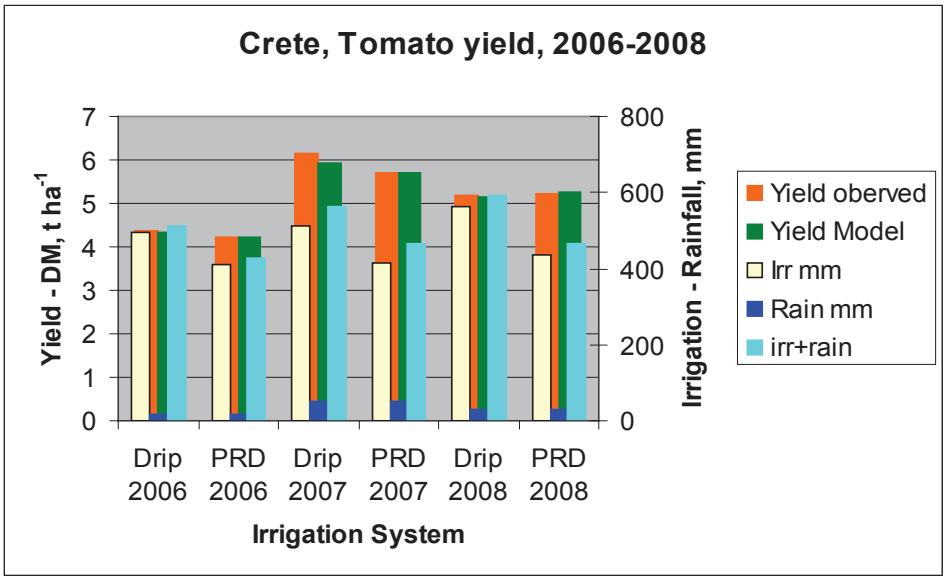
Crete, Tomato yield, 2006-2008
Yield - DM, t ha-1
0
1
2
3
4
5
6
7
800
600
400
200
0
Irrigation - Rainfall, mm
Drip 2006
PRD 2006
Drip 2007
PRD 2007
Drip 2008
PRD 2008
Irrigation System
Yield oberved
Yield Model
Irr mm
Rain mm
irr+rain

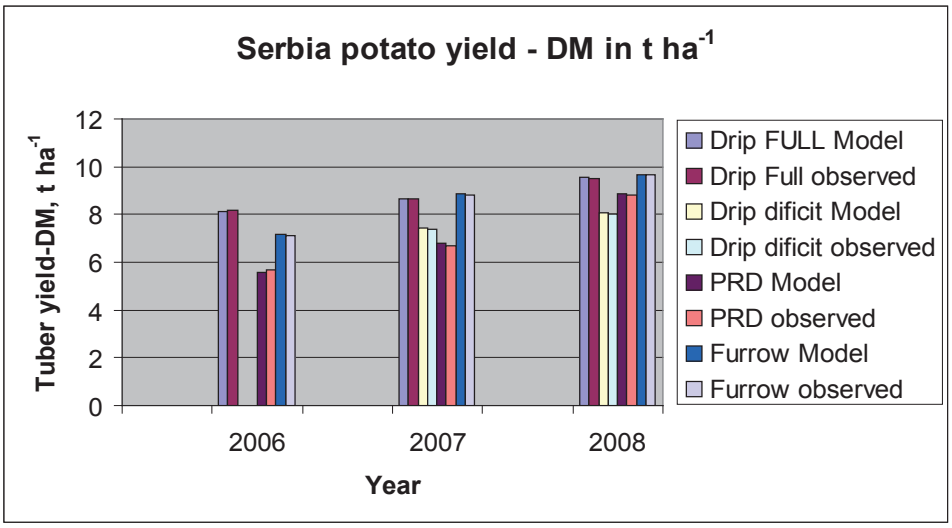

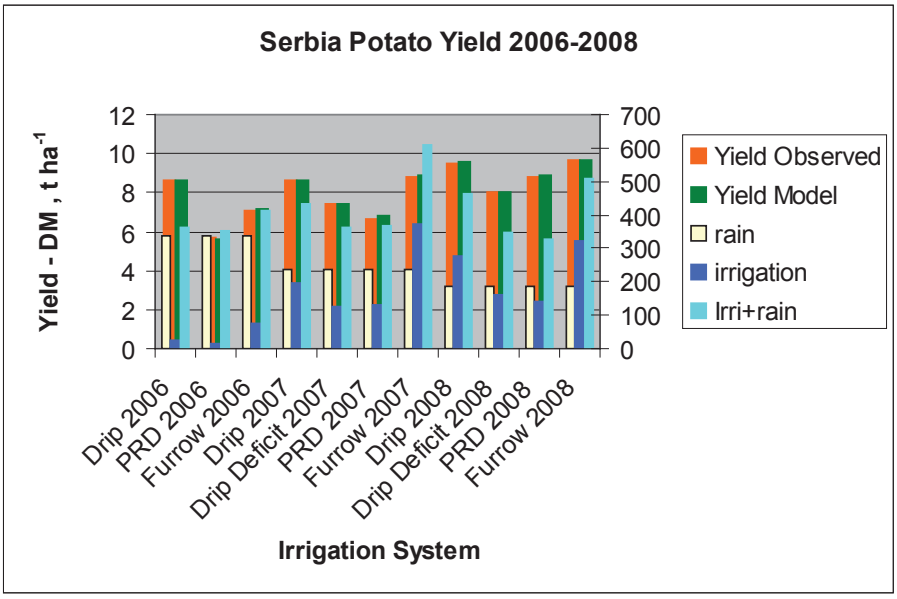

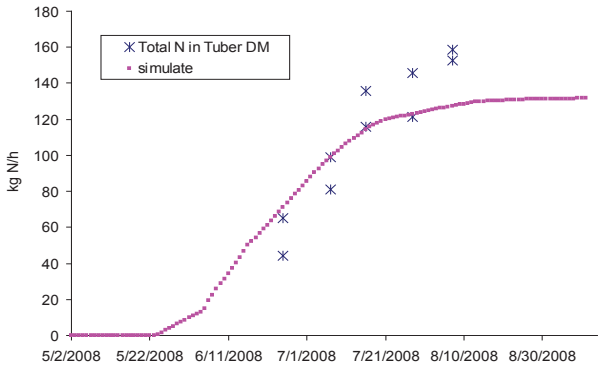

Serbia. Total N in tuber DM measured and simulated data obtained from fully irrigated potato crops with sand filter water treatment during 2008 season.

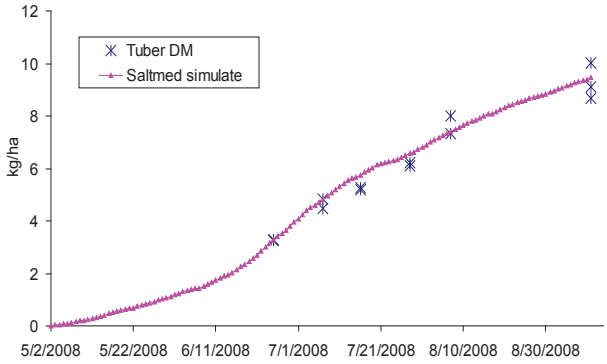

Serbia Tuber DM measured and simulated data obtained from fully irrigated potato crops with sand filter water treatment during 2008 season.

Soil Moisture and soil nitrogen modelling results

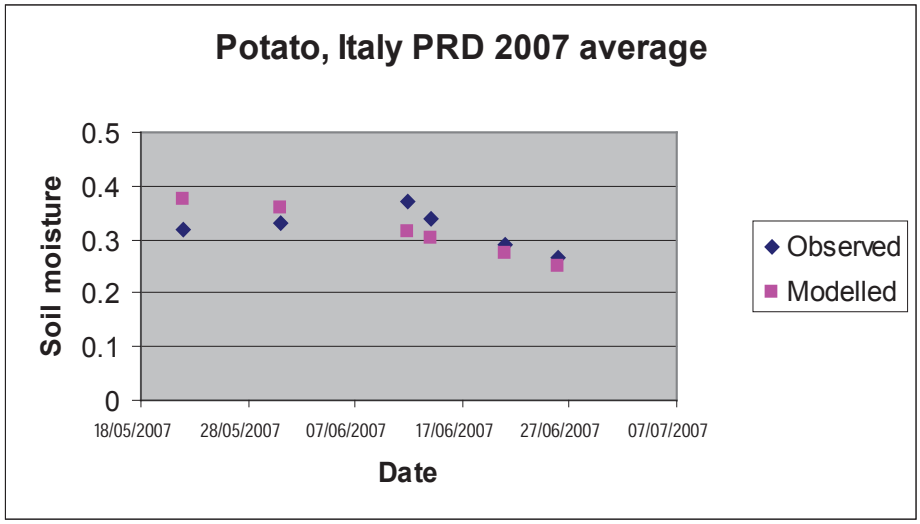

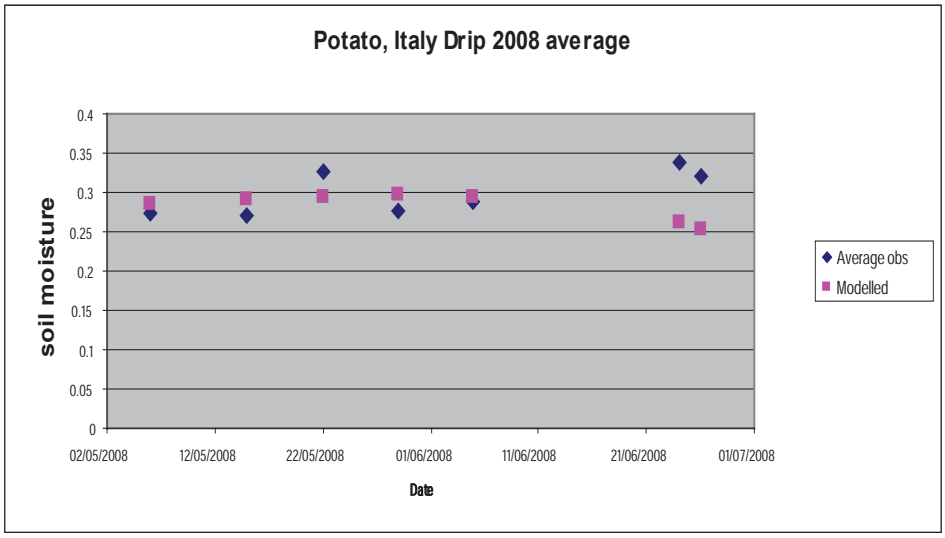
Potato, Italy Drip 2008 average
soil moisture
0.4
0.35
0.3
0.25
0.2
0.15
0.1
0.05
0
02/05/2008
12/05/2008
22/05/2008
01/06/2008
11/06/2008
21/06/2008
01/07/2008
Date
Average obs
Modelled

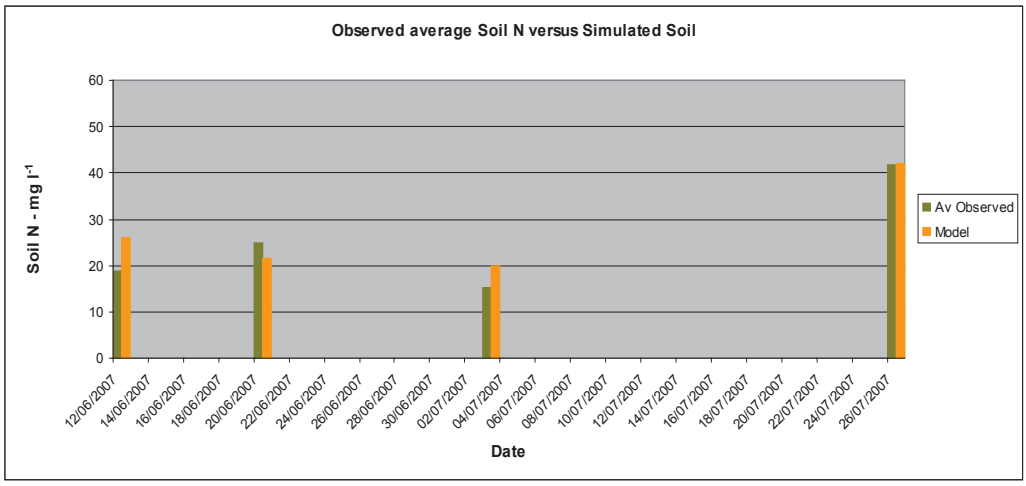
Observed average Soil N versus Simulated Soil
Soil N - mg l-1
60
50
40
30
20
10
0
12/06/2007
14/06/2007
16/06/2007
18/06/2007
20/06/2007
22/06/2007
24/06/2007
26/06/2007
28/06/2007
30/06/2007
02/07/2007
04/07/2007
06/07/2007
08/07/2007
10/07/2007
12/07/2007
14/07/2007
16/07/2007
18/07/2007
20/07/2007
22/07/2007
24/07/2007
26/07/2007
Date
Av Observed
Model

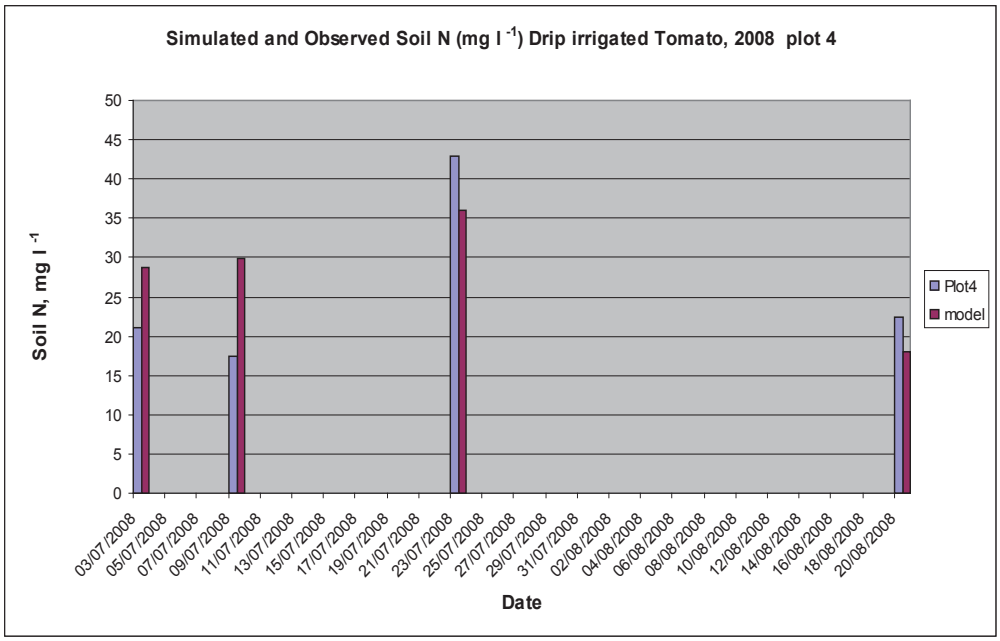
Simulated and Observed Soil N (mg l -1) Drip irrigated Tomato, 2008 plot 4
Soil N, mg l -1
50
45
40
35
30
25
20
15
10
5
0
03/07/2008
05/07/2008
07/07/2008
09/07/2008
11/07/2008
13/07/2008
15/07/2008
17/07/2008
19/07/2008
21/07/2008
23/07/2008
25/07/2008
27/07/2008
29/07/2008
31/07/2008
02/08/2008
04/08/2008
06/08/2008
08/08/2008
10/08/2008
12/08/2008
14/08/2008
16/08/2008
18/08/2008
20/08/2008
Date
Plot4
model

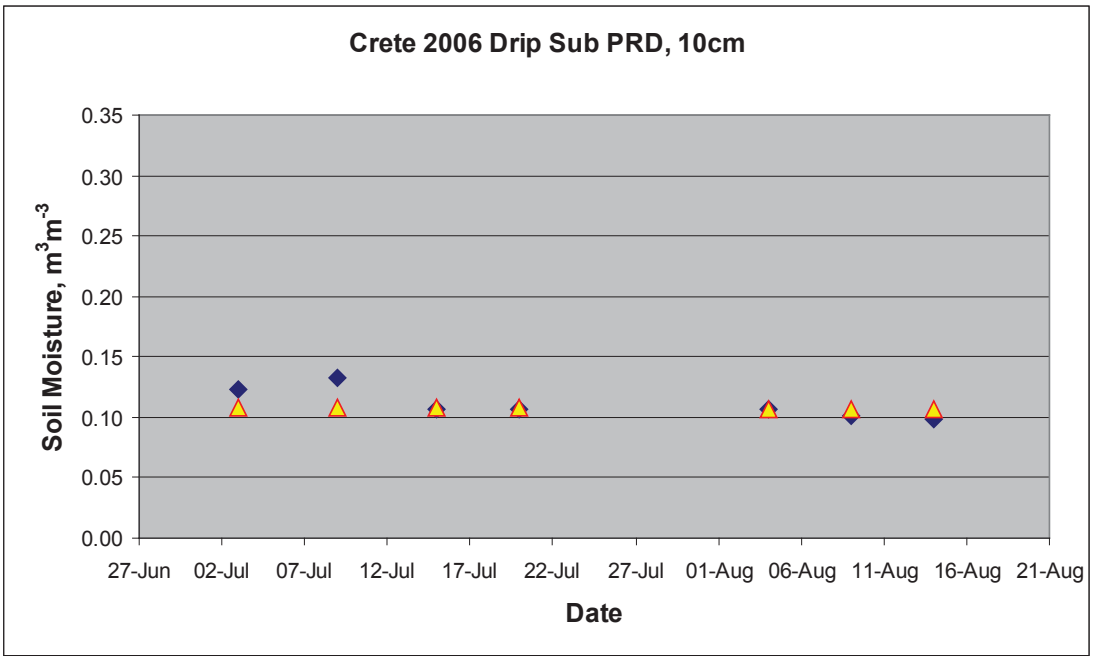
Crete 2006 Drip Sub PRD, 10cm
Soil Moisture, m3m-3
0.35
0.30
0.25
0.20
0.15
0.10
0.05
0.00
27-Jun
02-Jul
07-Jul
12-Jul
17-Jul
22-Jul
27-Jul
01-Aug
06-Aug
11-Aug
16-Aug
21-Aug
Date

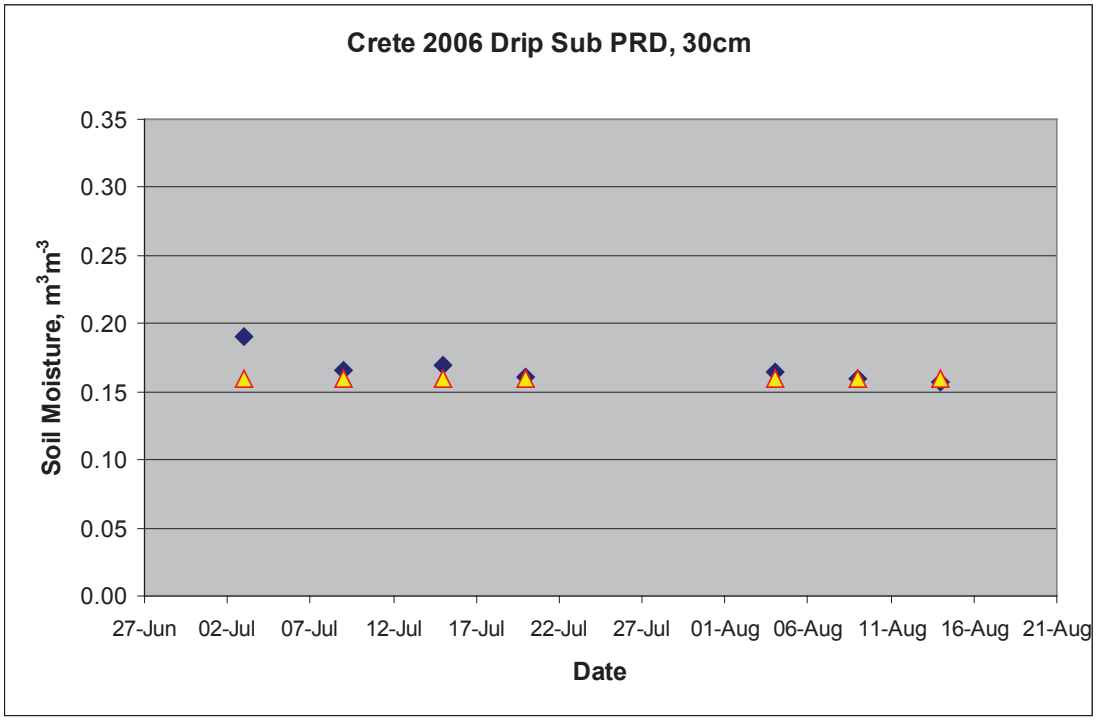
Crete 2006 Drip Sub PRD, 30cm
Soil Moisture, m3m-3
0.35
0.30
0.25
0.20
0.15
0.10
0.05
0.00
27-Jun
02-Jul
07-Jul
12-Jul
17-Jul
22-Jul
27-Jul
01-Aug
06-Aug
11-Aug
16-Aug
21-Aug
Date

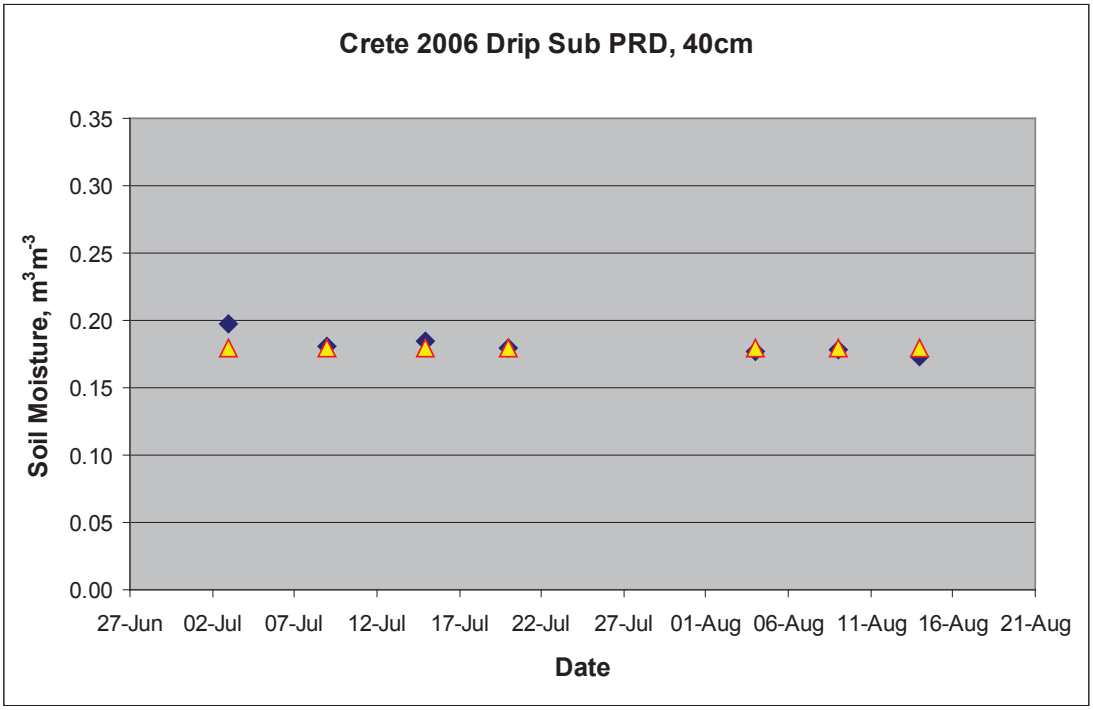
Crete 2006 Drip Sub PRD, 40cm
Soil Moisture, m3m-3
0.35
0.30
0.25
0.20
0.15
0.10
0.05
0.00
27-Jun
02-Jul
07-Jul
12-Jul
17-Jul
22-Jul
27-Jul
01-Aug
06-Aug
11-Aug
16-Aug
21-Aug
Date

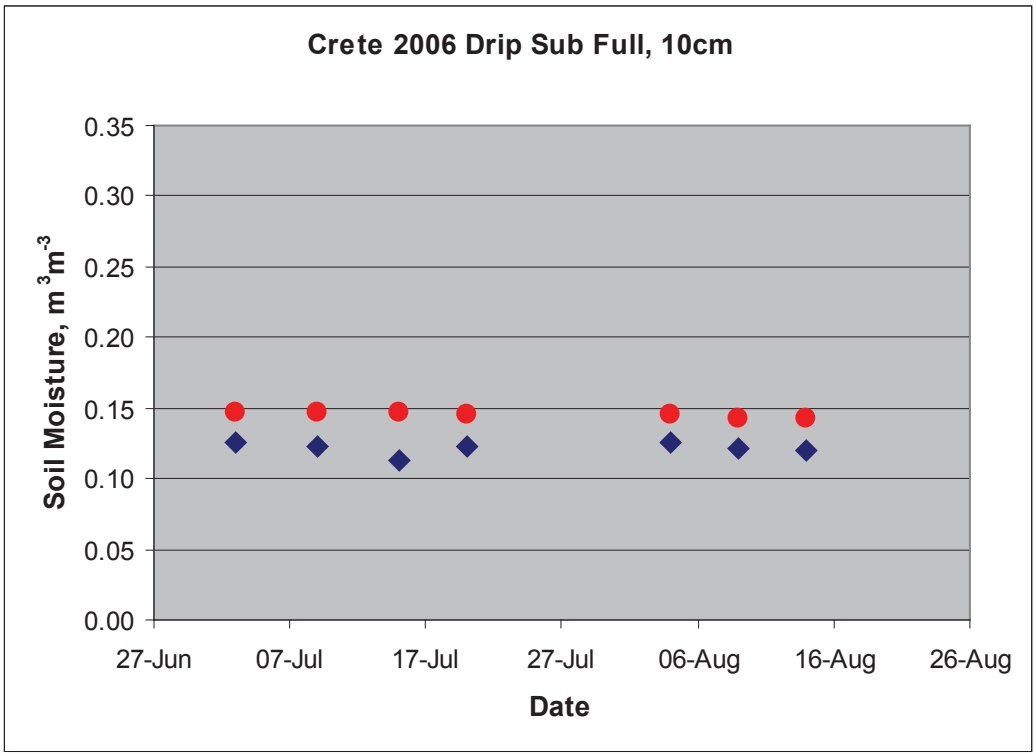
Crete 2006 Drip Sub Full, 10cm
Soil Moisture, m3m-3
0.35
0.30
0.25
0.20
0.15
0.10
0.05
0.00
27-Jun
07-Jul
17-Jul
27-Jul
06-Aug
16-Aug
26-Aug
Date

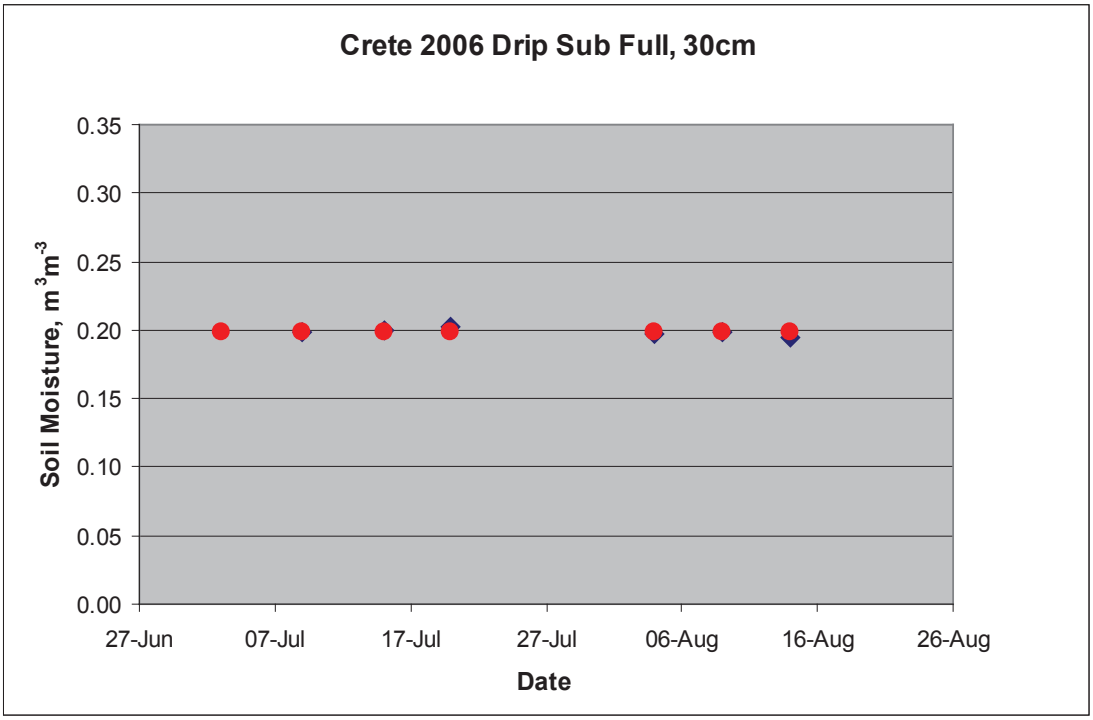
Crete 2006 Drip Sub Full, 30cm
Soil Moisture, m3m-3
0.35
0.30
0.25
0.20
0.15
0.10
0.05
0.00
27-Jun
07-Jul
17-Jul
27-Jul
06-Aug
16-Aug
26-Aug
Date

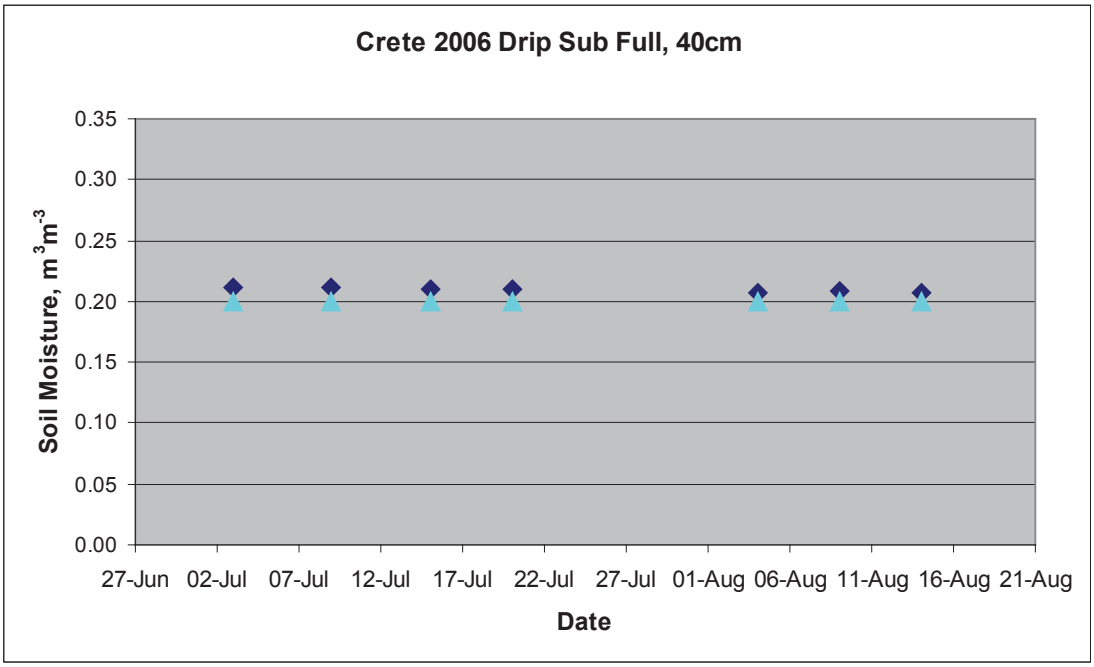
Crete 2006 Drip Sub Full, 40cm
Soil Moisture, m3m-3
0.35
0.30
0.25
0.20
0.15
0.10
0.05
0.00
27-Jun
02-Jul
07-Jul
12-Jul
17-Jul
22-Jul
27-Jul
01-Aug
06-Aug
11-Aug
16-Aug
21-Aug
Date

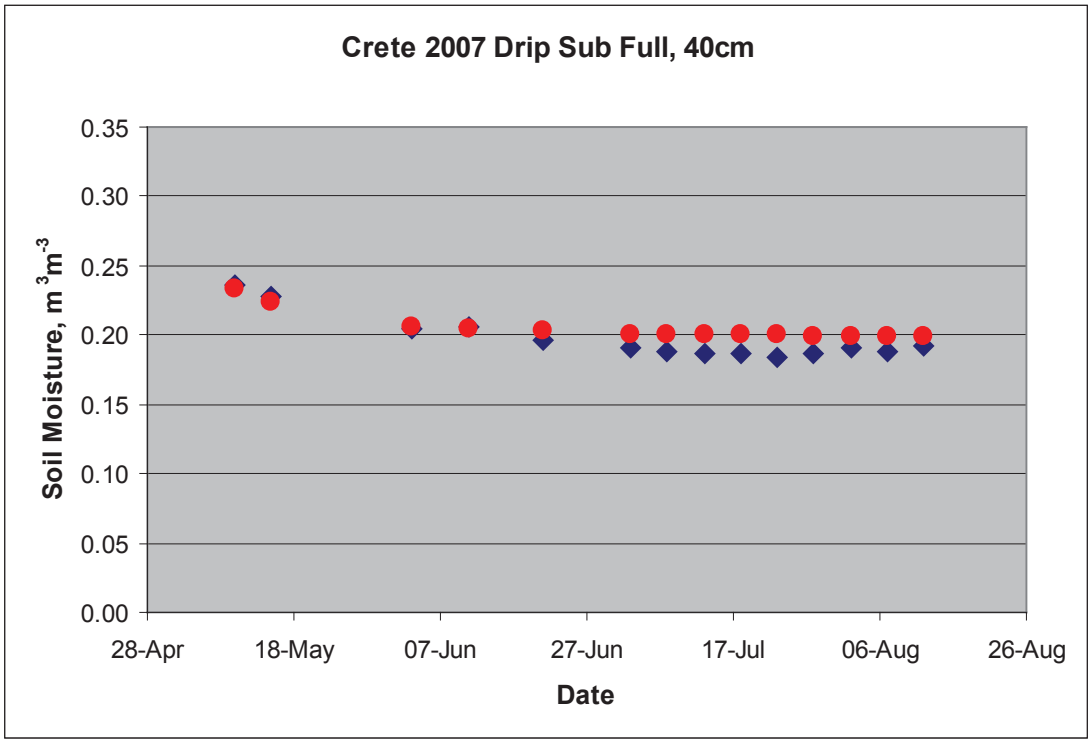
Crete 2007 Drip Sub Full, 40cm
Soil Moisture, m 3m-3
0.35
0.30
0.25
0.20
0.15
0.10
0.05
0.00
28-Apr
18-May
07-Jun
27-Jun
17-Jul
06-Aug
26-Aug
Date

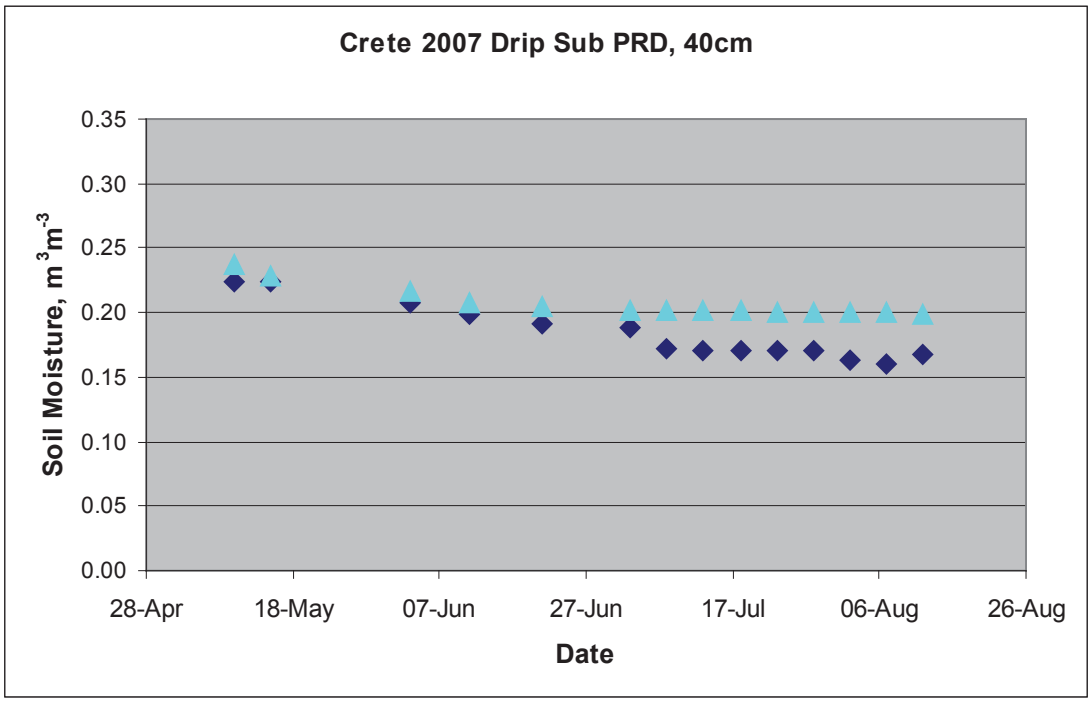
Crete 2007 Drip Sub PRD, 40cm
Soil Moisture, m 3m-3
0.35
0.30
0.25
0.20
0.15
0.10
0.05
0.00
28-Apr
18-May
07-Jun
27-Jun
17-Jul
06-Aug
26-Aug
Date

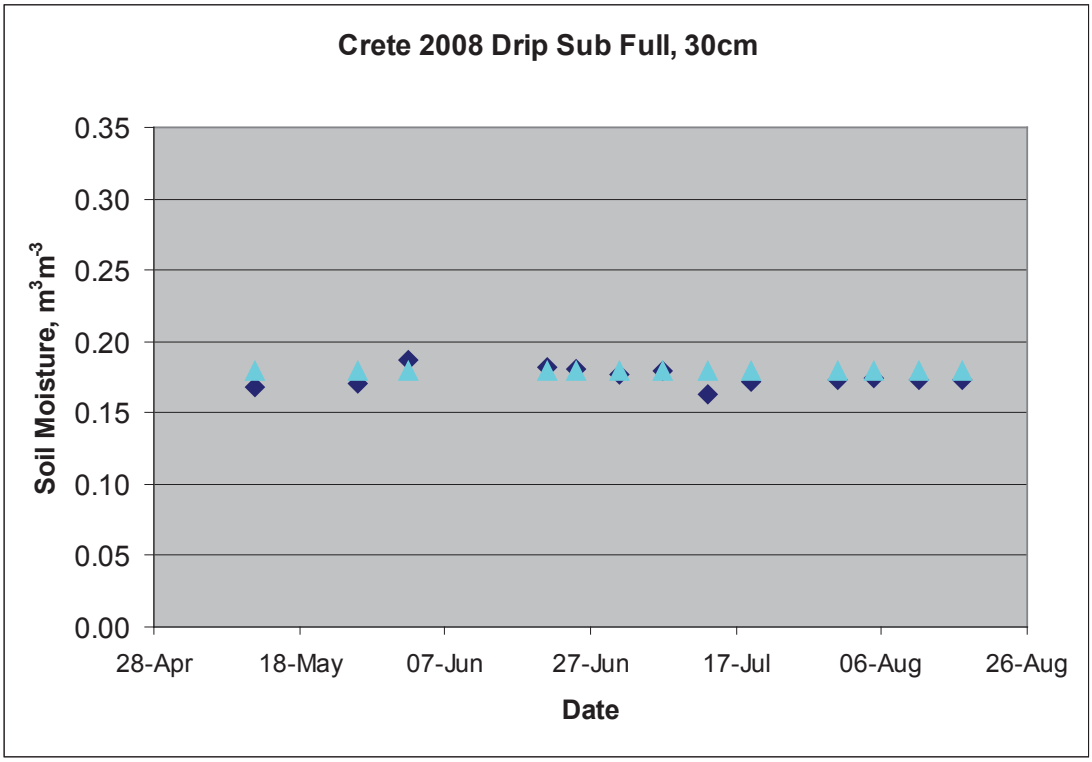
Crete 2008 Drip Sub Full, 30cm
Soil Moisture, m3m-3
0.35
0.30
0.25
0.20
0.15
0.10
0.05
0.00
28-Apr
18-May
07-Jun
27-Jun
17-Jul
06-Aug
26-Aug
Date